Imbalance of inhibitory control and excitatory drive associated with cognitive deficits in Alzeimer's disease and aging

Thèse

Iason Keramidis

Doctorat en neurobiologie
Philosophiæ doctor (Ph. D.)

Québec, Canada

Imbalance of inhibitory control and excitatory drive associated with cognitive deficits in Alzheimer's disease and aging

Thèse

Iason Keramidis
Doctorat en Neuroscience
Philosophiæ Doctor (PhD)

Sous la direction de:

Yves De Koninck, directeur de recherche

Résumé

La maladie d'Alzheimer (MA) est la maladie neurodégénérative la plus courante et la cause prédominante de la démence sénile (caractérisé par une perte de mémoire et de raisonnement) et du déclin cognitif. Elle résulte d'une dégénérescence des neurones et d'une atrophie sévère qui commence dans les lobes temporal, pariétal et frontal et dans le gyrus cingulaire, puis dans des régions sous-corticales telles que l'hippocampe et le noyau de Meynert. Des observations récentes chez les patients atteints de la MA ont fait état d'une activité cérébrale anormale, commune à d'autres troubles neurologiques avant la perte des neurones. L'hyperexcitabilité neuronale se manifeste tôt dans la MA, ce qui entraîne une hyperactivité corticale et hippocampique et parfois même une activité épileptiforme et des crises chez la souris et l'homme. Cependant, les mécanismes sous-jacents à l'hyperexcitabilité dans le cerveau de la maladie d'Alzheimer restent obscurs. Une hypothèse importante suggère que l'accumulation d'amyloïde-β perturbe la signalisation inhibitrice médiée par le $GABA_A$.

Le vieillissement normal est également associé à un déclin des fonctions cognitives, indépendamment de tout trouble neurodégénératif. Les causes du déclin cognitif associé au vieillissement (DCAV) sont multiples, mais le facteur clé est l'équilibre entre l'excitation et l'inhibition synaptiques. Comme dans le cas de la maladie d'Alzheimer, une hyperactivité neuronale dans l'hippocampe, une région du cerveau impliquée dans la formation et la rétention de la mémoire, ou une absence de désactivation du réseau du mode par défaut (DMN) ont été décrites dans les troubles cognitifs associés au vieillissement. Pourtant, dans le cortex préfrontal, une région du cerveau cruciale pour les fonctions exécutives, une réduction manifeste de la ramification dendritique se produit avec le vieillissement, entraînant une diminution de la transmission synaptique excitatrice et une augmentation de l'entrée inhibitrice.

Les études présentées dans cette thèse visent à identifier les altérations de la transmission synaptique conduisant aux déficits cognitifs associés à la MA et à l'ARCD mais visent également à dévoiler les mécanismes potentiels sous-jacents à l'hyperactivité neuronale. Dans la MA, les résultats présentés ici montrent une perte de fonction de l'extrudeur de chlorure neuronal KCC2, responsable du maintien de la robustesse de l'inhibition médiée par le $GABA_A$. La restauration de KCC2 chez les souris porteuses de mutations liées à la maladie d'Alzheimer a permis d'inverser les déficits de mémoire spatiale et les

dysfonctionnements sociaux, reliant la dyshoméostasie des chlorures au déclin cognitif lié à la maladie d'Alzheimer. Avec le vieillissement normal, un sous-ensemble de souris a développé des déficits de mémoire non spatiale, un comportement de type anxieux et un dysfonctionnement social. Dans ce sous-ensemble de souris âgées atteintes de troubles cognitifs, les niveaux de protéines synaptiques inhibitrices clés étaient élevés dans le cortex préfrontal médian (CPM). L'activation optogénétique des neurones GABAergiques du CPM a modifié le comportement des jeunes souris et a reproduit certaines des déficiences cognitives observées chez les vieilles souris souffrant de troubles cognitifs. D'autre part, lorsque la stimulation optogénétique a été utilisée pour générer un modèle d'hyperactivité neuronale soutenue et chronique dans l'hippocampe de jeunes souris, les niveaux de protéines synaptiques excitatrices et inhibitrices ont été réduits, ce qui indique une perturbation générale de la transmission synaptique. Enfin, et surtout, lorsque l'on compare les protéines modifiées lors d'une stimulation optogénétique chronique chez des souris de type sauvage à celles modifiées par des mutations et des pathologies dans les modèles de la maladie d'Alzheimer, seules quelques protéines sont exprimées différemment. Ces résultats suggèrent que l'hyperactivité neuronale pourrait contribuer directement à la perturbation de la transmission synaptique et à la neuropathologie liée à la MA.

En résumé, le déclin cognitif peut se produire avec une inhibition à la fois exagérée et diminuée. Ces deux voies opposées, la première étant observée dans le déclin cognitif lié à l'âge et la seconde étant typique de la MA, perturbent de manière unique le fonctionnement normal du cerveau, ce qui entraîne à son tour un déclin cognitif. Une appréciation de ces résultats peut avoir des implications pour les interventions thérapeutiques dans les deux conditions.

Dans l'ensemble, les travaux présentés dans cette thèse soulignent non seulement la contribution de l'altération de la transmission inhibitrice dans le développement du déclin cognitif dans la MA et le vieillissement, mais décrivent également l'implication de l'hyperactivité neuronale dans la perturbation des synapses et la neurodégénération.

Abstract

Alzheimer's disease (AD) is the most common neurodegenerative disorder and the predominant cause of senile dementia (characterized by a loss of memory and reasoning) and cognitive decline. It results from neuron degeneration and severe atrophy initiating from the temporal, parietal and frontal lobe, the cingulate gyrus and the hippocampus following by subcortical regions such as the the nucleus basalis of Meynert. Recent observations have reported an abnormal brain activity in AD patients, common to other neurological disorders prior to the neuron loss. Neuronal hyperexcitability manifests early in AD which leads to cortical and hippocampal hyperactivity and sometimes even epileptiform activity and seizures in mice and humans. However, the mechanisms underlying hyperexcitability in the AD brain remains elusive. A prominent hypothesis suggests that amyloid-β accumulation disrupts $GABA_A$-mediated inhibitory signaling.

Normal aging is associated also with a decline in cognitive function independently of any neurodegenerative disorder. The causes of aging associated cognitive decline (ASCD) are multifaceted but a key factor is the imbalance between synaptic excitation and inhibition. Similar to AD, neuronal hyperactivity in the hippocampus, a brain region involved in memory formation and retention, or failure of deactivation of the Default Mode Network (DMN) has been described in ASCD. Yet, in the prefrontal cortex, a brain region crucial for executive functions, an overt reduction in the dendritic branching occurs with aging resulting in diminished excitatory synaptic transmission together with an increase in the inhibitory input.

The studies presented in this thesis aim to identify alterations in synaptic transmission leading to cognitive deficits associated with AD and ARCD but also aim to unveil potential mechanisms underlying neuronal hyperactivity. In AD, the results presented here show a loss of function of the neuronal chloride extruder KCC2, responsible for maintaining the robustness of $GABA_A$-mediated inhibition. Restoring KCC2 in mice carrying AD-linked mutations reversed spatial memory deficits and social dysfunction linking chloride dyshomeostasis with AD-related cognitive decline. With normal aging, a subset of mice developed non-spatial memory impairments, anxiety-like behavior, and social dysfunction. In this subset of cognitively impaired old mice, the levels of key inhibitory synaptic proteins were elevated within the medial prefrontal cortex (mPFC). Activating mPFC GABAergic neurons optogenetically altered the behavior of young mice and mimicked some of the cognitive impairments found in the old, cognitively impaired mice. On the other hand, when

optogenetic stimulation was used to generate a model of sustained, chronic neuronal hyperactivity in the hippocampus of young mice, both excitatory and inhibitory synaptic proteins levels were reduced pointing to a general disruption of synaptic transmission. Finally, and more importantly, when we compared the proteins altered upon chronic optogenetic stimulation in wild-type mice to that altered due to mutations and pathology in AD models, only a few proteins where differently expressed. These results suggest that neuronal hyperactivity could contribute directly to the disruption of synaptic transmission and the neuropathology linked to AD.

To sum up, cognitive decline can occur with both exaggerated and diminished inhibition. These two opposing paths, with the first seen in age-related cognitive decline, and the second being typical to AD, uniquely disrupt normal brain functioning which in turn leads to cognitive decline. An appreciation of these findings can have implications for therapeutic interventions in the two conditions.

Taken together, the work presented in this thesis not only highlights the contribution of altered inhibitory transmission in the development of cognitive decline in AD and aging, but also describes the involvement of neuronal hyperactivity in synapse disruption and neurodegeneration.

Table of contents

List of figures

List of abbreviations

AD	Alzheimer's disease
Aβ	Amyloid-β peptides
NFTs	Neurofibrillary tangles
K^+	Potassium
Cl^-	Chloride
GABA	Gamma Aminobutyric Acid
CA1	cornu Ammonis 1
KCC2	Potassium chloride co-transporter 2
5xFAD	5 Familial Alzheimer's Disease
APP	Amyloid Precursor Protein
NL-G-F	KM670/671NL (Swedish); APP V717I and APP E693Q mutations
NonTg	Non-Transgenic
mPFC	medial Prefrontal Cortex
CaMKIIa	calcium/calmodulin-dependent protein kinase II
MWT	Morris Water Task
ARCD	Aging-Related Cognitive Decline
$GABA_AR$	Gamma Aminobutyric Acid alpha Receptor
DMN	Default Mode Network
E/I	Excitation/Inhibition
GAD	Glutamic Acid Decarboxylase
VGAT	vesicular GABA transporter
TM	Transmembrane domains
HCO_3^-	Bicarbonate
IPSCs	Inhibitory Post-Synaptic Currents
Geph	Gephyrin gene

mIPSCs	miniature Inhibitory Post-Synaptic Currents
E_{Cl}	electrochemical equilibrium potentials of Cl^-
IPSPs	Inhibitory Post-Synaptic Potentials
NMDA	N-methyl-D-asparate
AMPA	a-amino-3-hydroxy-5-methyl-4-isoxazolepropionic acid
KA	kainic acid
ER	Endoplasmic Reticulum
KAR	Kainate Receptor
$[Cl^-]_i$	Intracellular chloride concentration
TMD	Transmembrane domain
NTD	N-terminal domain
CTD	C-terminal domain
EM	Electron Microscopy
BDNF	Brain Derived Neurotrophic Factor
ERK1/2	Extracellular signal-regulated kinase 1/2
REST	Repressor element-1 silencing factor
RE-1	Repressor element 1
WNK1	Lysine deficient protein kinase 1
WNK3	Lysine deficient protein kinase 3
SPAK	SPS1-related proline/alanine-rich kinase
ORS1	oxidated stress-response kinase 1
PKC	Protein kinase C
TrkB	Tropomyosin receptor kinase B
CREB	cAMP response element-binding protein
BACE1	β-site cleaving enzyme
sAPPβ	soluble APP beta

sAPPα	soluble APP alpha
PSEN1	presenilin 1
PSEN2	presenilin 2
LTP	Long-Term Potentiation
DS	Down Syndrome
FTDP-17	Frontotemporal dementia with parkinsonism linked with chromosome 17
MCI	Mild Cognitive Impairment
CSF	Cerebrospinal Fluid
TTX	tetrodotoxin
PET	Positron Emission Tomography
PIB	Pittsburgh compound B
fMRI	functional Magnetic Resonance Imaging

To all rodents used in research. Σε εσένα, γλυκιά μου γιαγιά, που φρόντισες έναν ασθενή με άνοια για χρόνια και τελικά κατέληξες να υπέφερες κι εσύ από τη ίδια νόσο, Αλτζχάιμερ. To all the caregivers across the globe.

"Bear in mind that the wonderful things you learn in your schools are the work of many generations, produced by enthusiastic effort and infinite labor in every country of the world. All this is put in your hands as your inheritance in order that you may receive it, honor it, add to it, and one day faithfully hand it on to your children. Thus do we mortals achieve immortality in the permanent things which we create in common"
Albert Einstein, *in a speech to children*

Acknowledgements

First and foremost, I would like to express my sincere thanks and my deepest gratitude to my mentor, Dr. Yves De Koninck, for his guidance, supervision, and encouragement to my projects over the years but also his support, enthusiasm and trust to my ideas and work. His wisdom, patience and dedication to his work and students has been truly inspirational to me. I feel incredibly privileged to have him as my PhD supervisor. Thank you for teaching me how to think outside the box and integrate all the information to make sense of scientific data.

My deepest appreciation further extends to my supervisory committee, Drs. Caroline Menard and Christophe Proulx for their advice throughout my committee meetings and hallway conversations.

I am grateful for Dr. Antoine Godin's friendship and support. His help and assistance with analyzing and interpreting the data presented in this thesis was invaluable. I would also like to give my thanks to all the people that have helped and collaborated on my projects over the years, including Drs. Majid H Mohajerani, Benoit Gosselin, Katerina Papanikolopoulou, Brendan McAllister and Gabriel Gagnon-Turcotte.

Many thanks to all the members of the Yves De Koninck lab, past and present, in particular, Drs. Annie Castonguay and Feng Wang for being incredibly supportive. Thanks to my colleagues and friends Irene, Nicolo, Melina, Sahara, Amalia, Banshi, Jonathan, Johanna, Isabel, Dominique, Jackye and many others for making life at CERVO worthwhile.

Finally, my heartfelt thanks to my family, my mother and father; Maria and Christos, my brother, Alexandros, and my sister-in-law Marita for all their love and support.

Foreword

This thesis summarizes the research I conducted during my doctoral studies in Neuroscience at Université Laval since September 2016 under the supervision of Prof. Yves De Koninck in CERVO Brain Research Centre affiliated with Université Laval.

Throughout these years I had the opportunity to work on several projects which are presented in this thesis, and all had something in common. They address changes in neural activity and synaptic transmission under different pathological conditions. Thus, in Chapter 1, I review the literature focusing on Alzheimer's disease, aging-related cognitive decline, synaptic neurotransmission and, chloride regulation.

Chapter 2 presents the results contained in a manuscript submitted for peer review on *Brain* entitled: "Restoring neuronal chloride extrusion reverses cognitive deficits linked to Alzheimer's disease mutations". For this article I am a co-first author and I contributed to designing and planning all the experiments. I performed all the biochemical experiments, the surgeries for the chloride imaging (*ex vivo* or *in vivo*) and the social interaction behavioral testing. Analysis was performed jointly by Brendan McAllister, Julien Bourbonnais, Feng Wang, Antoine G Godin, Yves De Koninck and I. Brendan McAllister, Yves De Koninck and I wrote the manuscript.

Chapter 3 presents the results contained in a manuscript currently in preparation for submission entitled: "A subset of aged mice develops cognitive decline associated with prefrontal cortex synaptic alterations". For this article, I contributed to designing, planning, and conducting all the experiments. Analysis and interpretation were performed by Antoine G Godin, Yves De Koninck and I. Reza Hazrati performed part of the behavioral testing. Gabriel Gagnon-Turcotte and Benoit Gosselin provided the hardware and the software for the *in vivo* electrophysiology recordings. I wrote the manuscript in collaboration with Yves De Koninck.

Chapter 4 presents the results contained in a manuscript currently in preparation for submission entitled: "Hippocampal chronic optogenetic activation alters proteome and elicits synapse disruption". For this article, I contributed to designing, planning, and conducting all the experiments. Martina Samiotaki performed the mass spectrometry analysis. Data analysis and interpretation were performed by Katerina Papanikoloupoulou, Yves De Koninck and I. Johanna Alonso and I performed and analyzed the *in vivo* optrode recordings.

Romain Sansonetti performed the daily optogenetic stimulation. I wrote the manuscript in collaboration with Katerina Papanikolopoulou and Yves De Koninck.

Introduction

Despite the tremendous advancement in the field of medical science, our understanding of the mechanisms underlying neurodegeneration still remains feeble. Alzheimer's disease (AD) is the most common neurodegenerative disorder with approximately 500,000 individuals suffering from it in Canada, while more than 6.2 million people (aged 65 years old or more) suffering from AD alone in the United States (Rajan et al., 2021). This number is estimated to rise dramatically in the upcoming years mostly due to the human lifespan increase (Kowal, 2016). Among many risk factors for neurodegeneration and AD, aging remains the most impactful and given that in elderly populations neurodegeneration is common, one could argue that neurodegeneration is a manifestation of accelerated aging. However, a major contributor to our poor understanding of AD, and neurodegeneration in general, is the late onset and the relatively long asymptomatic nature of these devastating disorders. Thus, the controversy between the two, aging being a risk factor for neurodegeneration and neurodegeneration being a late onset phenotype, could only further muddle our understanding of the mechanisms of neurodegeneration. Is aging-related cognitive frailty and senile dementia so distinct to AD? Are there any common mechanisms contributing to the development of various dementia forms? How could aging and neurodegeneration give rise to so similar phenotypes in humans but also in non-human primates and rodents? These are key questions neuroscientists are trying to answer especially since cognitive frailty and dementia emerge as a major threat to our lives and only very few effective therapies have been identified to delay the progression of dementia and mitigate some symptoms.

Alzheimer's Disease is characterized by progressive memory loss and cognitive decline over the course of several years, with the symptoms often appearing years after the onset of pathological alterations in the brain of patients. The critical process contributing in the development of AD is postulated to be the aggregation of both amyloid-β (Aβ) protein fragments into plaques and phosphorylated tau protein into neurofibrillary tangles (NFTs) (Selkoe, 2001; Serrano-Pozo et al., 2011). These two hallmarks of the disease have been described already since 1906 by Dr. Alois Alzheimer with a Bielschowsky staining on the brain of his deceased patient Auguste Deter. Age is the main risk factor for the disease but also a discrimination factor between the early onset disease, where the symptoms occur prior to 65 years old (familial cases) and the late onset disease with the clinical phase starting after 65 years old. The typical clinical symptoms for the late onset patients include

progressive memory impairment, cognitive decline, paranoia, delusions, and loss of social appropriateness. Only 1% of the AD patients represent the familial cases (Bekris et al., 2010) with the first typical clinical symptoms starting between 30-65 years old but many other atypical symptoms follow, such as visual dysfunction, apathy, aphasia and/or executive dysfunction.

Recent observations on individuals carrying a genetic risk factor for AD, but also late onset patients and rodent models carrying several AD-linked mutations have reported an abnormal brain activity occurring early in the development of the disease (Palop and Mucke, 2016). Neuronal hyperexcitability manifests during early stages of AD (Palop and Mucke, 2016) leading to neocortical and hippocampal hyperactivity (Bassett et al., 2006; Bookheimer et al., 2000), and under certain conditions to epileptiform activity and seizures (Vossel et al., 2013).This aberrant brain activity is postulated to arise from a disruption of inhibitory transmission and specifically $GABA_AR$-mediated inhibition (Palop and Mucke, 2016) and/or blocking of glutamate reuptake (Zott et al., 2019). Similarly, one key factor of aging-related cognitive decline (ARCD) is hyperactivity in certain regions of the brain such as the hippocampus (Wilson et al., 2005) or the failure of deactivation of the Default Mode Network (DMN) (Miller et al., 2008). Reducing the hyperactivity via various pharmacological approaches improves cognition both in AD and ARCD suggesting that hyperactivity is a cause of cognitive decline and not a compensatory mechanism. Yet, ARCD has been associated with an increase in inhibitory input and subsequently a shift in the E/I balance towards inhibition in the prefrontal cortex (Bories et al., 2013; Luebke et al., 2004), a brain region critical for several cognitive functions. Thus, one could argue that cognitive deficits in AD and ARCD are better associated with alterations in synaptic transmission and an imbalance in the E/I ratio since the onset for these symptoms appears decades after the accumulation of plaques and NFTs (Perrin et al., 2009).

During my doctoral studies I have focused on studying alterations in synaptic transmission underlying cognitive deficits associated with AD and ARCD, but I have also tried to unveil potential mechanisms underlying neuronal hyperactivity. Synaptic transmission relies on finely tuned homeostatic processes that regulate the cellular concentration of several types of ions. Chloride homeostasis is one of these essential homeostasis processes. The robustness of $GABA_AR$ neurotransmission, the predominant inhibitory signal in the brain, depends on low intracellular chloride concentrations which allows influx of negatively charged chloride into the neuron when $GABA_ARs$ open. The

potassium-chloride cotransporter KCC2 is the key regulator of chloride levels in the mature CNS (Doyon et al., 2016; Rivera et al., 1999) and, therefore, of inhibitory signaling. KCC2 hypofunction limits chloride extrusion which in turn disrupts $GABA_A$ signaling leading to an imbalance in E/I, neuronal hyperactivity and confound synaptic plasticity. KCC2 hypofunction contributes to pathological conditions such as epilepsy (Huberfeld et al., 2007), neuropathic pain (Coull et al., 2003), and schizophrenia (Hyde et al., 2011). However, it remains unclear whether KCC2 hypofunction could contribute to the cognitive impairments occurring with aging and AD. This was one of the open questions I tried to address during my PhD and explore how changes in KCC2 function contribute to chloride dyshomeostasis, $GABA_A$ neurotransmission disruption, and cognitive impairments in AD.

While the aberrant brain activity reported in AD seems to arise from disinhibition, the imbalance in E/I observed in the medial prefrontal cortex with normal aging is manifested through an increase in the $GABA_A$-mediated inhibitory tone (Dickstein et al., 2007). In addition to the electrophysiological alterations, neurons undergo morphological changes with reduction in dendrite arborization and spine numbers being evident in pyramidal neurons of aged rodents and nonhuman primates (Bories et al., 2013; Duan et al., 2003). Spines represent key sites for excitatory synapses (Berry and Nedivi, 2017) and synaptic communication thus diminished spine numbers could reflect lower excitatory input in the PFC. Taking together all these pre-existing findings, I tried to understand whether ARCD in mice is associated with biochemical changes in the major excitatory and inhibitory synaptic proteins and whether by manipulating the E/I balance in the PFC, one could replicate some of the cognitive impairments linked with ARCD.

Finally, neuronal overexcitability has been linked to neuronal hyperactivity, aberrant network activity and the onset of various neurodegenerative disorders (Baroncelli et al., 2011; Bassett et al., 2006; Bookheimer et al., 2000; Khedr et al., 2011; Wong, 2010). The neuronal degeneration seems to occur due to the activation of signaling cascades which induce excitotoxicity (Choi, 1994). Yet it remains unknown whether neuronal hyperactivity is sufficient to promote synapse and neuronal loss and more importantly which are the potential mechanisms and key contributors of such degeneration driven by neuronal hyperexcitability. Thus, I tried to generate a paradigm of chronic neuronal hyperactivity (typical during early stages of AD) in the rodent hippocampus by optogenetics and then study the effect of such manipulation, by assessing the proteome changes followed this evoked neuronal hyperexcitability.

Chapter 1 - Literature Review

1.1 Alzheimer's disease

1.1.1 Overview

Alzheimer's disease (AD) is the most common neurodegenerative disorder and the most frequent cause of dementia in elderly. Other than progressive memory loss, the disease is associated with an overt cognitive decline such as loss of judgment and logic, loss of spatial consciousness and of trouble solving (McKhann et al., 2011; Selkoe, 2001). According to the World Alzheimer Report 2021, 23 to 35 million people suffer from the disease worldwide with this number estimated to rise to 131.5 million people by 2050 (Rajan et al., 2021). Age is the main risk factor of the disease (Carr et al., 1997) and also a discrimination factor between the early onset disease in which the symptoms start prior to 65 years old (familial cases), and the late onset disease with the clinical phase initiating after 65 years old (sporadic cases). About 1% of the patients represent the familial cases with the clinical symptoms starting between 30 to 65 years old (Bekris et al., 2010). These patients may develop additional symptoms to the typical described for the sporadic patients, such as visual disfunction, aphasia and executive dysfunctions.

The histopathological characteristics of the disease include the extracellular depositions of amyloid-β (Aβ) peptides in amyloid plaques and the intracellular formation of neurofibrillary tangles (NFTs) consisting of phosphorylated TAU (Selkoe, 2001; Serrano-Pozo et al., 2011). Histological analysis also reveals extensive cerebral synaptic and neuronal loss accompanied by gliosis (Hyman et al., 2012). Specific brain regions such as the temporal, parietal and frontal lobe and the cingulate gyrus have been identified as the first sites of Aβ deposition in pre-clinical AD patients (Palmqvist et al., 2017; Thal et al., 2002), which later in the disease progression undergo severe atrophy (Sperling et al., 2014). Yet, regions such as the hippocampal CA1, the subiculum, the amygdala, the nucleus basalis of Meynert, the locus coeruleus and the dorsal raphe are also subject to extensive neuronal degeneration (Thal et al., 2002). On the other hand, TAU aggregates are commonly found in the medial temporal lobe later in the progression of the disease (after 60 years of age). The NFTs formation initiates in the entorhinal cortex and propagates to the hippocampus and beyond to the limbic and associated areas (Crary et al., 2014; Jagust, 2018). The anatomical pattern of TAU propagation in patients suggests that misfolded TAU is released by neurons with NFTs and taken up by connected cells, leading to recruitment

of endogenous TAU to the misfolded state, supporting the prion-like properties of TAU (Jucker and Walker, 2018).

Aβ is a secreted peptide produced by a 2 step enzymatic cleavage of Amyloid Precursor Protein (APP), first by β-secretase (BACE1) followed by γ-secretase. Several peptides of Aβ can be produced because of the amyloidogenic cleavage of APP ranging from 38 to 43 amino acids in length. The most prominent form is the Aβ40, however Aβ42 appears to be critical for the aggregation of Aβ and the formation of amyloid plaques (Hardy and Selkoe, 2002). TAU is a cytosolic protein essential for the microtubule assembly and neuronal trafficking. Its function is regulated by post-translational modifications; mostly phosphorylation in 85 distinct serine, threonine, and tyrosine residues. Phosphorylation of specific TAU sites and/or TAU hyperphosphorylation are postulated to result in lower affinity of the protein to the microtubules and its (mis)sorting and aggregation into the dendrites (Zempel and Mandelkow, 2014). The deposition of amyloid plaques is detrimental to the surrounding neurons and in parallel, Aβ seems to exaggerate the toxicity of TAU (Bu et al., 2018; He et al., 2018). The formation of plaques and NFTs seems to precede the onset of very mild dementia in AD, and dementia seems to better correlate with the synaptic and neuronal loss associated with AD (Morris and Price, 2001). These observations support the hypothesis that plaques initially and NFTs later, accumulate for 10-15 years prior the onset of any symptoms and mediate the pathophysiology of the preclinical phase of the disease (Perrin et al., 2009) (**Figure 1.1.1**).

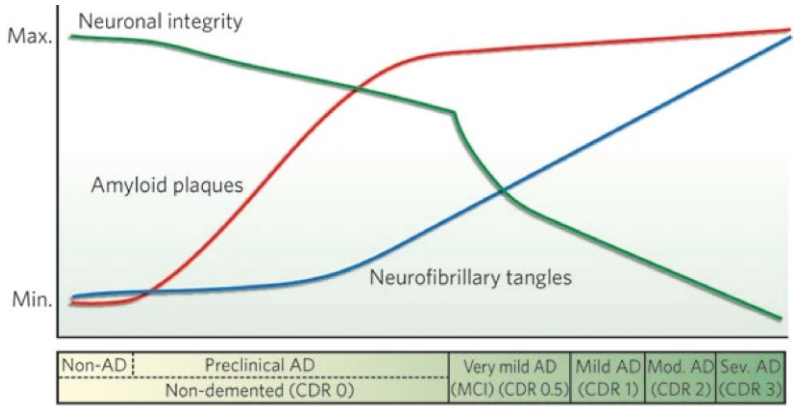

Figure 1.1.1. The clinical stages of Alzheimer's disease

The 'very mild', 'mild', 'moderate' and 'severe' mild cognitive impairment (MCI) are associated with abundant Aβ plaques deposition (red line) and a gradual accumulation of NFTs (blue line). However, the onset of MCI better correlates with the occurrence of synaptic and neuronal loss (green line). Modified from (Perrin et al., 2009).

AD can be clustered in families and can be specifically inherited in an autosomal dominant fashion. Familial AD is mostly caused by missense mutations in *APP* or in *PSEN1* and/or *PSEN2*. However, the majority of the AD cases might have a genetic determinant, such as a polymorphic allele which predisposes to the disease, but does not cause it. An example of this is apolipoprotein E (APOE) polymorphic alleles that have been found to predispose strongly to the development of AD (Strittmatter et al., 1993) (although the APOE-ε2 allele appears to be neuroprotective (Talbot et al., 1994)). Interestingly there are no mutations in *MAPT*, the gene encoding for TAU, that have been associated with AD (Wang and Mandelkow, 2015). Mutated TAU typically gives rise to other types of dementia, with an overt deposition of tau in neurofibrillary tangles but not amyloid deposition, such as frontotemporal dementia with parkinsonism linked to chromosome 17 (FTDP-17) (Hutton et al., 1998; Spillantini et al., 1998). Despite the cause of AD, familial or sporadic, the two forms of AD are often indistinguishable, but for the earlier age of the onset in the familial forms. Both the histopathological phenotypes and the clinical symptoms of the common sporadic AD and the autosomal dominant forms are quite similar (Hardy and Selkoe, 2002). Thus, this phenotypic similarity between the two forms, strongly suggests that the mechanisms linked to the onset of the familial disease, are also common to the development of the sporadic disease. Moreover, the findings supporting that profound neurofibrillary tangles formation leading to fatal neurodegeneration are not sufficient to induce amyloid deposition and plaques formation (Lewis et al., 2001) indicate that NFTs formation are downstream of the changes in Aβ proteolysis and amyloid aggregation (Hardy et al., 1998).

AD remains untreated to date and the only therapeutic agents available are simply aiming to temporarily reduce the symptoms and/or delay the symptom progression. Early neurochemical studies based on the pioneering work of Carlsson and Hornykiewicz in Parkinson's disease (Hornykiewicz, 2002) led to the prevalent view that modulation of cholinergic transmission can offer a symptomatic treatment of Alzheimer's disease. The profound loss of cholinergic cortical intervention from the nucleus basalis of Meynert led to the use of cholinesterase inhibitors in AD patients (Summers et al., 1986). However, all the currently approved therapies based on cholinesterase inhibitors are marginally effective and do not alter the course of the disease (Lleó et al., 2006). The ineffectiveness of cholinesterase inhibitors largely relies in their selectivity and the fact that other neurotransmitters are disturbed. The catecholamine innervation to the cortex is also affected (Adolfsson et al., 1979) and most prominently the neuronal loss due to the NFTs formation

in the cortex results in a functionally significant deficiency in glutamatergic neurotransmission (Hardy et al., 1987).

Another treatment approach is focused on Aβ immunization. Several experimental studies, but also clinical trials, have shown that immunization against Aβ can effectively reduce the Aβ levels in the brain and in some cases improve memory impairments (Janus et al., 2000; Morgan et al., 2000; Nicolll et al., 2003; Schenk et al., 1999; Sevigny et al., 2016). The initial clinical trials had to be stopped since some of the AD patients participating in the study (but not the healthy volunteers) developed meningoencephalitis (Winblad and Blum, 2003). However, the Aβ-targeting monoclonal antibody aducanumab developed by Biogen, recently, was finally granted an accelerated FDA approval even if the data supporting the efficacy of the treatment were not strong or convincing to many.

Finally, approaches including γ-secretase or BACE1 inhibitors have been suggested and tested without yielding any encouraging results. Both types of inhibitors significantly reduced the Aβ production (Bateman et al., 2009; Egan et al., 2018), however blocking γ-secretase worsens the cognitive decline (Doody et al., 2013), while blocking BACE1 significantly increased the rate of cognitive decline (Egan et al., 2018). Due to these adverse results, development of therapeutic agents inhibiting γ-secretase or BACE1 have been halted and ongoing clinical trials were withdrawn.

Since most of the attempts focusing on removing Aβ or reducing its production have been largely unsuccessful, TAU has received considerable recent scrutiny. In addition to AD, TAU is implemented in the pathology of several other neurodegenerative disorders, called tauopathies. Thus, the development of an effective AD treatment targeting TAU could result in prosperous therapeutic agents for a group of other diseases. The strategy followed so far to intervene and block the detrimental effects of TAU have focused on reducing its phosphorylation. Memantine, has been used to activate the PP2A phosphatase with early clinical trials showing short-term improvements in cognition following treatment (Jiang and Jiang, 2015). In addition, kinase inhibitors, such as lithium, an inhibitor of GSK3β (Stambolic et al., 1996) have shown to reduce phospho-TAU (p-Tau) levels in the CSF of patients with MCI and improved cognition (Forlenza et al., 2011). Unfortunately, as in the case of Aβ, TAU immunotherapies have been largely unsuccessful (Pedersen and Sigurdsson, 2015; Sigurdsson and Sigurdsson, 2016). This is probably due to the fact that NFTs are intracellular, hence targeting TAU with antibodies could be demanding, however some studies have shown that antibody fragments against TAU can effectively reduce TAU levels *in vivo* (Ising et al., 2017; Nisbet et al., 2017).

1.1.2 Amyloid Precursor Protein and Amyloid-β

The Amyloid Precursor Protein (APP) is a single pass transmembrane protein encoded by the *APP* gene located on the chromosome 21 (Gralle and Ferreira, 2007). The *APP* gene contains 18 exons and spans for more than 170 kb (Yoshikai et al., 1990). Alternative slicing of *APP* produces three isoforms containing 695, 751 and 770 amino acids, with the APP_{695} being the predominant isoform expressed in neurons (Kang et al., 1987). Homolog proteins to human APP have been identified in other animal models such as *Drosophila melanogaster*, *Ceanorhabditis elegans* and *Danio rerio*, while other APP-like proteins have been identified in mammals (Zheng and Koo, 2006). Interestingly the sequence encoding for Aβ is not conserved between species suggesting that this domain of APP is not involved in the physiological function of the protein (Zheng and Koo, 2006) (**Figure 1.1.2**).

As its name suggests, APP acts as the precursor protein to produce amyloid-β peptides (Aβ) which play a crucial role in the development of AD, however its physiological function still remains elusive. APP is processed and cleaved in two distinct pathways producing active fragments that have different functions (**Figure 1.1.3**). The amyloidogenic pathway produces the soluble APP beta (sAPPβ) peptide and Aβ by the subsequent cleavage of APP from the β-site cleaving enzyme (BACE1) and the presenilin-containing γ-secretase (De Strooper et al., 2012). BACE1 is an aspartic acid protease that cleaves APP either at the Asp+1 site of Aβ or at a secondary site (Glu+11) in the extracellular side of APP (Tan and Evin, 2012). Gamma secretase on the other hand is a multi-protein complex consisting of presenilin 1 (PSEN1), nicastrin, APH-1, PEN-2 (presenilin enhancer 2) and CD147, with PSEN1 mediating the intramembranous proteolysis of APP (Wolfe et al., 1999). Interestingly APP is transported to the axon by kinesin-I along with β-secretase and presenilin-1 suggesting that the proteolysis and the secretion of Aβ occurs in axonal membrane compartment (Kamal et al., 2001). In the non-amyloidogenic pathway APP is cleaved by α-secretase (ADAM10) producing soluble APP alpha (sAPPα), preventing the production of Aβ (Kuhn et al., 2010). The Aβ monomers produced by the amyloidogenic cleavage of APP can further aggregate into soluble oligomers, soluble fibrils and insoluble fibrils which form amyloid plaques (Haass, 2010).

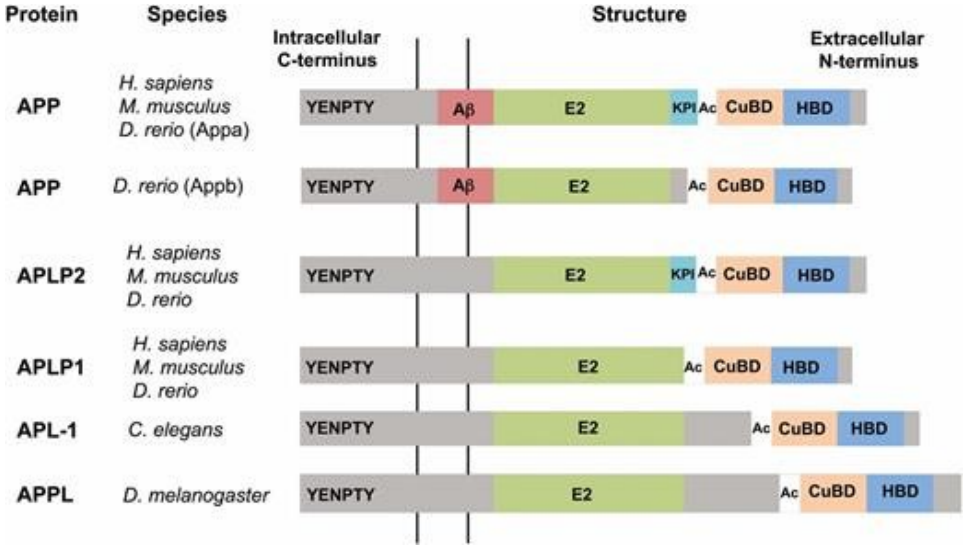

Figure 1.1.2. The structure of APP in various animal species.

The extracellular domains E2, the acid domain (Ac), the cooper binding domain (CuBD) and the heparin-binding domain and the intracellular YENPTY domain are highly conserved across species. A Kunitz protease inhibitor domain (KPI) is found only in APP and APLP2. The Aβ sequence is only present in APP. Modified from (Nicolas and Hassan, 2014).

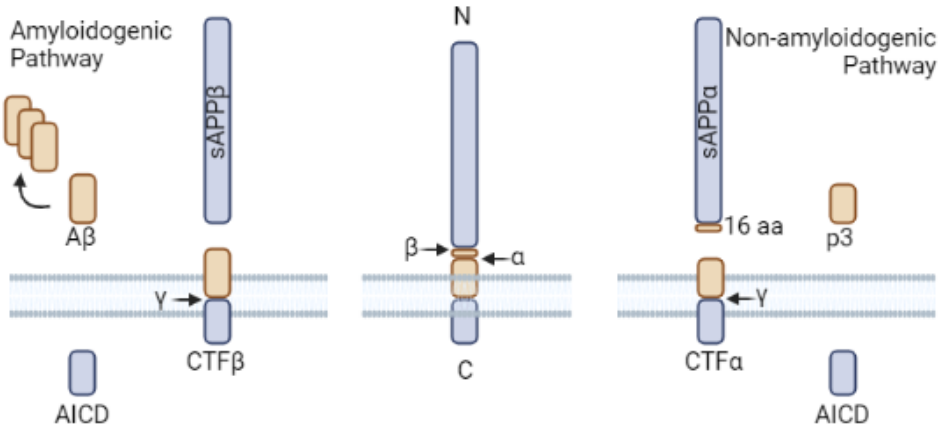

Figure 1.1.3. APP processing and cleaving pathways

The Non-amyloidogenic processing of APP by α-secretase (ADAM10) within the Aβ region prevents Aβ generation and produces sAPPα and p3 peptide which are secreted. Cleavage by β-secretase results in the secretion of Aβ and sAPPβ during the amyloidogenic pathway. Created with BioRender.com

The Aβ aggregation and amyloid plaques deposition in the brain of AD patients and the resulting neuronal loss have been the main focus in AD research and the amyloid cascade hypothesis (Hardy and Higgins, 1992). Several mutations associated with AD have been found in the *APP* gene and the enzymes mediating APP processing. For instance three mutations in the COOH-terminus of APP and the codon 717 of the protein substitute valine to isoleucine, phenylalanine or glycine (Chartier-Harlin et al., 1991; Van Duijn et al., 1991; Goate et al., 1991) resulting in high production of Aβ42 (Herl et al., 2009) due to looser binding of γ-secretase to APP and a shift of PSEN1 from the ε cleavage site (Dehury et al., 2020). Most of the *APP* mutations linked with early-onset AD are localized near the α- or γ-cleavage site such as the: I716V, V715M, T714I, T714A, N694D, E693G, E693K and A673V. However, there are mutations in *APP* which are neuroprotective and prevent the development of AD in carriers. An example represents the A673T substitution in the exon 16 of *APP* which has been identified first in a Caucasian individual aged 65 years old who died by ischemic neurovascular disease but had no signs of AD (Peacock et al., 1993). This polymorphism was characterized extensively later in a study conducted in approximately 1,800 Icelanders in which carriers of the A673T had 1.47 fold odds to reach the age of 85 and above and did not develop AD (Jonsson et al., 2012). The A673T mutation has a protective effect against AD due to the reduction of the cleavage of APP by BACE1 at the β-cleavage site (Jonsson et al., 2012).

It is evident that the loss of function of APP, by itself, is not sufficient to induce AD, although, depletion of APP can give rise to seizure activity in mice (Steinbach et al., 1998). It is the increase in the total Aβ levels or a shift in the ratio of Aβ40 to Aβ42 that is associated with the development of AD. Incubation of primary hippocampal cultures with media containing fibrils of Aβ results in neuronal loss (Yankner et al., 1989). Several studies have shown that the synaptic transmission alterations linked to AD occur in the early stages of the disease and are independent of the amyloid plaques formation (Hsia et al., 1999). Moreover, clinical trials aiming to reduce Aβ formation and deposition in patients have been unsuccessful so far (Egan et al., 2018; Honig et al., 2018; Salloway et al., 2014) and even the recently approved Aducanimab antibody treatment raised a lot of concerns for its efficacy (Sevigny et al., 2016). An additional clinical trial testing another antibody-based treatment just released its phase 3 report showing that cognitive decline was 27% slower in individuals with MCI due to AD pathology receiving the treatment for 18 months (van Dyck et al., 2022). However the community is still concerned about the high incidence of brain hemorrhage reported in some participants of the trial and patients (Reish et al., 2023). It is still subject to

debate which forms (if any) of Aβ are toxic and sufficient to induce the neural circuit impairments associated with the disease and the resulted neuronal loss. Interestingly, a recent study have shown that the binding of Aβ oligomers in the synapses and the subsequent blockage of hippocampal LTP is prevented upon depletion of APP (Wang et al., 2017).

APP is associated also with another disease, Down Syndrome (DS). Individuals with DS carry three copies of the chromosome 21 resulting in triplication of the *APP* gene which greatly increases the risk for AD in individuals with DS. Both diseases have been associated with neurodegeneration and seizures or epileptic activity in humans (Menéndez, 2005; Rissman and Mobley, 2011) and rodents (Deidda et al., 2015; Palop et al., 2007). The comorbidities between the two diseases suggest that some common neuropathological mechanisms may exist and are potentially linked to APP and or Aβ accumulation. Overexpression of APP gives rise to network hyperexcitability and epileptiform activity in mice (Born et al., 2014; Johnson et al., 2020; Kreis et al., 2021), consistent with the findings in patients of DS (Menéndez, 2005).

APP is abundantly expressed in presynaptic boutons where it interacts with several presynaptic proteins (Kohli et al., 2012). It also seems to play a role in neurite outgrowth through an interaction with Reelin and integrins (Hoe et al., 2009) and negatively controls synapse formation (Priller et al., 2006). In parallel, trophic factor deprivation could trigger cleavage of APP by BACE1 with the cleaved amino-terminal fragment of APP binding to death receptor 6 which subsequently initiates axonal pruning by caspase 6 activation (Nikolaev et al., 2009). Homo- or heterodimers of APP with the amyloid precursor-like protein 2 (APLP2) have been found to participate in trans-cellular adhesion too (Soba et al., 2005).

Recent observations indicate that APP is highly expressed in inhibitory GABAergic neurons and is part of the inhibitory metabotropic $GABA_BR$ complex (Schwenk et al., 2015). This interaction of APP with the $GABA_{B(1a)}R$ sushi domains seems to mediate axonal expression of the $GABA_BR$ and as a result augments presynaptic inhibition (Dinamarca et al., 2019) (**Figure 1.1.4**). The formation of the APP $GABA_BR$ complexes also protect APP from BACE1 cleavage and potential reduces the Aβ secretion (Dinamarca et al., 2019). In addition, Rice and colleagues have shown that soluble APP released followed α-secretase cleavage binds to presynaptic $GABA_BRs$ and regulate the presynaptic release of the neurotransmitter (Rice et al., 2019). Finally, APP interacts with KCC2 and ensures the stability and function of the latter at the surface of neurons (Chen et al., 2017; Shen et al., 2022) controlling the robustness of inhibitory neurotransmission.

The majority of the secreted Aβ are peptides of 40 amino acids (Aβ 40) but the longer 42 amino acids peptides (Aβ42) have the propensity to aggregate and produce fibrils (Jarrett et al., 1993). Several studies have shown that Aβ in various aggregation states when added to neuronal preparations gives rise to electrophysiological phenotypes (Freir et al., 2001; Hartley et al., 1999; Hsieh et al., 2006; Kessels et al., 2013; Kim et al., 2001; Stéphan et al., 2001). High levels of Aβ have been found to reduce glutamatergic synaptic transmission and LTP and increase long-term depression (Hsia et al., 1999; Hsieh et al., 2006; Walsh et al., 2002). Desensitization of synaptic NMDARs and aberrant activation of peri-synaptic GluN2B containing NMDARs or mGluRs can promote long-term depression and spine retraction (Hsieh et al., 2006; Li et al., 2009). On the other hand, altered synaptic activity and specifically elevated excitatory transmission can modulate the secretion of Aβ (Kamenetz et al., 2003). Taken together, these findings suggest a negative feedback loop mechanism maintaining neuronal activity under control and preventing secretion of Aβ and that disruption of this loop could contribute to the development of AD.

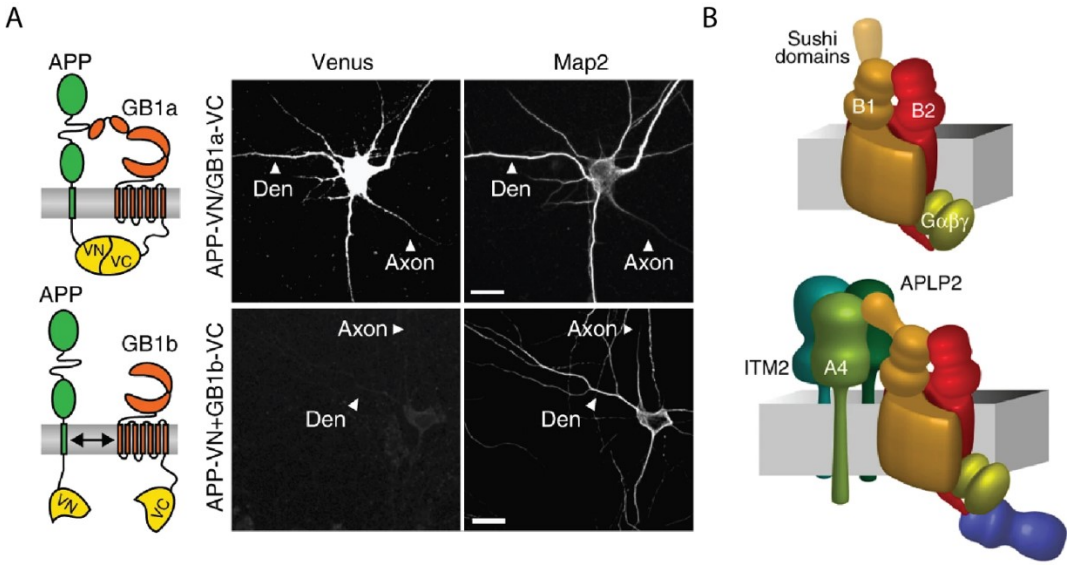

Figure 1.1.4. The APP and $GABA_BR$ complexes protect APP from cleavage

(**A**) Schematic illustration of APP and $GABA_{B(1a)}R$ complexes and the lack of complexes with $GABA_{B(1b)}R$. The formation of the complexes allows the reconstruction of Venus (N-terminus Venus fragment (VN) and C-terminus Venus fragment (VC)) and emission of fluorescence shown in the confocal images of hippocampal neurons expressing APP-VN and $GABA_{B(1a)}R$-VC but not in neurons expressing APP-VN and $GABA_{B(1b)}R$-VC. (**B**) Graphical illustration of the structural of the $GABA_BR$ and the sushi domains of the 1a subunit (top). At the bottom an illustration of the complex between $GABA_BR$ and APP (A4) facilitated via the interaction of the latter and the sushi domains of the receptor. Adapted by and modified from (Dinamarca et al., 2019; Schwenk et al., 2015).

Other than synaptic depression, high levels of Aβ seem to induce excessive neuronal activity both in the cortex and the hippocampus of rodents (Busche et al., 2008, 2012; Zott et al., 2019). In addition, it is becoming clear that Aβ accumulation measured by $CSF_{Aβ}$ and PET-amyloid imaging, initiates more than 20 years before the onset of symptoms in people at risk of AD (Bateman et al., 2012). This early detection of Aβ in clinic correlates with fMRI findings of hippocampal hyperactivity and impaired deactivation of the default-mode network (Bakker et al., 2012; Bookheimer et al., 2000; Dickerson et al., 2005; Hedden et al., 2009; Sperling et al., 2009) consistent with the experimental findings in rodents (Palop and Mucke, 2016). Application of soluble Aβ dimers in wild-type mice results in hippocampal hyperactivity (Busche et al., 2012) probably mediated by an Aβ-dependent block of glutamate reuptake resulting in neuronal hyperexcitability (Zott et al., 2019) or due to functional impairment of inhibitory interneurons (Busche et al., 2012; Verret et al., 2012) and a decline of $GABA_A$ input (Limon et al., 2012). Monomers and dimers of Aβ40 have been found to also enhance presynaptic glutamate release and thereby promote neuronal hyperactivity (Fogel et al., 2014).

Taken together, APP and its amyloidogenic product, Aβ, appear to be involved in regulating synaptic plasticity and neural activity on the circuit and network level. APP loss of function and/or accumulation of soluble Aβ in high concentrations in AD may represent thus a potential mechanism inducing neuronal hyperactivity, neural circuits dysfunction and network hypersynchrony (Palop and Mucke, 2016; Zott et al., 2018).

1.1.3 Tau and neurofibrillary tangles

Tau is a microtubule associated protein (MAP) encoded by the *MAPT* gene (Goedert et al., 1988, 1989) which promotes the organization and stability of the cytoskeleton but also facilitates the axonal transport in the nervous system (Wang and Liu, 2008). Six isoforms have been identified in the human CNS produced via alternative slicing of its transcript (Goedert et al., 1989). These isoforms vary in the number of the microtubule binding sites in the carboxy-terminal of the protein (having either 3R or 4R) and the number of the N-terminal repeats (having 0N, 1N or 2N) (Andreadis et al., 1992). The number of the microtubule binding repeats influence the binding affinity of Tau to the cytoskeleton (Geschwind, 2003) while the N-terminal repeats are postulated to influence the association of TAU with the plasma membrane and the nucleus (Arrasate et al., 2000).

The hyperphosphorylation of Tau in its 85 potential phospho-residues (all present in the 2N4R isoform of Tau) reduces the binding affinity of the protein to tubulin and results in a loss of function phenotype. Free p-Tau can accumulate and precipitate in endoplasmic aggregates called neurofibrillary tangles (NFTs) which can induce neuronal dysfunction and neurodegeneration (Geschwind, 2003). Tau is a natively unfolded protein which has no tendency to aggregate by itself and yet post-translational modifications, such as phosphorylation, result in modifying the processes of Tau oligomerization and aggregation and inducing the formation of the NFTs in disease. Elevated levels of non-mutated tau in the human CNS are typical for numerous neurological disorders called Tauopathies, such as AD, Pick's disease and Progressive Supranuclear Palsy (PSP) while mutations of Tau affecting again the binding of Tau to microtubules or increasing the levels of 4R TAU have been linked to Frontotemporal dementia with Parkinsonism-17 (FTDP-17) (Götz et al., 2019; Reed et al., 2001). No mutations on *Tau* have been found in AD patients, however NFTs are present and propagate in the brain following prion-like properties (Jucker and Walker, 2013)

Under physiological conditions Tau is localized in the axon terminals in mature neurons where it remains bound to the microtubules promoting microtubule assembly and/or maintenance of stability of previously formed microtubules. In immature neurons however, Tau is equally distributed in the soma and dendrites and becomes primarily axonal with neuronal polarization. Interestingly the intracellular localization of Tau during development is mediated by an increase of 4R isoforms and reduced phosphorylation (Drubin and Kirschner, 1986; Drubin et al., 1984; Mandell and Banker, 1996). In tauopathies, Tau accumulates in the soma, the dendrites and spines instead of the axon and eventually deposits in tangles. But free Tau in the soma or the dendrites can interact with other proteins that normally does not interact with. An example of an abnormal interaction represents the trapping of JIP1 protein, a component key for the kinesin axonal transport, in the soma by p-Tau (Ittner et al., 2009).

Tau can also undergo N- or O-glycosylation, ubiquitination, acetylation, truncation, and oxidation, totaling about 63 unique post-translation modifications identified in physiological and pathological conditions (Morris et al., 2015). However, phosphorylation remains the predominant modification which appears to be essential for neuronal plasticity (Götz et al., 2019). Most of the potential phosphorylation residues of Tau are clustered in the proline rich region or the carboxy-terminal region of the protein, hence the tandem mass spectrometry approaches used so far seem suboptimal in detecting specific phosphorylation

sites linked to physiological or pathological functions of the protein. Recent observations support that phosphorylation of Tau in specific residues and not hyperphosphorylation per se mediate most of the pathological and toxic effects of the protein in disease (Hanger et al., 2009; Keramidis et al., 2020; Nishimura et al., 2004; Papanikolopoulou and Skoulakis, 2014; Wang and Mandelkow, 2015).

A lot of effort has been put in understanding the physiological function of tau. To this end, several transgenic lines reducing or depleting the expression of tau in the CNS have been introduced. Surprising for most of the cases, reducing or depleting Tau in rodent models elicit neither functional nor morphological changes (Van Hummel et al., 2016) mainly due to the overexpression of other MAP homologs which compensate for the loss of Tau. However, in some *tau knock-out* animals a deficit in long-term potentiation or long-term depression has been observed in the hippocampus (Ahmed et al., 2014; Kimura et al., 2014), suggesting an involvement of tau in synaptic plasticity. Tau as mentioned above is primarily localized in the axon, however small amounts of Tau are present in the dendrites and the spines where it interacts with tubulin, F-actin, Src kinases and thus alters the structure of the dendrites cytoskeleton but also the synaptic scaffold and signaling (Morris et al., 2011), key elements for synaptic plasticity. Phosphorylated tau has been found to interact with the PSD95-NMDAR complex; while NMDA activation seems to alter the phosphorylation of Tau and its interaction with Fyn (Mondragón-Rodríguez et al., 2012). NMDAR serves as a substrate of Fyn and the phosphorylation of NR2 subunits has been shown to induce synaptic excitotoxic downstream signaling in pain, epilepsy and neurodegenerative disorders (Salter and Kalia, 2004).

Other electrophysiological findings in TAU *knock-out* mice indicate that loss of Tau function results in a profound resistance to seizures induced by disinhibition, excitotoxins or Aβ (Ittner et al., 2010a; Roberson et al., 2007, 2011) linking TAU to neuronal overexcitability and network hypersynchrony. These last findings also link Tau and the amyloid-β induced synaptic impairments which will be discussed extensively later (section 1.1.4). Interestingly, in AD, oligomeric Aβ induces de novo synthesis of Tau in the soma and the dendrites through a Fyn mediated activation of the ERK/ribosomal protein S6 signaling (Li and Götz, 2017). In addition, Aβ has been found to alter the phosphorylation or the distribution of Tau from the axon to the somatodendritic compartment (Zempel et al., 2010). This regulation of Tau expression, trafficking, and post-translation modification from Aβ results in a gain of function phenotype of Tau which can further mediate the Aβ-induced neuronal dysfunction. Thus, one could argue that the effect of Tau in synaptic plasticity and neuronal excitability

in AD is manifested by Aβ, however Tau can induce network hypersynchrony in other brain disorders independently of Aβ (Shao et al., 2022).

1.1.4 Amyloid-β dependent modulation of synaptic transmission

Synaptic plasticity is regulated by the release probability of various neurotransmitters and the calcium presynaptic concentration. When the neurotransmitter release probability is low in excitatory synapses, high frequency stimulations are necessary for potentiation. These synapses act as a high pass filters responding mainly to coordinated, synchronized firing patterns but not infrequent action potentials (Abbott and Regehr, 2004). In contrast, excitatory synapses with high neurotransmitter release probability act as low pass filters and better respond to single action potentials (Abbott and Regehr, 2004) and tend to show reduced potentiation in response to coordinated stimulation.

Amyloid-β is released in the synapses by either the non-amyloidogenic or the amyloidogenic pathway where it can have various physiological functions on synaptic transmission but also synaptic activity can modulate Aβ production (Cirrito et al., 2005). Elevated neuronal activity enhances the production of Aβ and when neuronal activity is blocked the levels of Aβ are reduced (Kamenetz et al., 2003). When the metabotropic glutamate receptors 2/3 are activated a subsequent decrease in presynaptic glutamate release follows which in turn reduces drastically the levels of Aβ in the hippocampus (Cirrito et al., 2005). Additionally, when synaptic activity is blocked with TTX the levels of Aβ are reduced (Cirrito et al., 2005). This activity dependent release of Aβ seems to be regulated by clathrin-mediated endocytosis of APP and processing from β- and γ-secretases (Cirrito et al., 2005). Activity-dependent release of Aβ has been observed in pathological conditions, such as induced epileptiform activity (Cirrito et al., 2005) or in physiological processes, during wakefulness (Kang et al., 2009). The same observations are supported also by the earlier development of plaques in patients with temporal lobe epilepsy (Mackenzie and Miller, 1994). In addition, a study conducted in rat hippocampus slices showed that fast spike bursts (typical during seizures) produce a high Aβ42/Aβ40 ratio via a calcium dependent synaptic vesicle exocytosis mechanism (Dolev et al., 2013).

In turn, Aβ can control synaptic activity via a feedback loop (**Figure 1.1.5**). Low levels of Aβ (in the picomolar range) potentiates synaptic transmission through pre-synaptic activation of a7-containing nicotinic acetylcholine receptors (Puzzo et al., 2008). Activation

of presynaptic nicotinic receptors elevate intracellular calcium concentration which increases the probability of synaptic vesicle release containing glutamate (Puzzo et al., 2008). Blocking or removing the nicotinic receptors indeed blocks synaptic plasticity and further reduces the secretion of Aβ (Wei et al., 2010). Glutamate release results in activation of NMDARs and AMPARs and the induction of LTP, however, the potentiation is only due to the presynaptic facilitation mediated by activation of nicotinic receptors and not due to alterations in NMDAR or AMPAR currents in the postsynaptic side.

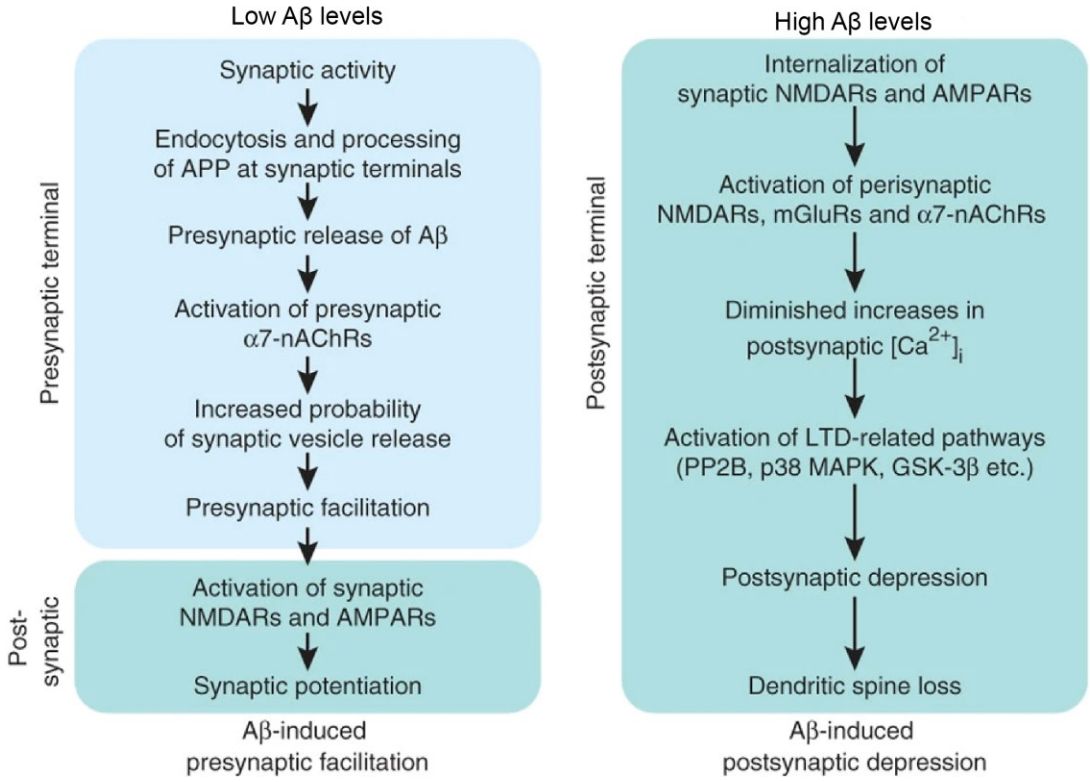

Figure 1.1.5. Aβ-dependent modulation of synaptic transmission

Low levels of Aβ induce pre-synaptic facilitation via activation of a7 containing nicotinic acetylcholine receptors and increased probability of glutamate release. This results in synaptic potentiation. In contrast, high abnormal levels of Aβ induces LTD-related mechanisms which result in post-synaptic depression and loss of dendritic spines. Modified from (Palop and Mucke, 2010a).

Elevated levels of Aβ (at the nanomolar range) can have the opposite effect and cause synaptic depression (Puzzo et al., 2008). The Aβ-dependent synaptic depression is

mediated through several mechanisms which modify the synapse strength by internalization (Roselli et al., 2005; Snyder et al., 2005) or desensitization of NMDARs and AMPARs (Liu et al., 2004) and/or dendritic spines collapse (Hsieh et al., 2006; Snyder et al., 2005). High peri-synaptic Aβ levels induce endocytosis of NMDAR via the a-7 nicotinic receptor activation and dephosphorylation of the NMDAR NR2B subunits resulting in overall reduction of NMDAR surface expression (Snyder et al., 2005). In parallel, Aβ appears to block glutamate uptake at synapses (Li et al., 2009; Zott et al., 2019) resulting in high glutamate concentrations in the synaptic cleft. Elevated glutamate activates synaptic NMDARs which ultimately results in desensitization of the NMDARs and synaptic depression. Glutamate can also spillover and activate the peri-synaptic NMDARs containing NR2B subunits or the metabotropic glutamate receptors and facilitate LTD (Li et al., 2009; Liu et al., 2004). Finally, there are several reports suggesting that high levels of Aβ can induce downstream effects to NMDAR activation such as activation of STEP-cofilin, p38 MAPK and GSK-3β signaling cascades (Li et al., 2009; Tackenberg and Brandt, 2009; Wang et al., 2004). Activation of these signaling pathways ultimately weakens connectivity between synapses, alters the dynamics of dendritic spines and promotes synaptic loss which impairs networks that underlie learning and memory (Walsh et al., 2002; Wei et al., 2010).

1.1.5 Neuronal network dysfunction in Alzheimer's disease

Alzheimer's disease, like many other neurological disorders, such as schizophrenia, epilepsy, DS, and autism, have been associated with an abnormal brain activity. In AD neuronal networks associated with successful encoding and retention of memories are altered, even during the early stages of the disease, before the symptoms onset (Anticevic et al., 2012; Canter et al., 2016; Sperling et al., 2009). These network alterations include hyperactivity or deactivation of specific brain regions, aberrant oscillatory rhythms and network hypersynchrony (Palop and Mucke, 2016), with all these alterations appearing in brain regions where the pathology of AD initiates and Aβ starts to deposit (Celone et al., 2006; Palmqvist et al., 2017; Persson et al., 2008) suggesting that Aβ can underly these aberrant network activity in patients.

Aβ can cause various detrimental effects on neurons and other cells types in the brain resulting in cell death (De Strooper and Karran, 2016). However, Aβ can induce deficits

in synaptic plasticity and neuronal circuits function way before the neuronal loss (Palop and Mucke, 2010a). Soluble Aβ oligomers, accumulating years before the Aβ plaques, are sufficient to evoke neuronal and network dysfunction (Cleary et al., 2004; Lesné et al., 2013; Selkoe, 2008; Shankar et al., 2008). Hence, tracing the propagation and the deposition of Aβ in the brains of AD patients could help identify brain networks that are susceptible to Aβ-induced dysfunction long before the overt neuronal loss. The development of C-Pittsburgh compound B (PIB) and florbetapir F-18, two positron emission tomography (PET) tracers have allowed detection of Aβ across the course of AD (Klunk et al., 2004; Wong et al., 2010). In parallel, brain activity can be monitored by functional magnetic resonance imaging (fMRI), PET or EEG recordings while the patients perform attention-demanding cognitive tasks. In healthy individuals, cognitive tasks typically increase fMRI signals in specific brain regions such as the hippocampus, but at the same time, cause silencing of other brain regions composing the default mode network (DMN) (Raichle et al., 2001). The radioligand tracers retention in PET studies have identified regions of the DMN as the sites of initial deposition of Aβ in AD patients and correlation of these findings to fMRI studies suggest that accumulation of Aβ is fundamental for the cognitive and memory decline related to activity changes within the DMN (Greicius et al., 2004; Palmqvist et al., 2017; Sperling et al., 2009).

The DMN is a network of functionally connected brain regions including the precuneus, posterior cingulate cortex, lateral and inferior parietal cortex and parts of the temporal and medial prefrontal cortex (Raichle et al., 2001). All together, these brain regions are co-activated during rest and inwardly oriented mental activity such as passive thinking, remembering, and planning, but also daydreaming and mind wandering (Raichle et al., 2001). The DMN becomes deactivated during outwardly directed mental tasks and this deactivation can act as a valuable predictor of good cognitive performance (Sperling et al., 2010). Notably, activation of the hippocampus during cognitive tasks without the deactivation of the DMN has been associated with impaired memory formation even in healthy individuals (Anticevic et al., 2012; Palop and Mucke, 2016). In addition, synchrony of activation and deactivation between the various brain regions of functional networks is crucial for cognitive performance and desynchronized circuits may underlie cognitive dysfunction (Palop and Mucke, 2016).

In AD and particularly during early stages of the disease, fMRI studies have revealed a remarkably consistent brain activity during memory-related tasks. In healthy individuals with overt Aβ deposition (Sperling et al., 2009), cognitively normal carriers of the APOE-ε4 allele (Bassett et al., 2006; Bookheimer et al., 2000; Filippini et al., 2009; Kunz et al., 2015),

patients with MCI (Bakker et al., 2012; Celone et al., 2006; Dickerson et al., 2005) and pre-symptomatic carriers of AD-related mutations (Quiroz et al., 2010) tasks a hippocampal hyperactivity and reduced deactivation of the DMN have been observed during memory-encoding (**Figure 1.1.6**). During later stages however, the activity of the hippocampus is reduced but the DMN activity remains high during cognitive-related tasks (Celone et al., 2006; Sperling et al., 2009). Interestingly, the Aβ accumulation seems to reach a plateau while the MCI starts in AD and does not increase further during the progression of the disease (Villemagne et al., 2011), however the cognitive performance of the patients keeps deteriorating. The latter could be then an consequence of the network dysfunction manifestations in the DMN and the hippocampal silencing (Damoiseaux et al., 2012).

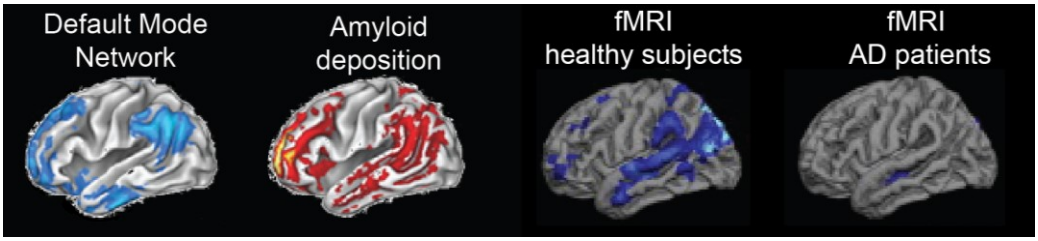

Figure 1.1.6. Aberrant network activity in Alzheimer's disease patients

The default mode network labelled in blue (left) and the PiB radioligand retention (red) in AD patients (center left). The fMRI activity (deactivation) in young healthy subjects during memory-related tasks (center right) and the fMRI deactivation in old AD patients. Modified from (Buckner et al., 2005; Sperling et al., 2009).

The hippocampal hyperactivity during the early stages of the disease have been hypothesized to act as a compensatory mechanism of the brain for the cognitive decline (Dickerson et al., 2004). It appears however that this hyperactivity underlies the early learning and memory impairments (Bakker et al., 2012; Putcha et al., 2011). Treatment of MCI patients with levetiracetam, an antiepileptic drug, reversed the hippocampal hyperactivity and improved the performance of the patients to a pattern-separation task (Bakker et al., 2012, 2015). Yet, Aβ deposition in the hippocampus follows the accumulation in the temporal, parietal, and frontal lobe which cannot explain the early hyperactivity of the hippocampus. 20 to 35 year old asymptomatic carriers of APOE-ε4 present task-induced hippocampal hyperactivity and alteration in the DMN activity (Filippini et al., 2009). It is

therefore probable that the hippocampal hyperactivity is related to the DMN alterations, a notion that is supported by the interconnection of the DMN with the limbic system which was revealed after deep brain stimulation of the fornix in AD patients (Laxton et al., 2010).

Other than abnormal activation or deactivation of neuronal networks in AD patients, network hypersynchrony has been observed in patients and animal models of the disease. Fluctuations in network synchrony are normally associated with physiological changes in brain states (Destexhe et al., 1999; Palva et al., 2005), however network hypersynchrony is pathological and is related to the induction of epileptiform discharges and seizures (Dominguez et al., 2005). Development of AD is considered a risk factor for epileptic seizures in humans (Romanelli et al., 1990). The incidence of epileptic activity in AD is around 15% (Horváth et al., 2016), however when comparing the incidence of seizures between individuals with AD and people with other forms of dementia, the first have a 7-8 fold higher incidence (Amatniek et al., 2006). More importantly, people with early onset AD are more likely to undergo seizures than the late onset patients (Sherzai et al., 2014) and the AD patients who had seizures or epileptic activity show faster progression of cognitive deterioration than patients without detectable seizures (Irizarry et al., 2012; Vossel et al., 2016).

Network hypersynchrony and epileptiform activity has been reported also in rodent transgenic lines carrying various mutations linked to AD. Overexpression of mutated APP and/or mutated PSEN1 results in the development of spontaneous epileptiform activity or to lower thresholds for chemically induced seizures (Born et al., 2014; Lalonde et al., 2005; Palop et al., 2007; Siwek et al., 2015). Notably, the L166P substitution in *PSEN1,* which results in a really aggressive familial form of AD, promotes the development of seizures as early as in adolescence in humans (Moehlmann et al., 2002). But it is not just Aβ that induces network hypersynchrony in mice. The presence of mutated TAU is sufficient to cause aberrant network activity (Maeda et al., 2016; Morris et al., 2011) and at the same time, endogenous TAU seems to promote the Aβ-dependent epileptiform activity since genetic suppression of TAU in mice overexpressing human APP can reduce the occurrence of seizures (Roberson et al., 2007; Shao et al., 2022). Finally, recent observations suggest that TAU is involved in the development of epileptic activity in other brain disorders and conditional ablation of the protein from excitatory neurons specifically, can reduce the epilepsy and the lethality linked to this overt cerebral activity (Shao et al., 2022).

The vast majority of individuals with DS (approximately 84%) who end up having dementia also develop seizures (Lai and Williams, 1989), suggesting that overexpression of

wild type APP could actually replicate the epilepsy-like phenotypes seen in familial AD. Similar to what happens in DS patients, duplication of the *APP* gene in some early onset AD cases have been also linked to epileptic activity during childhood or adolescence, long before the onset of dementia (McNaughton et al., 2012). Thus, regardless of the mechanism involved in the development of this aberrant brain activity, whether it is Aβ, TAU or overexpression of APP, seizures and network hypersynchrony appears to manifest in early stages of the disease prior to the onset of the typical clinical symptoms and it could present a potential key point for effective therapeutic interventions in AD.

1.1.6 Inhibitory disruption in Alzheimer's disease

Neuronal hyperexcitability and network hypersynchrony manifest during early stages of AD (Busche and Konnerth, 2016; Palop and Mucke, 2016; Zott et al., 2018). This leads to neocortical and hippocampal hyperactivity (Bassett et al., 2006; Bookheimer et al., 2000; Dickerson et al., 2005) and under certain conditions, to epileptiform activity and seizures, as discussed before, both in rodents (Busche et al., 2008; Verret et al., 2012; Zott et al., 2019) and humans (Cretin et al., 2016; Lam et al., 2017; Vossel et al., 2016, 2017). Hyperexcitability can also disrupts neuronal rhythms such as gamma oscillations (Guillon et al., 2017; Iaccarino et al., 2016; Verret et al., 2012). Oscillatory rhythms are promoted and regulated predominantly by the activity of inhibitory GABAergic interneurons (Buzsáki and Draguhn, 2004). The net inhibitory input of interneurons onto excitatory neurons (but other interneurons too) generates precise rhythms that regulate and coordinate the firing patterns of excitatory neurons (Sohal et al., 2009). This action of interneurons in controlling the rhythms within brain networks is in line with the observations suggesting that oscillatory network activity is disrupted in AD but also other neurological disorders such as schizophrenia, autism and epilepsy (Herrmann and Demiralp, 2005; Palop and Mucke, 2016).

The initial observations indicating that an inhibitory input disruption underlies the hyperactivity observed in the brains of transgenic mice carrying AD-linked mutations were made by Busche and colleagues (Busche et al., 2008). In this work, clusters of hyperactive neurons have been identified in the proximity of plaques (stained with Thioflavin-S) in the hippocampus of mice in *in vivo* calcium imaging recordings. These hyperactive neurons were inhibited by application of diazepam, a benzodiazepine which increases the open

probability of $GABA_A$Rs (Busche et al., 2008). More importantly, application of gabazine, a $GABA_A$R antagonist, increased the firing frequency of all neurons in the hippocampus but the relative increase in the already hyperactive neurons was smaller compared to neurons with normal baseline activity (Busche et al., 2008). Altogether, these observations suggest that disruption of $GABA_A$R-dependent neurotransmission underlies the neuronal hyperactivity. In addition, enhancing GABAergic activity was found to rescue the circuit dysfunction reported in AD transgenic mice but also after acute application of Aβ (Busche et al., 2015). Specifically, treatment with midazolam or clonazepam, two benzodiazepines which act as agonists of $GABA_A$R, restore normal slow-wave oscillatory rhythms in transgenic mice but also in the brain of wild-type mice exposed to Aβ (Busche et al., 2015) (**Figure 1.1.7**). In this last study, treatment with clonazepam (at low doses 0.05 mg/kg) was sufficient to restore learning performance during a spatial memory test in mice, while previous studies have shown that high doses of benzodiazepines (4.5 mg/kg) can actually worsen memory performance (Tampellini et al., 2010).

Several other studies have reported loss of gamma oscillatory activity in transgenic mice carrying AD-linked mutations (Cramer et al., 2012; Gurevicius et al., 2013; Verret et al., 2012), suggesting that these animals could have impaired inhibitory interneuron function. Diminished gamma power has been associated with reduced firing of parvalbumin positive (PV^+) inhibitory interneurons in mice (Lapray et al., 2012; Verret et al., 2012). Notably, injection of Aβ in the hippocampus resulted in the reduction of firing rates of fast bursting interneurons which typically represent PV^+ cells (Villette et al., 2010). Aβ application seems to also increase excitatory but decrease inhibitory postsynaptic currents in excitatory pyramidal neurons (Kurudenkandy et al., 2014). Decreased inhibitory input to hippocampal excitatory neurons have been shown to impair learning and memory retention in mice (Andrews-Zwilling et al., 2012), highlighting the importance of interneurons and inhibitory tone in cognition.

The mechanisms by which inhibitory input in excitatory neurons is disrupted in AD remain to be fully elucidated, however recent observations have started to shed light on this question. In the hAPP-J20 mice, a transgenic line for which epileptiform activity and network hypersynchrony has been well characterized (Palop et al., 2007), the downregulation of the voltage-gated sodium channel subunit Nav1.1 specifically in interneurons seems to give rise to the aberrant network activity and cognitive decline associated with AD (Verret et al., 2012). Notably, by restoring the levels of Nav1.1 in interneurons, the action potential kinetics of these neurons were accelerated and these changes were sufficient to restore normal

gamma oscillatory rhythms and reduce network hypersynchrony in hAPP-J20 mice (Martinez-Losa et al., 2018). The levels of Nav1.1 have been found to be reduced also in patients with AD (Verret et al., 2012), highlighting this voltage-gated sodium channel as a potential target for restoring interneuron dysfunction in patients and specifically gamma rhythms. This last feature might be crucial since gamma power appears to drop before the onset of epileptiform discharges in the hAPP-J20 (Martinez-Losa et al., 2018) and low gamma oscillations have been associated with disrupted memory encoding in humans with epilepsy (Matsumoto et al., 2013).

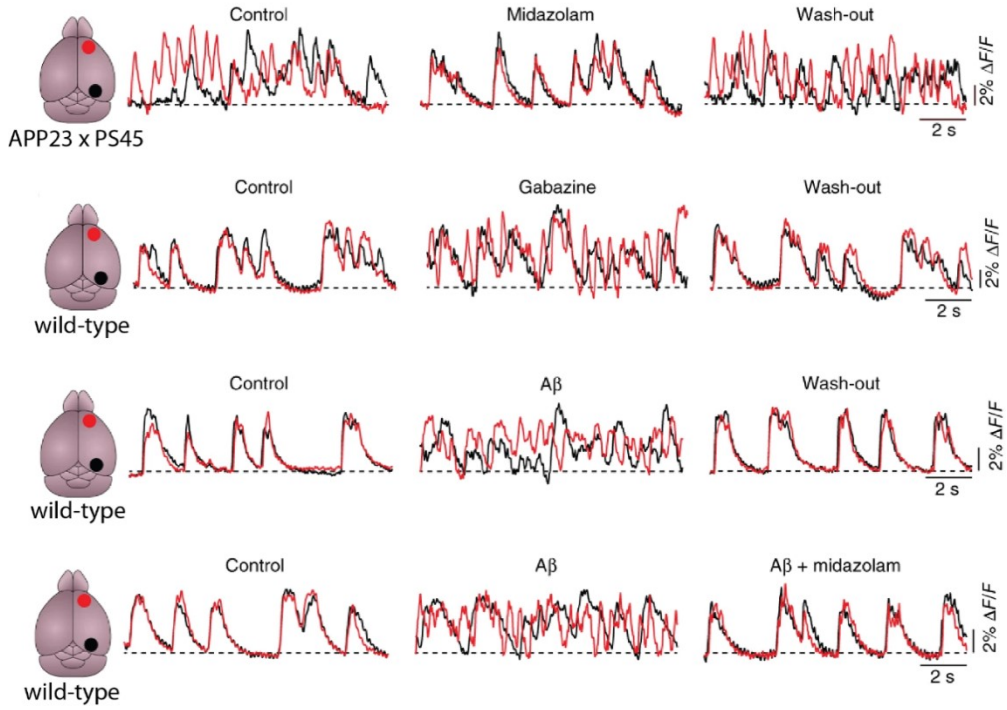

Figure 1.1.7. Aβ-dependent slow waves circuit dysfunction is restored by benzodiazepines

The slow-wave activity of the neocortex is altered in AD transgenic mice (APP23 x PS45) but also upon Aβ application. This disrupted circuit activity can be restored upon midazolam treatment and can be reproduced in wild-type mice upon gabazine application. Modified from (Busche et al., 2015).

The detrimental effect of Aβ in inhibitory neurotransmission can also be mediated by disruption in the $GABA_AR$ activation and downstream signaling. Yet, until recently there were only few indications that the GABA receptors are affected by neurodegeneration and AD

(Rissman and Mobley, 2011), although the majority of the studies investigating the GABA receptors were focused on the hippocampus. Only a modest decrease in the binding of benzodiazepines have been reported for the $GABA_AR$ in the hippocampus and the cortex in AD (Chu et al., 1987; Lanctôt et al., 2004). However, the specific subunit composition of the $GABA_AR$ seems to undergo alterations during the disease progression, which could in turn alter the function of the receptors. The mRNA levels of $GABA_AR$ subunits α1, α2, α4, δ, and β2 and of α1, α5, and β3 (refer to section 1.3.3) are respectively lower in the prefrontal cortex and the hippocampus (Luchetti et al., 2011; Mizukami et al., 1998; Rissman et al., 2003). A more recent study however, revealed lower mRNA levels of the α1 and γ2 subunit while an upregulation of the α2, β1 and γ1 subunits was reported in the temporal cortex of AD brains (Limon et al., 2012). In the same study, the GABA currents amplitude was reduced and the $GABA_ARs$ were desensitized faster in temporal cortices from AD brains (Limon et al., 2012). The reduction in GABA currents can be supported by the alterations in the composition of the $GABA_AR$ subunits in AD, with α2 and γ1 containing receptors being less sensitive to GABA (Bonnert et al., 1999; Lorenzo et al., 2020; Mortensen et al., 2012).

Consistently, in AD brains the level of Gephyrin, an inhibitory post-synaptic scaffolding protein (refer to section 1.3.3), are reduced with increasing disease severity, however, in late stages the levels of Gephyrin recover either due to advanced age or as a compensatory mechanism to the overt brain activity (Agarwal et al., 2008). Moreover, in cortical regions with abundance of plaques it has been reported a significant reduction in GABAergic (and glutamatergic) perisomatic terminals in excitatory neurons (Garcia-Marin et al., 2009). Thus, the notion that the GABAergic synapse is spared during neurodegeneration and AD appears to be outdated and the reduction of the GABAergic signaling or the disruption of GABAergic synapses could underlie the disinhibition, hyperexcitability and hypersynchrony associated with AD.

But it is not just the composition and the kinetics of the $GABA_AR$ which could result in disinhibition. $GABA_AR$ allow for bidirectional transport of Cl^- depending on the Cl^- gradient across the membrane. When $[Cl^-]_i$ is low, activation of $GABA_ARs$ results in influx of the negatively charged Cl^- and the hyperpolarization of the cell (Kahle et al., 2008; Kaila, 1994). The Cl^- gradient is regulated in mature CNS neurons primarily by the potassium-chloride cotransporter KCC2 which under normal conditions extrudes Cl^- from the neuron maintaining the robustness of GABAergic inhibitory signaling (Kahle et al., 2008). Alterations in the expression, cellular distribution and function of KCC2 can lead to disrupted GABAergic inhibition (Lorenzo et al., 2020). Several recent observations point to a shift in E_{GABA} upon

injection of Aβ in the mouse brain or in the brain of AD transgenic mice or in APP overexpressing systems (Bie et al., 2022; Chen et al., 2017; Doshina et al., 2017; Kreis et al., 2021; Zhou et al., 2021) supporting a disruption in chloride homeostasis in AD. In addition, KCC2 protein levels have been found to be decreased in the frontal lobe of sporadic AD patients (Doshina et al., 2017) but also after injection of Aβ in the hippocampus of rodents (Bie et al., 2022). Interestingly, overexpression of APP in cortical neurons seems to decrease the expression of KCC2 and result in a diminished GABA response (Doshina et al., 2017), but another study showed that APP interacts directly with KCC2 and protects it from its degradation (Chen et al., 2017). KCC2 hypofunction occurs in the development of other neurological disorders for which disinhibitions and/or seizures are reported, including epilepsy (Huberfeld et al., 2007), neuropathic pain (Coull et al., 2003) and schizophrenia (Hyde et al., 2011). Thus, $GABA_A$ signalling disruption in AD could result from Cl^- dyshomeostasis caused by KCC2 hypofunction and thus restoring Cl^- regulation could serve as a valuable target for reversing disinhibition in AD.

1.1.7 Amyloidogenic mouse models

The amyloidogenic mouse models differ with respect to the genetic design features used for their generation. Most of the first-generation amyloidogenic transgenic lines were based on overexpression of transgenes carrying mutations found in familial AD (Götz and Ittner, 2008). On the other hand, the second-generation animal models of AD are based on homology-directed recombination aiming to insert mutations (*knock-in*) linked to AD in the murine mouse gene or modify and humanize an endogenous gene (Saito et al., 2014). There are however few non-genetic animal models of AD for which intracranial injections of Aβ (or TAU) aggregates are performed to recapitulate several aspects of AD (Meyer-Luehmann et al., 2006; Morales et al., 2011). For all these three approaches the goal is to reproduce biochemical and histological changes on the cellular level or cognitive impairment or the temporal and spatial characteristics of AD-linked neurodegeneration.

Generally, an amyloidogenic mouse model needs to show synaptic and neuronal degeneration and histological findings of plaques starting from specific brain areas and then affect several other brain regions. These cellular changes should induce at some point progressive impairment of various behavioral functions, similar to the ones observed in AD patients.

The first amyloidogenic transgenic line was developed by overexpressing the human *APP* gene carrying the V717F mutation under the neuron-directed platelet derived growth factor-β promoter (Games et al., 1995) followed by the APP23 transgenic line carrying the more commonly studied Swedish *APP* mutation (*APP*^{swe} mutant K670N/M671L) expressed under the brain-specific Thy1 promoter (Sturchler-Pierrat et al., 1997). These single-gene transgenic lines displayed overt Aβ aggregation and plaque formation across the brain, yet such histological findings were shown after several months. Combinatorial approaches have been utilized to introduce to mice more than one AD-related genes in order to augment and accelerate the pathology. Such example is the widely used APP/PS1 mouse model which has been developed by co-injecting two plasmids in the pronucleus of the zygote, one encoding for the *APP*^{swe} mutant and the other for the ΔE9 PS1 mutant (Jankowsky et al., 2001).

The 5xFAD line, one of the transgenic lines used here, combines the expression of the *APP* Swedish, Florida (I716V) and London (V717I) mutations as well as the M146L and L286V mutation of the *PSEN1* gene (Oakley et al., 2006). The transgenes were co-injected in the pronucleus and utilize the Thy1 mouse promoter to control the expression in neurons, in the brain. The 5xFAD line is maintained as hemizygotes on a B6/SJL hybrid background where both transgenes are co-expressed as a single transgene indicating that the exogenous DNA has been inserted in the same genomic locus. Later the line was backcrossed to a congenic C57BL6 background (Jawhar et al., 2012). These mice recapitulate several AD-related cellular phenotypes such as plaques formation (starting at 2 months of age), gliosis, synaptic and neuronal loss but they also develop progressive cognitive decline. Interestingly, female mice express the *APP* transgene more robustly than males and subsequently they generate higher levels of Aβ (Oakley et al., 2006). In terms of behavioral phenotypes, the 5xFAD mice develop working memory impairments at 4 to 5 months of age (Oakley et al., 2006), spatial memory deficits at 6 months of age (Xiao et al., 2015) and long-term contextual-fear-conditioning memory impairments at 4 months of age (Kimura and Ohno, 2009). Social behavior deficits and some motor impairments have been reported at 9 months of age also (O'Leary et al., 2018).

The 5xFAD mice and all the other overexpressing lines might offer several advantages on studying the effect of genes expressed exogenously, however they still display several disadvantages. The most prominent is actually intrinsic to the way these transgenic lines are generated. The insertion site or the number of copies cannot be controlled and thus the expression rate is difficult to be regulated or the expression patterns

of the transgenes can be altered due to potential integration artifacts (Saito et al., 2014, 2016). In addition, all the non-coding sequences are not incorporated into the sequences inserted, so slice variants are impossible to be studied (a key disadvantage concerning TAU-based animal models) (Götz et al., 2018). These and many other caveats of overexpression systems are minimized in the second-generation, *knock-in* animal models where the murine genes of interest are humanized, or AD-linked mutations are inserted in the endogenous gene (Pang et al., 2021; Saito et al., 2014, 2019).

Humanizing the mouse *APP* gene is extremely easy since the homology to the human gene rounds to 96.6% and only three amino acids are different within the Aβ sequence. However, no Aβ plaques are produced in the mouse brain by just humanizing the murine *APP* gene as predicted (Saito et al., 2014). When mutations linked to AD are introduced in the humanized *APP* gene (specifically the Swedish and the Beyreuther/Iberian I716F mutations), then Aβ deposits by 6 months of age (Saito et al., 2014). The addition of the Artic mutation E693G to the previous *knock-in* mice results in the formation of plaques as early as 2 months of age in the APP^{NL-G-F} mice (Saito et al., 2014). The APP^{NL-G-F} display age-dependent memory impairments and similar to the 5xFAD, the Aβ pathology appears to be more severe in the females (Masuda et al., 2016).

The development of cognitive decline and AD-related pathology in general in the APP^{NL-G-F} line without the overproduction of APP represents a great advantage over the earlier transgenic lines overexpressing APP or presenilin-1. APP has not been found to be overexpressed in humans with AD, and its overproduction might have secondary effects which are not found to patients. Actually, APP/PSEN1 overexpression has been reported to lead to overproduction of APP cleavage products other than Aβ, such as the C-terminal fragments of APP (CTF-β), which is more toxic than Aβ and does not accumulate in typically in AD.

1.2 Aging and cognitive decline

1.2.1 Overview

Aging can be defined biologically as a progressive deterioration of physiological processes which will ultimately result in the organism's death (Gilbert, 2000). The rate of aging however differs greatly between species but also within the same species or even between different tissues of the same organism. These differences can result from different rates in DNA repair pathways, in the deterioration of metabolic processes, the protein synthesis regulation, cell death specific mechanisms and cell reproduction capacity (Aubert and Lansdorp, 2008). Yet, aging can lead to an increase in the risk of disease development (Rose, 2009), and especially in neurodegenerative disorders (Hou et al., 2019). This is primarily due to the fact that the brain consists mainly of postmitotic cells which are especially sensitive to the detrimental effects of aging (Hou et al., 2019).

It is generally believed that as we grow older, we become wiser (Hedden and Gabrieli, 2004) but, in some cases, aging could be unsuccessful, with memory loss and cognitive decline greatly affecting the elderly. With the human lifespan increasing the past decades, mainly due to the development of successful treatments for various diseases of the youth and middle age, a greater fraction of the human population is touched by aging-related cognitive decline (Bishop et al., 2010). When we think of memory impairments in aging, most of the times we refer to AD since nearly 50% of the adults over 85 years old develop AD (Hebert et al., 2003a). Yet, non-pathological aging of the nervous system can also lead to cognitive decline and memory loss independently of any neurodegenerative disorder. During normal aging, the deterioration in cognitive performance is not dependent on neuronal loss as in AD or other neurodegenerative disorders. However, aging remains the most impactful risk factor for AD, so one could argue that this neurodegenerative disorder resembles accelerated aging and neuronal loss could also appear during normal aging if the human lifespan increases more.

During aging a profound decline in the ability of forming new episodic memories has been found in demented old adults, but also the ability to process information quickly and robustly and to invoke executive functions are diminished. These behavioral phenotypes seem to start relatively early in the adult lifespan, around the age of 60 (Hedden and Gabrieli, 2004). On the other hand, short-term and semantic memory appears to decline only very late in life (Hedden and Gabrieli, 2004). Finally, there are other forms of memory which seem

to be relatively unaffected by aging such as autobiographical memory (which is typically perturbed in AD patients (El Haj et al., 2016)), or emotional and implicit memory.

Various brain regions/structures are associated with memory formation and retention, such as the hippocampus, the perirhinal and entorhinal cortices. An extensive body of literature reports changes in neuronal plasticity with aging in these brain regions including changes in long-term potentiation (LTP), neuronal excitability, and alterations in structural and functional synaptic transmission (Burke and Barnes, 2010; Disterhoft and Oh, 2007; Rosenzweig and Barnes, 2003). However, over the past years, the medial prefrontal cortex (mPFC) and other cortical areas received a lot of attention and were associated with cognitive decline and other neuropsychological changes linked to normal aging (Bishop et al., 2010; Hedden and Gabrieli, 2004; Morrison and Baxter, 2012). In addition to executive function impairments, cognitive flexibility deterioration, attention, and language deficits (Gallagher and Burwell, 1989; Gallagher and Rapp, 2003; Morrison and Baxter, 2012), there are several reports supporting an emergence of depressive episodes in the elderly too (Blazer, 2000) which are also correlated with neurophysiological changes in the mPFC.

Taken together, these behavioral alterations require specific care for the elder populations creating a great economic burden to modern human societies. It is therefore important to understand the basic mechanisms of aging and their contribution to the onset and the progression of cognitive decline to develop effective interventions and treatments. However, isolating and understanding the age-associated changes of the nervous system is extremely challenging for various reasons (Hedden and Gabrieli, 2004). Most of the elders undergo other pathological conditions which could affect the brain or contribute to cognitive frailty (such as diabetes and hypertension). In addition, aging studies rely on comparisons between different age groups, and they are not based on tracking changes in physiology and behavior longitudinally. Finally, along with the age-related deterioration in cognition, other mental changes occur in parallel and thus correlating behavioral alterations with functional changes in the aging brain is particularly challenging. The use of experimental rodent and primate models to study aging over the past years has greatly expanded our understanding of the biological mechanisms of senescence. Numerous studies have demonstrated functional and structural alterations in primates and rodents that are similar to those observed during aging in humans, thus providing us with valuable data to facilitate the study of the neurobiological correlates of neuropsychological alterations observed during aging (Gallagher and Rapp, 2003; Hof and Morrison, 2004).

1.2.2 Aging-related cognitive decline

While aging is a process occurring throughout the brain, alterations within the PFC and the hippocampus are at the spotlight of cognitive aging research since they support memory formation and cognitive functions that are liable to decline during aging. Several high order behaviors relying primarily on the activity of the PFC appear to decline across aging. The cognitive mechanisms which support strategic planning, organize and modify information for working memory, support the ability to select and change between several sources of information, and accelerate the perception of rules and cues greatly decline with age (Hedden and Gabrieli, 2004) (**Figure 1.2.8**). In addition to these, long-term episodic memory associated with the activity of the medial temporal lobe deteriorates with aging and it drastically worsen during the later decades of life (Park et al., 1996).

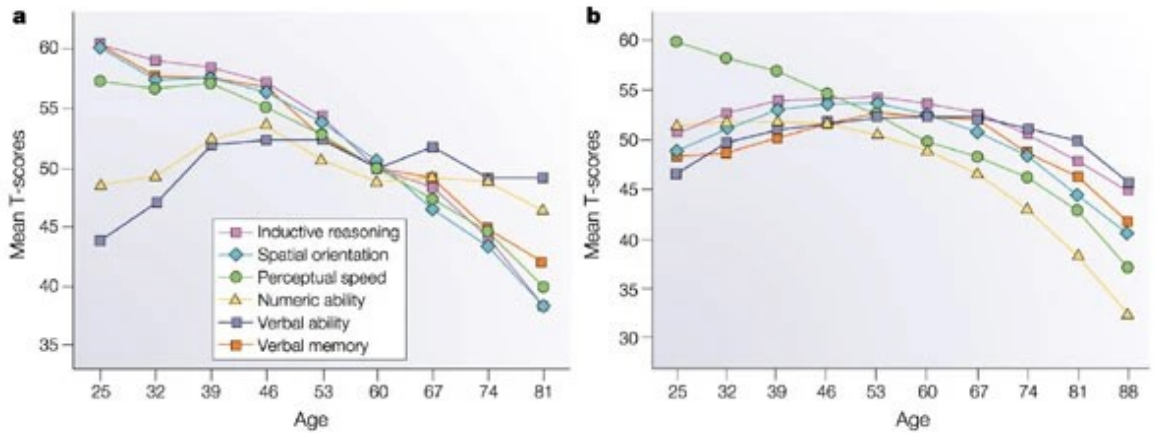

Figure 1.2.8. Prefrontal- dependent cognitive decline during aging

Data collected from (**a**) cross-sectional and (**b**) longitudinal studies showing an early life improvement in several cognitive aspects assonated with the function of the PFC, which finally decline with age in humans (Hedden and Gabrieli, 2004).

Alterations in frontal cortex reduce executive functions even in nondemented elders, yet this reduction can influence memory on the long term. Remembering sources or time details of previous episodes rely on executive functions (Schacter et al., 1991; West, 1996). Moreover, the act of retrieving memories is dependent on executive functions such as

controlled processing and strategic elaboration during the memory formation. Longitudinal and cross-sectional studies have revealed different trajectories of cognitive performance across aging. Linear decline as a function of age, after the age of 60, has been observed in episodic memory, reasoning, and orientation ability (Schaie, 1996) (**Figure 1.2.8**). Perceptual speed, the ability to compare and recognitive distinctive patterns or cues, seems to show a life-long decline (Schaie, 1996). Other cognitive impairments seem to appear only during the late life. Verbal memory, vocabulary and semantic knowledge remain stable until late in life (Hedden et al., 2005). Tasks which rely on knowledge and short-term memory that involves verbal storage show great decline only after the age of 70 (Grégoire and Van der Linden, 2007; Hedden et al., 2005). The relative stability of semantic memory into late life may be indicative of elders using accumulated knowledge and experience to formulate effective strategies when performing complex tasks, whereas younger adults would rely on superior processing capacity and speed.

Interestingly, when the cognitive performance is correlated with the time of mortality, it appears that cognitive decline accelerates 3-6 years before death (Wilson et al., 2003). This observation suggests that the existence of underlying pathologies that precipitate changes which could be related to cognitive aging. On the other hand, physiological aging is characterized by a progressive loss of cognitive performance.

Similar to humans, some experimental animal models develop PFC dependent cognitive deficits with aging (**Figure 1.2.9**). Both rodents and non-human primates exhibit working and episodic memory impairments during aging (Barense et al., 2002; Bizon et al., 2009; Bloss et al., 2010; Dumitriu et al., 2010; LaSarge et al., 2007; Simon et al., 2010) allowing researchers to study the neurobiology underlying age-related cognitive decline and memory loss. Delayed response tasks are widely used to access PFC-dependent working memory impairments in non-human primates and rodents. For instance, a subpopulation of aged primates present working memory deficits characterised by impairments in retaining information for a long period of time during tasks with or without a spatial component or show deterioration in performance for tasks requiring rule learning or rule alterations (Chang et al., 2005; Luebke et al., 2010, 2004; Rapp and Amaral, 1989).

The rodent PFC is not as elaborate as in primates however there is an abundance of evidence supporting that the rodent PFC has high anatomical and function homology with the primate PFC (Brown and Bowman, 2002; Kesner and Churchwell, 2011; Uylings et al., 2003). Yet, rodents are still capable of various complex behaviors similar to primates. In delay response task in which rats should remember a position or an object over a short

duration, aged rats display significant decline in performance as compared to young rats (Beas et al., 2013; Bories et al., 2013). In addition, a subpopulation of aged rats have been found to develop working memory deficits associated with retention of spatial memory for a long period of time (Frick et al., 1995; Wong et al., 2006). Taken together, the behavioral analysis of aged rodents provides an index of memory and executive function which can be associated with molecular, structural, and functional alterations of the aging brain supporting cognition.

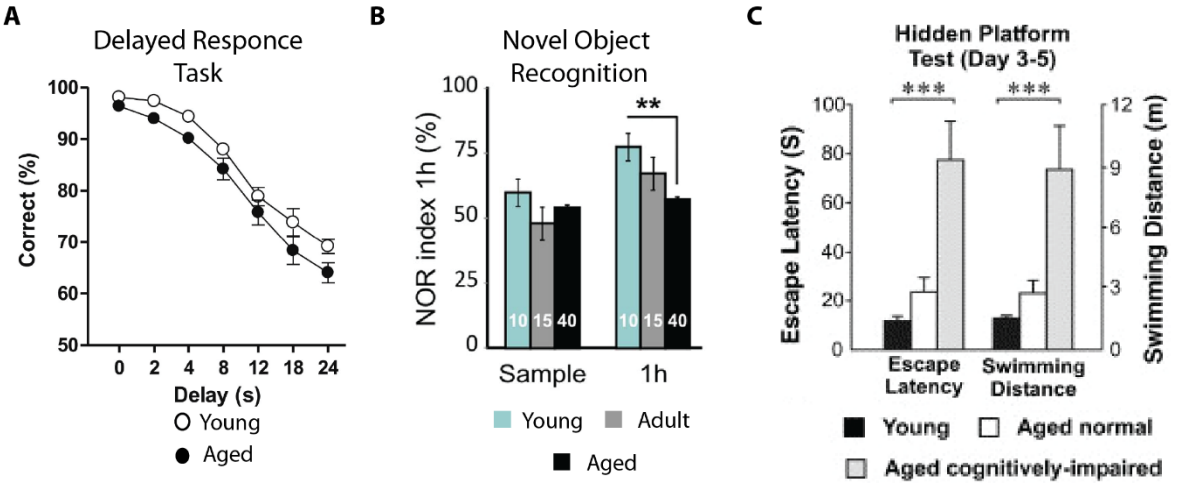

Figure 1.2.9. Working memory deficits in aged rodents

(**A**) The performance of aged rats in a delayed response working memory task is significantly lower at the sessions with the longest delay as compared to the performance of young rats. (**B**) Aged rats display short-term working memory deficits in an object discrimination task as compared to young or adult rats. (**C**) Spatial working memory deficits in a subset of aged rats in a test where the rats need to find a hidden platform based on visual cues surrounding the maze. Modified from (Beas et al., 2013; Bories et al., 2013; Wong et al., 2006).

1.2.3 Structural and morphological changes of the aging brain

A typical misconception about the aging brain is that neuronal loss is overt as in several neurodegenerative disorders such as Alzheimer's or Parkinson's disease. Multiple post-mortem and *in vivo* studies have revealed that neuronal loss does not seem to have a significant role in the development of cognitive decline or memory loss in senescence. Since

a decrease in neuronal density does not explain the brain size reduction concomitant with aging, early work from Scheibel suggested that attrition of the dendritic arborization and a reduction in cortical layers could account for the volume reduction (Scheibel et al., 1975, 1976). Indeed, more recent work has validated these initial observations showing that the brain shrinks with normal aging and this loss in volume arises from a reduction in synaptic densities (Masliah et al., 2006; Morrison and Hof, 2007; Resnick et al., 2003) (**Figure 1.2.10**).

The aging-associated volume decline, however, is not uniform across the entire brain (**Figure 1.2.10**). In fact, some brain regions, and specific structures, such as the prefrontal and temporal cortex, are more vulnerable, showing greater reduction in volume as compared to others (Rajah and D'Esposito, 2005; Resnick et al., 2003; West, 1996). Specifically, structures in the PFC show the largest volume reduction during aging with an estimated 5% decrease in volume every decade after the age of 20 (Raz et al., 2004). Both in humans and non-human primates this volume reduction in the PFC correlates with a decrease in synaptic density (Bourgeois et al., 1994; Liu et al., 1996). There are other cortical areas which remain unaffected by aging such as the anterior cingulate gyrus or the primary visual cortex. Interestingly, another sub-cortical brain region that connects to the PFC, the striatum, undergoes age-related reduction in volume (Raz et al., 2003). Consistent with the volumetric changes in the striatum across aging, dopamine concentration, dopamine transporter and dopamine D2 receptor density diminish with age in the PFC (Goldman-Rakic and Brown, 1981; Volkow et al., 1996, 1998).

Apart from the grey matter density, aging affects also the density of the white matter in the brain (Guttmann et al., 1998) (**Figure 1.2.10**). Once again, the most affected brain region seems to be the PFC, where the greatest changes in the white matter are observed (Bartzokis et al., 2003; Head et al., 2004). White matter loss has been associated with a decline in executive functions and perceptual speed but also with poor immediate and delayed memory (Gunning-Dixon and Raz, 2000). This is not a surprise since PFC white matter abnormalities could influence the connectivity of the PFC to other brain structures such as the hippocampus and the striatum.

The macroscale structural changes associated with aging reflect the sum of the microscale alterations in the morphology of neurons (**Figure 1.2.10**). Yet again, the age-related neuronal morphological changes are selective and unique between various brain regions. Early reports suggested that an extensive reduction in the dendritic branching occurs with aging in the entorhinal cortex and the hippocampus (Scheibel et al., 1976) and

later reports reproduced the same findings for neurons in the layer II of the para-hippocampal gyrus in individuals with dementia (Buell and Coleman, 1981). Similarly, a decrease in dendritic branching has been observed in the medial PFC in humans (Brabander et al., 1998) supporting that the morphology of pyramidal neurons in the PFC (the major neuon type in the cortex (Elston et al., 2011)) are susceptible to the effects of aging.

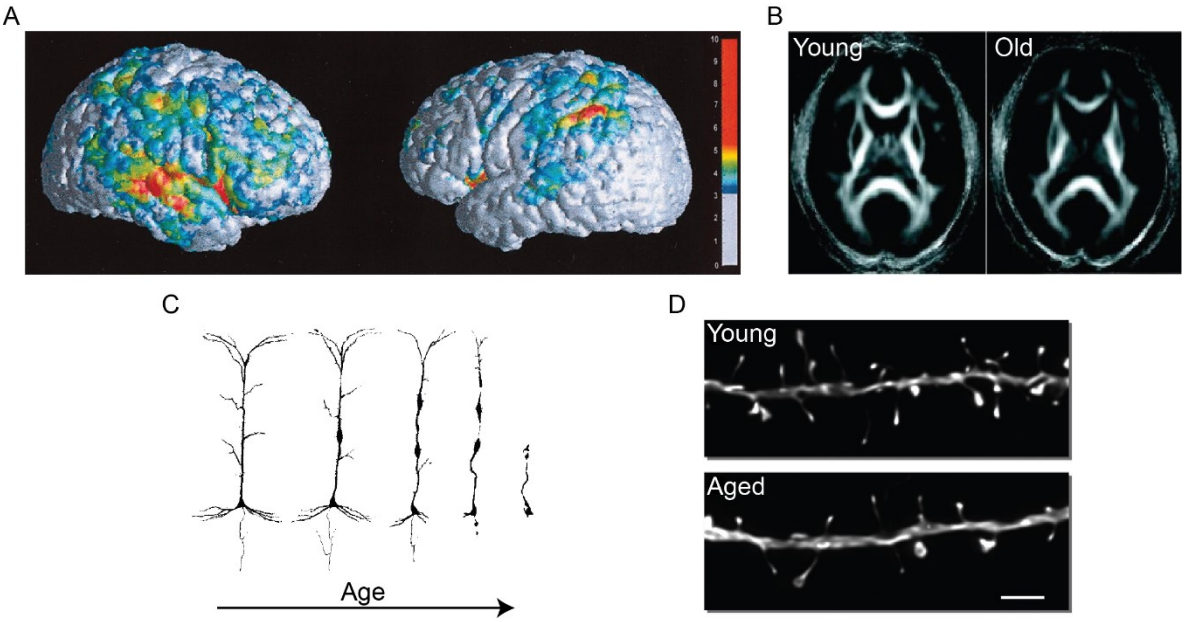

Figure 1.2.10. Aging-related macro- and micro-scale brain structural and morphological alterations

(**A**) The tissue loss in gray matter of the inferior frontal, insular and posterior temporal cortical regions during aging. The color represents the calculated average loss (Modified from (Resnick et al., 2003)). (**B**) The white matter loss in elderly. The greater decrease is focused in the anterior cortex (Modified from (Head et al., 2004)). (**C**) Reduction in dendritic arborization with aging in the entorhinal cortical neurons in humans (Modified from (Scheibel et al., 1976)) (**D**) Loss of spine density and specifically of thin spines in the dendrites of layer III pyramidal neurons in non-human primates (Modified from (Dumitriu et al., 2010)).

Age-dependent neuronal morphological changes have been observed in the PFC of aged rats too. Dendritic branching is reduced with age in pyramidal neurons of various cortical layers in rats, both in the apical and basal dendrites (Bories et al., 2013; Grill and

Riddle, 2002). Consistently, the geometry of the dendritic tree is altered in the PFC of non-human primates during aging (Dumitriu et al., 2010; Luebke et al., 2010). However, dendritic morphology studies in the rat hippocampus show a trend of an increase in the dendritic branching at a late age (Pyapali and Turner, 1996; Turner and Deupree, 1991), but the width or the extent of the distal dendrites are significantly reduced in the hippocampus of old monkeys (Luebke and Rosene, 2003).

In addition to dendritic arborization, spine density is reduced with aging in the PFC pyramidal neurons. Spines are dendritic post-synaptic structures which receive input from pre-synaptic boutons and have been divided in three distinct categories: mushroom, thin, and stubby (Harris and Kater, 2003). Mushroom spines have a relatively large head, are structurally stable and support strong synaptic currents while thin spines are small structures with high plasticity which form non-perforated synapses (Kasai et al., 2003; Matsuzaki et al., 2001). Mushroom spines have been associated with long-term memory formation while thin spines are thought to mediate learning (Bourne and Harris, 2007). The function of stubby spines still remains elusive. Morphological and electron microscopy studies suggest a profound loss of spines in cortical pyramidal neurons both in rodents and non-human primates (Bloss et al., 2010, 2011; Bories et al., 2013; Dumitriu et al., 2010). Thin spines seem to be significantly more vulnerable and account almost for the half of the spines lost with aging in monkeys and the PFC (Dumitriu et al., 2010; Hara et al., 2012; Luebke et al., 2010). This last observation is crucial since the size of the thin spine's head correlates with the performance of monkeys to learn delayed response tasks suggesting that thin spines density reduction and the subsequent decline in synapse plasticity may be the primary contributor of the age-related cognitive decline.

1.2.4 Aging-dependent cortical synaptic activity alteration

As discussed above, several cognitive skills such as episodic memory, information processing speed and reasoning decline with age. Aging is thus associated with deficits in executive tasks; however, elderly people perform also worse on tasks requiring the suppression of previously learned rules, demonstrating a decline in cognitive flexibility (Hedden and Gabrieli, 2004). This aging-dependent cognitive decline has been associated with the structural alterations but also with neurophysiological changes in the brain (refer to section 1.2.3). The advent of neuroimaging technologies has allowed to measure the neuronal activity of the brain in healthy and demented individuals while they are performing

cognitive tasks. Similar to what has been reported for Alzheimer's disease patients, in the brain of the elderly, an overt disruption of neuronal networks is observed, and coordination of brain activity between brain regions that support high-order cognitive functions becomes less robust with aging (Andrews-Hanna et al., 2007).

It is generally believed that elderly show less activity in the frontal lobes while performing tasks requiring working memory (Cabeza et al., 1997; Grady et al., 1995; Logan et al., 2002). However, several other studies have reported a paradoxical activation of distinct frontal regions during memory encoding which are typically silent (or less active) in younger individuals (Cabeza et al., 2002; Reuter-Lorenz et al., 2000; Rosen et al., 2002). This additional activation of complementary PFC regions is hypothesized to act as a compensatory mechanism, possibly as part of a general-purpose mechanism to boost the performance of the brain in resolving demanding cognitive task (Cabeza, 2002; Grady, 2008) since it is often only seen in elders with high-performance (**Figure 1.2.11**). In addition, these increases in PFC activity often occur in contralateral areas to those activated in young individuals and reduce the hemisphere asymmetry seen normally in young people (**Figure 1.2.11**). At the same time, one could argue that the activation of complementary PFC regions is indicator of a less integrated network or a delocalized brain activity which again is consistent with the idea of a compensatory mechanism in elders (Cabeza, 2002; Cabeza et al., 2002).

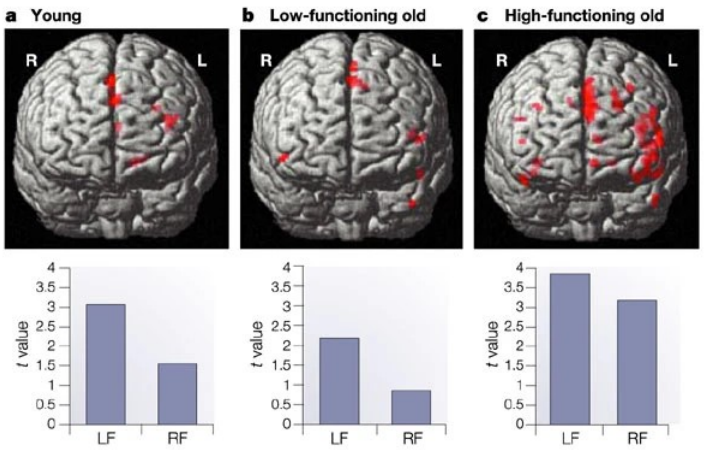

Figure 1.2.11. PFC activation in elders during memory encoding tasks

fMRI imaging of the human brain shows activation of the left PFC in young individuals when performing memory-based task. In low-performing elders however, the activity of the left PFC is reduced while in high-performing elders there is a bilateral activation of the PFC (LF: left frontal; RF: right frontal. Modified from (Hedden and Gabrieli, 2004).

Although functional neuroimaging studies provide great information and valuable insight into how regional alterations in brain activity are associated with cognitive decline in elders, they cannot provide any information regarding the underlying cellular and physiological chances accounting for the age-related cognitive decline. As discussed earlier, neuronal density is vastly preserved during normal aging however morphological changes in dendrites arborization combined with dendritic spines reduction manifest in senescence. These structural changes can result in alteration of electrical properties of neurons and their synaptic input which are likely to compromise the neuronal integrative performance (Kabaso et al., 2009; Spruston, 2008). Such electrophysiological changes have been reported in the hippocampus of aged rats for instance, where an increase of Ca^{2+} influx activates calcium-sensitive potassium currents which prolong neuronal hyperpolarization which subsequently could impair neuronal excitability and the maintenance of LTP (Foster, 2007; Rosenzweig and Barnes, 2003).

When it comes to the PFC, the passive electrophysiological properties of the neurons are greatly preserved during aging, with the resting membrane potential, the threshold to elicit an action potential, and the duration and rise time of the action potentials remaining unaltered (Burke and Barnes, 2006; Chang et al., 2005). Some changes in the input resistance of pyramidal neurons and the action potential amplitude time have been observed in the dorsal lateral PFC of aged monkeys, but these changes did not correlate with the cognitive performance of the animals (Chang et al., 2005).

The morphological changes occurring in neurons with aging have been shown to result in a reduction of excitatory synaptic transmission in non-human primates. Luebke and colleagues have demonstrated a decrease in the frequency of spontaneous excitatory post-synaptic currents in aged monkeys (Luebke et al., 2004) that represent a synaptic response to either an action potential dependent or an action potential independent release of glutamate from the pre-synaptic terminals (**Figure 1.2.12**). However, no similar reduction in the spontaneous excitatory post-synaptic currents was measured in the PFC of aged rats in another electrophysiological study (Bories et al., 2013) (**Figure 1.2.12**). Regardless, the overall reduction of excitatory input to pyramidal neurons reported in the primate prefrontal cortex could be supported by a decrease in post synaptic glutamate receptors (Hof et al., 2002). Indeed, it has been shown that GluR2 subunit is significantly reduced in the macaque or monkey prefrontal cortex with aging while the NMDAR1 subunit is primarily reduced in the superior temporal cortex (Hof et al., 2002).

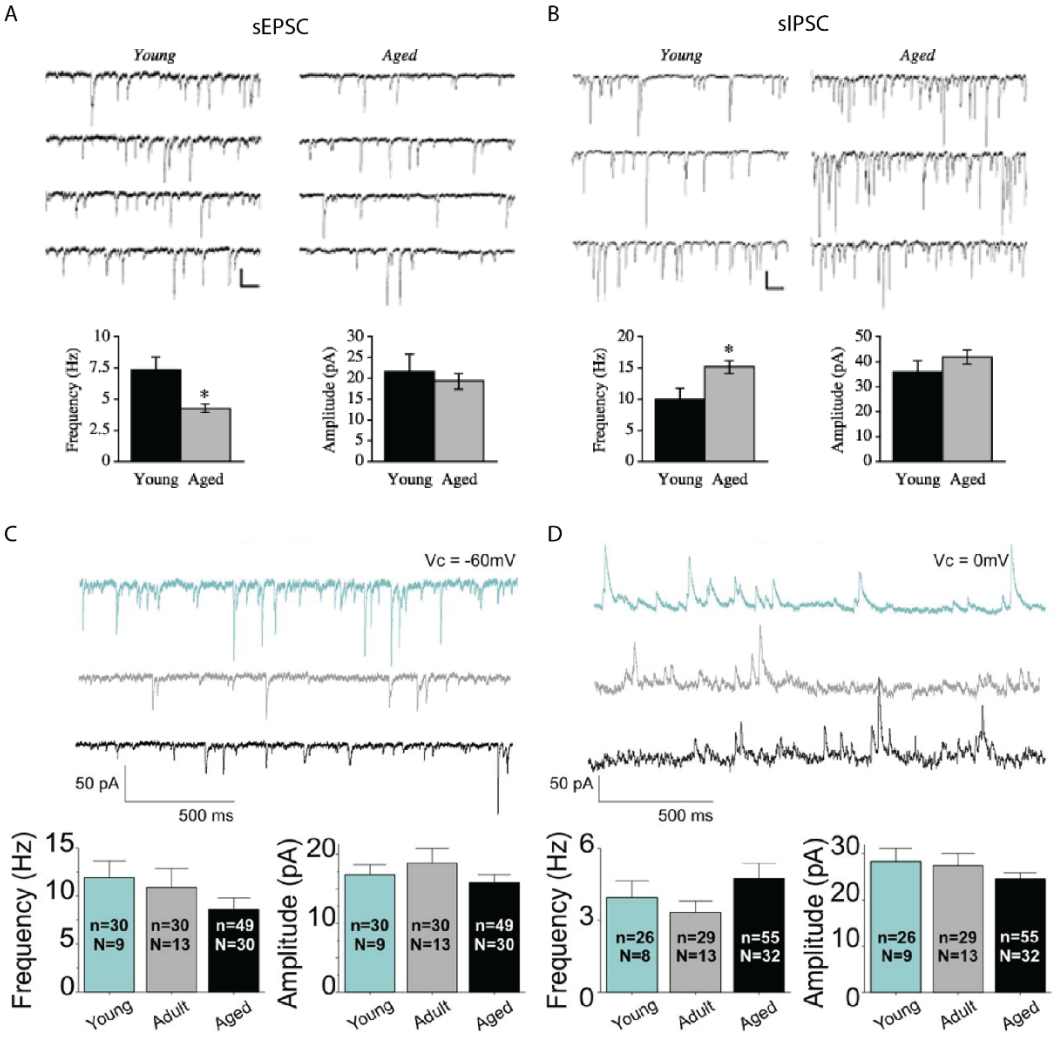

Figure 1.2.12. Spontaneous excitatory and inhibitory PSCs in layer 2/3 pyramidal neurons in aged monkeys and rats

(**A** - **B**) Representative traces of spontaneous EPSCs and IPSCs in young and aged monkeys showing a decreased frequency of sEPSCs and an increase frequency of sIPSCs in aged monkeys (modified by (Luebke et al., 2004)). (**C** – **D**) Representative traces of sEPSCs and sIPSCs in young (cyan), adult (gray) and aged (black) Fisher 344 rats. No changes are observed in the amplitude of the sEPSCs and sIPSCs (modified from (Bories et al., 2013)).

In contrast to the excitatory neurotransmission findings in the aged PFC, an increase in the inhibitory synaptic input to layer 2/3 pyramidal neurons have been observed in aged as compared to young monkeys (Luebke et al., 2004). This increase in the inhibitory input

was manifested as a higher frequency of spontaneous inhibitory post-synaptic currents (**Figure 1.2.12**) which could reflect an increase in the pre-synaptic action potential dependent release of GABA from interneurons. As with the excitatory post-synaptic currents, no increase in the frequency of spontaneous inhibitory post-synaptic currents was reported in the mPFC of aged rats, however a significant increase in the frequency of the miniature inhibitory post-synaptic currents have been measured in cognitively impaired aged rats (Bories et al., 2013). This change in the miniature inhibitory post-synaptic currents could indicate an increase in either the presynaptic release probability of GABA or a raise in the number of the functional synaptic sites. Hence, future studies should concentrate in understanding the changes occurring in GABAergic interneurons in the aged PFC and the contribution of this excessive inhibitory tone in the development of cognitive decline.

The PFC pyramidal neurons have a distinct electrophysiological property allowing them to maintain a sustained discharge activity in the absence of any external stimulus. Due to this unique property, and the sustained firing pattern of pyramidal neurons, it is postulated that prefrontal neurons could encode and maintain information precisely during the execution of memory tasks. In aged monkeys, an increase or a reduction in the repetitive action potential firing rates have been correlated with a low performance in delayed response tasks (Chang et al., 2005), suggesting that an equilibrium of sustained discharging activity in pyramidal neurons is crucial for information maintenance. The same observation was reported later while recording the repetitive firing rates *in vivo*, in the monkey PFC. With advanced age, the persistent firing rate was significantly reduced, and this reduction was specific for the neurons that normally keep discharging during the delay period of an frontal lobe dependent oculomotor delayed response task (Wang et al., 2011).

Other than changes in the excitability of excitatory neurons in the PFC and the inhibitory input to them described above, several presynaptic alterations in both the synthesis and the release of glutamate and GABA have been reported with aging. An approximate 15-20 % decrease in the glutamate concentration have been reported during aging by several studies (Dawson et al., 1989; Jing et al., 2016; Segovia et al., 2001a; Wallace and Dawson, 1990). This reduction in glutamate levels is probably originating from a decrease in the activity of glutaminase which has been observed in the temporal cortex, the striatum and the hippocampus of aged rats (Segovia et al., 2001b; Wallace and Dawson, 1992). In contrast, no alteration in the levels of GABA have been reported in the aging brain so far. Although, several studies have shown a decrease in the glutamate decarboxylase enzymes levels which synthesize GABA during aging. GAD65 and/or GAD67 mRNA or

protein levels have been found to be reduced in the auditory, and barrel cortex, but also in the hippocampus of aged rodents (Burianova et al., 2009; Liguz-Lecznar et al., 2014; Ling et al., 2005; Shi et al., 2004). These changes in the GAD expression may play a role in restricting changes in plasticity, even if they do not really translate to changes in GABA levels per se (Rozycka and Liguz-Lecznar, 2017).

Finally, the density or the composition of some glutamate or GABA receptors have been reported to be altered during aging and could explain some of the electrophysiological changes discussed above. A general reduction in NMDA receptor density has been observed in most of the cortex, the striatum and the hippocampus across aging (Segovia et al., 2001a). In the mPFC of aged non-human primates, the most profound change in the NMDAR composition is a reduction in the expression of the NR2B subunit (Bai et al., 2004). Moreover, a decrease in the NMDAR binding affinity for glutamate and glycine has been measured in various cortical regions in the brain of aged mice as compared to young mice (Magnusson and Cotman, 1993a). In parallel, a decrease in the concentration and the binding affinity of the AMPA receptors have been observed again in the frontal and parietal cortex of aged mice (Magnusson and Cotman, 1993b). A more recent study revealed diminished levels of the GluR2 subunits in the mPFC of old monkeys (Hof et al., 2002).

Then, changes in the expression levels of different $GABA_AR$ subunits have been reported during aging, with these changes being very subtle and typically brain region specific (Rissman et al., 2007; Rozycka and Liguz-Lecznar, 2017). Distinct $GABA_AR$ subunit compositions can greatly affect the receptor kinetics, the ligand binding affinity and the ion specificity of the receptor (Rissman and Mobley, 2011). The α5 subunit which is normally highly abundant in the hippocampus and it is involved in the processes of learning and memory (Collinson et al., 2002) seems to decrease with age in the auditory thalamus (Richardson et al., 2013) and the motor and somatosensory cortex (Yu et al., 2006). The α1, β1, β2, γ1 and γ2 subunits have been found to decrease in expression in the aged rat auditory cortex while the α3 subunit was upregulated (Caspary et al., 2013). Consistently the γ2 subunit is decreased in the motor and somatosensory cortex and the hippocampus (Yu et al., 2006). The expression of the α1 subunit is also downregulated in the monkey hippocampus with aging, but an age-related increase has been described in the rat hippocampus (Gutiérrez et al., 1996; Rissman et al., 2007). All these subtle changes in the subunit composition of the $GABA_AR$ during aging can modify the physiology of the receptor and alter inhibitory synaptic transmission.

Taken together, it appears that ARCD is correlated with changes in the excitability of pyramidal neurons and an increase in the inhibitory input to excitatory neurons in the PFC. These synaptic activity alterations, typical to aging, may be distinct to the changes in synapse plasticity observed in AD, however they result in neuronal activity disruption and network dysfunction, giving rise to memory loss and cognitive decline (Bishop et al., 2010; Burke and Barnes, 2006, 2010; Morrison and Baxter, 2012).

1.3 Synaptic Transmission

1.3.1 Overview

Central nervous system (CNS) neurons communicate with each other either electrically or chemically in sites named synapses (Heuser and Reese, 1977). The electrical communication takes place between two neurons physically connected to one another via gap junctions which contain intercellular channels called connexins allowing for ions and small molecules exchange (Hormuzdi et al., 2004). Electric synapses allow rapid transfer of pre-synaptic currents into post-synaptic potentials which can generate action potentials at the post-junction cell. The chemical communication, on the other hand, occurs when an electrical event in one neuron is translated into neurotransmitters release in the synaptic cleft (Hammond, 2015). The synaptic cleft represents the region in which the pre-synaptic terminal of one neuron comes in proximity (~ 20 nm) to the post-synaptic density of a second neuron (Berry and Nedivi, 2017). Upon release, the neurotransmitters bind to their receptors located on the post-synaptic cell (Heuser and Reese, 1977) and depending on the nature of the neurotransmitter they can excite or inhibit the post-synaptic cell.

Neurotransmitters are generally divided in excitatory or inhibitory with the first activating the post-synaptic neuron and resulting in the firing of an action potential and the latter inhibiting the neuron and blocking the formation of an action potential. However, other factors can determine the effect of a neurotransmitter on the post-synaptic cell. At rest, the membrane of a neuron is mainly permeable to potassium (K^+) and to a lesser extent to sodium (Na^+). This neuronal membrane permeability results in a negative resting membrane potential of approximately -70 mV (Kandel and Spencer, 1961). Binding of a neurotransmitter to its receptor can increase the permeability of the plasma membrane to specific ion(s), and subsequently shift the membrane potential towards the reversal potential of the ion(s). The reversal potential of an ion is the potential where there is no net flow across the membrane.

Release and binding of glutamate, the predominant excitatory neurotransmitter, result in the opening of ligand-gated cation channels and mainly an influx of Na^+ which depolarizes the membrane. In contrast, when an inhibitory neurotransmitter, such as gamma-aminobutyric acid (GABA), is released, it activates either $GABA_A$ or $GABA_B$ receptors causing an influx of Cl^- or an efflux of K^+ respectively that hyperpolarize the membrane. Along these lines, it is not the binding of the neurotransmitters itself, or the receptor type that determines whether an excitatory or inhibitory action will follow. The

driving force of ions following the electrochemical gradient across the neuronal membrane determines the action of a neurotransmitter.

1.3.2 Glutamatergic Transmission

Glutamate is the predominant excitatory neurotransmitter in the CNS. In neurons it is synthesized by converting glutamine to glutamate (Rowley et al., 2012) and subsequently it is loaded to synaptic vesicles by the vesicular glutamate transporter (VGLUT or SLC17) (Danbolt, 2001) (**Figure 1.3.13**). When released in the synaptic cleft it acts by binding to three different types of ionic receptors: NMDA, AMPA or kainic acid (KA). Opening of the NMDA receptor allows for influx of Na^+ and Ca^+ and an efflux of K^+, while AMPA and KA receptors allow for the influx of Na^+ or Ca^+ depending on the subunit composition in the case of AMPA receptors. Extracellular glutamate is taken up by glutamate transporters (EAATs) which use the sodium gradient to transport glutamate against its concentration gradient (Vandenberg and Ryan, 2013) (**Figure 1.3.13**). Glutamate transporters are abundantly expressed in astrocytes that represent the major site of glutamate re-uptake but they are expressed also in the pre- and post-synaptic cells (Hertz and Zielke, 2004; Magi et al., 2019). In astroglia, glutamate is converted to glutamine again in an ATP-dependent process which does not have neurotransmitter properties, it is released from glia via glutamine transporters and taken back from neurons via another glutamine transporter (**Figure 1.3.13**).

Activation of NMDARs requires the binding of glutamate and of a co-agonist such as glycine or D-serine. They form heterotetrameric channels composing typically of two GluN1 (or NR1) glycine binding subunits and two glutamate binding subunits (GluN2A to 2D or NR2A-D) or a mix of GluN2 and GluN3 (or NR3) subunits (Hansen et al., 2018). At resting membrane potential, Mg^{2+} ions enter the NMDAR pore and block any ion flux through the channel; however, this block is released upon depolarization (Nowak et al., 1984). This property of the NMDA receptor grants a voltage-dependency to the channel for its function. NMDARs are highly permeable to Ca^{2+} allowing an inward Ca^{2+} current to the neuron upon activation. This influx of Ca^{2+} acts as a secondary messenger triggering several signaling pathways important for synaptic plasticity (Paoletti et al., 2013). However, excessive glutamate release and subsequent intracellular Ca^{2+} load could result in excitotoxicity and initiation of cell death signalling cascades as well (Sattler and Tymianski, 2001).

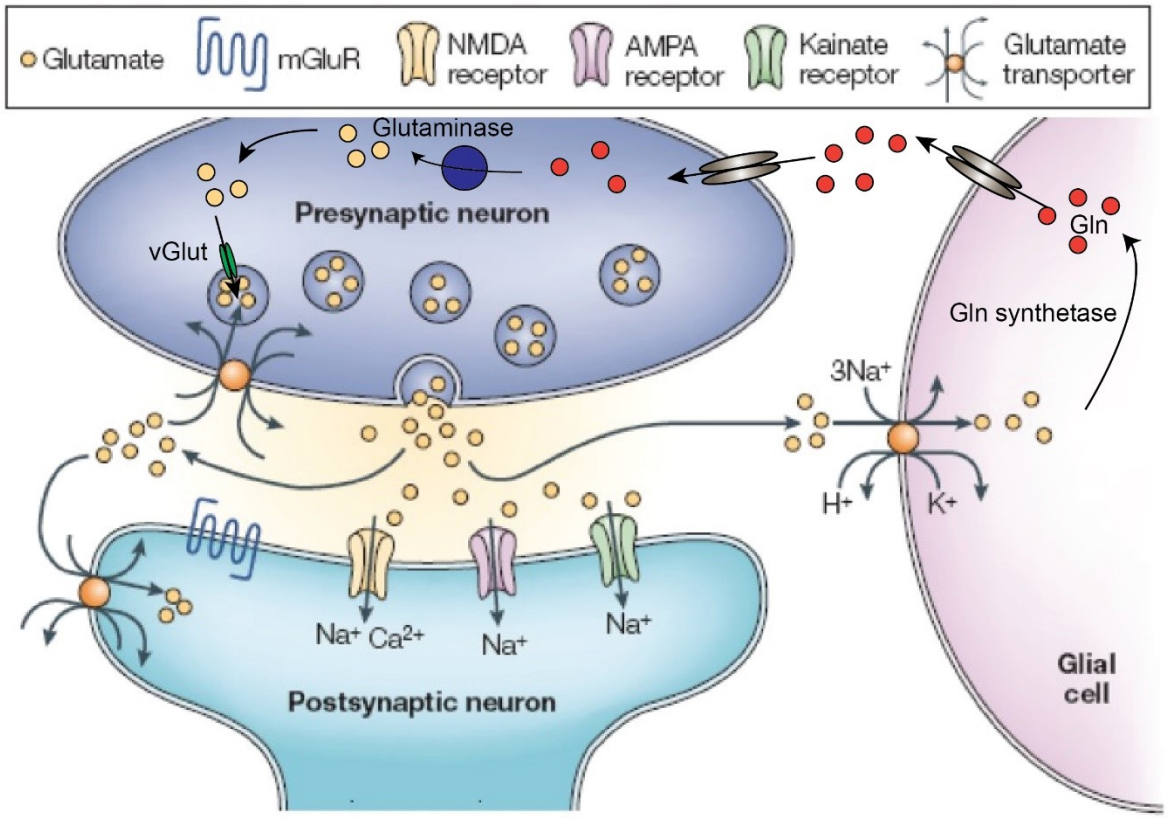

Figure 1.3.13. Glutamatergic synapse.

In the pre-synaptic terminals, glutamate is synthesized by glutamine and loaded to synaptic vesicles by the vesicular glutamate transporter (vGlut). Upon release to the synaptic cleft, glutamate binds to NMDA, AMPA or Kainate receptors. The extracellular concentration of glutamate is kept low by glutamate re-uptake mediated by glutamate transporters primarily expressed in glia cells. In glia, glutamate is converted to glutamine are released by glutamine transporters and transferred to the neurons again via other glutamine transporters. Modified from (Attwell and Gibb, 2005).

AMPA receptors are the principal inotropic glutamate receptors mediating fast excitatory transmission. They are composed of four types of subunits encoded by distinct genes, GRIA1-4 (or GluA1-4) (Béïque and Huganir, 2009). AMPARs are assemble as two identical heterodimers in the endoplasmic reticulum (ER) with the GluA1/2 being the most common AMPAR subtype in the CNS (Lu et al., 2009). The transport of AMPARs in the synaptic terminals is mediated by exocytosis of vesicles containing the receptors transferred by dynein or kinesin (Anggono and Huganir, 2012) but also via myosin and Ca^{2+}-dependent

transport (Correia et al., 2008). Halfway to the synaptic terminal, AMPARs reach the Golgi where they are glycosylated in an N-glycosylation site, a post-translational modification necessary for the AMPARs to become functional (Kandel et al., 2018). The presence of the GluA2 subunit in the AMPARs is crucial for their biophysical properties since GluA2-containing receptors are impermeable to Ca^{2+} while GluA2-lacking receptors are permeable to Ca^{2+} exhibiting an inward rectifying current (Béïque and Huganir, 2009). Excessive activation of AMPARs leads to the depolarization of neurons which ultimately can induce to hyperexcitation. This process along with an increase of expression of GluA2-lacking AMPARs results in an increase in Ca^{2+} influx which again can trigger cell death signaling pathways and excitotoxicity (Choi, 1994).

Kainate receptors (KARs) form also tetrameric complexes from distinct subunits as the NMDARs and AMPARs. There are five types of subunits composing the KARs: GluK1-5, from which GluK1 and GluK3 can form functional homo- or hetero-tetrameric receptors, while GluK4 and GluK5 need to partner with GluK1 or GluK3 subunits to form functional receptors (Lerma and Marques, 2013). They are ionotropic channels allowing the movement of sodium and potassium resulting in the depolarization of the post-synaptic neuron upon glutamate binding.

1.3.3 GABAergic Transmission and GABA Receptors

GABA is the predominant inhibitory neurotransmitter in the CNS, while glycine represents the main inhibitory neurotransmitter in the periphery (Smith and Kittler, 2010). GABA is synthesized from glutamate via an enzymatic reaction mediated by the glutamic acid decarboxylase (GAD) (**Figure 1.3.14**). There are two GAD isoforms known to decarboxylate glutamate to GABA: GAD65 and GAD67 (Martin and Barke, 1998). GAD67 is mainly found in the neuronal soma synthesizing the GABA which can be released by non-vesicular extrusion (Martin and Barke, 1998), while GAD65 is localized in synaptic terminals where it mediates the synthesis of GABA for vesicular release (Mower and Guo, 2001). When GABA is synthesized in the presynaptic terminals, the vesicular GABA transporters (VGAT) absorbs and stores GABA in synaptic vesicles based on the electrochemical gradient (Chaudhry et al., 1998) (**Figure 1.3.14**). When GABA is released by exocytosis in the synaptic cleft, it can saturate the GABA receptors in the postsynaptic membrane (Maconochie et al., 1994) or diffuse in the perisynaptic terminals where presynaptic terminals or glia reuptakes it through the action of GABA transporters (GAT) (Cavelier et al.,

2005) (**Figure 1.3.14**). However, the reuptake of GABA is not absolute and there is always a small concentration (approximately 1 μM) remaining in the extracellular space (Lerma et al., 1986).

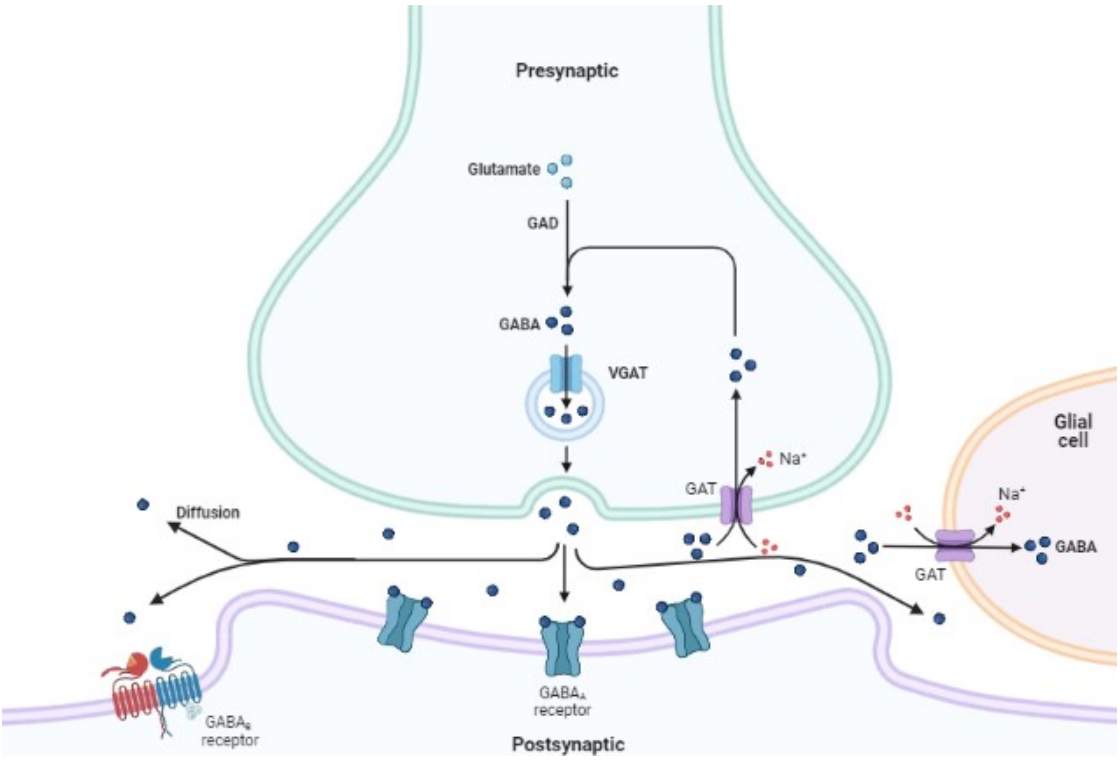

Figure 1.3.14. GABA synthesis, release, and reuptake in synaptic terminals.

GABA is synthesized in presynaptic inhibitory terminals by glutamate via an enzymatic reaction catalyzed by GAD. Then it is loaded in synaptic vesicles by the vesicular GABA transporter (VGAT) and released in the synaptic cleft. When released it can activate $GABA_A$ receptors in the post-synaptic cell or diffuse and bind to the perisynaptic $GABA_B$ receptors. Reuptake of GABA by surrounding neurons and glia is mediated by the activity of GABA transporters (GAT) (created with BioRender.com).

GABA can act upon three types of receptors: the ionotropic $GABA_A$ or $GABA_C$ and the metabotropic $GABA_B$ receptors, with each receptor having distinct localization and kinetic patterns. $GABA_A$ receptors are heteropentameric ligand-gated ion channels consisting of a large amino-terminal extracellular domain and four transmembrane domains (TMs) with a large intracellular domain spanning between TM3 and TM4 (**Figure 1.3.15**). $GABA_AR$ subunits are encoded by 19 different genes which are grouped into eight

subclasses depending on sequence homology. These subclasses include six α (1-6) subunits, three β (1-3) subunits, three γ (1-3) subunits, three ρ (1-3) subunits and one δ, ε, π, and θ subunits each (Luscher et al., 2011). Different subunit combinations result in many distinct functional $GABA_AR$ receptors. The most common subunit composition of $GABA_AR$ in the CNS sums two α, two β and one γ subunits (Olsen and Sieghart, 2009) (**Figure 1.3.15**).

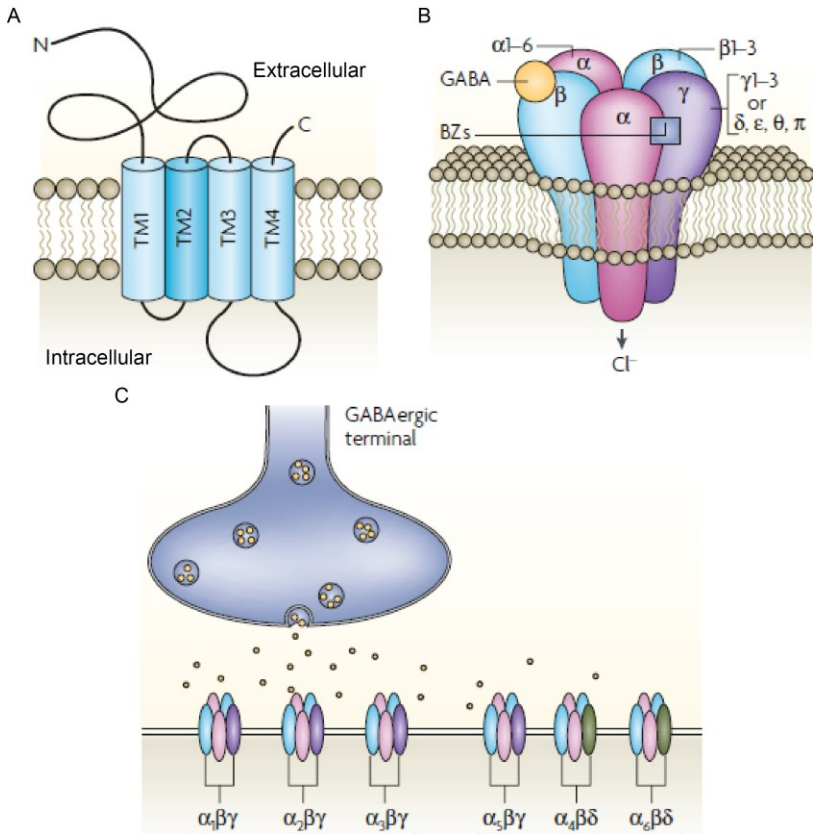

Figure 1.3.15. $GABA_AR$ subunits composition

(**A**) $GABA_AR$ subunits consist of an extracellular amino terminal domain (where GABA binds), four transmembrane domains (TMs) and an intracellular loop between TM3 and TM4. (**B**) The assembly of 5 subunits form a functional $GABA_AR$. (**C**) The localization of each distinct receptor is determined by its subunit composition, and it could be either synaptic or extrasynaptic. Modified from (Jacob et al., 2008).

$GABA_A$ receptors are ligand-activated Cl^- channels, but they are also permeable to bicarbonate (HCO_3^-). Activation of the receptors by two molecules of GABA results in the

influx of chloride and to a lesser extend to an efflux of HCO_3^- from the neuron (Kaila, 1994). $GABA_A$Rs localized in the post-synaptic terminal have relative low affinity to GABA (Glykys and Mody, 2007), allowing the receptors to respond selectively to very high concentrations of GABA in the cleft (Mody et al., 1994). Thus, activation of $GABA_A$R gives rise to very fast and transient inhibitory postsynaptic currents (IPSCs) known as phasic inhibition (Farrant and Nusser, 2005). This form of synaptic inhibition is considered to be crucial for neuronal communication, precision of action potentials firing, and synchronicity of neuronal rhythms (Buzsáki and Chrobak, 1995; Cobb et al., 1995; Somogyi and Klausberger, 2005). However, the response of the post-synaptic terminal to the activation of $GABA_A$R relies on the driving force for Cl^- which is determined by the difference between the electrochemical equilibrium potentials of Cl^- (E_{Cl}) and the membrane potential of the post-synaptic neuron (Kahle et al., 2008). At rest, the E_{Cl} remains very close to the membrane potential, therefore a minor change in the intracellular Cl^- can result to significant shifts in E_{Cl} (Doyon et al., 2016). The mechanisms regulating neuronal Cl^- gradient and their role in $GABA_A$-mediated fast-hyperpolarizing inhibition will be discussed extensively later.

Another determinant of the $GABA_A$-mediated phasic inhibitory strength is the confinement of the $GABA_A$Rs at the post-synaptic terminals. The inhibitory post-synaptic scaffolding protein Gephyrin represents a key factor for the clustering of the $GABA_A$R at the synapse. It forms multimeric complexes with several inhibitory synaptic proteins and the cytoskeleton while it is found to self-assemble in hexagonal lattice (**Figure 1.3.16**) (Betz, 1998; Choii and Ko, 2015). Depletion of gephyrin (*Geph*$^{-/-}$) results in reduction of puncta of $GABA_A$R α2-3, β2/3 and γ2 in mice which diminishes miniature inhibitory postsynaptic currents (mIPSCs) (Kneussel et al., 1999, 2001; Lévi et al., 2004). In addition, genetic knock out of γ2 subunits reduces the detected clusters of gephyrin and $GABA_A$Rs indicating that gephyrin interacts with $GABA_A$ receptors via specific receptor subunits (Essrich et al., 1998). Neuroligins have been identified also as interactors of gephyrin with neuroligin 2 localized specifically in inhibitory synapses (Poulopoulos et al., 2009; Varoqueaux et al., 2004). The interaction between neuroligin 2 and neurexins, attached in the presynaptic terminal membrane, allows the alignment of the pre- and post-synaptic components of an inhibitory synapse (**Figure 1.3.16**). Neuroligin 2 is also crucial for the clustering of gephyrin in the post-synaptic density (Poulopoulos et al., 2009) and subsequently for the clustering of the $GABA_A$Rs. Enhancing the expression of neuroligin 2 in mice increases the frequency of mIPSCs but not the amplitude of the events (Hines et al., 2008).

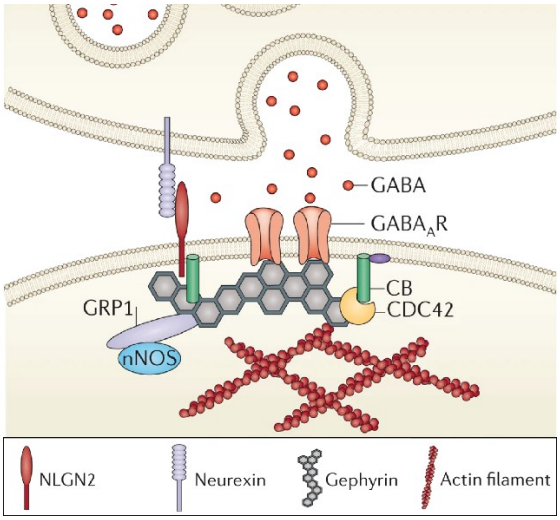

Figure 1.3.16. Gephyrin scaffold in GABAergic synapses.

Gephyrin auto-assembles in a hexagonal lattice forming multimeric complexes that interact with filamentous actin, Neuroligin 2 and $GABA_A$Rs. Neuroligin 2 in the post-synaptic density interacts with neurexin anchored in the pre-synaptic membrane allowing the alignment of the pre- and post-synaptic components. Modified from (Tyagarajan and Fritschy, 2014).

$GABA_C$ receptors represent a subclass of the $GABA_A$ receptors, and they are composed of ρ subunits only. They are Cl^- permeable ligand-gated channels responsible for the fast-hyperpolarizing inhibition in response to GABA binding.in the outer retina and particularly the horizontal and bipolar cells (Lukasiewicz, 1996).

$GABA_B$ receptors are metabotropic receptors for GABA which are linked through G-proteins to potassium channels (Gassmann and Bettler, 2012). $GABA_B$Rs are composed of principal $GABA_{B1a}$, $GABA_{B1b}$ and $GABA_{B2}$ subunits (Pin and Bettler, 2016) forming the core of the receptor. The $GABA_{B1}$ subunits are essential for the ligand binding whereas the $GABA_{B2}$ subunits are involved in the expression of the receptor as a dimer at the neuronal membrane (Pinard et al., 2010). They can be expressed both in the pre- and the post-synaptic excitatory or inhibitory terminals. In the pre-synaptic terminal $GABA_B$R mediate feedback inhibition and prevent further GABA release. In the post-synaptic cell, binding of GABA to $GABA_B$Rs activates rectifying K^+ channels that generate slow inhibitory postsynaptic potentials (IPSPs) which hyperpolarize the membrane (Pin and Bettler, 2016).

1.3.4 Chloride regulation

The nature of GABAergic transmission is greatly influenced from changes in the gradient of Cl^- (Kaila et al., 2014) and to a lesser extend to HCO_3^- (Staley, 1994). The membrane potential V_m at which there is no net flux of Cl^- through the $GABA_AR$ accounts for the reversal potential for GABA or E_{GABA}. When the intracellular concentration of Cl^- ($[Cl^-]_i$) is higher than the electrochemical gradient, the E_{Cl} is more positive to the V_m. Then opening of $GABA_AR$ will result in efflux of Cl^- and a depolarization of the neuronal membrane. In the opposite situation, when $[Cl^-]_i$ is low, the E_{Cl} is more negative to the V_m resulting in an influx of Cl^- through the $GABA_AR$ upon its activation and hyperpolarization of the membrane. The permeability of $GABA_AR$ to HCO_3^- results to a slightly more depolarizing E_{GABA} than the expected if the receptor was permeable only to Cl^- (Farrant and Kaila, 2007).

Most of the mature CNS neurons maintain a low $[Cl^-]_i$ (~ 7 mM) allowing for a hyperpolarizing effect of GABA upon activation of $GABA_ARs$ (Kahle et al., 2008) (**Figure 1.3.17**). Hyperpolarization of the neuronal membrane decreases the V_m which subsequently raises the threshold for an action potential to fire. In contrary, during embryonic development the $[Cl^-]_I$ remains high (~ 25 mM) resulting to a depolarizing effect of GABA and therefore a decrease in the action potential firing threshold (Ben-Ari, 2002; Ben-Ari et al., 2007; Zhang et al., 1991) (**Figure 1.3.17**).

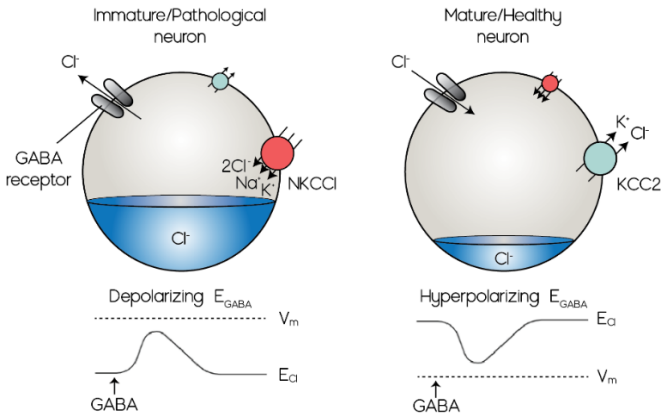

Figure 1.3.17. GABA switch during development and in pathological conditions.

The neuron on the left represents an immature or a neuron undergoing pathology where NKCC1 levels are relatively high causing accumulation of Cl^- thus reversing the Cl^- gradient leading to a Cl^- efflux upon $GABA_AR$ activation. In contrast, in mature healthy neurons protein levels of KCC2 are high in the membrane maintaining low intracellular Cl^- levels resulting in a robust inward electrochemical gradient for Cl^- and a hyperpolarizing E_{GABA}. Adapted from (Kahle et al., 2008).

However, it is not only during development that GABA acts as an excitatory neurotransmitter. During some phases of the circadian cycle, GABA release has an excitatory effect in the suprachiasmatic nucleus (De Jeu and Pennartz, 2002). In addition, in the basolateral amygdala and the parietal and perirhinal cortices, GABA is found to be depolarizing in fast-spiking interneurons, but not in pyramidal neurons (Martina et al., 2001), suggesting that GABA could have different effects in various neuronal subtypes depending on the $[Cl^-]_i$ in the mature CNS. Finally, in many neurological disorders and diseases, changes in the Cl^- gradient renders GABA excitatory in the mature CNS and contributes to the onset of symptoms associated with such disorders/diseases (Kaila et al., 2014).

The $[Cl^-]_i$ is regulated in the majority of mammalian cells by a group of cation-chloride cotransporters (CCCs) (Kaila et al., 2014) encoded by the Solute Carrier family 12 (*slc12*) genes. These cotransporters are electroneutral trans-membrane transporters enabling secondary active transport by exploiting the ionic gradient set by the Na^+/K^+ ATPase to transfer Cl^- (**Figure 1.3.18**). The first members of this gene family were isolated from the teleost *Pseudopleuronectes americanus* and the shark *Squalus acanthias* leading to the identification of their mammalian homologues (Gamba et al., 1993; Hebert et al., 2003b). There are four potassium-chloride cotransporters (KCC1-4); two sodium-potassium-chloride cotransporters (NKCC1-2) and a sodium-chloride cotransporter NCC. In the CNS two CCCs have been found to set the gradient for Cl^-, the Na^+-K^+-Cl^- cotransporter NKCC1 and the K^+-Cl^- cotransporter KCC2 (**Figure 1.3.18**). NKCC1 mediates the uptake of Cl^- by transporting 2 anions of Cl^- along with a K^+ and a Na^+ cations, by exploiting the Na^+ gradient (**Figure 1.3.18**). KCC2, on the other hand, extrudes Cl^- by transporting one Cl^- ion against its concentration gradient by using the K^+ outward gradient (**Figure 1.3.18**). But KCC2 can act as a bidirectional transporter depending on the chemical concentration gradients of the transported ions (Delpire and Lauf, 1991). Since the transport through KCC2 is driven by the K^+ driving force, any mechanisms altering K^+ concentrations, such as changes on the activity of the Na+/K+ ATPase (Ikeda et al., 2004) or elevated neuronal activity (Futamachi et al., 1974) can impact the activity of the transporter and disrupt Cl^- homeostasis (Doyon et al., 2011).

Until recently, KCC2 was considered to be specifically expressed in neurons where it defines the strength of inhibition and the water transport and cell volume regulation. However, recent observations have identified three splice variants of KCC2 in pancreatic insulin-secreting β-cells (Kursan et al., 2017). Like most of the CCCs, KCC2 and NKCC1 can be targeted by commonly used diuretics (Payne et al., 2003) such as bumetanide and

furosemide. Bumetanide has a high affinity for NKCC1 (K_i 0.1 µM) while its affinity for KCC2 is approximately 500 times lower (K_i 25 – 50 µM). Thus, bumetanide at low doses could be used as a relatively specific inhibitor for NKCC1. On the other hand, furosemide inhibits both KCC2 and NKCC1 almost equally. Due to the low affinity of these blockers to KCC2, their use to modulate the activity of KCC2 in the CNS will have minimal effects while the effect on NKCC1 expressed in the periphery and kidneys will be predominant. As such, more specific and selective modulators for KCC2 have been identified by two recent pharmacological screening studies (Delpire et al., 2009; Gagnon et al., 2013). VU024551 and VU0463271 have been identified as specific blockers for KCC2 without any substantial effect on NKCC1 but they may also bind to several Gq-GPCRs or other proteins (Delpire et al., 2009, 2012), leading to other unspecific effects (Sivakumaran et al., 2015). CLP257 and its prodrug CLP290 have been identified as KCC2 activators which effectively reduce $[Cl^-]_i$ in neurons (Gagnon et al., 2013). Prochlorperazine dimaleate (PCPZ), an antipsychotic drug of the family of the piperazine phenothiazines has also been identified as a good KCC2 activity enhancer but the mechanisms of its action remain elusive (Liabeuf et al., 2017).

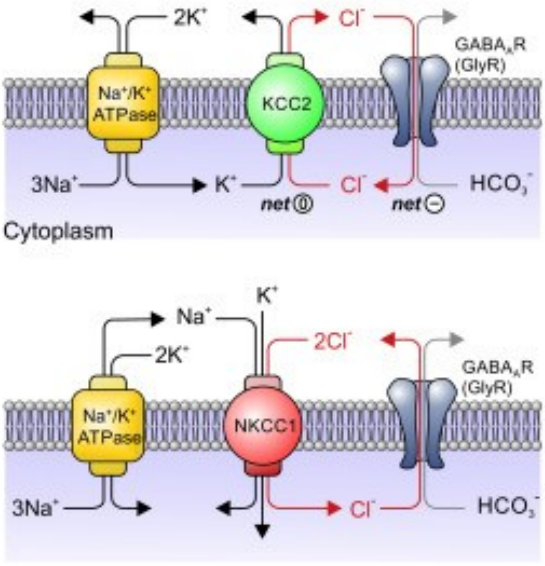

Figure 1.3.18. Chloride regulation in neurons.

KCC2 and NKCC1 exploit the ionic gradient set by the Na^+/K^+ ATPase to transport Cl^- across the plasma membrane. KCC2 extrudes Cl^- from the neurons maintaining low intracellular Cl^- allowing for the influx of Cl^- through $GABA_AR$ and membrane hyperpolarization. NKCC1 mediates Cl^- efflux and loading the neurons with Cl^- resulting in an outflux of Cl^- through the $GABA_AR$. Modified from (Doyon et al., 2016).

1.3.5 KCC2 structure, function, cellular distribution, and regulation

KCC2 is encoded by the *slc12a5* gene located on the 9th or the 20th chromosome in mice or in humans respectively (Sallinen et al., 2001). Due to alternative promoters and first exons, two isoforms of KCC2 are expressed in the CNS: the KCC2a and KCC2b (Uvarov et al., 2007). KCC2b represents the major isoform in the adult brain while KCC2a isoform is very low or absent in the mature cortex, hippocampus, thalamus and cerebellum (Markkanen et al., 2014). However, during development, both isoforms are detected in the CNS with KCC2a being the predominant isoform in the hypothalamus, the brain stem and the spinal cord (Markkanen et al., 2014). Interestingly, null mutant mice for either the KCC2 exon 5 (Hübner et al., 2001) or the exon 4 (Tornberg et al., 2005) are lethal, but KCC2b deficient mice survive for up to 2 weeks but finally die due to overt seizures (Uvarov et al., 2007) suggesting that KCC2a isoform is crucial during development while KCC2b is essential for the mature CNS. At the subcellular level, the two isoforms rarely colocalize, with KCC2b being concentrated at the plasma membrane of the neuronal soma, while KCC2a is expressed in dendrites together with KCC2b but without any overlap between the two (Markkanen et al., 2014).

KCC2 is also expressed in the pancreas where both KCC2a and KCC2b are detected, along with a new variant of the protein which was identified to be expressed specifically in pancreatic cells (Kursan et al., 2017). This novel isoform (KCC2a-S25) is produced by slicing resulting in lack of the exon 25 and it is expressed in various endocrine pancreatic cells where it modulates insulin secretion (Kursan et al., 2017).

KCC2 consists of 1116 amino acids with 12 a-helices transmembrane domains (TMD), a short N-terminal (NTD) and a long C-terminal intracellular tails (CTD) (Payne et al., 1996). The intracellular NTD and CTD of KCC2 contain regulatory phosphorylation sites, while the TMD are involved in determining the ion affinity of the transporter (Chamma et al., 2012; Payne et al., 1996; Williams et al., 1999). The CTD also contains an ISO domain too that allows KCC2 to transport under isotonic conditions (Mercado et al., 2006). The predicted molecular weight of the protein is 123.6 kDa (Payne et al., 1996) however KCC2 is detected as two bands in an immunoblot. The first band represents monomeric KCC2 at approximately 140 kDa which does not correspond to the predicted molecular weight of the protein. This is because the protein is typically glycosylated in the large extracellular loop

between the TMD5 and TMD6 (Blaesse et al., 2006; Payne, 1997). The second band is detected above 250 kDa and represents the dimers of KCC2 (Uvarov et al., 2009).

Electron microscopy (EM) analysis of the native functional KCC2 confirms the immunoblot findings showing that KCC2 exists as monomers and dimers in solutions (Agez et al., 2017). As a monomer KCC2 is organized in two major domains connected with a linker (Agez et al., 2017). The extracellular domain is formed by two ordered linkers between the TM5-6 and TM7-8 and the TMD and CTD are linked through the TM12 and a scissor helix (Xie et al., 2020).(**Figure 1.3.19**). When in dimer, KCC2 is organized in four domains with the TMDs and CTDs coinciding perpendicular to the plasma membrane surface and the CTD of one subunit attaching the TMD of the other subunit (Xie et al., 2020) (**Figure 1.3.19**). The dimer maintains its formation due to the interactions between the two CTDs and the hydrophobic interactions between the TM11 and TM12 (Xie et al., 2020). The N-terminal peptide includes two highly negative regions which insert in the cavity of the dimer and block the transport (Xie et al., 2020; Zhang et al., 2021). Interestingly, both isoforms of KCC2 can form dimers *in vivo* and in overexpression systems (HEK 293 cells), either as homodimers or heterodimers (Uvarov et al., 2009). Some other studies have identified KCC2 as trimers and tetramers in brain lysates (Blaesse et al., 2006; Mahadevan et al., 2014) suggesting that KCC2 forms oligomers as other CCCs commonly do (Hartmann and Nothwang, 2015), but still the presence of KCC2 oligomers is debated.

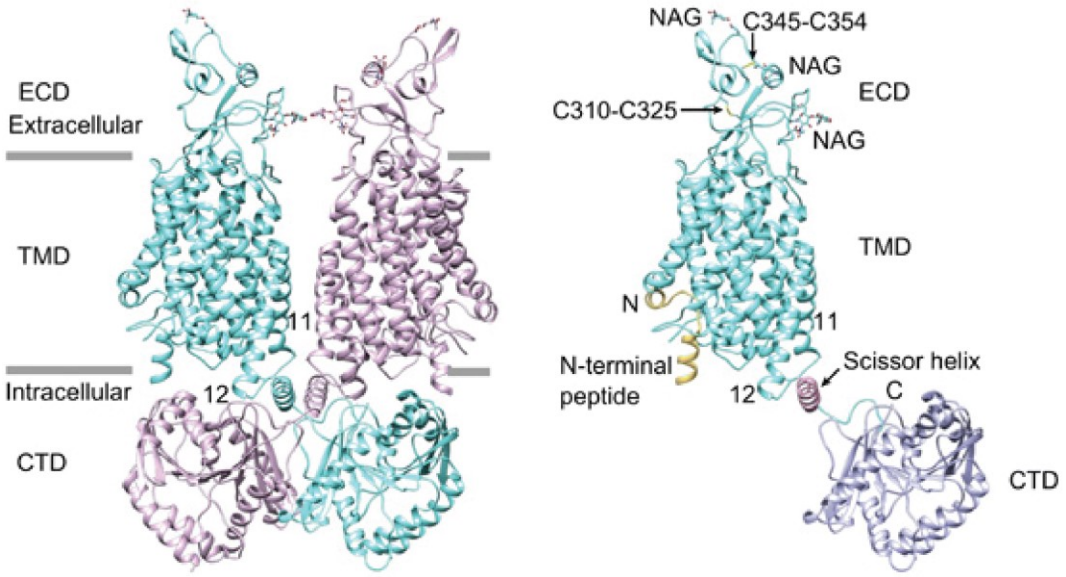

Figure 1.3.19. Secondary structure of KCC2 monomer and dimer.

Graphical representation of the human KCC2 dimer folding (left) and the secondary structure of a single subunit of KCC2 (monomer; right). Modified from (Xie et al., 2020).

KCC2 is detected both in the cytosol and the plasma membrane where it mediates Cl^- extrusion. When in the membrane it is distributed exclusively in the neuronal soma and the dendrites, while it is excluded from the axon (Báldi et al., 2010). This specific subcellular distribution justifies the high $[Cl^-]_i$ in the axon which in turn results to a more depolarizing E_{Cl} (Price and Trussell, 2006). However, even between the soma and the dendrites the levels of KCC2 could vary a lot. For instance in the hippocampal pyramidal neurons, KCC2 is mainly localized in the spine heads adjacent to asymmetric synapses, while it is highly expressed both in the soma and the dendrites of interneurons in the hippocampus (Gulyás et al., 2001). The high levels of KCC2 in the dendritic spines are also crucial for the formation of excitatory synapses. The majority of the excitatory synapses are formed on dendritic spines, and most of the inhibitory synapses are localized on the dendritic shafts (Harris, 1999; Klausberger and Somogyi, 2008). When KCC2 is suppressed during development, the maturation of dendritic spine fails and the number of functional excitatory synapses decreases drastically (Li et al., 2007). Thus, the cellular distribution of KCC2 not only controls the levels of $[Cl^-]_i$ across different cellular compartments, it allows also the formation of functional synapses and contributes to synaptic plasticity.

Like many membrane proteins, the activity and function of KCC2 is regulated by transcriptional and post-translational modifications. KCC2 is undergoing phosphorylation and dephosphorylation in specific residues in the NTC or the CTD (Cordshagen et al., 2018) but also it is susceptible to recycling, cleavage and changes to its quaternary structure. In addition, several proteins have been identified to interact directly with KCC2 and modulate its function (Chen et al., 2017; Ivakine et al., 2013; Mahadevan et al., 2017).

At the transcriptional level, KCC2 is regulated by many mechanisms which mostly control the developmental upregulation of its expression and the GABA shift. One of these mechanisms involves the activation of the KCC2b promoter by the early growth response 4 (Egr4) transcription factor (Ludwig et al., 2011). Egr4 is activated in response to Brain Derived Neurotrophic Factor (BDNF) and activation of the extracellular signal-regulated kinase 1/2 (ERK1/2) in immature neurons resulting in an upregulation of KCC2 expression (Ludwig et al., 2011). Another transcriptional regulator of KCC2 is the repressor element-1 silencing factor (REST). Inhibition of REST and its interaction with the dual repressor elements-1 (RE-1) allows for transcription of KCC2b and the shift of GABA from depolarizing to hyperpolarizing (Yeo et al., 2009), again in response to BDNF.

Membrane expression of KCC2 and functional activation/de-activation is primarily mediated via phosphorylation and dephosphorylation of the protein (**Figure 1.3.20**). Low

phosphorylation of the transporter is generally associated with enhanced chloride extrusion. The best characterized phosphorylation residue of KCC2 involved in its functional regulation is the S940 located in the CTD of the protein (Côme et al., 2019). This residue is phosphorylated by the protein kinase C (PKC) and has been implemented in the regulation of the cell surface stability of KCC2 and as a result to a better Cl^- extrusion capacity of neurons (Lee et al., 2007).The constrain of KCC2 to the plasma membrane of excitatory synapses is confined by the interaction of S940 phosphorylated KCC2 and the actin cytoskeleton (Chamma et al., 2013). Dephosphorylation of KCC2 at S940 results in lateral diffusion of the transporter and degradation of the protein via calpain protease cleavage (Chamma et al., 2013; Lee et al., 2011; Silayeva et al., 2015; Zhou et al., 2012). The dephosphorylation of KCC2 seems to be triggered by elevated synaptic activity, NMDAR activation and Ca^{2+} flux which leads to PP1 activation that mediates the KCC2 S940 dephosphorylation (Chamma et al., 2013; Kahle et al., 2013; Lee et al., 2011; Silayeva et al., 2015) (**Figure 1.3.20**).

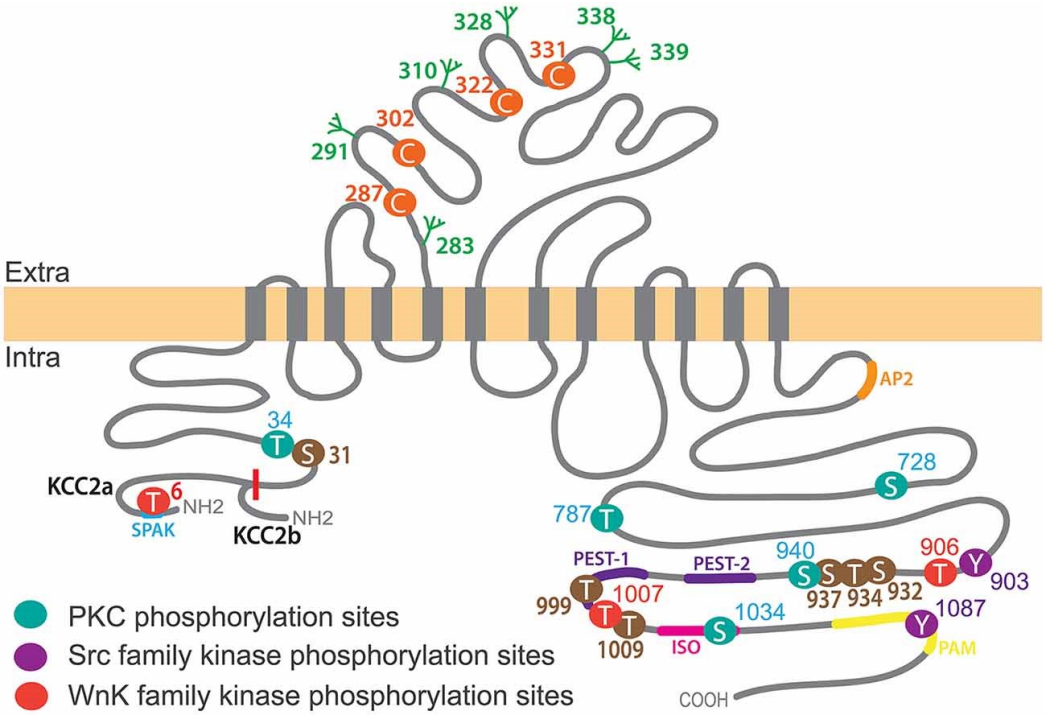

Figure 1.3.20. The phosphorylation and glycosylation residues of KCC2.

KCC2 is a transmembrane protein with 6 N-glycosylation sites (green) between the TM5 and TM6 and several cysteine residues (orange) for ion transport. At the intracellular side, KCC2 has several serine and threonine residues that can be targeted and phosphorylated by kinases Phosphorylation and de-phosphorylation of specific residues alters the function of the transporter. Modified from (Côme et al., 2019).

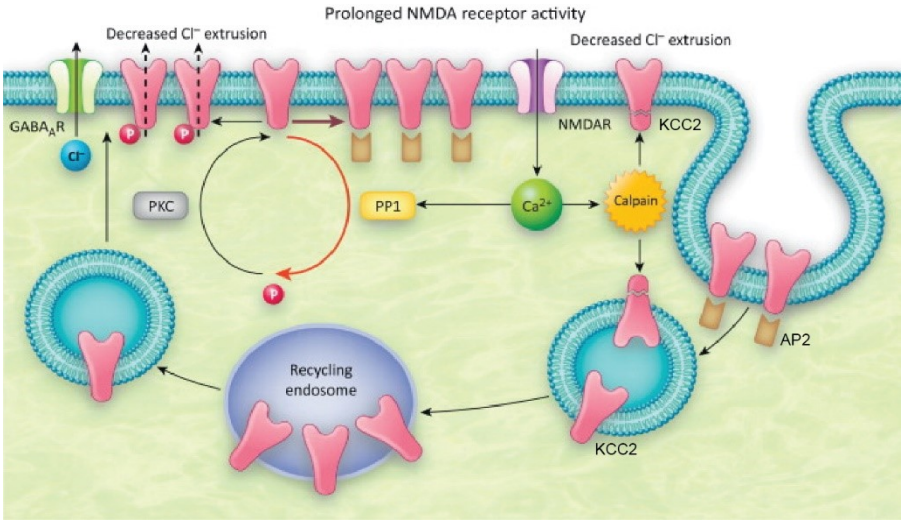

Figure 1.3.21. Activity-dependent regulation of KCC2 surface expression.

Increased activation of NMDAR and Ca^{2+} influx activates a signalling cascade which results in dephosphorylation of KCC2 S940 from PP1 and KCC2 endocytosis or triggers calpain and KCC2 degradation. Modified from (Kahle et al., 2013).

Autophosphorylation and activation of lysine deficient protein kinases 1 and 3 (WNK1 and WNK3) activates the SPAK/OSR1 complex which phosphorylates KCC2 at T906 and T1006 (or T1007 in human) (Alessi et al., 2014; Friedel et al., 2015) (**Figure 1.3.21**). Phosphorylation in these two threonine residues results in low expression of KCC2 in the membrane and KCC2 enrichment in the cell soma, while dephosphorylation of KCC2 allows for KCC2 targeting in the membrane of dendrites and a hyperpolarizing E_{GABA} (Friedel et al., 2015). This signaling pathway is involved in the cell volume regulation by the response of WNK1 to the osmotic stress with increase in $[Cl]_i$ preventing the autophosphorylation of the kinase (Kahle et al., 2010; Piala et al., 2014).

Phosphorylation of KCC2 from the Src family of protein kinases at two tyrosine residues (Y903 and Y1087) can also modify the cell surface expression of the transporter. The addition of a phosphoryl-group to these two tyrosines results in reduced membrane expression and increased lysosomal degradation of KCC2 (Lee et al., 2010). However, work from another group suggests that phosphorylation of Y1087 promotes clustering and oligomerization of KCC2 enhancing Cl^- extrusion (Watanabe et al., 2009). Finally, KCC2 phosphorylation at S932, T934 and T937 have shown to augment KCC2 function, while

phosphorylation at T1008 has shown to diminish Cl^- extrusion in HEK293 overexpression systems (Cordshagen et al., 2018; Weber et al., 2014).

Another key signaling mechanism that leads to KCC2 downregulation or decrease in KCC2 activity is mediated by BDNF activation of the tropomyosin receptor kinase B (TrkB) (Rivera et al., 2002). The subsequent effect of TrkB autophosphorylation results in activation of phospholipase Cγ (PLCγ) and cAMP response element-binding (CREB) or the activation of the src homology 2 domain containing transforming protein (Shc) and the Akt/Erk kinases (Rivera et al., 2004) (**Figure 1.3.22**). This signaling mechanism has been reported in various pathological conditions such as epilepsy (Rivera et al., 2002, 2004), spinal cord injury (Boulenguez et al., 2010) and neuropathic pain (Coull et al., 2005). In the latter, BDNF is found to be released by microglia after nerve injury (Coull et al., 2005) and selective blockage of the spinal cord microglia or of the BDNF/TrkB signaling reverses inflammation or morphine-induced Cl^- extrusion (Ferrini et al., 2013; Groth and Aanonsen, 2002).

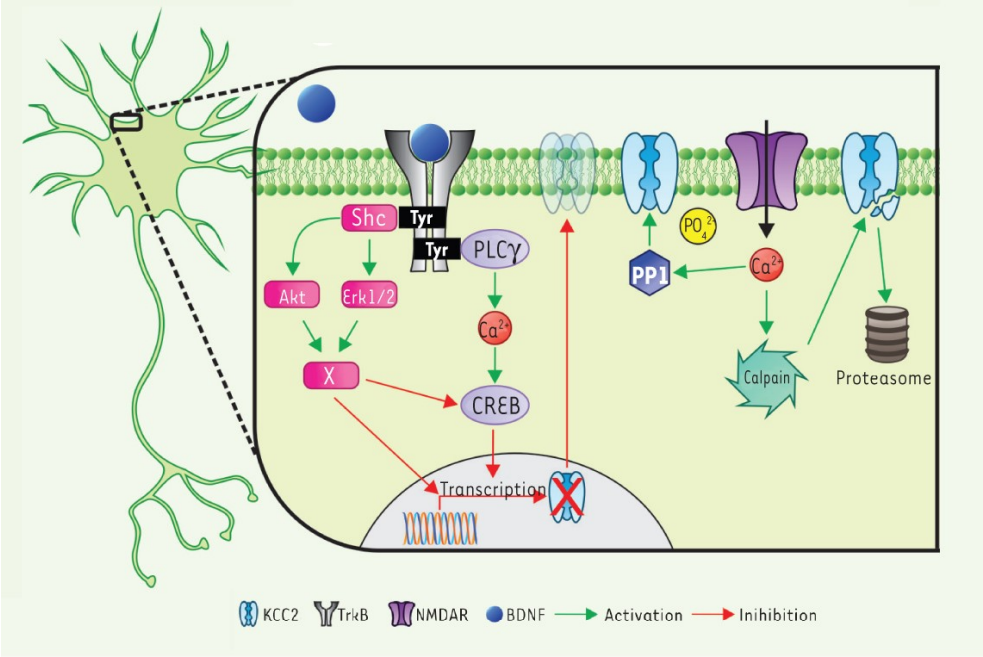

Figure 1.3.22. BDNF/TrkB signaling pathway mediating KCC2 downregulation.

BDNF binding to TrkB receptors results in PLCγ or Shc and Akt/Erk activation of CREB and transcriptional KCC2 downregulation. In addition, Ca^{2+} influx through NMDAR causes cell surface KCC2 decrease via PP1 mediated dephosphorylation of KCC2 and/or calpain proteolysis of KCC2. Modified from (Bergeron et al., 2014).

1.4 Rationale and Objectives

Alzheimer's disease has been associated with an abnormal brain activity common to other neurological disorders such as epilepsy, Down Syndrome, autism and frontotemporal dementia (Baroncelli et al., 2011; Palop and Mucke, 2016; Rubenstein and Merzenich, 2003; Vattikuti and Chow, 2010; Wong, 2010; Yizhar et al., 2011a). Normal brain neuronal activity importantly relies on the balance between synaptic excitation and inhibition. Subtle disruption of this balance is postulated to result in cognitive decline and neurodegeneration (Bookheimer et al., 2000; Dickerson et al., 2005; Palop and Mucke, 2009). Specifically, in AD, aberrant brain activity arises from neuronal hyperexcitability due to disruption of $GABA_A$-mediated inhibitory signaling (Verret et al., 2012). Transient seizure-like network hyperactivity has been described in the prefrontal cortex (medial orbitofrontal cortex and the anterior cingulate cortex), the posterior cingulate cortex, the precuneus and the hippocampus of AD patients (Lam et al., 2017; Palop and Mucke, 2016; Vossel et al., 2013). Hyperactive neurons contributing to seizure-like events have been observed in the proximity of amyloid plaques (Busche et al., 2008) but also, soluble amyloid-β *per se* is sufficient to evoke neuronal hyperactivity (Busche et al., 2012). Yet, it is still debatable whether the aberrant neuronal activity is evoked by the accumulation of Aβ or the deposition of Aβ is augmented by neuronal hyperexcitability (Bero et al., 2011).

Several hypotheses have emerged on the origin of neuronal hyperexcitability in AD. Disruption of $GABA_A$-mediated signaling and loss of inhibition arises as the most prominent mechanism of neuronal hyperexcitability and cognitive decline. The robustness of $GABA_A$ receptor neurotransmission depends on low intracellular chloride concentrations, so that negatively-charged chloride will flow into the cell when $GABA_A$ receptors are opened. In mature CNS, a key regulator of chloride levels and, therefore, of inhibitory signaling, is the potassium-chloride cotransporter KCC2 (Doyon et al., 2016; Rivera et al., 1999). KCC2 hypofunction limits neuronal chloride extrusion and disrupts $GABA_A$ signaling. Notably, it has been reported that KCC2 levels are reduced in the frontal lobe of sporadic Alzheimer's disease patients (Doshina et al., 2017). It remains an open question whether KCC2 hypofunction and subsequently impaired neuronal chloride transport contribute to cognitive decline and the onset of AD.

Similar disruption in the balance between synaptic excitation and inhibition has been reported in patients with mild-cognitive impairment (MCI) and senile dementia (Andrews-Hanna et al., 2007; Bakker et al., 2012; Burke and Barnes, 2006). However, the aging-linked

changes in the E/I balance differ between brain regions. Neuronal hyperexcitability has been reported early in the hippocampus of patients with MCI (Putcha et al., 2011), while an increase in the intrinsic inhibitory tone has been observed in the PFC of elderly people (Legon et al., 2016). Similarly, distinct cognitive skills deteriorate with aging. Working and episodic memory, executive function, planning, attention and rule perception drastically decline with aging (Hedden and Gabrieli, 2004; Park et al., 1996). This decline in executive functions in senescence has been linked to morphological and structural changes in the PFC pyramidal neurons along with an overt spine density reduction resulting in neurophysiological changes (Andrews-Hanna et al., 2007; Morrison and Baxter, 2012). In addition, electrophysiology studies in aged rodents and non-human primates revealed that PFC pyramidal neurons receive excessive inhibitory input (Bories et al., 2013; Luebke et al., 2004), supporting a decrease in the E/I ratio and a shift towards inhibition. Thus, understanding the contribution of the neurophysiological changes observed in the PFC and the mechanisms supporting the alterations in the E/I ratio during aging are crucial for preventing cognitive decline in senescence and restoring normal neuronal activity.

An abnormally active neuron can be as disruptive to the function of a neuronal circuit as can an abnormally silent neuron. Aberrant neuronal activity and disrupted firing patterns can impair synapse formation and synaptic strength important for memory and other cognitive functions (Turrigiano and Nelson, 2004). This so-called activity-driven neuropathology could have potential implications for neurodegenerative disorders such as AD. So far, pathogenic factors crucial for the development of AD are thought to cause synaptic and neuronal degeneration in disease. The changes in network activity are postulated to be secondary manifestations of previous degeneration (Palop and Mucke, 2010b). However, recent observations support the concept that in AD neuronal overexcitability can give rise to neuronal hyperactivity and eventually network disruption which in turn augment the production of pathogenic factors and activate signaling cascades of neuronal death (Yamamoto et al., 2015; Zott et al., 2019). Yet, both possibilities are not mutually exclusive and can present key elements of a vicious cycle in AD facilitating the disease progression. Thus, understanding the mechanisms inducing and sustaining neuronal hyperactivity under non-pathological conditions and in disease is crucial for targeting specific components of this vicious cycle and design innovative potential therapeutic strategies.

Therefore, the principal objectives of my thesis were:

1. **To determine the contribution of chloride transport impairments in the development of cognitive decline in mice carrying Alzheimer's disease-linked mutation** (Chapter 2)

   The KCC2 membrane levels and the neuronal chloride transport rate through KCC2 were measured in mouse lines carrying Alzheimer's disease-related mutations. Following this, the memory and cognitive performance of these mice was assessed after preventing or restoring KCC2 function with a KCC2 enhancer compound to validate the possibility of targeting chloride transport to fight against dementia associated with AD.

2. **To assess whether aging-related cognitive decline is associated with altered excitation and inhibition ratio in the medial prefrontal cortex** (Chapter 3)

   Cohorts of adult and old male mice were tested in a battery of behavioral tasks to correlate cognitive decline with changes in synaptic proteins levels. Then optogenetics were utilized to activate inhibitory neurons in the mPFC and shift the E/I ratio towards inhibition in adult and old mice and validate the effect of such manipulation in cognitive performance.

3. **To validate whether evoked neuronal hyperactivity is sufficient to induce synaptic and neuronal degeneration at the proteome level** (Chapter 4)

   To address this, optogenetics were adopted to generate a model of chronic neuronal hyperactivity in the hippocampus of wild-type and the 5xFAD transgenic mice. The proteome changes occurring after a month of daily optogenetic stimulation were analyzed and gene-ontology analysis was performed to access whether chronic neuronal hyperactivity replicates pathological features linked to AD.

Chapter 2 – Restoring neuronal chloride extrusion reverses cognitive deficits linked to Alzheimer's disease mutations

Iason Keramidis[1,2,*], Brendan B McAllister[3,*], Julien Bourbonnais[1], Feng Wang[1], Dominique Isabel[1], Romain Sansonetti[1], Phil Degagne[3], Justin P Hamel[1], Mojtaba Nazari[3], Samsoon Inayat[3], Annie Barbeau[1], Lionel Froux[1], Antoine G Godin[1,2], Majid H Mohajerani[3], Yves De Koninck[1,2]

1 CERVO Brain Research Centre, Québec Mental Health Institute, Québec, QC, Canada.

2 Department of Psychiatry and Neuroscience, Université Laval, Québec, QC, Canada.

3 Canadian Centre for Behavioural Neuroscience, University of Lethbridge, Lethbridge, AB, Canada.

* These authors contributed equally to this work

Correspondence to: Yves De Koninck: yves.dekoninck@neuro.ulaval.ca

2.1 Résumé

La désinhibition au cours des premiers stades de la maladie d'Alzheimer est censée provoquer un dysfonctionnement du réseau et une hyperexcitabilité conduisant à des déficits cognitifs. Cependant, le mécanisme moléculaire sous-jacent reste inconnu. Nous montrons ici que, chez les lignées de souris porteuses de mutations liées à la maladie d'Alzheimer, une perte du co-transporteur de potassium-chlore de la membrane neuronale KCC2, responsable du maintien de la robustesse de l'inhibition médiée par le $GABA_A$, se produit de manière présymptomatique dans l'hippocampe et le cortex préfrontal. La réduction des niveaux de KCC2 était inversement corrélée à l'augmentation, liée à l'âge, de l'amyloïde-β 42 (Aβ42). La perte de KCC2 a entraîné une altération de l'homéostasie du chlore. L'administration d'Aβ42 a provoqué une réduction de la membrane de KCC2. La prévention de la diminution de KCC2 a protégé contre la détérioration de l'apprentissage et l'hyperactivité corticale. Par ailleurs, le rétablissement du KCC2 après sa réduction a permis d'inverser efficacement les déficits de mémoire spatiale et le dysfonctionnement social, ce qui a permis d'établir un lien entre le dérèglement du Cl- et le déclin cognitif lié à la MA. Ces résultats révèlent que l'hypofonctionnement du KCC2 est une cible viable pour restaurer la fonction cognitive au cours de la la maladie d'Alzheimer, elle confirme l'engagement de la cible, le lieu de l'intervention thérapeutique et son efficacité.

2.2 Abstract

Disinhibition during early stages of AD is postulated to cause brain network dysfunction and hyperexcitability leading to cognitive deficits. However, the underlying molecular mechanism remains unknown. Here we show that, in mouse lines carrying AD-related mutations, a loss of neuronal membrane potassium-chloride co-transporter KCC2, responsible for maintaining the robustness of $GABA_A$-mediated inhibition, occurs pre-symptomatically in the hippocampus and prefrontal cortex. KCC2 downregulation was inversely correlated with the aged-dependent increase in amyloid-β 42 (Aβ42). Loss of KCC2 resulted in impaired chloride homeostasis. Acute administration of Aβ42 caused a downregulation of membrane KCC2. Preventing the decrease in KCC2 using long term treatment with CLP290 protected against deterioration of learning and cortical hyperactivity. In turn, restoring KCC2, using short term CP290 treatment, following the transporter reduction effectively reversed spatial memory deficits and social dysfunction, linking chloride dysregulation with AD-related cognitive decline. This reveals KCC2 hypofunction as a viable target for treatment of AD-related cognitive decline, it confirms target engagement, where the therapeutic intervention takes place, and its effectiveness.

2.3 Introduction

Aberrant brain activity has been reported in pre-symptomatic AD patients (Vossel et al., 2013) and in rodents carrying AD-linked mutations (Palop et al., 2007). This abnormal brain activity appears to arise from neural hyperexcitability due to disrupted $GABA_A$-mediated inhibitory signaling (Verret et al., 2012) near Aβ plaques (Busche et al., 2008). Conversely, overexpression of tau suppresses neuronal activity and counteracts the Aβ-dependent neuronal hyperactivity (Angulo et al., 2017; Busche et al., 2019)

While hyperexcitability has been associated with cognitive decline (Dickerson et al., 2005; Palop and Mucke, 2009; Yizhar et al., 2011a), loss of inhibition per se, especially through loss of synaptic specificity due to impaired chloride homeostasis, arises as a potential mechanism of memory deficits (Ferando et al., 2016). The potassium chloride cotransporter KCC2 is responsible for maintaining a low intracellular chloride concentration ($[Cl^-]_i$) in neurons by extruding chloride, preserving the robustness of $GABA_A$ signaling (Doyon et al., 2016). Notably, it has been reported that KCC2 levels are reduced in the frontal lobe of sporadic AD patients (Doshina et al., 2017), and that amyloid fibril injection in the CA1 of rodents can downregulate KCC2 protein (Bie et al., 2022). Here we address the

hypothesis that KCC2 hypofunction underlies cognitive deficits in two mouse lines carrying AD-linked mutations resulting in Aβ pathology.

2.4 Materials and methods

Animal Subjects

Experimental protocols were approved by the committee for animal protection of Université Laval (CPAUL) and the University of Lethbridge Animal Care Committee in accordance with the guidelines from the Canadian Council on Animal Care.

Male B6SJL-Tg(APPSwFlLon,PSEN1*M146L*L286V)6799Vas/Mmjax mice (5xFAD) were purchased from the Jackson Laboratory (#34840-JAX) and bred with female B6SJLF1/J mice (The Jackson Laboratory, #100012). These breeders were used to produce both 5xFAD mice and littermate NonTg control mice for the present experiments. Two separate 5xFAD colonies were maintained at the CERVO Brain Research Centre and the Canadian Centre for Behavioural Neuroscience (CCBN). Breeding pairs of C57BL/6-App<tm3(NL-G-F)Tcs> knock-in mice ($APP^{NL\text{-}G\text{-}F/NL\text{-}G\text{-}F}$) (Saito et al., 2014), were provided by RIKEN Center for Brain Science, Japan (RBRC #06344). The $APP^{NL\text{-}G\text{-}F/NL\text{-}G\text{-}F}$ colony was maintained at the CCBN. Mice were housed on a 12 h light/12 h dark cycle, and all experiments were performed during the light cycle. Food and water were provided without any restrictions.

Both sexes were included in each group tested for any experiment conducted. For the behavioral testing, group 1 consisted of 6-month-old vehicle-treated 5xFAD mice (*n* = 14, 7 males), CLP290-treated 5xFAD mice (*n* = 14, 8 males), and vehicle-treated NonTg mice (*n* = 14, 7 males); group 2 consisted of 6-month-old vehicle-treated 5xFAD mice (*n* = 13, 6 males), CLP290-treated 5xFAD mice (*n* = 16, 8 males), CLP290-treated NonTg mice (*n* = 13, 6 males), and vehicle-treated NonTg mice (*n* = 10, 3 males); and group 3 consisted of 9-month-old vehicle-treated 5xFAD mice (*n* = 10, 5 males) and CLP290-treated 5xFAD mice (*n* = 10, 5 males). One NonTg mouse (female) in group 1 became ill and died after completing the Morris water task (MWT), so only 13 NonTg mice were tested on subsequent behavioral tests. For the *in vivo* multi-unit electrophysiology, the group of mice tested consisted of 9-month-old CLP290-treated 5xFAD (*n* = 6, 3males) and vehicle-treated 5xFAD (*n* = 7, 3 males).

Drugs and viral constructs

The viral constructs were produced by the Canadian Neurophotonics Platform Viral Vector Core. The AAV2/9.CaMKIIa.SuperClomeleon (RRID: SCR_016477) was purified on an iodixanol gradient from cell culture at 1.8 x 10^{13} GC mL^{-1}.

CLP290 was dissolved in 20% 2-hydroxypropyl-ß-cyclodextrin (HPCD) at 10 mg mL-1. A fresh solution of CLP290 was prepared daily. The administration was performed *per os* (P.O.) by gavage 1-4 hours prior to the behavioral experiments or brain collection for histology or chloride imaging. A 20% HPCD solution was used as vehicle treatment. For the short-term treatment (group 1 and group 2), mice received a single dose of CLP290 (or Vehicle) daily for the duration of the behavioral testing. For the long-term CLP290 treatment (group 3), the mice received CLP290 or vehicle daily starting at 4 months of age and continuing until the completion of testing in the Morris Water Maze task at 9 months of age.

Stereotaxic surgeries and viral injections

For all surgeries, mice were anesthetized with 1.5-4 % isoflurane and placed in a stereotaxic apparatus (Stoetling Co.) on a heating pad.

For the *ex vivo* chloride imaging experiments, 100 nL of AAV2/9.CaMKIIa.SuperClomeleon was injected unilaterally into the mPFC at Rostro-Caudal (R/C) + 1.8 mm, Medial-Lateral (M/L) ± 0.3 mm and Dorso-Ventral (D/V) - 2.0 mm from Bregma of 3-month-old 5xFAD and NonTg or into the CA1 region of the dorsal hippocampus at R/C - 2.5 mm, M/L ± 2.0 mm and D/V - 1.4 mm of 5-month-old 5xFAD or NonTg mice using a glass capillary and a NANOLITER2020 injector (World Precision Instruments LLC). Imaging was performed 4 weeks after viral injection.

For the *in vivo* chloride imaging experiments, 300 nL of AAV2/9.CaMKIIa.SuperClomeleon was injected unilaterally into the prefrontal cortex at + 2.3 mm R/C, + 0.3 mm M/L and -1.5 mm D/V from Bregma of 3-month-old 5xFAD and NonTg mice, as described above. Imaging was performed, again, 4-weeks post viral injection.

For the *in vivo* electrophysiology experiments, mice were implanted with neocortical, hippocampal, and muscular electrodes made from Teflon-coated stainless steel wire. For neocortical local field potential (LFP) recording, bipolar electrodes (vertical tip separation = 0.6 mm, bare diameter 50.8 µm) were implanted in the left retrosplenial cortex (RSC) at R/C

-2.5 mm, M/L 0.7 mm and D/V -1.1 mm, and in the right barrel cortex at R/C -0.1 mm, M/L 3.0 mm and D/V -1.4 mm. For hippocampal LFP recording, a monopolar electrode (bare diameter 50.8 µm) was implanted in the CA1 region of the right hippocampus at R/C -2.5 mm, M/L 2.0 mm and D/V -1.1 mm. For electromyography (EMG) recording, a multi-stranded wire (gauge 40) was implanted into the neck musculature using a 25-gauge needle. The reference electrode was placed under the skull overlying the cerebellum. The exposed electrode wires were clamped between two receptacle connectors (Mill-Max Mfg. Corp.), and the headpiece and connectors were secured to the skull using C&B Metabond and dental cement. After the final recording, electrode tip positions were marked by passing current through the electrodes (0.1 mA for 5 seconds), and tip placement was verified by histology.

Preparation of brain slices

Mice were anesthetized with 30% urethane in saline, and the brain was dissected and immersed briefly in ice-cold cutting saline containing the following: 204.68 mM sucrose, 2.5 mM KCl, 1 mM $CaCl_2$, 2 mM $MgCl_2$, 1.25 mM NaH_2PO_4, 25 mM $NaHCO_3$, 25 mM Glucose, 0.4 mM Na-Ascorbate and 3 mM Na-Pyruvate. 300 µm coronal slices were obtained with a Leica vibratome. Slices recovered for 30 min at 32 °C in an immersion chamber in an oxygenated 1:1 mix of cutting saline and ACSF (126 mM NaCl, 5 mM KCl, 2 mM $CaCl_2$, 2 mM $MgCl_2$, 10 mM glucose, 26 mM $NaHCO_3$ and 1.25 mM NaH_2PO_4; pH 7.35 and 295 mOsm), followed by 30 min recovery at room temperature in an immersion chamber in oxygenated ACSF.

For the CLP290 experiments, slices were obtained 3 hours post CLP290 or Vehicle administration. Slices recovered for 15 min at 32 °C in an oxygenated 1:1 mix of cutting saline and ACSF followed by 15 min recovery at room temperature in oxygenated ACSF.

Ex vivo chloride imaging

Coronal brain slices expressing SuperClomeleon (Grimley et al., 2013) were transferred to a perfusion chamber and perfused with ASCF (2 mL min^{-1}) at room temperature. Fluorescence lifetime imaging microscopy (FLIM) was performed as previously described (Ferrini et al., 2013) using two optical setups, a Zeiss 880 laser-scanning microscope and a polygonal mirror Video-rate Microscopy System (VMS; Bliq Photonics) coupled with an 80 MHz femtosecond-pulsed Ti-Sapphire laser set at 800 nm. This excitation

wavelength was chosen to minimize the acceptor excitation. For the Zeiss microscope, FLIM images (1 per 10s) were acquired with a 20x Plan-Apochromat water immersion objective (Zeiss, 1.0 NA), and FLIM images were generated onto a TCSPC module PMC-100-1 detector (Becker & Hickl GmbH). For the VMS, images were acquired with a 16x objective (Nikon, 0.8 NA) and FLIM images (31 Hz) were generated onto a SPC-150N TCSPC module with a HPM-100-40 detector (Becker & Hickl GmbH). The VMS allowed concurrent intensity detection (Chroma ET473/24m (donor channel) and Chroma ET530/30x (green channel)). All FLIM acquisitions were achieved using a bandpass filter (Chroma, ET473/24m) to collect only the donor emission.

Fluorescence lifetime values of CaMKIIa positive neurons in layer 2/3 of the mPFC and the CA1 pyramidal layer of the hippocampus were acquired under three conditions: i) ACSF with low extracellular KCl (5 mM); ii) ASCF with low extracellular KCl (5 mM) and 5 µM bicuculline, 10 µM CQNX and 50 µM APV; and iii) ACSF with high extracellular KCl (15 mM) as well as bicuculline, CQNX and APV. For the CLP290 experiments, fluorescence lifetime values of CA1 pyramidal neurons were acquired under the same conditions within 5h following the CLP290 or vehicle administration. Each FLIM image corresponds to 10 seconds acquisitions. The experiment was divided into the three conditions described above. We acquired 2.5 minutes (15 images) using the ACSF with low extracellular KCl (5 mM); then either 15 minutes or 10 minutes of acquisition, for the mPFC and the CA1 experiments respectively (90 and 60 images), using ACSF with low extracellular KCl (5 mM) including blockers; and, finally, 15 min of acquisition using the ACSF with high extracellular KCl (15 mM) including blockers.

FLIM Analysis

For each acquisition, the user delineated cell bodies of neurons in individual regions of interests (ROIs). The instrument response function (IRF) was acquired by using an 80 nm gold nanoparticle to generate a second-harmonic signal. Using a custom script, the FLIM histogram was generated by pooling all the pixels in the ROIs for each timepoint. Every time point (10 seconds) of the experiment was fitted using a mono-exponential decay and the fluorescence lifetime (τ) was estimated. The IRF was taken into account during the fit.

For each neuron analyzed, a Hill-Slope was fitted into the temporal evolution of lifetimes to estimate the initial and final lifetime values (for 5 mM and 15 mM KCl ASCF, respectively). The maximum slope of the lifetime (units of ns per min) was estimated upon

15 mM KCl application using a plateau followed by an exponential plateau function. Neurons that did not have enough photons in the FLIM acquisition (300 photons), a stable lifetime during the 5 minutes before the potassium increase, or did not respond, meaning no significant increase of lifetime was observed after the potassium increase, were excluded from the analysis (32 and 93 NonTg neurons and 41 and 62 5xFAD neurons were excluded from the mPFC and the CA1 analysis, respectively). Fit examples can be seen in **Suppl. Figure 2.5**.

In vivo chloride imaging

Mice were anesthetized intraperitoneally with a mix of 100 mg ketamine, 15 mg xylazine and 2.5 acepromazine per kg, and placed in a head fixing microscope platform (Stoelting Co, Wood Dale, IL). The scalp was removed, and a chamber was formed using dental cement. The skull was thinned in a circle (a diameter of approximately 2 mm) above the prefrontal cortex using a dental drill and the remaining bone was removed with a 32G needle to open a cranial window over the imaged region. The chamber was filled with HEPES-buffered ACSF (126 mM NaCl, 2.5 mM KCl, 2 mM $CaCl_2$, 2 mM $MgCl_2$, 10 mM D-glucose and 10 mM HEPES; pH 7.0; 290 mOsm), and the dura was carefully removed.

After the surgery was completed, the mice were transferred under a multiphoton Video-rate Microscopy System (VMS; Bliq Photonics, Quebec City, QC) system. The tunable femtosecond Ti:sapphire laser (InSight® X3™, Spectra-Physics Inc) was set to 840 nm to excite Cerulean (CRF), the FRET donor of SuperClomeleon chloride sensor (13). The emitted CRF and YFP signals were separated by a long-pass dichroic mirror (Semrock, FF509-Di01). Additional band-pass emission filters were used for Cerulean (Chroma, ET480/40m) and YFP (Chroma, ET540/40m). A 40x NIR Apo water immersion objective (Nikon, 0.8 NA) was used for all imaging sessions Panoramic images of 1000 x 500 pixels at a rate of 32 Hz (video-rate) were acquired up to 200 µm in depth from the visible surface and with a pixel size of 0.204 µm. For each field of view, an image stack of 5 seconds acquisition, with approximately 160 frames was recorded.

In vivo ratiometric chloride analysis

Acquired image stacks of the in vivo chloride imaging, were registered with a custom MATLAB script implemented on the graphics processing unit (GPU) of a computer using the computer unified device architecture (CUDA) library as previously described (Wang et al.,

2018). The rigid body translation alignment based on the 2D cross-correlation used both YFP and CRF signals to correct excessive movement. The out-of-focus frames were automatically deleted during the registration. Following this, an average projection of the registered image stack was generated as the single representative images of the field. Rectangular ROI was assigned manually in the cytoplasm of individual visible neurons. A background ROI was defined in a region without any visible neurons. The average fluorescence intensity inside the ROIs was measured for YFP and CRF separately. The ratiometric chloride concentration of individual neurons, R (or FRET Ratio), was calculated using the formula $R = (YFP-YFP_b)/(CRF-CRF_b)$, where YFP and CRF are the fluorescence intensity values measured for each neuron, and YFP_b and CRF_b the fluorescence values in the background ROI from the same field. The neurons with low signal-to-noise ratio ($YFP/YFP_b < 5$ or $CRF/CRF_b < 5$) were excluded to ensure the consistency of the data. The dependency of the calculated FRET ratios on the laser intensity was validated by imaging the same ROIs in a field at varying laser powers (**Suppl. Figure 2.6 C**). The FRET ratio was independent of the laser intensity at a given imaging depth (**Figure. 2.2H**). Furthermore, the calculated mean imaging depth of the 5xFAD vs. NonTg mice was comparable and the depth distribution of the imaging fields for each mouse did not vary (**Suppl. Figure. 2.6 B**).

In vivo multi-unit electrophysiology

The setup for chronic multi-unit recording in freely moving mice consisted of a large plexiglass box, into which the lidless home cage was placed. A tethered recording probe connected to a commutator (NeuroTek, Inc.) was inserted into the implanted connector. After at least 1 week of recovery post-surgery, mice were habituated to the recording setup and probe for 5 days, with the habituation time gradually increasing from 1 to 3 hours per day. After habituation, LFP/EMG activity was recorded on 3 consecutive days for 3 hours per day, at approximately the same time each day. All habituation/recording was conducted during the light phase. Recordings were conducted longitudinally at 6 and 9 months of age in mice that received long-term daily treatment with CLP290 or vehicle starting from 4 months of age, including on habituation/recording days. On those days, drug administration was performed immediately before the start of habituation/recording.

LFP/EMG activity was amplified, filtered (0.1-4000 Hz) and digitized at 16 kHz using a Digital Lynx SX Electrophysiology System (Neuralynx, Inc.). Data were recorded and stored on a local computer using Cheetah software (Neuralynx, Inc.). Analysis was performed offline. Sleep scoring was performed in 6-second intervals to define periods of

wakefulness, rapid eye movement (REM) sleep, and non-REM (NREM) sleep. For sleep scoring, the raw EMG activity was filtered (90-1000 Hz), rectified and integrated using a 4-second moving window, and thresholded to detect periods of mobility. Power in the slow wave/delta band (0.5-4 Hz) was calculated for the RSC LFP signal and thresholded using values between 0.04-0.1 mV2/Hz (depending on the mouse) to detect slow-wave activity. NREM sleep was scored when the mouse was immobile and exhibited slow-wave activity. For detecting REM sleep, the ratio of theta power (6-10 Hz) to total power of the hippocampal LFP signal was calculated. When this ratio was above 0.4-0.6 (depending on the mouse) and the mouse was immobile, REM sleep was scored. All remaining periods were considered wakefulness. After sleep scoring, spectral power of the neocortical and hippocampal LFP signals during NREM sleep was calculated for different frequency bands (30-60, 60-120, and 120-200 Hz) using Welch's method. Sleep structure (i.e., the percentage of total recording time spent in each state) and spectral power were averaged across the 3 recording days for each mouse.

Immunohistochemistry

Mice were anesthetized with 30% urethane in saline and perfused intracardially with 0.1 M PBS followed by 4% paraformaldehyde in PBS. Brains were dissected and stored in the same fixative for 15 hours and cryoprotected in 30% sucrose in 0.1 M PBS after. Coronal slices of the mPFC and the hippocampus were cut at 40 µm on a Leica vibratome and permeabilized in PBS with 0.2% Triton X-100 (3 x 10 min). Sections were incubated for 15 hours with the primary antibody (rabbit polyclonal KCC2, 1:1000, Millipore catalog # 07-432) diluted in PBS (with 0.2% TritonTM X-100) containing 4% normal goat serum (Sigma catalog # S26-100ML). After washing in PBS, slices were incubated for 2 hours at room temperature with the secondary antibody conjugated with the desired fluorochromes (Cy3-conjugated goat anti-rabbit, 1:500, Jackson Labs catalog # 111-165-003). Finally, slices were rinsed in PBS (3 x 10 min), mounted on slides (SuperfrostTM Plus Microscope Slides, Thermo Fisher Scientific catalog # 12-550-15) and cover-slipped using an aqueous antifade mounting media (Abcam catalog # ab104139). Negative control staining was performed by incubating sections with only the secondary antibody following the same protocol (**Suppl. Figure. 2.7 A).**

Confocal microscopy and images acquisition

Confocal images were acquired with a Zeiss LSM710 laser scanning microscope using a MBS 405/488/555/639 beam splitter or a Zeiss LSM880 laser scanning microscope using a MBS 488/555/639 beam splitter and the same oil immersion objective (Plan-Apochromat 63x/1.4 Oil DIC). Each channel was imaged sequentially to avoid crosstalk and unique emission filters were used for each fluorophore. The laser power and the PMT (Photo-Multiplier Tube) voltage were set to optimal values to limit pixel saturation and avoid excessive photobleaching. The laser power, polarization voltage, filters, dichroic mirrors, and scan speed were kept constant for each unique dataset and between controls and comparable samples to ensure a valid comparison for the pixel intensity analysis of KCC2 expression. Images were acquired at 12 bits and 2048x2048 pixels 0.103 um with pixel size.

Global KCC2 intensity and KCC2 sub-cellular profile analysis

Fluorescence confocal images of the mPFC layer II/III and the CA1 of the hippocampus were acquired. To quantify the global intensity of KCC2 expression in the brain regions of interest, we manually outlined the ROIs and quantified the mean fluorescence intensity within each ROI. The intensity of the immunostaining background noise was defined for several ROIs where KCC2 is known to be absent (i.e. the bundle of fibers in the forceps minor of the corpus callosum; **Suppl. Figure. 2.7B**) and subtracted from the KCC2 mean intensity values of each ROI as previously described (Ferrini et al., 2020; Lorenzo et al., 2020). We compared the global intensity of at least 8 images per animal, for several animals per condition for each distinct dataset.

A custom MATLAB algorithm, coined MASC-π (Ferrini et al., 2020), was utilized to perform the membrane analysis of subcellular intensity as previously described (Dedek et al., 2019). Briefly, for each confocal image acquired the membrane of randomly and blindly selected neurons (for which a continuous membrane across the entire cell body circumference was identified) was manually delineated. For each pixel in the ROIs defining individual neurons, the distance to the closest membrane segment was calculated to generate a distance map with the neuronal membrane defined as zero (**Figure. 2.1I**). The mean intensity per pixel and the standard deviation of the KCC2 fluorescence was computed as a function of the distance to the membrane. This approach provides an unbiased estimate of the membrane KCC2 expression and excludes any potential effect of neuronal loss in the measurement of KCC2 protein levels within the brain regions of interest.

Morris water task

The test was performed in a circular tank (154 cm in diameter, 50 cm deep), with three distinct visual cues placed outside the tank to facilitate spatial navigation. The tank was filled with water (22 ± 1 °C) to a height of 40 cm. Non-toxic white tempera paint was added to the water to make it opaque. A hidden escape platform (11 cm in diameter) was situated 1 cm below the surface of the water in one of the tank quadrants. The location of the platform remained fixed throughout training. For acquisition training, mice performed 4 trials per day for 8 consecutive days. On a given day, mice were released into the pool from each of the 4 cardinal directions, with the order of the start locations pseudo-randomly determined. A trial was terminated when the mouse located the hidden platform, after which the mouse was left on the platform for 10 s before being removed from the tank. If a mouse did not locate the platform within 60 s, a maximum latency score was assigned, and the mouse was guided to the platform. On the 9th day, 24 h after the completion of acquisition training, a probe test was conducted. This consisted of a single 60 s trial with the platform absent from the tank. Tracking software (Water 2100, HVS Image) was used to quantify the following measures for each acquisition training day: average latency to find the platform, average path distance to the platform, and average swim speed. For the probe test, the average proximity to the platform's previous location was measured.

Unconditioned social preference

The unconditioned social preference test was based on a three-chamber task, with two side compartments (35 x 20 cm) with differently colored walls (one with black walls and the second with white walls), separated by a smaller middle compartment with large horizontal white and black gratings on its walls. Mice were allowed to explore freely the three-chamber apparatus containing an inverted metallic cup in each large compartment for 10 min prior testing to habituate with the new environment. After, a sex- and age-matched conspecific was placed in one of the two inverted cups and an object in the other. The test mouse was then transferred to the apparatus and left to explore the compartments for an additional 10 min. The test mice were assigned to a random testing order. Movement was recorded by a camera located on the top of the apparatus and analyzed offline by ANY-maze (Stoetling Co.). Behavioral analysis was performed blind to the treatment. The times in the social and neutral chambers were calculated as the time spent by the test mouse in the compartment containing the social partner and the time spent in the object (neutral) compartment, respectively.

Statistical analysis

The statistical analysis was performed with GraphPad Prism 9 (GraphPad software, San Diego, CA). The two-group null-hypothesis significance was tested with Student's t-test and the normality of the samples' distributions was tested with an Anderson-Darling or a Shapiro-Wilk test. One-way analysis of variances (ANOVA) was used to analyze the difference of independent groups followed by a Fisher's LSD test. Multi-group designs with two categorical variables were analyzed by two-way ANOVA with a *post hoc* Tukey test for multiple comparisons. A repeated-measures ANOVA with a Dunnett's post-hoc comparison was utilized to compare values obtained from the same subjects at different time points. For the datasets not showing a normal distribution, differences between groups were tested with a Mann-Whitney non-parametric test. Data are reported as mean ± SEM with N (or n) indicating the number of mice, unless otherwise specified. P values < 0.05 were considered statistically significant.

Data availability

All data supporting the findings of this study are presented within the paper and the Supplementary Material files. Data supporting Figures 1- 4 and Supplementary Figs. 1-13, are available as Source Data File. Other data necessary to interpret and replicate the findings and methods of this article are available upon request. Codes and custom software/algorithms are available upon request.

2.5 Results

KCC2 is downregulated in the medial prefrontal cortex and the hippocampus of 5xFAD and APP^{NL-G-F} mice

In brains from 2-, 4- and 6-month-old 5xFAD mice and their age-matched non-transgenic littermates (NonTg), we measured via immunohistochemistry global and membrane KCC2 expression in both the mPFC layer II/III and the hippocampal CA1 pyramidal layer. We found that KCC2 global labeling intensity was reduced in layer II/III of the mPFC at all ages (**Figure. 2.1A** and **2.1B**), while membrane KCC2 was significantly reduced in 4- and 6-month-old, but not 2-month-old, 5xFAD mice compared to NonTg (**Figure 2.1A** and **2.1C**). In the hippocampal CA1, both global and membrane KCC2 levels were reduced at 6 months (**Figure 2.1D**, **2.1E** and **2.1F**) but not 4 months in 5xFAD mice (**Figure 2.1E** and **2.1F**). Comparable downregulation of KCC2 was observed in 9-month-old

APP^{NL-G-F} mice for both the mPFC and the CA1 (**Figure 2.1G and 2.1H**). In contrast, when we measured global and membrane KCC2 levels in the nucleus accumbens, a region with lower Aβ plaque load compared to the neocortex and hippocampus, at 6 months of age (Oblak et al., 2021), there was no KCC2 reduction in the 5xFAD mice as compared to NonTg mice (**Suppl. Figure 2.8**). In addition, we quantified the mean area of the individual neurons we analyzed, and we did not find any difference in neuronal surface area that could account for the decrease in KCC2 membrane expression (**Suppl. Figure 2.9**).

We also measured the levels of KCC2 protein and of soluble Aβ42 in frontal lobe samples from 2-, 4- and, 6-month-old 5xFAD and NonT mice. We found that the levels of soluble Aβ42 increase while KCC2 levels decrease with age in the 5xFAD mice, but not in NonTg mice (**Suppl. Figure 2.10A** and **2.10B**). At 6-months of age, KCC2 levels were negatively correlated to the levels of Aβ 42 (**Suppl. Figure 2.10C**). We finally found a significant reduction in the membrane KCC2 levels in neurons incubated with 10 μM Aβ42 as compared to neurons incubated with scramble (**Suppl. Figure 2.11**) suggesting that KCC2 downregulation is downstream the amyloid pathology.

Impaired neuronal chloride extrusion capacity in 5xFAD mice

To test for accompanying deficits in neuronal chloride extrusion capacity, we virally transduced the Cl^- sensor SuperClomeleon (Grimley et al., 2013) under the CaMKIIa promoter in 5xFAD and NonTg mice, targeting the mPFC and hippocampal CA1 in 4-month-old and 6-month-old mice, respectively (**Suppl. Figure 2.5A**, **2.5B**, **2.5D** and **2.5E**). In brain slices taken from these mice we performed time-resolved FRET measurements of Cl^- while we stepped extracellular K^+ ($[K^+]_e$) from 5 to 15 mM (**Figure 2.2A**, **2.2B**, **2.2D** and **2.2E** and **Suppl. Figure 2.5C** and **2.5F**) to reverse the KCC2 transporter. The rate of Cl- accumulation resulting from the raised $[K^+]_e$ was significantly slower in the mPFC of 4-month-old 5xFAD mice compared to NonTg mice (**Figure 2.2C**) and at 6 months in the CA1 (**Figure 2.2F**), reflecting weaker Cl^- transport capacity in the 5xFAD mice. We did not observe a difference in the diameter of neurons following the increase in extracellular K^+ which could suggest a neuronal volume change accommodating the Cl- influx (**Suppl. Figure 2.12**). Also, to ensure the difference measured was not due to an effect of the slice preparation, we performed SuperClomeleon-based ratiometric measurements of $[Cl^-]_i$ *in vivo* (**Figure 2.2G** and **2.2H**) in the prefrontal cortex of NonTg and 5xFAD mice (**Suppl. Figure 2.6A**). We found that the median FRET ratio of pyramidal neurons from 5xFAD mice was significantly lower as

compared to NonTg neurons, indicating higher $[Cl^-]_i$ (**Figure 2.2l**), while the estimated imaging depth did not differ between 5xFAD and NonTg mice (**Figure 2.2l**).

Short-term CLP290 treatment improves memory retention and social behavior in 5xFAD mice

Previous reports identified the CLP257 family of drugs, including CLP290, as KCC2 enhancers (Gagnon et al., 2013) which effectively restore KCC2 expression in various pathological conditions (Chen et al., 2017; Ferrini et al., 2017; Lorenzo et al., 2020; Sullivan et al., 2021). To validate whether CLP290 can enhance membrane KCC2 levels in 6-month-old 5xFAD mice, we analyzed global and membrane KCC2 expression in the mPFC, as described above (**Figure 2.3A**). Short-term daily treatment with CLP290 (100 mg kg^{-1}) significantly increased global and membrane KCC2 in 5xFAD mice as compared to vehicle-treated mice (**Figure 2.3B**). Acute treatment of hippocampal neurons with 1μM CLP257 also restored membrane KCC2 after its reduction by Aβ42 (**Suppl. Figure 2.11**).

Having verified that CLP290 can restore KCC2 levels in 5xFAD mice, we next tested whether CLP290 also rescues behavioral function in these mice. Vehicle- and CLP290-treated 5xFAD mice were tested for spatial and non-spatial memory, anxiety-like behavior, and social behavior (**Figure 2.3C**). Vehicle-treated NonTg mice were also tested, to verify that 5xFAD mice are impaired in the tests used. In the MWT, a test of spatial learning and memory, all groups showed a comparable learning curve during the acquisition phase, with performance improving across days (**Figure 2.3D**). Averaging across all days, the NonTg mice performed significantly better than both 5xFAD groups, and there was no significant difference between the vehicle- and CLP290-treated 5xFAD mice. The swim speed during the acquisition phase was not significantly different between the three groups (**Suppl. Figure 2.13A**). On the following probe test, the vehicle-treated 5xFAD mice performed significantly worse than the NonTg mice, searching further away from the platform's previous location, indicating a spatial memory impairment, and CLP290 treatment significantly reduced this spatial memory deficit (**Figure 2.3E** and **2.3F**).

In tests of cued and contextual fear memory, we also observed a significant impairment in the 5xFAD mice, with the 5xFAD mice exhibiting less freezing than the NonTg mice, suggesting worse memory (**Suppl. Figure 2.13B**). However, unlike the spatial memory impairment in the MWT, this fear memory impairment was not improved by CLP290 treatment.

In the elevated plus-maze (EPM) test of anxiety-like behavior, the ratio of time spent in the open arms to the closed arms was significantly lower in the NonTg mice than the

vehicle-treated 5xFAD mice but not the CLP290-treated 5xFAD mice, although the vehicle- and CLP290-treated mice did not differ significantly (**Suppl. Figure 2.13C**). The total number of arm entries was comparable between all the groups (**Suppl. Figure 2.13C**). In the three-chambered unconditioned social preference task, NonTg mice showed a significant preference for the social chamber over a neutral chamber, but the vehicle-treated 5xFAD mice did not (**Figure 2.3G** and **2.3H**). CLP290 treatment restored the social preference in the 5xFAD mice (**Figure 2.3G** and **2.3H**). As early as 4 months of age, the 5xFAD mice display social preference deficits in this unconditioned behavioral paradigm, as compared to age-matched NonTg mice (**Suppl. Figure 2.13D**). When we measured the maximum speed and the distance travelled during the social preference test, there were no significant differences between the three groups, suggesting that there are no motor deficits in 5xFAD mice (**Suppl. Figure 2.13E**). CLP290 did not alter social preference in NonTg mice, as expected (**Suppl. Figure 2.13F**). In conjunction with our histological data showing a KCC2 deficit already at 4 months of age in the mPFC of 5xFAD mice (**Figure 2.1B** and **2.1C**), these results suggest that social preference deficits may be an early behavioral sign of Cl- transport dysregulation in the mPFC. In contrast, the lack of reported spatial memory deficits in 5xFAD mice at 4 months of age (Richard et al., 2015) is consistent with our finding of lack of KCC2 in the hippocampus at that age in 5xFAD mice (**Figure 2.1E** and **2.1F**).

Long-term CLP290 treatment prevents cortical hyperactivity and spatial learning deficits in 5xFAD mice

Finally, we asked whether long-term treatment with CLP290 is sufficient to prevent KCC2 downregulation, as well as cortical hyperactivity and spatial learning and memory deficits measured late in the progression of the disease. 5xFAD mice were treated daily with CLP290 or vehicle, beginning at 4 months of age. At 6 months, this treatment had effectively protected against KCC2 downregulation in the mPFC (**Suppl. Figure 2.14**) but did not decrease the number or size of plaques (**Suppl. Figure 2.15**). In another experiment, mice were treated daily for 5 months, and their spatial learning and memory was assessed at 9 months of age in the MWT. The swim speed during the acquisition phase was not significantly different between the CLP290- and vehicle-treated groups (**Suppl. Figure 13E**). Even at this late stage of disease, the 5xFAD mice were able to acquire the task, with performance improving significantly from the first day to the final day in both groups (**Figure 2.3I**). We noted that the performance of the two groups converged by day 5 of acquisition, with both groups maintaining a fairly stable plateau thereafter. Therefore, we focused our analysis on the early phase of acquisition (days 1-4). Averaging across days, spatial learning

was significantly better in the CLP290-treated mice relative to the vehicle-treated mice, in terms of both path length and latency (**Figure 2.3I** and **Suppl. Figure 2.13G**). Examining within groups, performance in the CLP290 group showed a significant improvement by day 2 of acquisition, whereas the vehicle group showed no significant improvement even by day 4. On the probe test, there was no significant difference between groups, consistent with the convergent performance of the two groups across the late phase of acquisition training (**Figure 2.3I**). In summary, even at an advanced stage of disease progression, long-term CLP290 treatment was effective at preventing spatial learning impairments.

Another group of mice was also treated daily with CLP290 or vehicle for 5 months, up to 9 months of age. Spontaneous multi-unit activity in the neocortex and hippocampus was recorded longitudinally at 6 and 9 months while the mice were freely moving in their home cages (**Figure 2.4A** and **2.4B**). At 6 months, there was no significant difference between the vehicle- and CLP290-treated mice in the power of gamma (30-120 Hz) or high-frequency (120-200 Hz) oscillations in the RSC during NREM sleep. However, by 9 months of age, gamma and high-frequency power were significantly greater in the vehicle-treated mice than the CLP290 treated mice (**Figure 2.4C**). Similar results were observed in the barrel cortex, though the effects were less pronounced and did not reach statistical significance at 9 months (**Suppl. Figure 2.16**). The greater effect in the RSC could be due to this region's status as part of the brain's default mode network. This network exhibits elevated activity at rest, which has been linked to increased regional Aβ concentrations and plaque deposition (Bero et al., 2011). In the hippocampus, a significant interaction between age and CLP290 treatment was observed for the high-frequency band but not for gamma power (**Figure 2.4D**). Long-term CLP290 treatment did not affect the sleep structure of the mice (**Suppl. Figure 2.17).** These results suggest that long-term CLP290 treatment prevents the age-dependent emergence of cortical hyperactivity in 5xFAD mice.

2.6 Discussion

We present evidence for KCC2 hypofunction in the mPFC and CA1 of both 5xFAD and APP^{NL-G-F} mice, which contributes to cognitive and social dysfunctions. This KCC2 hypofunction appears to be downstream to amyloid-β accumulation, and is consistent with reports associating Aβ with deficits in inhibition (Palop and Mucke, 2016). Indeed, soluble Aβ has been reported to induce cortical (Busche et al., 2015) and hippocampal hyperactivity (Busche et al., 2012) due to disrupted inhibitory input (Verret et al., 2012). The conclusion

that KCC2 hypofunction is downstream of Aβ accumulation is consistent with several lines of evidence from clinical research suggesting that Aβ pathology is not directly responsible for producing the cognitive decline associated with AD (Erten-Lyons et al., 2009; Lacoursiere et al., 2022). First, deposition of Aβ pathology in the brain begins long before cognitive symptoms become pronounced (Perrin et al., 2009; Sperling et al., 2014). Second, some people exhibit abundant Aβ pathology with no detectable cognitive impairment (Crystal et al., 1988). Third, treatments that effectively reduce amyloid in the brain have largely proven ineffective at reversing cognitive symptoms and disease progression (Egan et al., 2018; Honig et al., 2018; Salloway et al., 2014). These findings suggest that Aβ initiates a pathological process that, once sufficiently advanced, can no longer be reversed by targeting Aβ itself. This is a key reason why it is necessary to develop treatments that target components of the cascade downstream of Aβ, such as KCC2.

The global increase in the power of gamma and high-frequency oscillations during NREM sleep shown here are conforming with observations of elevated gamma power in the neocortex or hippocampus of other AD-like transgenic lines (Gurevicius et al., 2013; Ittner et al., 2014; Palop and Mucke, 2016) and in patients (Van Deursen et al., 2008), and with impaired inhibitory function resulting from diminished KCC2. Our findings of cognitive deficits are also consistent with the observation that loss of LTP specificity in aging is directly associated with diminished KCC2, which confounds synapse specificity of LTP (Ferando et al., 2016). While impaired Cl^- homeostasis by itself can be a substrate of the hyperexcitability associated with some AD syndromes through both disinhibition (Doyon et al., 2016) and ensuing enhanced NMDA receptor function (Hildebrand et al., 2016), elevated neural activity has been reported, in turn, to reduce KCC2 function (Rivera et al., 2004). This positive feedback loop has the potential for yielding an unclamped spiral of escalating hyperexcitability, eventually resulting in excitotoxicity. Attempting to restore Cl^- homeostasis through blocking the Cl^- importer NKCC1 in AD (Taubes et al., 2021) appears a less promising target, first because it is not brain-specific, but more importantly because it does not restore Cl^- extrusion capacity from the cells and thus does not protect the cells from Cl^- loads nor spatially constrain inhibition (Cordero-Erausquin et al., 2005; Doyon et al., 2011, 2016; Ferrini et al., 2020; Lorenzo et al., 2020).

2.7 Acknowledgments

The authors thank Di Shao and Cesar Benavente for animal husbandry and genotyping, and Emily Hagens, Sophia Fraser, Audrey Golsteyn, Farhanuddin Mohammed, Louisabelle Gagnon and Catherine Couture for assistance with drug treatments and behavioral experiments. The authors also thank Takashi Saito and Takaomi C. Saido (RIKEN Center for Brain Science, Japan) for providing the $APP^{NL-G-F/NL-G-F}$ knock-in mice used to establish a colony at the CCBN.

Funding:

Weston Brain Institute Transformation Research grant TR192089 (MHM, YDK)

Canadian Institutes of Health Research (CIHR) grant FDN - 159906 (YDK)

Canada Research Chair program (YDK)

Canadian Institutes of Health Research (CIHR) grants 390930 and 156040 (MHM)

Fonds de recherche du Québec – Santé (FRQ-S) Junior 1 Scholar, 269555 (AGG)

Sentinel North Partnership Research Chair on Probing Life and the Environment with Light (AGG)

Natural Sciences and Engineering Research Council of Canada (NSERC) grant 06507 (AGG)

Norampac Research grant on Alzheimer's and Related Diseases through Laval University (IK)

Fondation de la famille Lemaire Research grant on Alzheimer's and Related Diseases through Laval University (IK)

NSERC Postdoctoral Fellowship (BBM)

2.8 Author Contributions

Iason Keramidis and Brendan B McAllister contributed equally to this study.

Conceptualization: IK, BBM, AGG, MHM, YDK

Methodology: IK, BBM, JB, FW, AB, LF, AGG, MHM, YDK

Investigation: IK, BBM, JB, FW, DI, RS, PD, JPH, MN, SI, AB, LF

Visualization: IK, BBM, AGG, YDK

Funding acquisition: MHM, YDK

Supervision: AGG, MHM, YDK

Writing – original draft: IK, BBM, YDK

Writing – review & editing: IK, BBM, FW, AGG, MHM, YDK

Competing interests: The authors declare no competing interests.

2.9 Figures

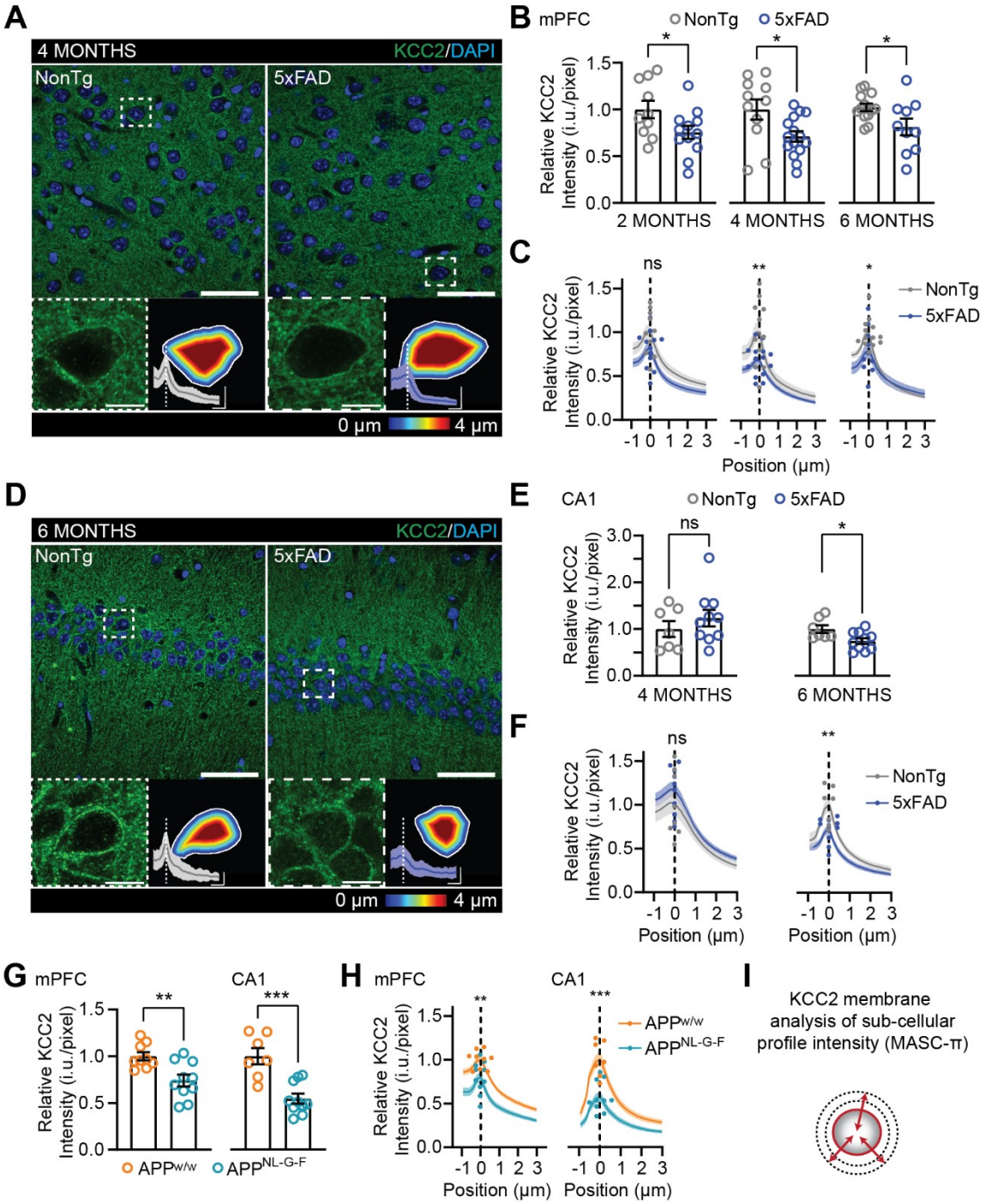

Figure 2.1. Changes in global and membrane KCC2 expression in the mPFC and hippocampal CA1 regions of 5xFAD and APP^{NL-G-F} mice

(**A** and **D**) Confocal images showing KCC2 immunostaining in mPFC LII/III (**A**) and the CA1 (**D**) of 5xFAD vs. NonTg mice (KCC2 in green, DAPI in blue; Scale bar: 50 µm). Insets show KCC2-expressing neurons from ROIs (Scale bar: 10 µm). On the right, examples of KCC2 sub-cellular profile

intensities. The color-coded maps illustrate the distance from the membrane. The graphs represent the KCC2 intensity as a function of the distance to the membrane (Scale bars: vertical 1000 intensity units, horizontal 2 µm). (**B** and **E**) Global index KCC2 analysis of the mean KCC2 pixel intensity in mPFC LII/III of 2-, 4- and 6-month-old 5xFAD vs. NonTg mice (**B**) and the CA1 of 4- and 6-month-old 5xFAD vs. NonTg mice (E). (**C**) Mean KCC2 intensity profiles across the plasma membrane of individually identified 5xFAD (blue) and NonTg (gray) neurons in the mPFC (5xFAD: n_2 = 1163, n_4 = 1537, n_6 = 912, from N_2 = 12, N_4 = 15, N_6 = 10 mice, respectively; NonTg: n_2 = 932, n_4 = 1164, n_6 = 974 neurons from N_2 = 10, N_4 = 11, N_6 = 13 mice, respectively). (**F**) KCC2 subcellular intensity profile of individual neurons from 5xFAD (blue) vs. NonTg (gray) mice in the CA1 (5xFAD: n_4 = 625, n_6 = 608 from N_4 = 10 and N_6 = 10 mice, respectively; NonTg: n_4 = 360, n_6 = 523 from N_4 = 8 and N_6 = 7 mice, respectively). (**G**) Pixel intensity of KCC2 immunostaining in 9-month-old $APP^{NL\text{-}G\text{-}F}$ vs. $APP^{w/w}$ mice in the mPFC (left) and the CA1 (right). (H) Average KCC2 intensity profiles in $APP^{NL\text{-}G\text{-}F}$ (cyan) vs. $APP^{w/w}$ (orange) mice in the mPFC (left) and CA1 (right) ($APP^{NL\text{-}G\text{-}F}$: n_{mPFC} = 742 and n_{Ca1} = 746 neurons from N_{mPFC} = 10 and N_{CA1} = 10 mice, respectively; $APP^{w/w}$: n_{mPFC} = 880, n_{CA1} = 594 neurons from N_{mPFC} = 10 and N_{CA1} = 7 mice, respectively). (**I**) Scheme of the KCC2 membrane analysis of subcellular profile intensity (MASC-π). Circles in **B**, **E** and **G** represent single mice. Data are presented as mean ± SEM. * P < 0.05; ** P < 0.01 & ***P < 0.001; ns = non significant.

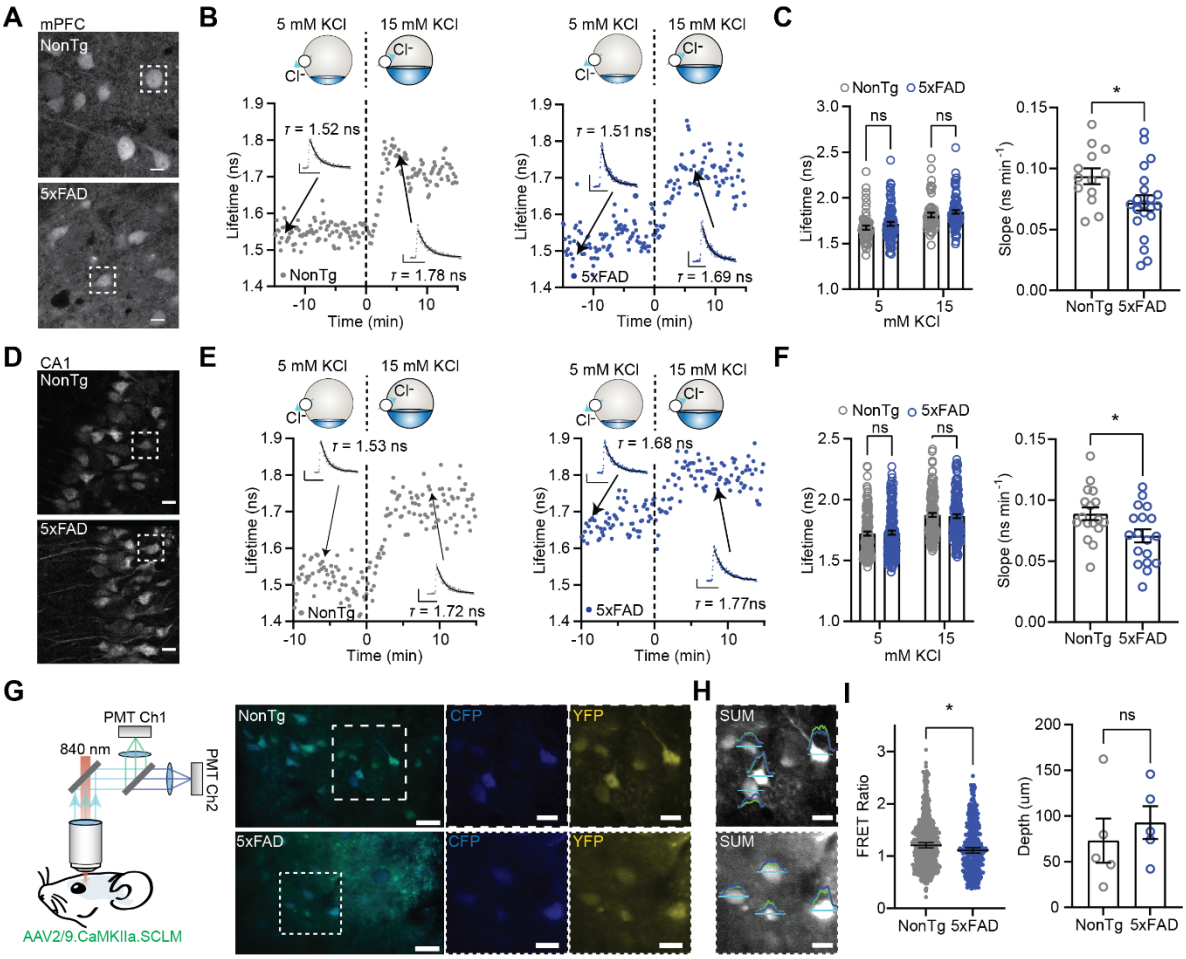

Figure 2.2. Impaired chloride transport in 5xFAD mice

(**A** and **D**) FLIM images of 5xFAD and NonTg CaMKIIa-positive neurons expressing SuperClomeleon in mPFC (**A**) and hippocampal (**D**) slices (Scale bars: 10 µm). (**B**) Timelapse recording of Cl^- accumulation in the cell body of selected NonTg (gray) and 5xFAD (blue) neurons from the ROI in **A** upon 15 mM KCl extracellular application (dashed line). Insets show examples of fitted photon-distribution histograms during the low KCl condition (left) and upon 15 mM KCl application (right). Scale bars: vertical, 50 photons; horizontal, 5 ns. (C) The mean lifetime of NonTg and 5xFAD neurons during the baseline condition (5 mM KCl) and upon 15 mM KCl application (left; 5xFAD: n = 105 neurons from N = 10 mice; NonTg: n = 58 neurons from N = 7 mice). The rate of Cl- changes measured in 4-month-old 5xFAD and NonTg mPFC slices (right; 5xFAD: n = 21 slices from N = 10 mice; CTRL: n = 13 slices from N = 7 mice). (**E**) Timelapse recording of Cl- transport to the cell body of NonTg and 5xFAD CA1 neurons within ROIs shown in **D**. Insets display photon-distribution histogram examples at 5 mM (left) and 15 mM KCl (right). Scale bars: vertical, 50 photons; horizontal, 5 ns. (**F**) On the left, the average lifetime of 5xFAD vs. NonTg CA1 neurons at 5 mM and 15 mM

extracellular KCl (5xFAD: n = 133 neurons from N = 6 mice; NonTg: n = 122 neurons from N = 5 mice). On the right, the average rate of Cl^- changes measured in 6-month-old 5xFAD and NonTg hippocampal slices (5xFAD: n = 18 slices from N = 6 mice; NonTg: n = 17 slices from N = 5 mice). (**G**) Graphical illustration of the SuperClomeleon in vivo steady state imaging experimental setup, and representative images of the mean intensity of YFP and Cerulean merged (left) and split for the areas selected in dashed squares (right) in the prefrontal cortex of 4-month-old 5xFAD and NonTg mice (Scale bars: 20 µm and 10 µm for the selected areas). (**H**) Images of the sum of the CFP and YFP fluorescence intensity of the selected areas in (**G**) and intensity profiles of CFP (blue) and YFP (green) for the lines in cyan. (**I**) The median FRET ratio of 5xFAD vs. NonTg neurons (left; 5xFAD: n = 361 neurons from N = 5 mice; NonTg: n = 638 neurons from N = 5 mice) and the estimated mean depth of imaging (µm; right). * $P < 0.05$; *** $P < 0.001$; ns = non significant.

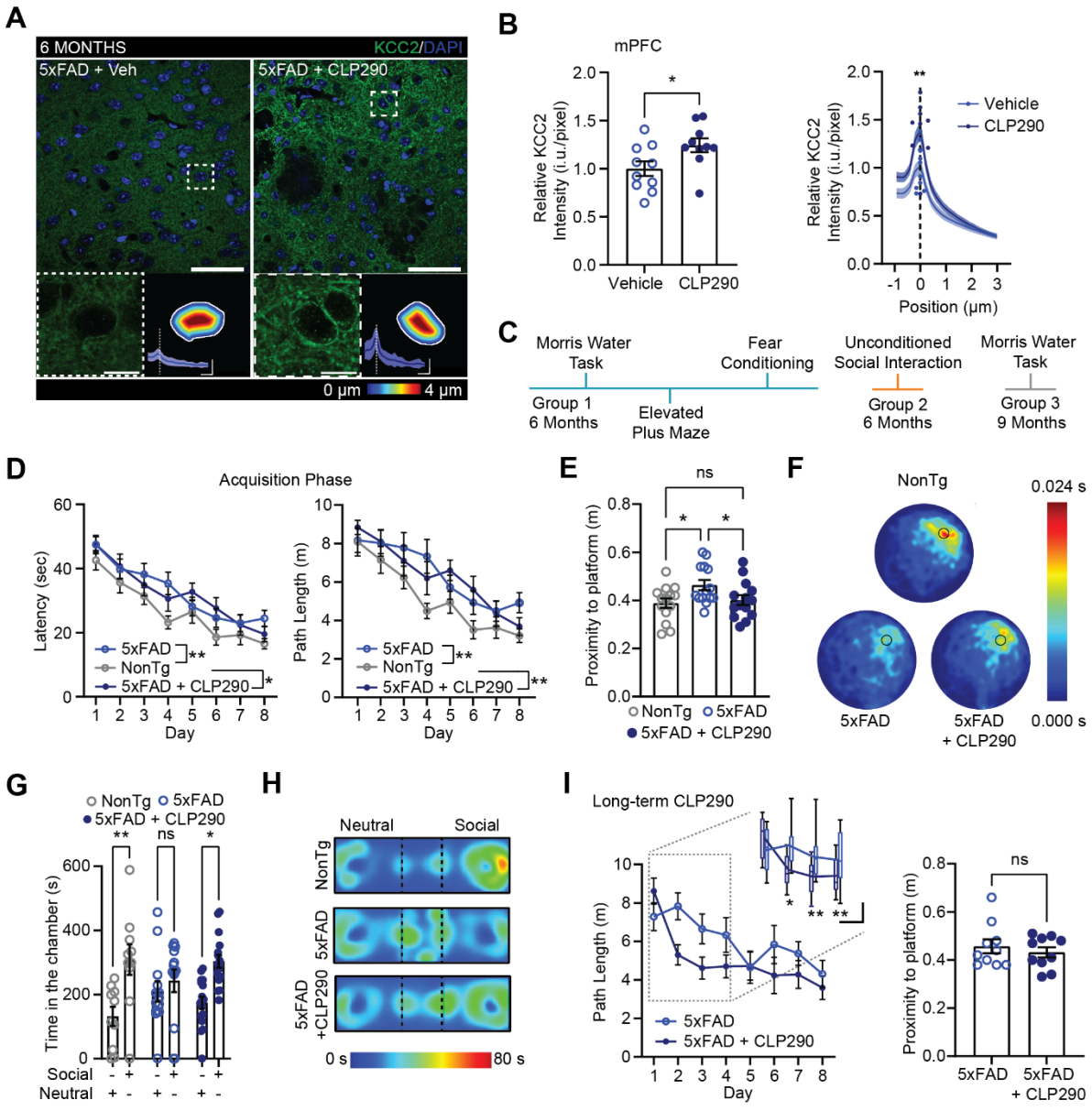

Figure 2.3. CLP290 enhances membrane KCC2 in 5xFAD mice and augments memory retention and social behavior

(**A**) Confocal images of mPFC slices stained for KCC2 from CLP290 vs. Vehicle treated 5xFAD mice (KCC2 in green, DAPI in blue; Scale bar: 50 µm). Insets show KCC2-stained neurons from ROIs (Scale bar: 10 µm). Color-coded maps illustrate the distance from the membrane and graphs represent the subcellular KCC2 intensity profile (Scale bars: vertical 1000 intensity units, horizontal 2 µm). (**B**) On the left, the mean global index KCC2 pixel intensity and on the right the mean KCC2 intensity profiles across the plasma membrane of CLP290- (blue circles; n = 919 neurons from N= 9 mice) and Vehicle-treated (filled dark blue dots; n = 985 neurons from N = 10 mice) 5xFAD mice. (**C**)

The chronological order of behavioral testing for the three CLP290 and Vehicle-treated experimental groups. (**D**) Learning curves measured by the latency to the platform (left) and the path length (right) during the acquisition phase of the Morris water task (MWT) in NonTg Vehicle-treated mice and CLP290- and Vehicle-treated 5xFAD mice. (**E**) The average proximity to the platform's previous location during the MWT probe trial. (**F**) Heat maps indicating the average time spent in each spatial bin (bin size = 1 cm2) during the probe trial of the MWT. The black circle in the top right quadrant represents the platform's position during acquisition training. (**G**) The time spent in the social vs. neutral chamber during the unconditioned social interaction test. (**H**) Heat maps representing the location of the animal's head during the social interaction test. (**I**) The swim path length during the acquisition phase of the MWT (left), and the average proximity to the platform's previous position during the probe trial test (right) of 9-month-old 5xFAD mice chronically treated with CLP290 vs. Vehicle. Inset shows the learning curve for the 4 first days of the acquisition phase (box-whisker plots with the 5-95 percentile; scale bars: vertical 2 m; horizontal: 1 day). Circles or dots in **B**, **E**, **G** and **I** represent single mice. Data are presented as mean ± SEM. * $P < 0.05$ & ** $P < 0.01$; ns = non significant.

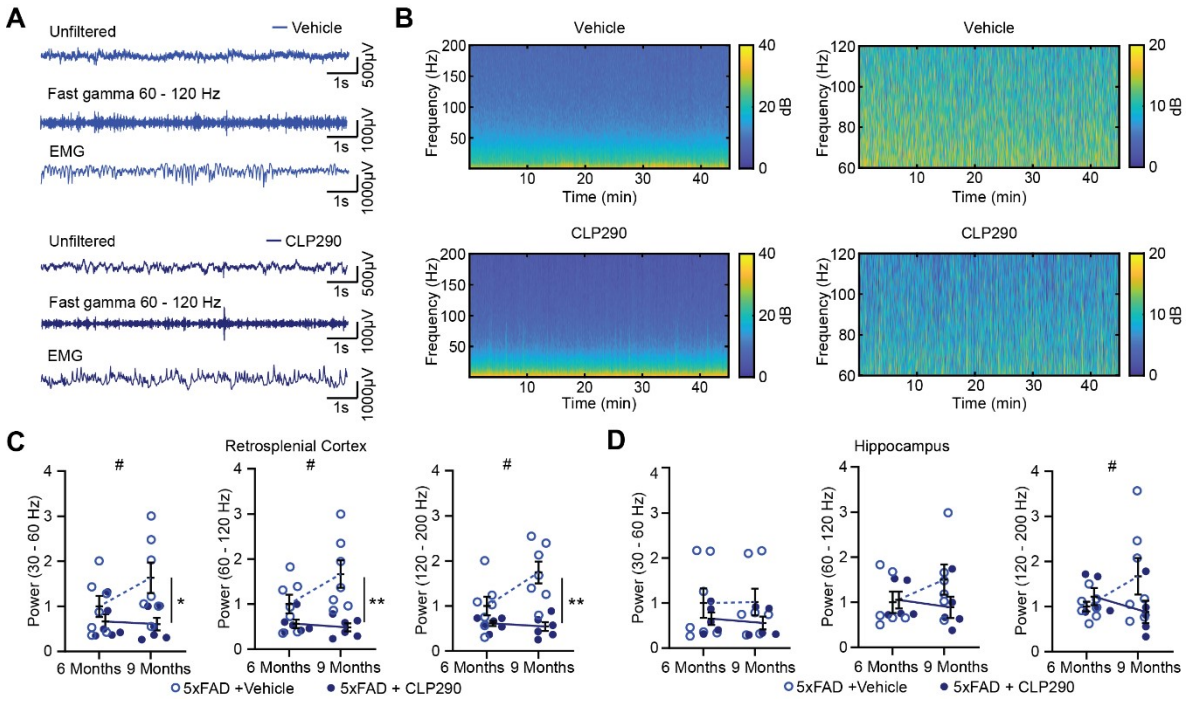

Figure 2.4. Long-term CLP290 treatment prevents cortical hyperactivity in 9-month-old 5xFAD mice.

(**A**) Traces of LFP activity in retrosplenial cortex (RSC), both raw and filtered in the 60-120 Hz (fast gamma) frequency band, and electromyography (EMG) activity from representative 5xFAD mice treated with either Vehicle (top) or CLP290 (bottom) for 5 months. The traces depict activity during non-REM (NREM) sleep. (**B**) Left: LFP wavelet spectrograms of RSC activity during concatenated NREM sleep episodes from the same mice as in A. Right: spectrograms generated from the same data, but scaled to highlight the difference in power in the fast gamma band. (**C**) The mean power of RSC activity in the slow gamma (30-60 Hz), fast gamma, and high-frequency (120-200 Hz) bands during NREM sleep in mice treated with either Vehicle (top) or CLP290 (bottom) for 5 months, beginning at 4 months of age. LFP recordings from freely-moving mice were conducted longitudinally at 6 and 9 months of age. For each figure, power is normalized to the mean of the Vehicle-treated group at 6 months of age. (**D**) Same as C, but for LFP recordings from the hippocampus. # $P < 0.05$ for the interaction between age (6 vs. 9 months) and drug treatment (vehicle vs. CLP290). * $P < 0.05$ & ** $P < 0.01$.

2.10 Supplementary materials

ELISA

For ELISA, brains were excised from anesthetized mice (30% urethane in saline) and the frontal lobe was dissected and harvested in sample tubes. The tissue was snap-frozen in liquid nitrogen and stored -80 °C until processing. Frozen PFC tissue was homogenized in RIPA buffer (50 mM Tris-HCl, 150 mM NaCl, 1% Triton X-100, 0.5% Na deoxycholate, 0.1% SDS; pH 8.0). Homogenates were incubated under constant agitation for 4 hrs at 4 °C for lysis. Lysates were centrifuged at 17,200 g and 4 °C for 10 min. Supernatants were collected and stored at -30 °C.

Levels of soluble Aβ42 in PFC samples were quantitated using the Human/Rat β Amyloid (42) ELISA kit (Wako catalog# 290-62601, LOT# PTN4256). Levels of KCC2 were quantified with the custom Mouse SLC12A5/KCC2 ELISA kit (LifeSpan BioSciences catalog# LS-F65788, LOT# 220764). All ELISAs were performed according to the manufacturer recommendations, and the plates were read at 450 nm using an Eon microplate reader (BioTek).

Amyloid-β plaques quantification

Coronal sections of the mPFC (40 µm) were incubated for 14 hours with the anti-D54D2 (1:1000, Cell Signaling catalog# 8243) diluted in PBS (with 0.2% TritonTM X-100) containing 10% normal goat serum. After washing with PBS, slices were incubated for 2 hours with the secondary Alexa Fluor™ 555-conjugated goat anti-rabbit (1:500, Invitrogen catalog# A21428). Slices were rinsed in PBS, mounted on slides and cover-slipped using aqueous antifade mounting media. Confocal images were acquired with a Zeiss LSM710 laser scanning microscope using a 20x Plan-Apochromat objective (0.8 NA). Images were acquired at 12 bits and 2048x2048 pixels, with 0.31 µm pixel size. For each image acquired, the amyloid plaques were automatically segmented using ilastik (version 1.4.0b13; www.ilastik.org) and a probability image was exported. The probability images were utilized to quantify the number of plaques per image and the area of each plaque using a custom MATLAB algorithm.

Cell culture incubation with Aβ42 and immunostaining

Neonatal rats (day 0) were sacrificed by decapitation, in accordance with the procedures approved by the committee for animal protection of Université Laval (CPAUL). The hippocampi were dissected and dissociated hippocampal neurons were prepared as previously described (PMID: 16049173). At DIV21, neurons were incubated for 15 hours with beta-amyloid (1-42; Aβ42) or beta-amyloid (1-42) Scramble (JPT Peptide Technologies catalog# SP-Ab-07-0.5 and SP-Ab-31-0.5, respectively) in culture media supplemented with 5 mM HEPES (pH 7.2). Thermo Fisher Scientific A-21449Aβ42 and Scramble were prepared at 220 µM in PBS and further diluted at a final concentration of 10 µM. Followed, neurons were treated with 1 µM of CLP257 or vehicle (0.01% DMSO) for 4 hours.

After treatment, neurons were fixed in 4% PFA solution (4% sucrose, 100 mM phosphate pH 7.2, 2 mM NaEGTA) at room temperature for 30 min, rinsed once with 100 mM glycine in PBS followed by 2 washes in PBS and permeabilized in PBS with 0.2 % Triton X-100 and 10% normal goat serum for 45 min at room temperature. Neurons were incubated for 15 hours at 4 °C with the primary antibodies (anti-KCC2, 1:1000, Millipore catalog# 07-432 and anti-NeuN, 1:1000, Millipore ABN91) diluted in PBS with 0.2 % Triton X-100 and 10% normal goat serum. After washing in PBS with 0.2 % Triton X-100, neurons were incubated for 2 hours at room temperature with the secondary antibodies (Cy3-conjugated goat anti-rabbit, 1:1000, Jackson Labs catalog# 111-165-003 and AlexaFluor™ 488-conjugated goat anti-rabbit, 1:1000, Thermo Fisher Scientific catalog# A-21449).

Confocal images were acquired with a Zeiss LSM880 laser scanning microscope using a 63x Plan-Apochromat oil objective (1.4 NA). Images were acquired at 12 bits and 2048x2048 pixels, with 0.066 µm pixel size. KCC2 subcellular profile analysis was performed as in brain sections to estimate the membrane KCC2 expression in individual neurons.

Fear conditioning

The fear conditioning test was conducted over 3 consecutive days. On day 1, the mice were conditioned to associate a context and auditory cue (tone) with a noxious foot shock. Each mouse was placed in the conditioning chamber (square shape, 33 × 33 cm) and, after a 120 s habituation period, a tone (2.1 kHz) was presented for 20 s. A foot-shock

(2 s, 0.5 mA) generated by a scrambled grid current generator (Lafayette Instrument, Model HSCK100AP) was administered concurrently with the final 2 s of the tone. In total, five tone-shock pairings were presented, with a 120 s interval between the start and end of each tone. The mouse was removed from the chamber 60 s after the final tone. The chamber was cleaned with 1% Virkon between mice. On day 2, cued fear memory was assessed. The mice were placed in a novel context (triangular shape with walls 23 cm in length, and a different floor type and wall color than the conditioning chamber). After 120 s, three tones were presented (20 s each, with a 120 s interval between the start and end of each tone). The chamber was cleaned with 70% isopropyl alcohol between mice. On day 3, mice were placed back in the original conditioning chamber for 300 s to assess contextual fear memory. The tests were video recorded for offline scoring using ANY-maze software (version 4.83w). The percentage of time spent exhibiting freezing behavior was measured as an indicator of fear memory. For cued fear memory, freezing was scored during the tone presentations (60 s total) on day 2. For contextual fear memory, freezing was scored across the entire session on day 3. Freezing was scored using the following parameters in ANY-maze: on threshold = 10; off threshold = 20; minimum duration = 1 s.

Elevated plus-maze test

The elevated plus-maze (EPM) apparatus was constructed of black plastic. It consisted of four arms (each 27 × 5 cm) in a plus-shaped configuration, with two opposing closed arms (20 cm high walls) and two opposing open arms, separated by an open center area (5 × 5 cm). The arms were elevated 50 cm above the ground. The entire structure was brightly illuminated. Mice were tested individually for a period of 5 min, starting in the center of the maze facing toward one of the closed arms. Between mice, the maze was cleaned with 1% Virkon to minimize scent cues. Activity in the maze was video recorded for manual off-line scoring of time spent in the open and closed arms, as well as the total number of arm entries. Entry into an arm was defined as a mouse placing all four paws on the arm.

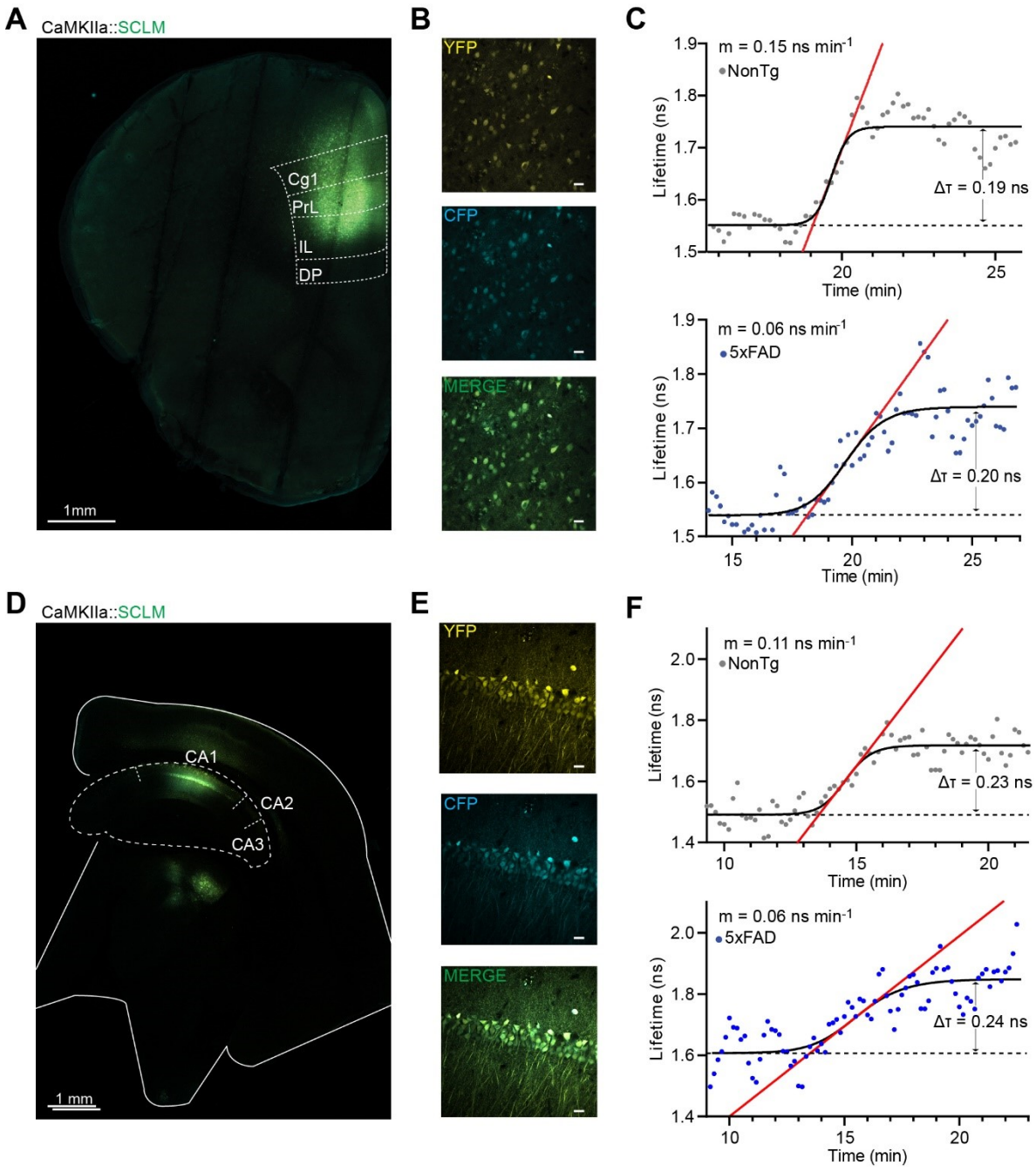

Suppl. Figure 2.5. AAV2/9.CaMKIIa.SuperClomeleon expression and representative examples of Hill-slopes.

(**A**) Confocal image of a mPFC slice infected with AAV2/9.CaMKIIa.SuperClomeleon in the prelimbic cortex (PrL). (**B**) Confocal images showing CaMKIIa positive neurons in LII/III of the PrL expressing SuperClomeleon (SCLM). (**C**) Representative linear Hill-slopes fitted to the FLIM lifetime measurements of an individual neuron derived from a 5xFAD and a NonTg mouse during the ex vivo chloride imaging. (**D**) Confocal image of a hippocampal slice expressing SuperClomeleon in the

pyramidal layer of the CA1. (**E**) Images of CA1 CaMKIIa positive neurons expressing SuperClomeleon. (**F**) Fitted Hill-slopes to the fluorescence lifetime as in C for a 5xFAD and a NonTg neuron in the CA1.

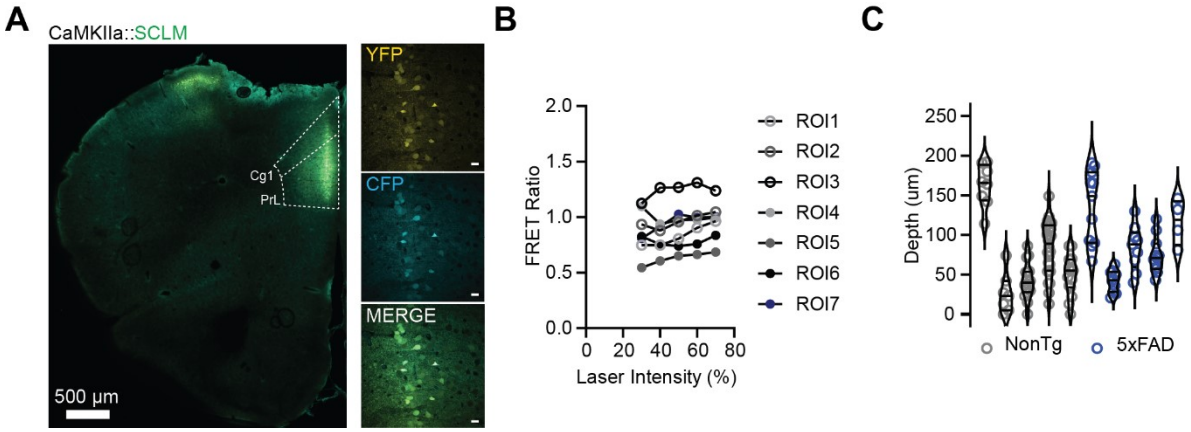

Suppl. Figure 2.6. FRET ratio is independent of laser intensity, and imaging depth was comparable between NonTg and 5xFAD mice

(**A**) Confocal image of the AAV2/9.CaMKIIa.SuperClomeleon (SCLM) infected mPFC from a NonTg mouse imaged during the in vivo chloride imaging experiment. (**B**) The FRET ratio of YFP to CFP for seven ROIs in the same field of view calculated for five different laser intensities in the mPFC of a NonTg mouse expressing SCLM. (**C**) The depth distribution of each field for every single mouse imaged. Each violin plot represents the probability density and the median of the depth distribution of a single mouse, while the dots represent the depth of the fields imaged from a given mouse.

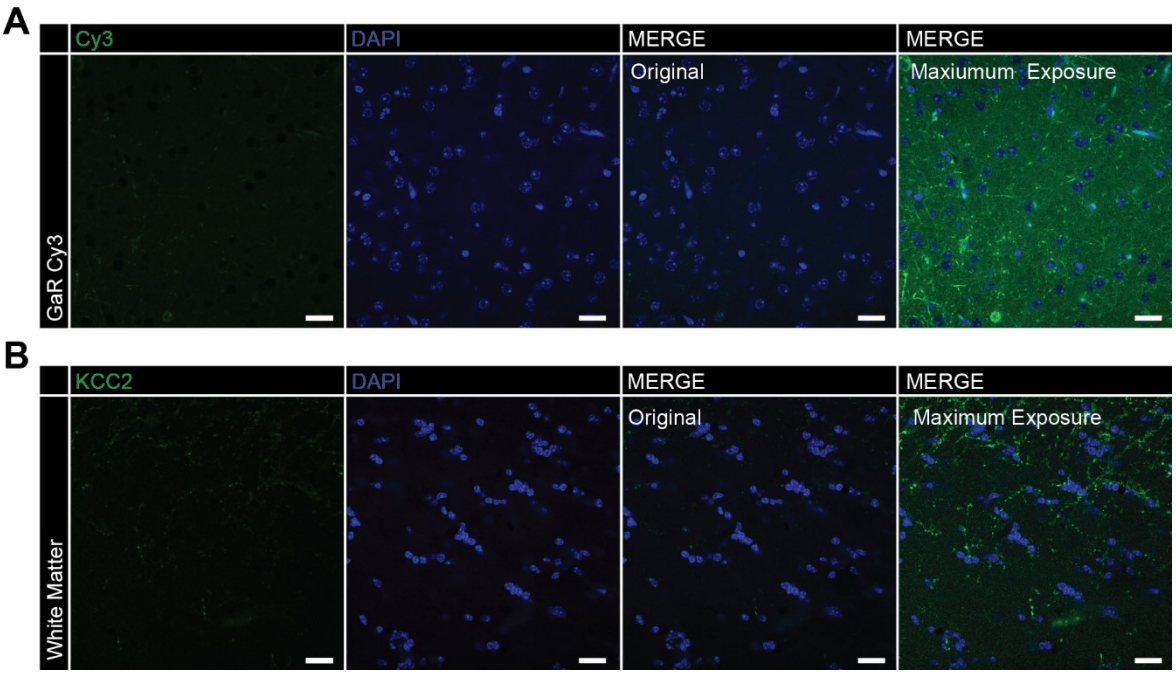

Suppl. Figure 2.7. Immunostaining negative controls and background staining in the corpus callosum.

(**A**) Confocal images of an mPFC slice incubated with Cy3-conjugated goat anti-rabbit (GaR Cy3; green. Nuclei were stained with DAPI (blue). For the merged image on the right, the brightness and contrast were adjusted for maximum exposure. Scale bar: 20 µm. (**B**) Confocal images showing KCC2 immunostaining in the forceps minor of the corpus callosum (KCC2 in green, DAPI in blue; Scale bars 20 µm) of a 5xFAD mouse. Brightness and contrast of the green channel was adjusted in the merged image on the right.

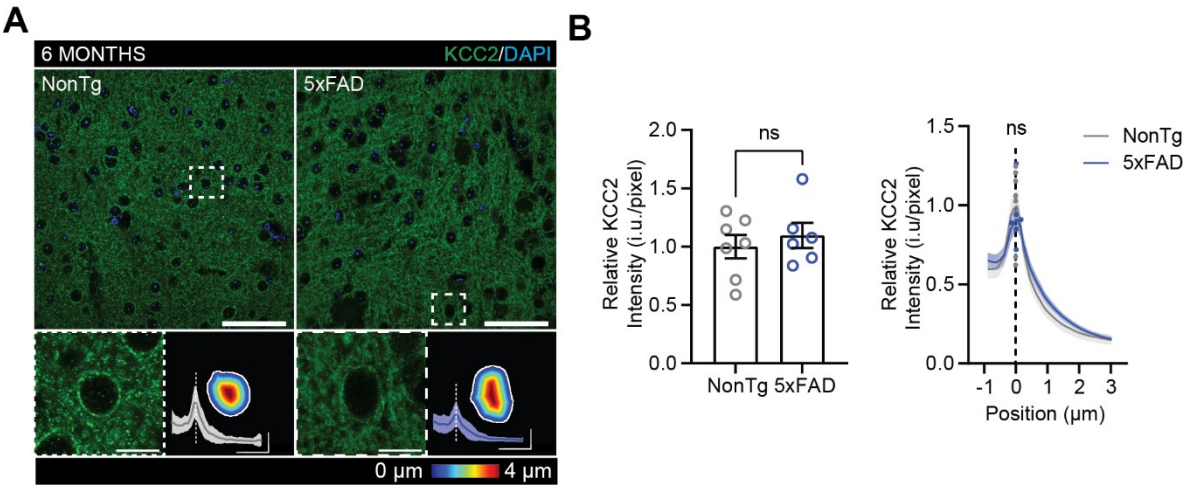

Suppl. Figure 2.8. KCC2 levels are unaltered in the nucleus accumbens of 6-months-old 5xFAD mice.

(**A**) Confocal images of mPFC slices stained for KCC2 from NonTg vs. 5xFAD mice (KCC2 in green, DAPI in blue; Scale bar: 50 µm). Insets show KCC2-stained neurons from ROIs (Scale bar: 10 µm). Color-coded maps illustrate the distance from the membrane, and graphs represent the subcellular KCC2 intensity profile (Scale bars: vertical 1000 intensity units, horizontal 2 µm). (**B**) The mean global KCC2 pixel intensity (left) and the mean KCC2 intensity profiles across the plasma membrane of 5xFAD (blue; *n* = 492 neurons from *N* = 6 mice) and NonTg (gray; *n* = 492 neurons from *N* = 7 mice) mice (right).

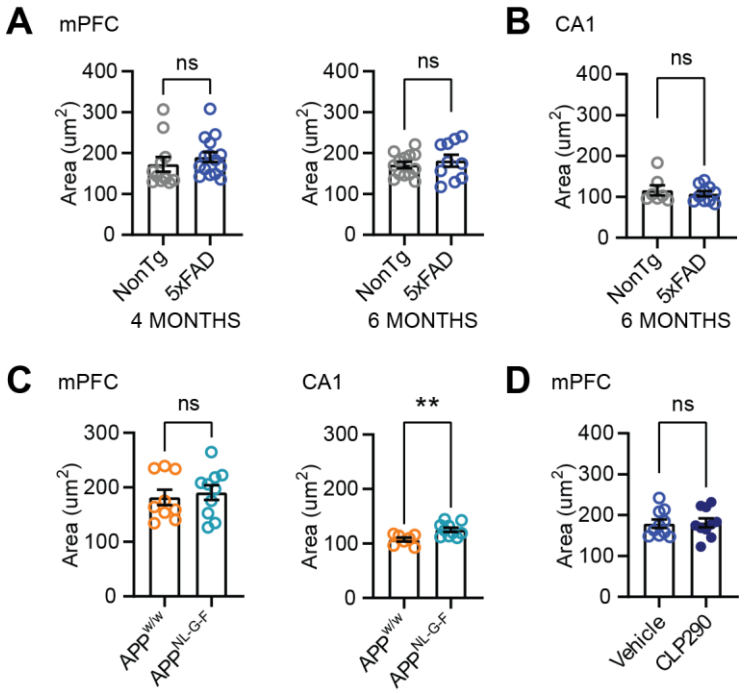

Suppl. Figure 2.9. The mean area of neurons analyzed for the membrane KCC2 expression.

(**A - B**) The average area of neurons selected for analysis of membrane KCC2 expression in the mPFC of 4- and 6-month-old 5xFAD and NonTg mice (**A**) and in the hippocampal CA1 of 6-month-old 5xFAD and NonTg mice (**B**). (**C**) The average area of neurons analyzed for their KCC2 membrane expression in the mPFC (left) and the CA1 (right) of 9-month old $APP^{w/w}$ and $APP^{NL\text{-}G\text{-}F}$ mice. A 17.29% increase in the neuronal surface of the $APP^{NL\text{-}G\text{-}F}$ mice was observed as compared to the $APP^{w/w}$ mice, which could contribute to an increase of $\boldsymbol{sqrt(17.29)}\%$ of the total membrane compartment. This 4.16% difference in membrane area is not sufficient to explain the 42.85% decrease in membrane KCC2 expression that we observed in the CA1 of $APP^{NL\text{-}G\text{-}F}$ mice. (**D**) The average area of neurons in the mPFC of CLP290- and Vehicle-treated 5xFAD mice. Data are presented as mean ± SEM. **P < 0.01 and ns = non significant.

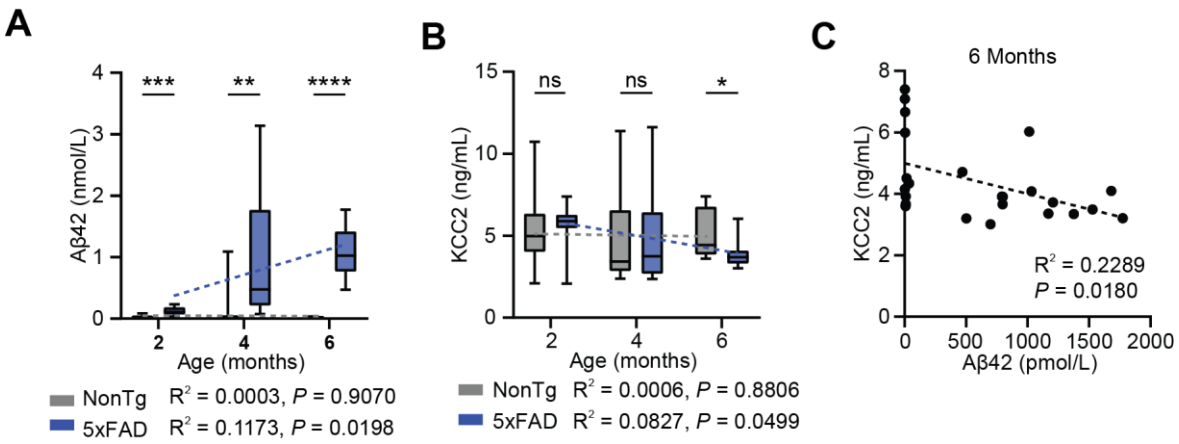

Suppl. Figure 2.10. Aβ42 and KCC2 levels are negatively correlated.

(**A**) The levels of soluble Aβ42 in the frontal lobe of 2-, 4- and 6-month-old 5xFAD (blue) and NonTg (gray) mice. The dashed lines represent the fitted linear regression equations of the Aβ42 levels vs. the age of the mice. (**B**) The total KCC2 protein levels quantified with an ELISA in the frontal lobe of 2-, 4- and 6-month-old 5xFAD (blue) and NonTg (gray) mice. The dashed lines represent the fitted linear regression equations of the KCC2 levels vs. age. (**C**) Pearson r correlation of the Aβ42 and KCC2 levels in the frontal lobe of 6-month-old mice. Data are presented as box plots and 5-95 percentiles whiskers. The R^2 and P values of the linear regressions are shown under the graphs. *P < 0.05; **P < 0.01; ***P < 0.001 & ****P < 0.0001. Dots in **C** represent individual mice.

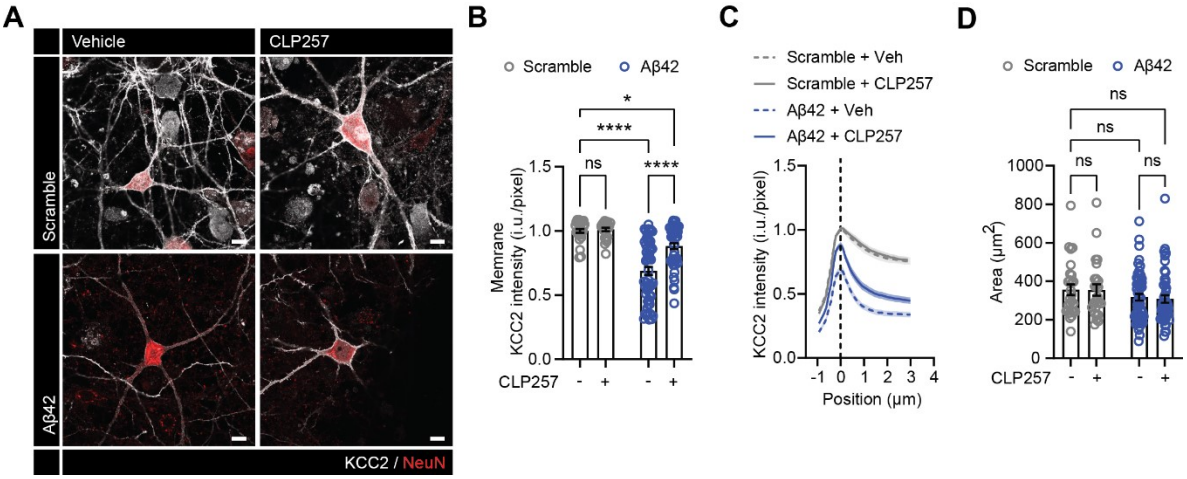

Suppl Figure 2.11. Aβ42 reduces membrane KCC2 levels in hippocampal cultured neurons.

(**A**) Representative confocal images showing KCC2 (gray) and NeuN (red) immunostaining in primary hippocampal cultured neurons incubated with Aβ42 or Scramble (Scale bars: 10 µm). (**B**) Mean membrane KCC2 intensity of individual neurons (Scramble - CLP257: *n* = 27 neurons from 2 coverslips; Scramble + CLP257: *n* = 25 neurons from 2 coverslips; Aβ42 - CLP257: *n* = 56 neurons from 4 coverslips; Aβ42 + CLP257: *n* = 50 neurons from 4 coverslips) (**C**) Mean KCC2 intensity profiles across the plasma membrane of individually identified neurons. (**D**) The average area of neurons analyzed for the membrane KCC2 expression. Data are presented as mean ± SEM. *P < 0.05; ****P < 0.0001 & ns = non significant.

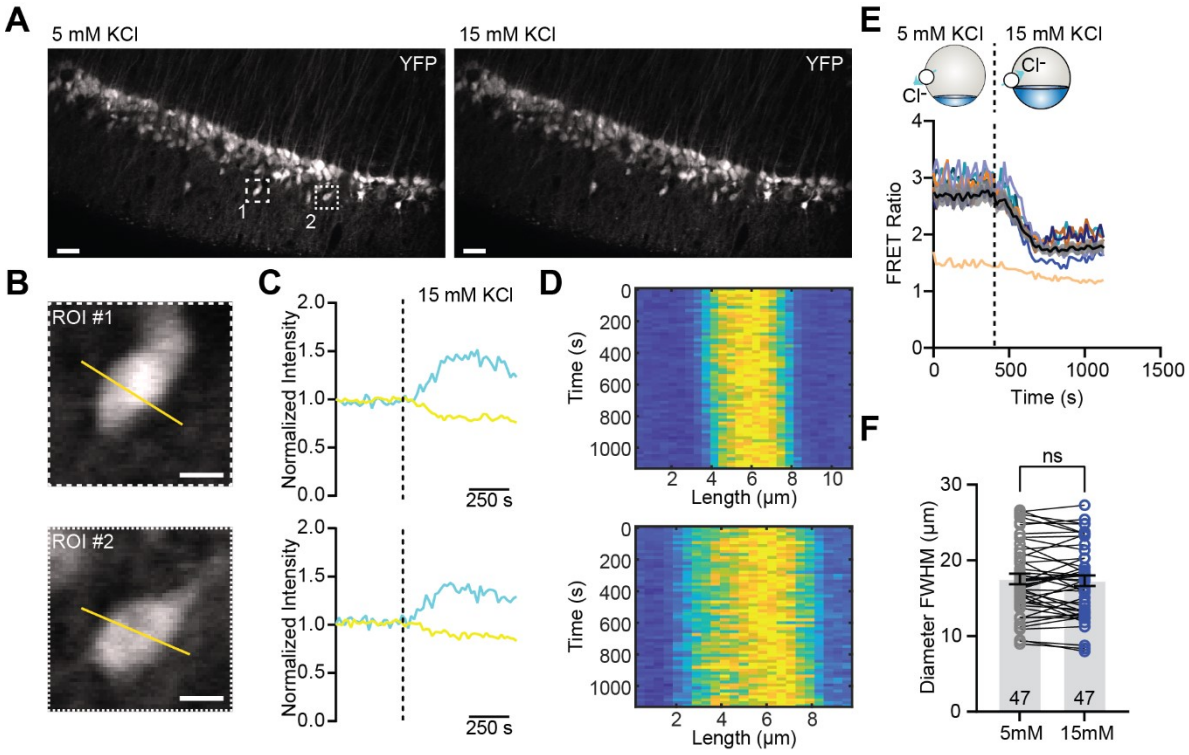

Suppl. Figure 2.12. Neuron cell body diameter is unaltered after stepping extracellular K+ from 5 to 15 mM.

(**A**) Two-photon images of the green fluorescence channel of CaMKIIa-positive CA1 hippocampal neurons transduced with SuperClomeleon in two different conditions. In the left the slices in ASCF with low extracellular KCl (5 mM) and in the right the same slice in ACSF with high extracellular KCl (15 mM). Scale bar 25 µm. (**B**) Neurons from selected ROIs in A (Scale bar 5 µm). The yellow dissecting lines were used to calculate the fluorescence intensity profile at each time point of the kymographs in **D**. (**C**) Normalized fluorescence intensity of CFP (cyan) and YFP (yellow) across time for the neurons selected in the ROIs. The dash line represents the time point when the extracellular solution was changed in ASCF with 15 mM KCl. (**D**) Kymograph presenting the intensity profile along the yellow line shown in **B** as a function of time. Each line was used to estimate the cell body diameter using the full width half maximum (FWHM) of each intensity profile. (**E**) Timelapse measurement of the intensity FRET ratio of all selected neurons from temporal acquisition in **A**. The black line shows the mean FRET ratio ± SEM (*n* = 8 neurons). (**F**) The mean FWHM neuron diameter for the 5 mM and 15 mM KCl ASCF conditions (*n* = 47 neurons from *N* = 5 slices). ns = non significant (paired t-test).

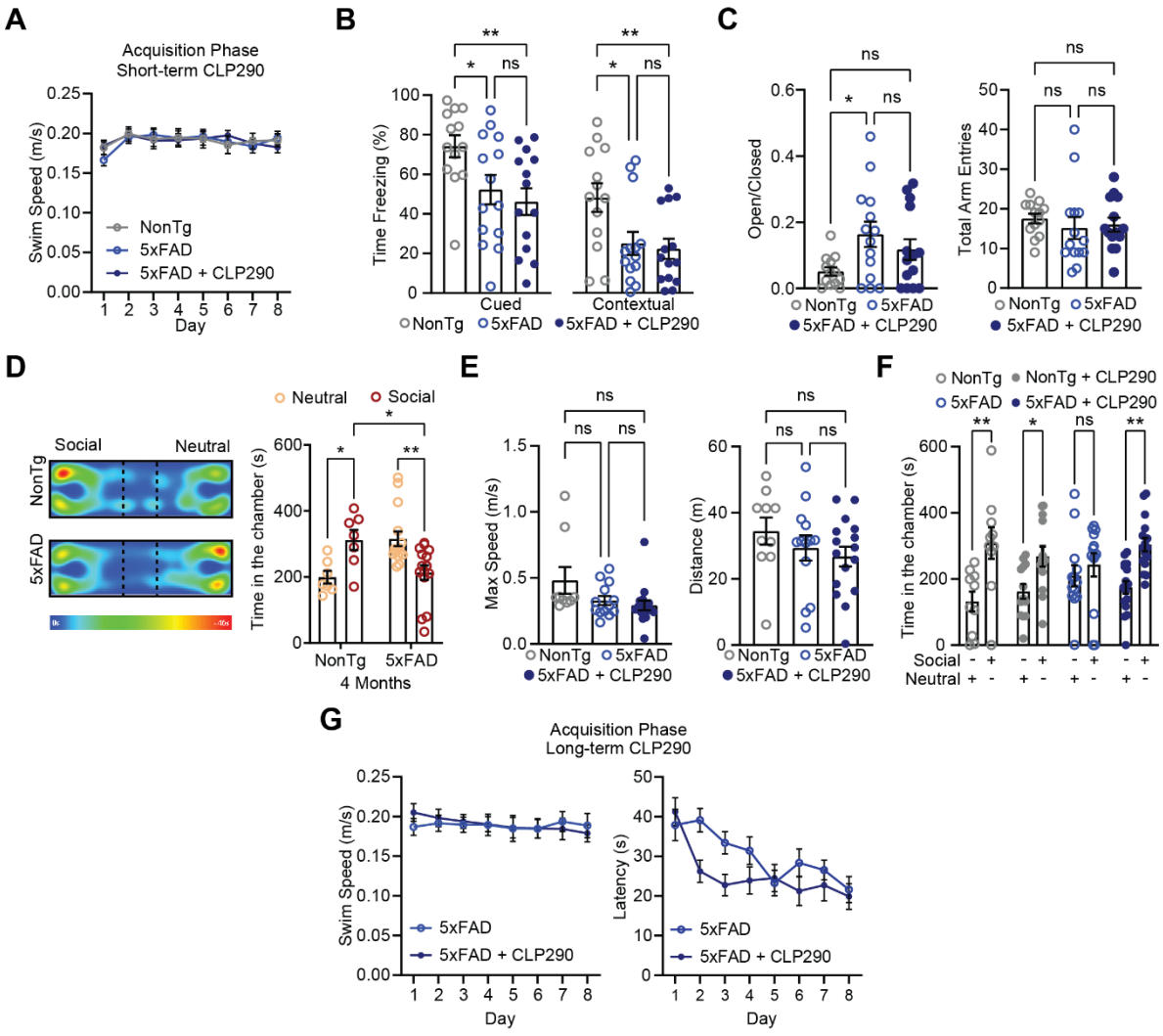

Suppl. Figure 2.13. The 5xFAD mice develop social preference deficits at 4 months of age.

(**A**) The average swim speed of CLP290-treated 5xFAD mice vs. vehicle-treated NonTg and 5xFAD mice for each day of the MWT acquisition phase. (**B**) The percentage of time spent freezing during the cued (left) and the contextual (right) fear conditioning test. (**C**) The open to closed arm time ratio in the EPM test (left), and the mean total entries into the open or closed arms of the EPM (right). (**D**) The time spent in the social chamber vs. the time spent in the neutral chamber in the unconditioned social interaction test of 4-month-old 5xFAD (*n* = 15) and NonTg mice (*n* = 7; right), and heat maps representing the location of the NonTg and 5xFAD mice during the same social interaction test (left). (**E**) The maximum speed and the distance travelled during the social interaction test. (**F**) The time spent in the social chamber vs. the time spent in the neutral chamber in the social interaction test by CLP290-treated or vehicle-treated 5xFAD and NonTg mice (**G**) The MWT acquisition phase mean swim speed (left) and latency to the platform (right) of 9-month-old 5xFAD mice receiving long-term

CLP290 vs. vehicle treatment. Circles or dots in **B**, **C** and **D** represent single mice. Data are presented as mean ± SEM. * $P < 0.05$ & ** $P < 0.01$; ns = non significant.

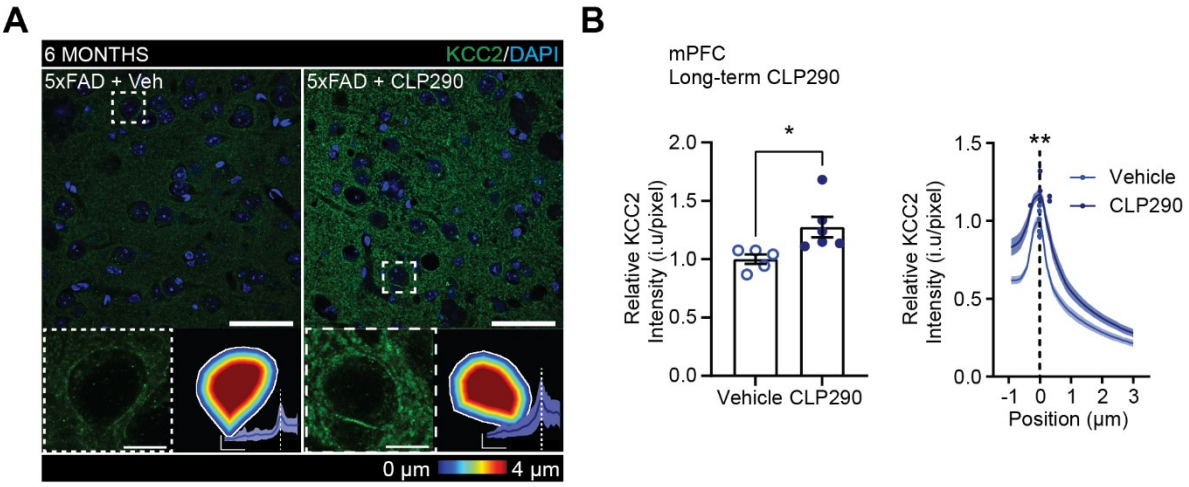

Suppl. Figure 2.14. Long-term CLP290 treatment prevents KCC2 loss.

(**A**) Confocal images of mPFC slices stained for KCC2 from long-term CLP290-treated vs. Vehicle-treated 5xFAD mice (KCC2 in green, DAPI in blue; Scale bar: 50 µm). Insets show KCC2-stained neurons from ROIs (Scale bar: 10 µm). Color-coded maps illustrate the distance from the membrane, and graphs represent the subcellular KCC2 intensity profile (Scale bars: vertical 1000 intensity units, horizontal 2 µm). (**B**) The mean global KCC2 pixel intensity (left) and the mean KCC2 intensity profiles across the plasma membrane of CLP290 (blue circles; *n* = 499 neurons from *N*= 6 mice) and Vehicle-treated (filled dark blue dots; *n* = 421 neurons from *N* = 5 mice) 5xFAD mice (right).

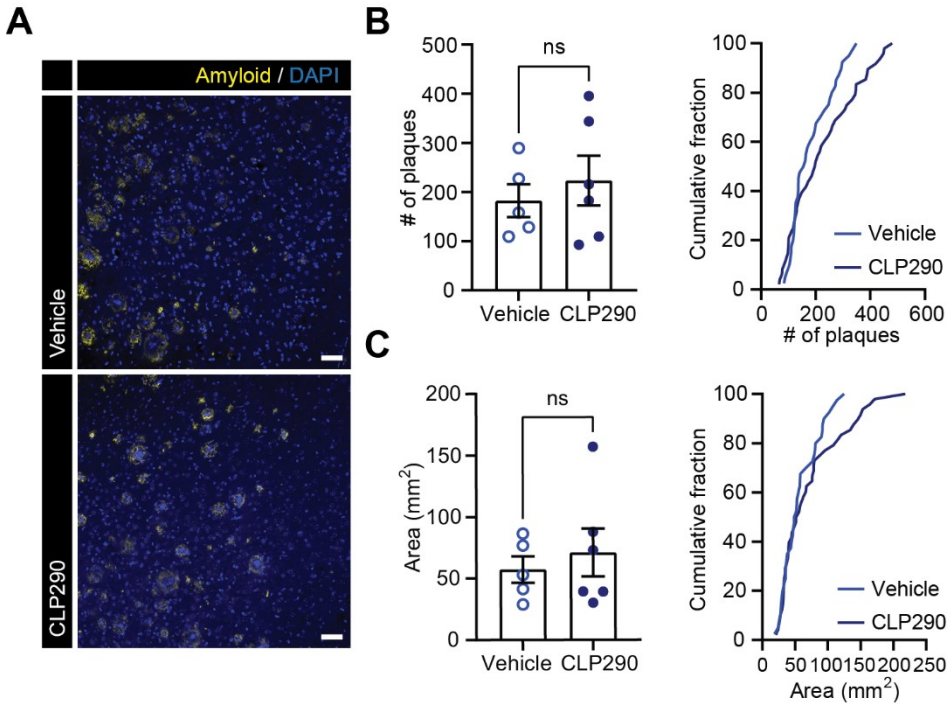

Suppl. Figure 2.15. Long-term CLP290 treatment did not reduce amyloid-β load.

(**A**) Confocal images of mPFC slices stained for amyloid-β plaques (anti-D54D2; yellow) from long-term CLP290-treated vs. Vehicle-treated 5xFAD mice (DAPI in blue; Scale bars 50 µm). (**B**) The mean number of plaques (left) and the cumulative distribution of the number of plaques in CLP290-treated vs. Vehicle-treated 5xFAD mice (Vehicle: *n* = 5 mice; CLP290: *n* = 6 mice). (**C**) The average plaque area (left) and the cumulative distribution of the plaques' area in CLP290-treated vs. Vehicle-treated 5xFAD mice. Data are presented as mean ± SEM. ns = non significant.

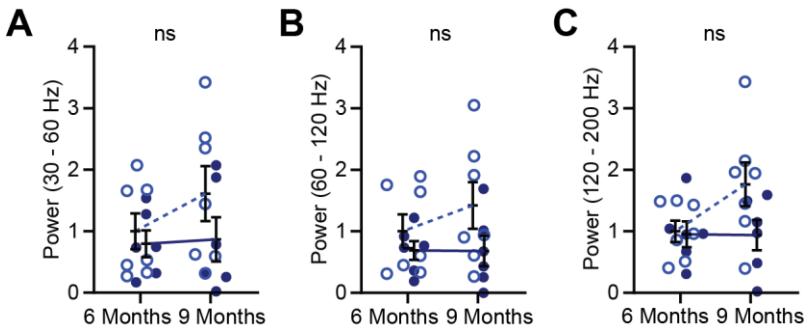

Suppl. Figure 2.16. LFP activity in the barrel cortex of 5xFAD mice treated with CLP290.

(**A - C**) The mean power of the slow gamma (**A**), fast gamma (**B**) and ripple band (**C**) LFP activity in the barrel cortex of Vehicle- and CLP290-treated 5xFAD at 6 and 9 months of age. Dots represent single mice. Data are presented as mean ± SEM. ns = non significant.

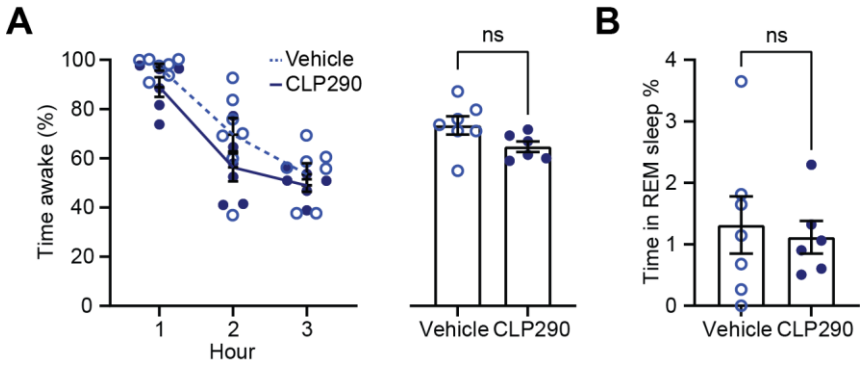

Suppl. Figure 2.17. Sleep structure is unaltered in 9-month-old 5xFAD mice treated long-term with CLP290.

(A) The percentage of time spent awake during each of the 3 hours of the recording session (left) and across the entire 3 hours (right; Vehicle: *n* = 7; CLP290: *n* = 6 mice). (**B**) The percentage of total time spent in REM sleep during the entire 3 hours of recording. Data are presented as mean ± SEM. ns = non significant.

Chapter 3 – A subset of aged mice develops cognitive decline linked to prefrontal cortex synaptic alterations

3.1 Résumé

Le vieillissement est le facteur de risque le plus important de la neurodégénérescence et il a été associé à un déclin de plusieurs fonctions cognitives liées à l'activité du cortex préfrontal (CPF). En effet, les neurones du CFP subissent plusieurs changements neurophysiologiques et morphologiques avec la sénescence, ce qui entraîne une modification de l'activité synaptique dans le CFP et plus particulièrement un déséquilibre de l'équilibre entre la neurotransmission excitatrice et inhibitrice en faveur de l'inhibition. Ici, nous avons identifié un sous-ensemble de souris âgées qui présentent déficits de la mémoire non spatiale, mais aussi un comportement de type anxieux et des troubles de la préférence sociale. Dans ce sous-ensemble de souris âgées présentant des déficits cognitifs, le rapport entre les niveaux de protéines PSD95 et Gephyrin était significativement plus faible, tandis que les niveaux de VGAT étaient significativement plus élevés dans le CPF par rapport à des souris âgées ou jeunes adultes cognitivement intactes. Enfin, l'activation optogénétique des neurones inhibiteurs corticaux a entraîné des déficits de mémoire et une réduction du comportement exploratoire. Dans l'ensemble, nos données indiquent une prédominance de l'inhibition chez les souris âgées atteintes de troubles cognitifs, que nous avons pu imiter chez les souris jeunes par l'activation optogénétique des neurones inhibiteurs et qui a permis de reproduire certains des déficits cognitifs observés chez les souris âgées.

3.2 Abstract

Aging is the most impactful risk factor for neurodegeneration and has been associated with a decline in several cognitive functions associated with the activity of the prefrontal cortex (PFC). Indeed, the PFC neurons undergo several neurophysiological and morphological changes with senescence resulting in altered synaptic activity in the PFC and specifically a shift of the balance between excitatory and inhibitory neurotransmission towards inhibition. Here, we identified a subset of old mice which show a decline in non-spatial memory, but also exhibit anxiety-like behavior and social preference impairments. In

this subset of cognitively impaired old mice the ratio of PSD95 to Gephyrin protein levels was lower while the levels of VGAT were significantly higher in the PFC as compared to cognitively intact old or adult young mice. Finally, optogenetic activation of cortical inhibitory neurons resulted in memory deficits and reduced explorative behavior. Altogether, our data indicate a shift towards inhibition in cognitively impaired old mice which we could mimic in young mice by optogenetic activation of inhibitory neurons and managed to reproduce some of the cognitive deficits we found in the old mice.

3.3 Introduction

Cognitive decline and dementia emerge as a major threat for modern societies. As human lifespan increases the prevalence of aging-related cognitive frailty rises too, largely in the form of Alzheimer's disease. Yet, non-pathological aging can lead to dementia and cognitive decline independently of neurodegeneration or neuronal death (Morrison and Hof, 1997). Nonetheless, age still remains the most impactful risk factor for neurodegeneration (Hou et al., 2019), hence understanding the basic mechanisms of aging and their contribution to the onset and the progression of cognitive decline is key for the development of efficacious interventions. The recent improvement of neuroimaging techniques greatly expanded our knowledge on neuronal network alterations occurring during aging in the brain and correlated them with various cognitive deficits (Bakkour et al., 2013; Hedden and Gabrieli, 2004). However, we still have not identified biomarkers of cognitive decline associated with senescence, or completely understood the molecular and functional changes occurring on the cellular level with normal aging.

Among the several brain structures associated with memory loss, the hippocampus appears to be the most vulnerable to aging (Rosenzweig and Barnes, 2003), with volume reduction, decreased number of spines, diminished synaptic plasticity and altered network activity reported both in humans and rodents (Andrews-Hanna et al., 2007; Burke and Barnes, 2010; Geinisman et al., 1986; Leal and Yassa, 2015; Nicholson et al., 2004; Scheff et al., 2007; Small et al., 2011; Tran et al., 2018). Along with memory loss, a decline in decision making, planning, attention and executive functions appear in an age-dependent manner (Hedden and Gabrieli, 2004; Herndon et al., 1997), with the prefrontal cortex (PFC) serving a key hub for such cognitive functions (Fuster, 2001; Miller and Cohen, 2003). Morphological and structural changes in the PFC pyramidal neurons along with overt spine density loss lead to neurophysiological changes linked to a decline in executive functions in

senescence in humans and non-human primates (Andrews-Hanna et al., 2007; Dumitriu et al., 2010; Luebke et al., 2010; Morrison and Baxter, 2012). Similarly, alterations in the neurophysiology and specifically the balance of excitatory to inhibitory neurotransmission (E/I ratio) in the rodent PFC have been associated with pathological conditions such as autism and schizophrenia (Lewis et al., 2005; Selimbeyoglu et al., 2017; Yizhar et al., 2011a) for which cognitive impairments is well characterized. Disruption of the E/I balance of the PFC, based on fMRI and computational modeling, has been recently reported also in aged individuals and has been correlated with memory loss and cognitive decline (Legon et al., 2016).

The level of excitation in the PFC is mainly regulated through inhibitory signals generated by the GABAergic interneurons (Baroncelli et al., 2011; Markram et al., 2004). In addition, inhibitory interneurons coordinate local network synchrony and establish crucial network dynamics which facilitate cognition (Buzsáki and Chrobak, 1995; Buzsáki and Draguhn, 2004). Blockage of mPFC GABA(A) receptors results in a profound working memory impairment (Auger and Floresco, 2015; Enomoto et al., 2011), while administration of GABA(B) antagonists augments working memory in rats (Bañuelos et al., 2014) through reduction of inhibitory input on pyramidal neurons produced by tonic activation of extrasynaptic GABA(B) receptors (Carpenter et al., 2016).

Electrophysiological studies revealed that mPFC pyramidal neurons receive excessive inhibitory input both in primates and rodents during aging (Bories et al., 2013; Luebke et al., 2004). Moreover, the protein levels of GAD67, the GABA synthesizing enzyme, are increased in the PFC of aged rats, whereas both GABA(B) receptor subunits are significantly reduced with aging and negatively correlated with working memory deficits (Bañuelos et al., 2014). These findings suggest a shift in the E/I ratio towards inhibition which could support the mPFC cognitive deficits associated with aging and may offer an area where we can intervene to alleviate cognitive deterioration in the elderly.

To investigate whether alterations in the mPFC E/I ratio contribute to the development of cognitive decline in rodents, we adapted behavioral tests and correlated the performance of adult and old male mice (21-25 weeks and 80-97 weeks respectively) with pre- and postsynaptic protein levels alterations. Moreover, we utilized optogenetics (Madisen et al., 2012; Yizhar et al., 2011a) to activate inhibitory neurons in the mPFC and validate the effect of such manipulation in the behavioral performance of adult and old male mice.

3.4 Materials and methods

Animal Subjects

All experimental protocols are approved by the animal protection committee of Université Laval (CPAUL) in accordance with the Canadian Council on Animal Care guidelines. Male C57BL/6J mice were purchased from the Jackson Laboratory (#000664) and maintained at the CERVO Brain Research Centre animal facility until they reached the appropriate age. Male Gad2-IRES-Cre were purchased from the Jackson Laboratory (#010802-JAX; Gad2tm2(cre)Zjh/J) and bred with female Ai32(RCL-ChR2(H134R)/EYFP) mice (Madisen et al., 2012) (The Jackson Laboratory, #012569) to produce the Gad2::ChR2-EYFP mice. All colonies were maintained at the CERVO Brain Research Centre. Mice were housed on a 12 h light/12 h dark cycle, with unrestricted access to food and water and the experiments were performed during the light cycle.

The group of old male C57BL/6J consisted of 43 mice in total aged between 80 to 97 weeks. From these 43 C57BL/6J mice, 22 mice were assigned to the Bad Performers (BP) group and 21 mice were assigned to the Good Performers (GP) group. The young C57BL/6J group consisted of 18 mice with an age of 21 to 25 weeks old. The group of the young Gad2::ChR2-EYFP consisted of 13 male mice aged between 27 to 33 weeks.

Surgical procedures

For the optogenetics experiments mice were anesthetized with isoflurane (3% induction, 1-2% maintenance) and placed in a stereotaxic table (Stoelting Co.), on a temperature control pad. The skin above the skull was removed and the skull surface was cleared of connective tissue with 10% peroxide and Etch-RiteTM (Pulpdent Corporation). A circular craniotomy of approximately 500 um was drilled above the medial prefrontal cortex with coordinates: Anterior-Posterior (AP) + 1.80 mm and Medial-Lateral (ML) + 0.30 mm. An optic-fiber cannula (200 um core and 0.37 NA) was lowered 1.80 mm (Dorsal-Ventral - 1.80 mm) and fixed on the skull with C&B Metabond® (Parkell Inc.). The mice were single-housed following the surgery and the experiments began at least one week later.

For the in vivo electrophysiology experiments mice were anesthetized with isoflurane, placed in a stereotaxic table, the scalp was removed, and the skull surface was cleared as before. A Fi-Wi optoelectric cannula (Doric Lenses, Canada) with one optical fiber (200-µm core; 0.66 NA; 1.6 mm long), three Tungsten microelectrodes (50-µm flat tip; 1.8 mm long) and an external silver wire reference was placed in the mPFC (AP: + 1.80 mm

and ML: + 0.30 mm) and fixed with C&B Metabond®. The reference wire was placed under the skin of the animal's neck. The mice were single-housed following the surgery and experiments began a minimum of a week later.

Optogenetic stimulation

Optical activation of ChR2-expressing Gad2 neurons was performed with a 470 nm LED diode (ThorLabs cat# M470F3) stimulus (87 sequences of 5 ms pulses at 40 Hz with 5 s delay between each sequence). The light was delivered through fiber optics connected to a rotary joint (Doric Lenses, Canada) and then to the LED diode. The intensity of light on the tip of the fiber was measured at 1 mW. The mice were acclimated to the handling, the connection of the removable fiber optic and the light stimulation for 5 days prior to the behavioral testing.

Novel Object Recognition

Mice were tested in a modified dark apparatus for Novel Object Recognition (NOR) consisting of a triangular zone (30 x 30 x 40) and a rectangular zone (40 x 25 cm) (Bories et al., 2013). The mice were placed in the triangular zone and allowed to explore the apparatus freely one day prior to the novel object task. The following day mice were allowed to explore two identical objects placed in the rectangular zone for 10 min and then returned to their homecage. One hour following the familiarization to the identical objects, a new copy of the identical object and a novel object were placed in the apparatus and the mice were allowed to explore the objects for 10 min. For the Gad2::ChR2-EYFP mice the test was repeated while the mice were optogenetically stimulated. The behavior was recorded by a camera located on the top of the apparatus and analyzed offline by ANY-maze (Stoetling Co.) or manually by a blinded observer for the mice receiving optogenetic stimulation. A NOR Performance Index (PI) was calculated by the ratio of the time interacting with the novel object to the total time of interaction with both objects. For each trial, distinct identical and novel objects were utilized.

Open Field

The test was performed in an opaque square Open Field (OF) apparatus (50 x 50 cm). The mice were placed in the center of the apparatus and left to explore the new environment for 10 min. The movement of the mice was recorded by a camera and analyzed offline with AnyMaze. To measure locomotor and explorative behaviour the total distance

travelled, and the maximum speed of the mice was calculated. The anxiety-like behavior was scored by measuring the time in the proximity of the apparatus' walls, defined by a zone of 10 cm surrounding the walls, and the time in the center of the apparatus. The test was repeated for the Gad2::ChR2-EYFP mice to score their performance during optogenetic stimulation.

Unconditioned social preference test

A modified three-chamber task was used to test the unconditioned social preference as previously described (Moy et al., 2004). The apparatus consisted of two compartments (35 x 20 cm) differently colored on the walls (one with black walls and the other with white walls), separated by a smaller compartment with horizontal white and black gratings on its walls. However, to allow uninterrupted exploration of the apparatus during the optogenetic stimulation phase for the Thy1::ChR2-EYFP and the Gad2::ChR2-EYFP mice, where the optic fiber would not allow the mice to move from one compartment to the other, the compartment separators were removed for all testing phases, for all the mice. An inverted wire mesh cup was placed in each large compartment. The test mice were introduced in the central compartment and allowed to habituate to the apparatus for 10 min. Then, a male age-matched social partner was placed under the cup of the social compartment and an object in the other, no-social compartment. The test mouse was returned in the small compartment and left to explore the apparatus for an additional 10 min. The behavior of the tested mice was recorded by a camera and analyzed offline by ANY-maze. The time to the social and neutral compartments were calculated as the time spent in the compartment with the social partner and the time spent in the object (neutral) compartment, respectively. The social interaction test was performed for an additional time for the Gad2::ChR2-EYFP mice while optogenetic stimulation was delivered.

Immunoblots

Prefrontal lobe tissue was obtained and homogenized with a pestle in RIPA buffer (50 mM Tris-HCl, 150 mM NaCl, 1% Triton X-100, 0.5% Na deoxycholate, 0.1% SDS; pH 8.0). The homogenates were incubated for 4 hours at 4 ^{o}C under constant agitation for lysis. Lysates were centrifuged at 4 ^{o}C, 17,200 g for 10 min and the supernatants were collected and stored at -30 ^{o}C until use. Samples were prepared at a 10ug/20µL concentration and denaturized for 5 min at 95 ^{o}C in Laemmli buffer. Proteins were run on 7.5% TGX Stain-Free polyacrylamide gels (Bio-Rad). Gels were transferred onto 0.2 µm PVDF membranes (Bio-

Rad) for western blot analysis. Membranes were blocked with 10% non-fat dry milk in TBST (0.2% Tween) and sequentially incubated with primary and secondary antibodies diluted in 5% non-fat milk TBST. The mouse monoclonal anti-PSD95 (SySy catalog #124011) and the rabbit polyclonal anti-NL2 (SySy catalog #129203), anti-VGLUT2 (SySy catalog #135403) and anti-VGAT (SySy catalog #131003) were used at 1:1000 dilution. The mouse monoclonal anti-Gephyrin (SySy catalog # 147111) and anti-NL1 (SySy catalog #129111) were used at 1:2000 dilution. Finally, the chicken polyclonal anti-GAPDH (Millipore catalog #Ab2302) was used at 1:10,000 dilution. The secondary goat anti-mouse IgG (H+L)-HRP conjugated (Invitrogen catalog #32460) and the secondary goat anti-rabbit IgG (H+L)-HRP conjugated (Invitrogen catalog #32430) were used at 1:2000 dilution while the rabbit anti-chicken IgY (H+L)-HRP conjugated (Jackon-ImmunoResearch catalog #303-035-003) was used at 1:10000 dilution. The intensity of bands on blots were measured with ImageJ (NIH). The protein levels were calculated by normalizing the intensity of each band to the intensity of the total protein loaded on the respective lane on the TGX Stain-Free gel and then to the normalized intensity of the same loading control sample (LC) which was run in every gel as previously described (Taylor et al., 2013).

In vivo electrophysiology

Mice were briefly anesthetized with 2% isoflurane and the wireless electro-optic headstage (Gagnon-Turcotte et al., 2019) was connected to the connector of the implanted Fi-Wi optoelectric cannula. Then, the mice were returned to their homecage to recover from the anesthesia. When awake, they were transferred to various arenas (such as an OF, the NOR arena or the three-chamber apparatus) and left freely to explore the new environments for 10 minutes while the spontaneous multi-unit activity in the mPFC was recorded. All the recordings were conducted approximately at the same time during the day and at the light phase.

The multi-unit activity was amplified, filtered (100 - 8000 Hz) and digitized at 16 kHz within the CMOS. The data were transmitted wirelessly (at 2.4 GHz) and stored on a local computer using a custom MATLAB (MathWorks) script. Analysis and spike detection was performed offline.

Spikes were detected using the non-linear energy operator (NEO) (Yang and Mason, 2017), a well-known low-complexity preprocessor, which consist of computing the following equation:

$$NEO(n) = n(x)^2 - x(n-1) \times x(n+1)$$

where $x(n)$ is n^{th} neural sample. The preprocessor output was then compared to a threshold, and the output of the comparison (greater on not) determines if a spike was detected using the following set or rules:

$$NEO(n), \begin{Bmatrix} if Neo(n) > threshold, a\ spike\ is\ detected \\ otherwise, no\ spike\ is\ detected \end{Bmatrix}$$

The threshold was based on a multiple of the estimated standard deviation of the noise (σ_{noise}) embedded in the recorded neural signal: $threshold = M \times \sigma_{noise}$, in which σ_{noise} was estimated using the median of the absolute deviation (MAD):

$$\sigma_{noise} \cong \frac{median[|x|]}{0.6745}$$

where x was the whole neural signal. Upon a detection event, the detection time was stored, the spike waveform was retrieved (27 samples after and 20 samples before the detection event, ~3.4 ms/spikes), the spike counter was increased, and the detection activity was stopped for ~3 ms to avoid multiple redetections of the same spike. The detection time stamps were used to compute the interspike activity intervals while the spike counter was used to determine the average firing rate.

Once the spike waveforms were collected, a clustering phase was performed to estimate the number of firing neurons and to associate each neuron to a specific spike waveform. For the clustering, a principal component analysis (PCA) algorithm was executed. Next, each spike was represented by a series of coefficients, representing the spikes in an orthogonal basis with the greatest variation. Then, each spike was compressed to a subset of 2 coefficients with the highest energy for classification. The optimal number of spike clusters was calculated using the Davies-Bouldin criterion (Davies and Bouldin, 1979) and the classification was performed using the k-means algorithm.

Statistical analysis

The statistical tests were performed with GraphPad Prism 9 (GraphPad Software) and MATLAB (MathWorks) scripts. The two-group null hypothesis significance was tested with a Mann-Whitney test whereas, the multi-group differences were analyzed with One-way ANOVA followed by a post-hoc Tukey test for multiple comparisons. Samples were tested for the normality of their distribution with an Anderson-Darling or a Shapiro-Wilk test. Multi-group analysis with two categorical variables was performed with a two-way ANOVA followed by a multiple comparisons Bonferroni test. Cluster analysis was conducted by a k-

means clustering with n = 1 vector and k = 2 clusters. *P values* < 0.05 were considered statistically significant.

3.5 Results

A subset of old mice develops cognitive deficits

We screened 43 old male C57BL6J mice, 80-97 weeks old, and a cohort of young mice (21-25 weeks old) for their performance in a novelty-based, non-spatial memory task. The old mice showed significantly lower performance in the 1 hour memory Novel Object Recognition (NOR) task as compared to the young mice (**Figure 3.1a** and **Suppl. Figure 3.5a**). Interestingly, approximately half of the old mice scored lower than the median of the group (**Figure 3.1a**), hence we used k-means clustering to assess whether the old mice can be grouped in two distinct clusters according to their NOR memory performance. The clustering analysis identified two clusters within the group (**Figure 3.1b**), thus we divided the group into the Good Performers (GP) and the Bad Performers (BP). Adding the NOR performance of young mice to the k-means analysis did not alter the previously identified clusters and the majority of the young mice were grouped with the GP (**Figure 3.1b**). To this end, the old GP performed equally well to the young mice, whereas the BP performed significantly worse than both the young mice and the GP (**Figure 3.1c**). The NOR performance index was not different during the familiarization phase between the groups, excluding any object location bias (**Suppl. Figure 3.5b**). The total time of exploration was significantly lower both during the familiarization and the 1 hour memory test for the GP and the BP as compared to the young group (**Suppl. Figure 3.5b**) which could suggest a poorer motivation for these mice. However, the average exploration time between the two subgroups of old mice was not different indicating that the lower NOR performance in the BP group reflects impaired memory.

The same cohorts of mice were also tested for their locomotor, explorative, anxiety-like and social behavior. The total distance traveled in the Open Field (OF) was relatively equal between the three subgroups (**Figure 3.1d**), however the time spent in the center of the OF arena was significantly lower in the BP subgroup as compared to the young group, suggesting an anxiety-like phenotype for this subgroup of old mice. The maximum speed in the OF arena was also significantly lower in both the GP and the BP group as compared to the young group (**Suppl. Figure 3.5c**). When tested for their social behavior based on an unconditioned social preference test, both the young and the GP mice spent significantly higher time in the social chamber as compared to the time spent in the neutral chamber, but

the BP showed a reduced preference for the social chamber (**Figure 3.1e**). In addition, the BP spent more time during the familiarization phase in the chamber which was selected as the social chamber in the testing phase (**Suppl. Figure 3.5b**) reflecting a location bias for this side of the apparatus and thus making the social chamber avoidance phenotype during the testing phase even more significant. On the other hand, the young and the GP did not show a preference for any of the chambers during the familiarization phase (**Suppl. Figure 3.5d**). Based on all the three behavioral tests together, the GP mice perform equally good with the young mice, while the BP separate themselves from the other old mice performing lower in every behavioral test (**Figure 3.1f**). Finally, the performance for all behavioral measurements were negatively correlated with age except for the time spent in the neutral chamber during the social preference test (**Figure 3.1g**) indicating a general cognitive deterioration with aging.

Overt increase in inhibitory synaptic protein levels in old, cognitively impaired mice

Alterations in gene expression and subsequently in protein levels in the brain can be regarded as a hallmark of cognitive aging (Hou et al., 2019; Lu et al., 2004). Changes in the molecular and biochemical composition of neurons can affect their synapses and impair synaptic plasticity (Turrigiano and Nelson, 2004; Wefelmeyer et al., 2016). Activity-dependent plasticity relies on both presynaptic and postsynaptic components (Choquet and Triller, 2013) regardless of the nature of the synapse. Thus, we measured the protein levels of several presynaptic proteins crucial for neurotransmitter release but also the levels of various postsynaptic scaffolding proteins which regulate receptors clustering in excitatory or inhibitory synapses.

The protein levels of neuroligin (NL) 1 and 2, which modulate synapse maturation and neural excitability of excitatory and inhibitory synapses respectively, were unaltered in the mPFC of BP or GP as compared to young mice (**Figure 3.2a** and **3.2b**). The ratio of the protein levels of NL1 to NL2 was also not significantly different between the three groups (**Figure 3.2b**). We did not observe any changes in protein levels of the scaffolding postsynaptic protein of excitatory synapses, PSD95, however the levels of the inhibitory counterpart Gephyrin were significantly higher in the BP and GP old mice as compared to young mice (**Figure 3.2c** and **3.2d**). The ratio of PSD95 to Gephyrin was significantly lower in both GP and BP mice as compared to the young mice but not different between the two groups of old mice (**Figure 3.2d**). Finally, the protein levels of the vesicular GABA

transporter (VGAT) were significantly higher in the BP as compared to young mice whereas the levels of the vesicular glutamate transporter were not significantly different between the three groups (**Figure 3.2e** and, **3.2f**). This quantification of synaptic proteins demonstrates that there is a significant increase in the levels of VGAT in the old cognitively impaired mice, consistent with the increase in mIPSC frequency previously described in cognitively impaired rodents (Bories et al., 2013).

The mPFC spontaneous activity tends to decrease in old mice

Previous studies indicate an age-dependent increase in the mPFC inhibitory tone in rodents and nonhuman primates (Bories et al., 2013; Luebke et al., 2004). Consistently, our measurements of excitatory and inhibitory synaptic proteins in GP and BP groups suggest a shift towards inhibition in the mPFC of old cognitively impaired mice. Thus, to explore underlying changes in neuronal activity within the mPFC in old mice we performed *in vivo* multi-unit recordings in a group of old and young mice. Due to the small number of mice available for the multiunit recordings we could not assign the old mice to a cognitively intact or impaired groups. All three old mice were grouped together, similar to the young mice. The spontaneous multi-unit activity in the mPFC was measured while the mice were exploring novel environments (**Figure. 3.3a**).

The mean interspike interval was increased in old mice during the 5 trials of novel environment exploration, but this increase did not reach statistical significance (**Figure. 3.3b**). Similarly, the distribution of the interspike interval of individual spikes detected from different electrodes in all the mice tested across the 5 trials appears to be shifted towards longer intervals in old mice, but this shift was not significantly different between young and old mice (**Figure. 3.3b**). Interestingly, the mean amplitude of the spikes detected from all the electrodes across the sum of the recordings performed was significantly different between young and old mice (**Figure. 3.3c**). These results demonstrate that the different age groups showed a comparable level of spontaneous activity but the amplitude of the spontaneous events in the mPFC during a novel environment exploration is reduced in old mice suggesting a loss of dendritic arborization.

Activation of mPFC GABAergic neurons in young mice induces cognitive deficits but has no effect on old cognitively impaired mice

Optogenetics and the use of opsins allow us to control the activity of specific neuronal populations acutely and study the effect of such manipulation on various experimental setups (Yizhar et al., 2011b). Here we utilized channelrhodopsin (ChR2) and the transgenic Gad2::ChR2-EYFP mice (Madisen et al., 2012) to activate the GABAergic interneurons in the mPFC LII/III of young mice (**Figure. 3.4a**). We tested these mice behaviorally prior to stimulation (No light; **Suppl. Figure 3.6a**) and during stimulation (470 nm; **Suppl. Figure 3.6b**). We used a high frequency stimulation protocol to activate the GABAergic interneurons in the mPFC since these neurons have been described to fire naturally in high frequencies and control oscillatory rhythms within cortical networks (Whittington et al., 1995). The expected outcome of such stimulation should be a decrease in the E/I ratio within the mPFC (**Suppl. Figure 3.6c**).

As shown before in the young C57BL6J mice, the young Gad2::ChR2-EYFP show a significant higher performance in the NOR, i.e. differentiating a novel object from a familiar object before the optogenetic stimulation (**Suppl. Figure 3.7a**). By contrast, optogenetic stimulation of these young Gad2::ChR2-EYFP resulted in memory performance deficits during the NOR test as compared to the performance prior stimulation (**Figure 3.4b**). The object exploration time during stimulation was unaltered suggesting that the memory performance reduction observed with stimulation is not a result of poor motivation (**Figure 3.4c**). Interestingly, when we tested the memory performance of old cognitively impaired Gad2::ChR2-EYFP (**Suppl. Figure 3.7a**) following optogenetic stimulation, there was no difference in the NOR performance index as compared to the performance prior stimulation (**Suppl. Figure 3.7b**).

In the OF test, light stimulation reduced the distance travelled within the arena in the young Gad2::ChR2-EYFP mice (**Figure 3.4d** and **3.4f**). The light stimulation also significantly decreased the time spent in the center of the arena (**Figure 3.4e** and **3.4f**) and surprisingly lowered the maximum speed of movement within the arena (**Figure 3.4g**). Thus, optogenetic activation of GABAergic neurons in the mPFC significantly lowers the motivation of young mice to explore novel environments and induces anxiety-like behavior.

Finally, when we tested this cohort of young Gad2::ChR2-EYFP mice for social preference behavior, we did not observe a significant preference for the social chamber at baseline, before the optogenetic stimulation (**Figure. 3.4h** and **Suppl. Figure 3.7c**). Thus, it is difficult to conclude whether the optogenetic activation of GABAergic neurons in these mice had an

effect in social preference behavior since there was no social preference to start with (**Figure 3.4h**). However, consistent with the findings in the OF test, the young Gad2::ChR2-EYFP mice travelled significantly less distance during stimulation in the three-chamber arena (**Fig. 4i** and **Supp. Figure 3.7d**) but the maximum speed was unaltered (**Figure 3.4j**). Altogether, these results indicate that activation of GABAergic neurons in young Gad2::ChR2-EYFP induces cognitive deficits similar to the ones observed in old cognitively impaired mice. In addition, such effect of GABAergic activation was occluded in old cognitively impaired Gad2::ChR2-EYFP mice.

3.6 Discussion

In the present study we present evidence for alterations in the balance of excitatory and inhibitory neurotransmission within the mPFC which contributes to the onset of cognitive deficits in mice. First, we identified a subset of old mice that display an overt cognitive decline. Second, this cognitive decline was correlated with an increase in presynaptic inhibitory proteins in the mPFC of old, cognitively impaired mice. Third, activating GABAergic neurons within the mPFC of young mice was sufficient to replicate the cognitive deficits presented in old, cognitively impaired mice, and, in the latter, activating inhibition did not yield further cognitive deficits, indicative of occlusion.

Altogether, these observations are consistent with previous work showing an increase in the inhibitory input to PFC pyramidal neurons in cognitively impaired rodents (Abdulla et al., 1995; Bories et al., 2013; Wong et al., 2006) and with studies demonstrating the detrimental influence of excessive inhibition in memory formation (Armenta-Resendiz et al., 2022; Fernandez et al., 2007; Meneses et al., 1993). Yet, our electrophysiology recordings in the mPFC of old mice during novel environment exploration suggest that, despite the age-dependent increase in both pre- and post-synaptic inhibitory markers, the spontaneous neuronal activity is preserved in old mice. Thus, these results call for additional studies on the mPFC neuronal activity in cognitively characterized old and young mice especially since most of the preceding work has employed patch-clamp slice recordings to measure excitatory and inhibitory post-synaptic currents. Finally, cognitive decline can be induced by elevated neuronal activity and disinhibition in Alzheimer's disease and other neurological disorders (Kehrer, 2008; Murray et al., 2014; Palop et al., 2007; Selimbeyoglu et al., 2017; Verret et al., 2012). Thus, preserving the E/I balance in the mPFC appears to be crucial for successful memory performance and cognition, and understanding the various mechanisms by which this balance is disrupted during normal aging, or in pathology will

allow for the development of prosperous therapeutic interventions to treat cognitive disorders.

3.7 Acknowledgments

The authors thank Cesar Benavente for animal genotyping and Caroline Menard and Cyril Bories for their invaluable comments on the behavioral data.

3.8 Author Contributions

IK and YDK designed the experiments. IK performed all the immunoblots, surgeries and the *in vivo* electrophysiology. IK and RH performed the behavioral experiments. IK and RS analyzed the behavioral data. IK, GGT and AGG analyzed the electrophysiology data. IK, AGG and YDK interpreted the data. GGT and BG provided the wireless electro-optic headstage. IK and YDK wrote the manuscript. YDK obtained funding and supervised all aspects of the present study. All the authors read and approved the final version of the manuscript.

3.9 Figures

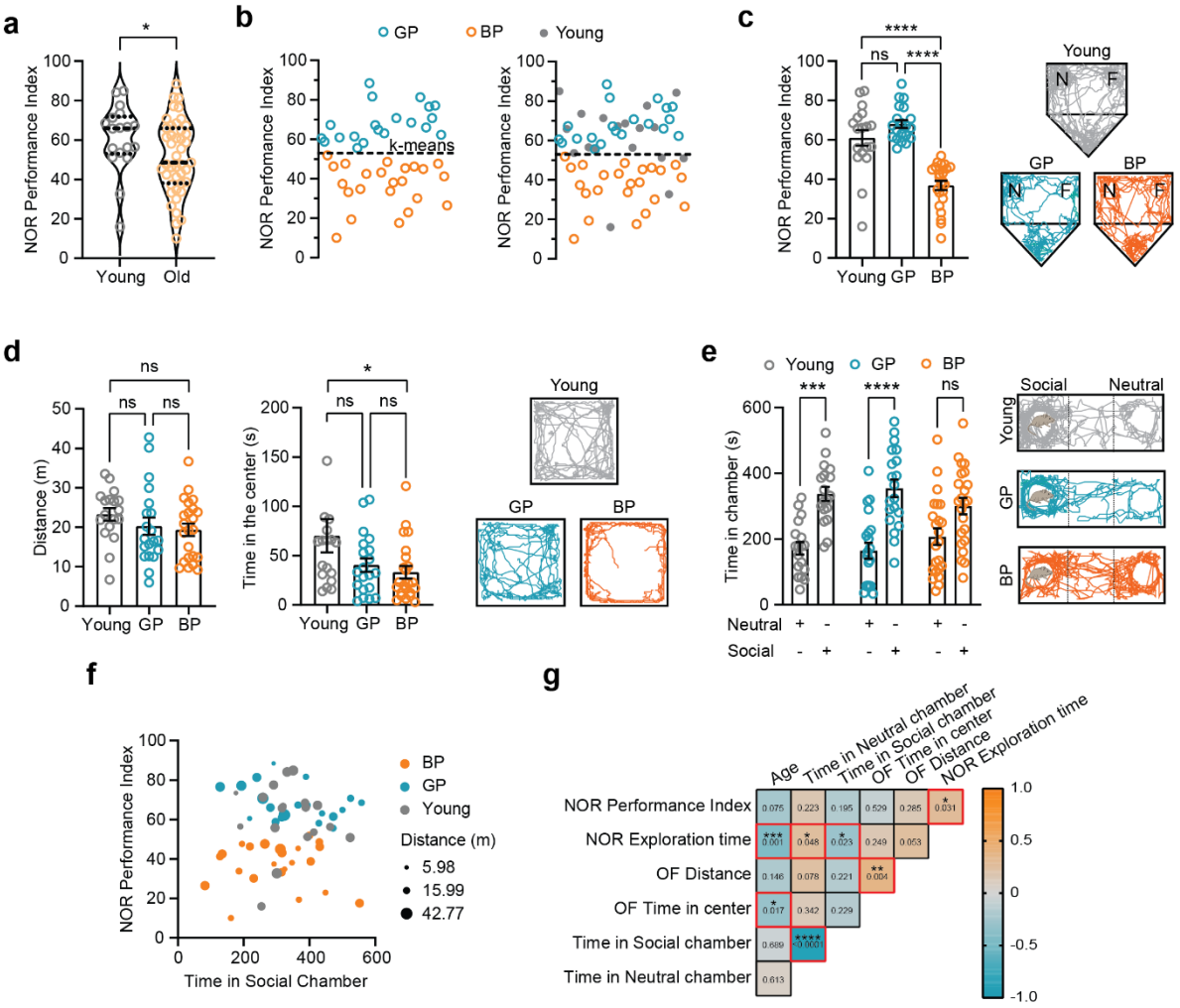

Figure 3.1. A subgroup of old mice develops cognitive deficits.

(**a**) The median Novel Object Recognition (NOR) performance index of the young and old mice (young: n = 18; old n = 43). (**b**) K-means clustering analysis identifying two distinct subpopulations within the old mice based on their NOR performance index (left). On the right the k-means clustering results when the young mice are added as data points. The dashed line represents the NOR Performance Index value threshold set based on the subgrouping. (**c**) The NOR performance index of the young, GP and BP groups and representative track plots of an individual mouse from each group during the NOR 1 hour memory test. (**d**) The average distance travelled during the Open Field (OF) test and the time spent in the center of the OF arena. On the right, representative track plots of a young, a GP and a BP mouse for the OF test. (**e**) The time spent in the social vs. the neutral chamber during the three chamber unconditioned social interaction test and representative track plots of mice belonging in the young, GP and BP group. (**f**) Clustering of the young, BP and GP group mice according to the behavioral measurements of NOR, social interaction and OF. (**g**) Pearson correlation

of various behavioral measurements and age. The color-coded scale represents the Pearson correlation coefficient r-value. P-values in the boxes refer to the strength of each correlation. Data in bar graphs are presented as mean ± SEM. Young: *n* =18; GP: *n* = 21 and BP: *n* = 22. * P < 0.05; ****P < 0.0001; ns = non significant.

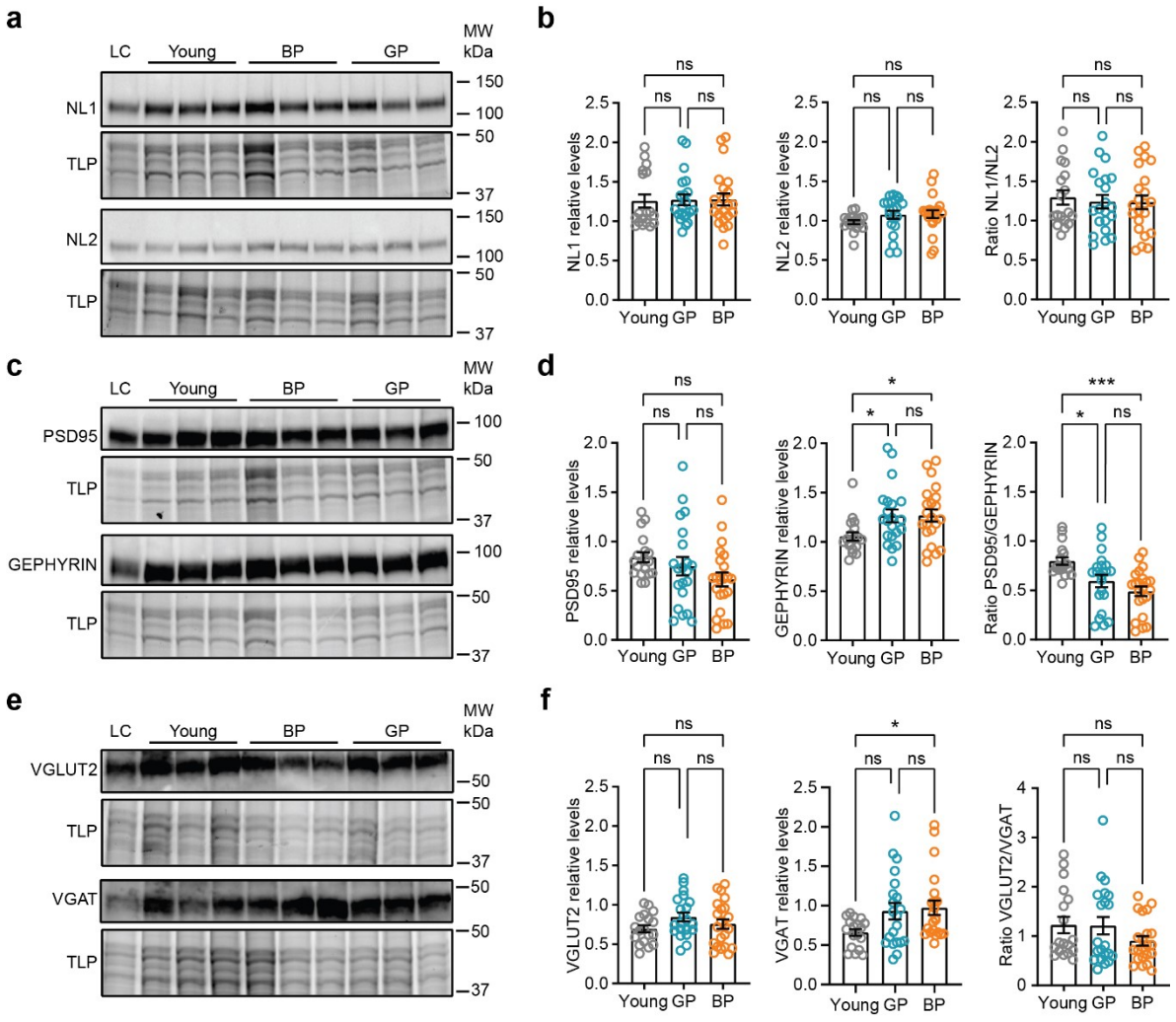

Figure 3.2. Pre- and post-synaptic inhibitory proteins are upregulated in old mice.

(**a, c, f**) Representative immunoblots for the levels of neuroligin I and neuroligin II (**a**), PSD95 and Gephyrin (**c**), and VGLUT2 and VGAT (**f**) in PFC homogenates of young, old BP and GP mice. (**b**) Quantification of neuroligin I (left), neuroligin II (middle) protein levels, and the ratio of the two (right). (**d**) Quantification of the protein levels of PSD95 (left) and Gephyrin (middle) and the ratio of PSD95 to Gephyrin (right). (**f**) Quantification of VGLUT2 (left) and VGAT (middle) protein levels and the ratio of the two (right). Data in bar graphs are presented as mean ± SEM. LC = loading control sample; BP = Bad Performers; GP = Good Performers; TLP = total lysate protein; NL1 = neuroligin I; NL2 = neuroligin II. Young: *n* =18; GP: *n* = 21 and BP: *n* = 22. * P < 0.05; ***P < 0.001; ns = non significant.

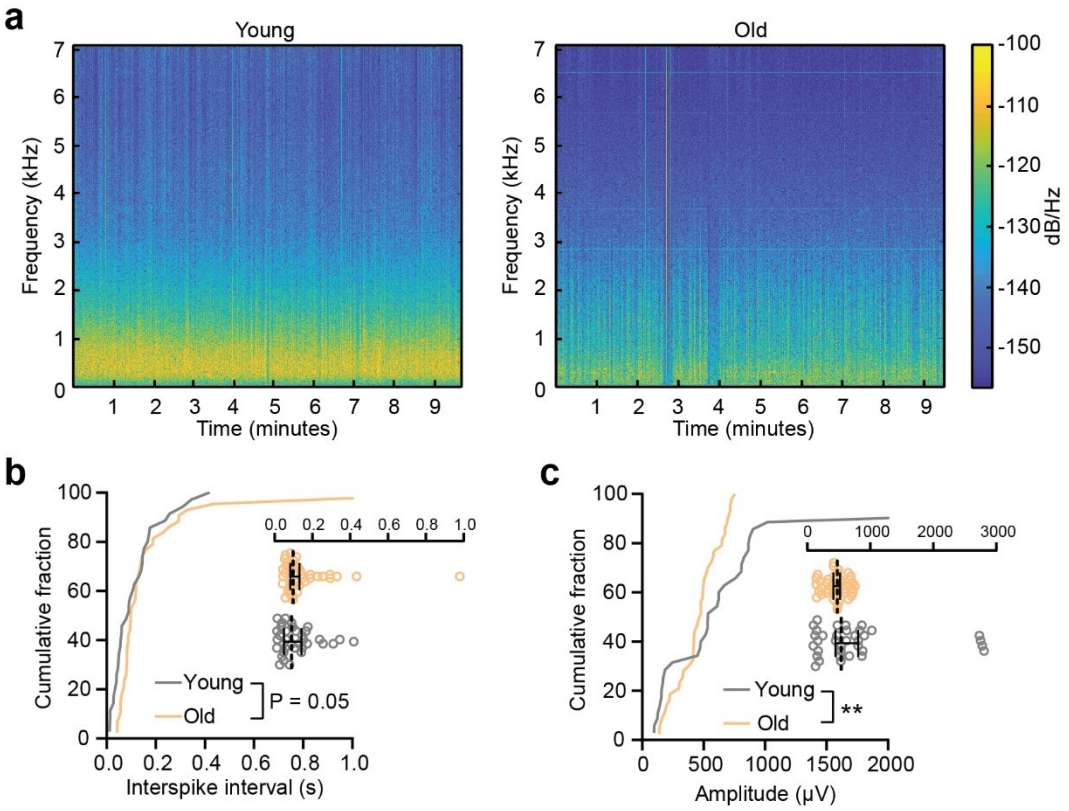

Figure 3.3. The mPFC spontaneous activity is unaltered in old mice but the amplitude of the events is reduced during exploration.

(**a**) Spike wavelet spectrograms of mPFC activity during open-field exploration in a young (left) and old (right) mouse. (**b**)The cumulative distribution of the interspike intervals for each clustered spike across all the recordings performed. The insets show the median interspike interval of spikes detected during each trial exploring a novel environment. The scale bar represents units of interspike intervals in seconds (Young: *n* = 35 spike clusters from *N* = 3 mice in gray; Old: *n* = 43 spike clusters from *N* = 3 mice in yellow). (**c**) The cumulative distribution of the amplitude of detected spikes in young and old mice. The insets (right; Young: *n* = 35 spike clusters from *N* = 3 mice in gray; Old: *n* = 43 spike clusters from *N* = 3 mice in yellow). **P < 0.01; ns = non significant, Kolmogorov-Smirnov test.

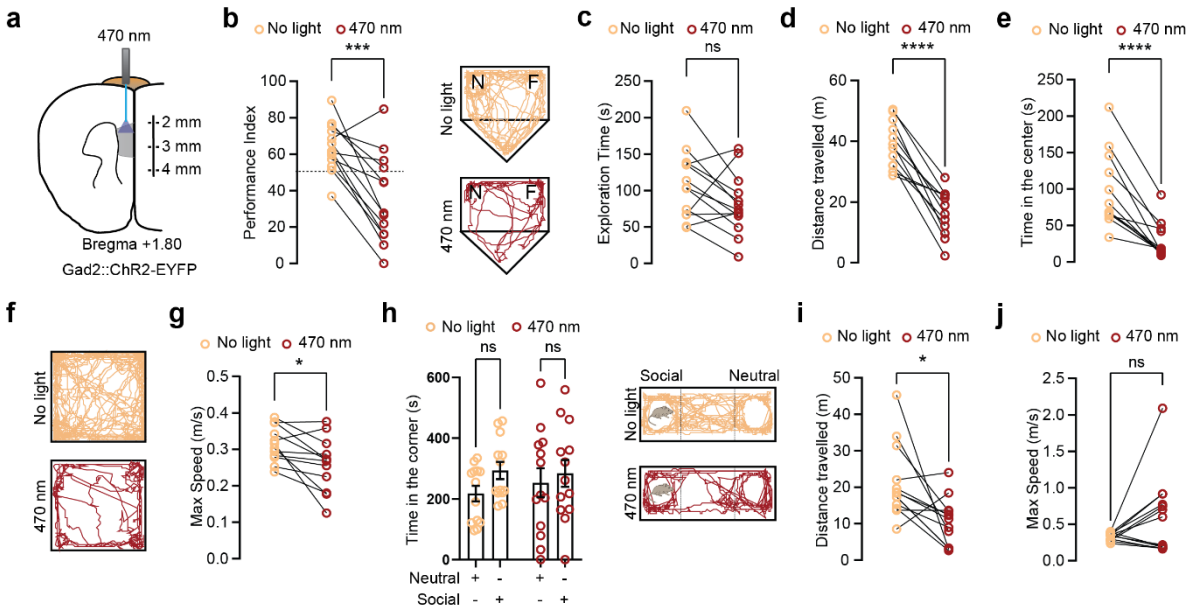

Figure 3.4. Activating GABAergic neurons in young mice induces cognitive deficits.

(**a**) Experimental setup for optogenetic activation behavioral experiments. The gray area marks the targeted brain region. Blue light (470 nm) was used to activate the ChR2 in the Gad2::ChR2-EYFP mice. (**b**) The NOR performance index of the young Gad2::ChR2-EYFP mice during baseline (No light, yellow) and upon stimulation (470 nm, red). Representative track plots of an individual mouse before and upon light stimulation during the NOR 1 hour memory test. (**c**) The time exploring the novel or the familiar object during the NOR 1 hour memory test. (**d - e**) The distance travelled (**d**), and the time spent in the center (**e**) of the open field arena during the baseline and upon stimulation by the Gad2::ChR2-EYFP mice. (**f**) Representative track plots of a mouse exploring the open field arena. (**g**) The maximum speed of Gad2::ChR2-EYFP mice in the open field arena. (**h**) The time spent in the social vs. neutral chamber during the unconditioned social interaction test (left) and track plots of a Gad2::ChR2-EYFP mouse in the three-chamber arena (right) before and during optogenetic stimulation. (**i - j**) The distance travelled (**i**) and the maximum speed (**j**) of Gad2::ChR2-EYFP mice during the social interaction test. Data are presented as mean ± SEM. Circles represent individual mice. No light and 470 nm: *n* = 13 mice. *P < 0.05; ***P < 0.001; ****P < 0.0001 and ns = non significant.

3.10 Supplementary materials

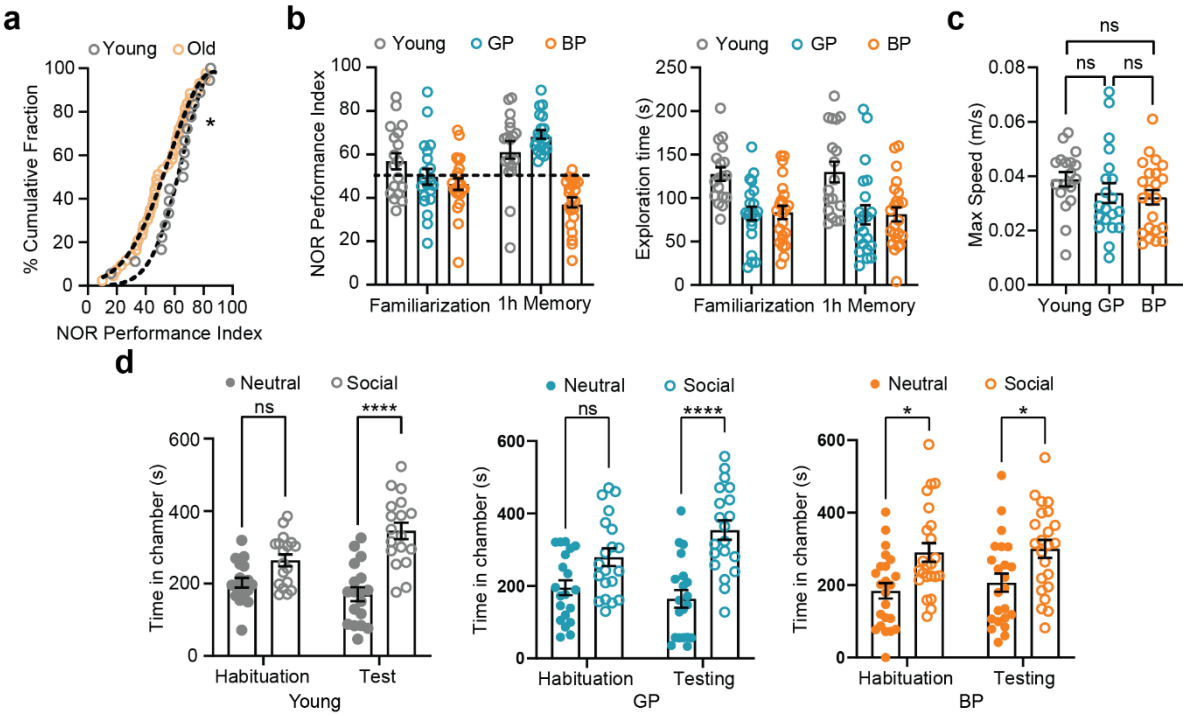

Suppl. Figure 3.5. Memory and social interaction deficits for the BP aged mice.

(**a**) Cumulative frequency distribution of the NOR performance index for the young and old mice. (**b**) The mean NOR performance index during the familiarization and 1 hour memory test phase for the young, GP and BP group and the total time exploring the two identical objects during the familiarization phase and the novel and familiar object during the test phase. (**c**) The maximum speed and the ratio of time spent in the center to the time spent close to the walls of the arena in the open field test. (**d**) The average time spent in the neutral (non-social) and the social chamber during the habituation and the social test phase for the young (left), the GP (center) and the BP (right) group. Bar graphs present the mean ± SEM. Young: *n* =18; GP: *n* = 21 and BP: *n* = 22. ** P < 0.01; ****P < 0.0001; ns = non significant.

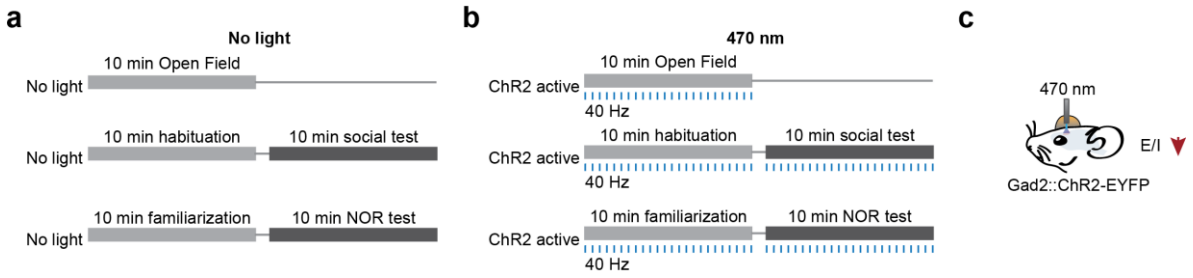

Suppl. Figure 3.6. Control of the mPFC E/I balance via ChR2 activation.

(**a**) Diagram illustrating the chronological order of behavioral testing for the Gad2::ChR2-EYFP mice and the light stimulation protocols during the stimulation phase. (**b**) The expected change in the mPFC E/I balance followed ChR2 activation in Gad2::ChR2-EYFP mice.

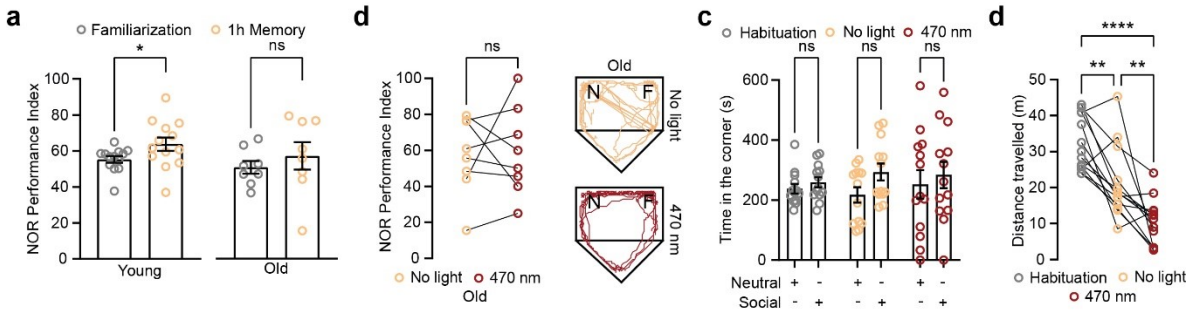

Suppl. Figure 3.7. Activating GABAergic neurons in old, cognitively impaired mice has no effect on non-spatial memory

(**a**) The NOR performance index of the young and old Gad2::ChR2-EYFP mice during the familiarization phase and the1 hour memory test. (**b**) The NOR performance index of the old, cognitively impaired Gad2::ChR2-EYFP mice during baseline (No light, yellow) and upon stimulation (470 nm, red). Representative track plots of an individual mouse before and upon light stimulation during the NOR 1 hour memory test. (**c**) The time spent in the social vs. the neutral corner during the social preference test. For the habituation stage, the neutral and social represent the corner for which an object or an animal will be placed during the social interaction stage respectively. (**d**) The distance travelled during each stage of the social preference test. Bar graphs present the mean ± SEM. Circles represent individual mice. Habituation, No light and 470 nm: *n* = 13 mice. **P < 0.01; ****P < 0.0001; and ns = non significant.

.

Chapter 4 – Hippocampal chronic optogenetic activation alters proteome and elicits synapse disruption

Iason Keramidis[1,2], Romain Sansonetti[1], Johanna Alonso[1,2], Martina Samiotaki[3], Katerina Papanikolopoulou[4], Yves De Koninck[1,2]

1. CERVO Brain Research Centre, Quebec Mental Health Institute; Québec, QC, Canada.
2. Department of Psychiatry & Neuroscience, Laval University; Québec, QC, Canada.
3. Institute for Bio-Innovation, Biomedical Sciences Research Centre Alexander Fleming, 34 Fleming Street, Vari, Greece.
4. Institute for Fundamental Biomedical Research, Biomedical Sciences Research Centre Alexander Fleming, 34 Fleming Street, Vari, Greece.

4.1 Résumé

La surexcitabilité neuronale peut perturber la formation et la force des synapses et provoquer des modifications synaptiques qui, à leur tour, donnent lieu à une hyperactivité neuronale et, finalement, à un traitement anormal global des circuits neuronaux. Un tel dysfonctionnement du réseau nuit à la fonction et à la survie des neurones, ce qui entraîne l'apparition de la neurodégénérescence. Néanmoins, les changements synaptiques séquentiels qui résultent d'une hyperactivité neuronale soutenue demeurent incompris. Pour y remédier, nous avons choisi l'optogénétique pour générer un modèle d'hyperactivité neuronale durable dans l'hippocampe. Nous avons appliqué ce modèle à des souris de type sauvage ainsi qu'à des souris 5xFAD présentant des mutations qui les prédisposent à développer la maladie d'Alzheimer. Nous avons analysé les modifications du protéome survenant après un mois de stimulation optogénétique chronique quotidienne. À la suite de ce protocole de stimulation, les protéines participant au métabolisme des lipides étaient principalement régulées à la hausse chez les souris 5xFAD. Par contraste, les protéines impliquées dans les processus biologiques tels que le traitement de l'ARNm, la traduction, la phosphorylation et, plus important encore, la signalisation synaptique étaient altérées chez les souris de type sauvage. Les protéines des synapses glutamatergiques et GABAergiques étaient régulées à la baisse chez les souris de type sauvage, indiquant une perturbation potentielle de la transmission synaptique à la suite d'une hyperactivité neuronale chronique. À leur tour, les modifications du protéome dans l'hippocampe des

souris de type sauvage ont entraîné une perte de mémoire spatiale et une augmentation surprenante de la sécrétion de Aβ42. Dans l'ensemble, ces résultats indiquent que la surexcitabilité et l'hyperactivité neuronales peuvent contribuer directement à la perturbation de la transmission synaptique, aux déficits de mémoire et au processus neurodégénératif associé à la maladie d'alzheimer.

4.2 Abstract

Neuronal overexcitability can disrupt synapse formation and strength and elicit synaptic changes which in turn give rise to neuronal hyperactivity, and eventually overall abnormal neural circuit processing. Such network dysfunction impairs neuronal function and survival, resulting in the onset of neurodegeneration. Yet, the sequence of synaptic changes that result from sustained neuronal hyperactivity remain elusive. To address this, we adopted an optogenetic stimulation strategy to generate a model of long-lasting neuronal hyperactivity into the hippocampus. We applied this to both wild-type mice as well as in the 5xFAD mice presenting mutations that confer susceptibility to develop Alzheimer's disease in humans. We analyzed the proteome changes occurring after a month of daily chronic optogenetic stimulation. Following this stimulation protocol, proteins participating in lipid metabolism were upregulated primarily in 5xFAD mice. By contrast, proteins involved in biological processes such as mRNA processing, translation, phosphorylation and, more importantly, synaptic signaling were lowered in wild-type mice. Both proteins of glutamatergic and GABAergic synapses were downregulated in wild-type mice indicating potential disruption of synaptic transmission following chronic neuronal hyperactivity. In turn, proteome changes in the hippocampus of wild-type mice resulted in spatial memory loss and surprisingly augmented Aβ42 secretion. Altogether, these findings indicate that neuronal overexcitability and hyperactivity can contribute directly to synaptic transmission disruption, memory deficits and the neurodegenerative process associated with Alzheimer's disease.

4.3 Introduction

Aberrant neuronal activity can impair synapse formation and strength resulting in disruption of synaptic plasticity. In turn, altered synaptic plasticity can reorganize synaptic connections ensuing runaway excitation or quiescence and eventually modify local neuronal circuits (Turrigiano and Nelson, 2004). For neural circuits to maintain their characteristic firing patterns, neurons within the network undergo homeostatic changes at the cellular

level, regulating synthesis and degradation of key synaptic proteins (Marder and Prinz, 2002; Wefelmeyer et al., 2016). Alterations perturbing these regulations have been linked with the onset of various brain disorders such as epilepsy and autism (Specchio et al., 2022). Neuronal hyperexcitability manifests early in Alzheimer's disease (AD) (Palop and Mucke, 2016; Zott et al., 2018), leading to cortical and hippocampal hyperactivity (Bassett et al., 2006; Bookheimer et al., 2000) and under certain conditions to epileptiform activity and seizures both in rodents (Busche et al., 2008; Verret et al., 2012) and humans (Vossel et al., 2017). Both amyloid-β (Aβ) and tau have been found to induce neuronal hyperactivity through distinct cellular mechanisms (Huijbers et al., 2019; Ittner et al., 2010b; Roberson et al., 2007; Verret et al., 2012; Zott et al., 2019). Concurrently, neuronal hyperactivity can increase Aβ secretion (Cirrito et al., 2005; Yamamoto et al., 2015) and promote pathological phosphorylation of Tau (Frandemiche et al., 2014). These observations suggest that Aβ and Tau can initiate a vicious cycle of neuronal hyperactivity in AD underlying neurodegeneration in disease. However, it still remains unknown whether neuronal hyperactivity alone can induce pathology mimicking neurodegeneration in AD.

Optogenetics has emerged as a powerful method to control the activity of genetically defined neurons allowing to study the function of selective brain circuits in physiological but also pathological conditions (Kim et al., 2017; Ruthazer et al., 2022; Yizhar et al., 2011b). Stabilized step function opsins (SSFOs) allow also for long-lasting activation of neural circuits with a brief light stimulation (Yizhar et al., 2011a). Such chronic optogenetic activation is necessary to model neurodegenerative disorders, such as AD, for which neuronal activity is altered for long periods of time. We adopted a similar approach to generate a model of chronic neuronal hyperactivity in the hippocampus of wild-type (WT) and transgenic mice carrying AD-linked mutations and demonstrate that evoked neuronal hyperactivity can disrupt synaptic signalling and facilitate an activity-driven neuropathology similar to AD.

4.4 Results

Optogenetic activation of the hippocampus in wild-type and 5xFAD mice using SSFO

To generate a model of chronic neuronal hyperactivity in the rodent hippocampus we virally transduced the SSFO-mCherry or tdTomato unilateral under the CaM kinase II promoter (CaMKIIa) into the CA1 of wild-type (WT) or 5xFAD (Oakley et al., 2006) male mice (**Figure 4.1A** and **4.1B**). We then inserted an optic fiber cannula above the CA1 and

stimulated the infected neurons for 4 weeks by blue light (**Figure 4.1A**). To validate if light stimulation of the SSFO evoked neuronal activity, we performed immunostaining for c-Fos on brain sections. Coronal sections of mice infected with AAV-CaMKIIa-SSFO-mCherry in the hippocampus showed mCherry labelling in the CA1, CA2 and CA3 (**Figure 4.1B**). Sixty minutes after light stimulation of CA1 neurons transduced with SSFO-mCherry, the ipsilateral CA1, CA3 and dentate gyrus (DG) neurons displayed increased c-Fos as compared to neurons of the contralateral side (**Figure 4.1C**). In mice infected with AAV-CaMKIIa-tdTomato, neurons in both the ipsilateral hippocampus were negative for c-Fos (**Suppl. Figure 4.5**).

Using extracellular recordings in anesthetized mice we assessed the light-induced changes in the activity of the CA1 region transduced either with the SSFO-mCherry or tdTomato (**Figure 4.1D**). In mice expressing the SSFO-mCherry, the multiunit spike rates within the CA1 increased for several minutes after a 2s light pulse as expected (**Figure 4.1E** and **4.1F**). Conversely, in tdTomato expressing mice, multiunit spiking activity did not increase following the brief light pulse (**Figure 4.1E** and **4.1F**). These results indicate that the SSFO is transduced in the hippocampus and can be activated by light stimulation to generate neuronal hyperactivity.

Chronic optogenetic stimulation of the hippocampus downregulated synaptic proteins and upregulated oxidative phosphorylation in wild-type mice

We sought to identify and quantify alterations in protein levels in response to sustain neuronal hyperactivity in the hippocampus of mice. We analyzed the hippocampi of wild-type mice expressing SSFO or tdTomato after 4 weeks of daily brief light stimulation (**Figure 4.1A**) using label-free liquid chromatography with tandem mass spectrometry (LC-MS/MS) proteomic analysis. We identified 859 proteins altered (**Figure 4.2A**). The chronic optogenetic stimulation in mice expressing SSFO significantly downregulates the expression of 620 proteins and only upregulates the expression of 239 proteins (**Figure 4.2A**). When we sorted the proteins altered for only the ones with a fold of change above or below 1.2, still the majority of them were downregulated (**Figure 4.2B**). Gene functional classification analysis with DAVID (Huang et al., 2009) showed that these proteins were mainly part of the cytoplasmic, nuclear and mitochondrial cellular components (**Figure 4.2C**). Yet, 53 proteins identified were part of the synapse (**Figure 4.2C** and **Suppl. Table 4.1**) suggesting that synaptic function is altered by evoked neuronal hyperactivity.

Gene Ontology (GO) enrichment analysis with STRING (Szklarczyk et al., 2021) revealed that modulation of synaptic transmission and synaptic signalling are two biological processes significantly downregulated by chronic optogenetic stimulation (**Figure 4.2D**). Protein transport, cytoskeleton organization and phosphorylation were other biological processes downregulated while translation and oxidative phosphorylation (OXPHOS) were upregulated (**Figure 4.2D**). Among the 33 synaptic signaling proteins downregulated, 15 proteins are enriched in glutamatergic synapses, while 5 are enriched in GABAergic synapses (**Figure 4.2E**). And yet there are several more proteins key for synaptic transmission that were found significantly downregulated in wild-type mice following chronic hippocampal hyperactivity (**Figure 4.2E** and **4.2F**). Finally, upregulation of OXPHOS and ATP metabolism (**Figure 4.2G**) indicated elevated mitochondrial activity following stimulation responsible for powering cell signaling cascades and neuronal activity (Hall et al., 2012).

Evoked chronic neuronal hyperactivity in the hippocampus of 5xFAD mice upregulates lipid metabolism

We adopted the same approach to induce neuronal hyperactivity in the hippocampus of 5xFAD mice, a transgenic line overexpressing mutations that have been linked to AD (**Figure 4.1A**). The chronic optogenetic stimulation in 5xFAD mice resulted in significantly upregulating the levels of 179 proteins while it resulted in downregulating the levels of only 63 proteins (**Figure 4.3A**). Consistently, the majority of the proteins showing the greatest fold of change following stimulation in 5xFAD mice were upregulated (**Figure 4.3B**). The altered proteins were primarily cytoplasmic and mitochondrial (**Figure 4.3C**). Only twelve proteins among them were identified as synaptic proteins (**Figure 4.3C**), representing approximately four times less proteins as compared to the altered proteins following stimulation in WT mice. From these synapse proteins, six are part of the glutamatergic synapse, one part of the GABAergic synapse and one has been described to participate in both excitatory and inhibitory synapses (**Figure 4.3D**).

GO enrichment analysis did not reveal any biological processes downregulated by chronic optogenetic stimulation, however proteins transport, organic acid metabolism and regulation of autophagy were upregulated (**Figure 4.3E**). Contrary to the wild-type mice, neurons in 5xFAD mice seem to favor fatty acid metabolism to produce the required energy for maintaining the elevated neuronal activity (**Figure 4.3F**). This is consistent with a

mitochondrial dysfunction previously reported in AD (Sorrentino et al., 2017) but also our proteomic analysis between wild-type and 5xFAD mice (**Suppl. Figure 4.6**). Functional classification of the proteins downregulated in 5xFAD mice as compared to WT mice revealed that the second most enriched cellular component is the mitochondria (**Suppl. Figure 4.6D**). The OXPHOS activity and ATP synthesis are diminished in 5xFAD neurons in the hippocampus (**Suppl. Figure 4.6D**).

Neuronal hyperactivity in wild-type mice induces spatial memory deficits and augments Aβ42 secretion

Hippocampal hyperactivity has been implicated in memory deterioration and AD pathogenesis (Palop and Mucke, 2016; Vossel et al., 2017). To explore whether the chronic optogenetic activation in the hippocampus of WT mice replicates some of the neurodegenerative processes involved in the pathogenesis of AD, we performed a hierarchical clustering analysis based on our proteomic analysis. Accordingly, we found that the WT+SSFO mice grouped together with the 5xFAD+tdTom or 5xFAD+SSFO while the WT+tdTom mice separated from the rest of mice according to the scalled changes in protein levels (**Figure 4.4A**). Interestingly, when we compared the proteins altered by stimulation in WT+SSFO mice to the ones altered due to the mutations and pathology in the 5xFAD mice, we identified only 356 proteins as differentially expressed (**Figure 4.4B** and Suppl. **Figure 4.7**). Among these proteins, GO analysis identified 17 proteins implicated in pathways related to AD (**Suppl. Table 4.2**), with 10 participating in OXPHOS and found upregulated in WT+SSFO mice (**Suppl. Figure 4.7**), further supporting the previous findings of a mitochondrial dysfunction in 5xFAD mice (**Suppl. Figure 4.6D**).

To examine how chronic hippocampal hyperactivity and the synaptic transmission changes (**Figure 4.2F**) observed following the optogenetic stimulation impact brain function, we performed behavioral testing of WT and 5xFAD mice. We adopted a modified version of the Y-maze alternation test allowing for the evaluation of spatial memory performance in mice (**Figure 4.4C**). We found that chronic optogenetic stimulation in the hippocampus of WT mice resulted in spatial memory deficits, more profound than the impairment seen in 6-months-old 5xFAD mice (**Figure 4.4D**).

Finally, since previous observations have linked neuronal and network hyperactivity with an increase in the secretion and deposition of amyloid-β in the brain of transgenic mice carrying several AD-linked mutations (Bero et al., 2011; Cirrito et al., 2005; Kamenetz et al.,

2003; Yamamoto et al., 2015), we sought to measure the levels of soluble Aβ40 and Aβ42 in the brain of WT mice following our chronic optogenetic stimulation protocol. In the brain of WT+SSFO mice the levels of soluble secreted Aβ42 were significantly increased by 330% as compared to the levels in the brain of WT+tdTom mice (**Figure 4.4E**). The levels of Aβ40 showed a trend of increase in the WT+SSFO mice, but this increase was not significantly different to the Aβ40 levels in the WT+tdTom (**Figure 4.4E**). Altogether, these results suggest that chronic neuronal hyperactivity is sufficient to induce synaptic transmission disruption and memory loss similar to that observed in the neurodegenerative process in AD, and also augments the amyloidogenic cleavage of App.

4.5 Discussion

We adopted optogenetics and a bi-stable step function opsin (SSFO) to induce chronic neuronal hyperactivity and examine the effect of such manipulation in the hippocampus of young wild-type and 5xFAD mice. We present evidence of: (1) an overt downregulation in the levels of both excitatory and inhibitory synaptic proteins and a potential upregulation of mitochondrial OXPHOS following neuronal hyperactivity in wild type mice; (2) an increase in the levels of proteins participating in lipid metabolism in 5xFAD; (3) spatial memory impairments in young mice expressing SSFO upon light stimulation; and (4) elevated levels of soluble Aβ42 in wild-type hippocampi following chronic optogenetic stimulation. Our findings strongly support the notion that rampant neuronal hyperactivity distorts cellular mechanisms regulating synthesis and degradation of synaptic proteins contributing to memory impairments.

Neurons in the hippocampus respond to high energy demands, to sustain an increase in neuronal activity, by generating ATP through oxidative phosphorylation (Hall et al., 2012). Consistently, our GO results based on the proteome analysis showed that neurons in the hippocampus of wild-type mice responded to the optogenetic activation by upregulating OXPHOS and respiratory chain reactions to fuel the increased firing (**Figure 4.2D** and **4.2G**). In contrast, such an effect was occluded in the 5xFAD mice, consistent with previous findings showing a mitochondrial dysfunction both in AD patients (Chandrasekaran et al., 1994) and AD-mimicking mice (Rhein et al., 2009). Instead, fatty acid catabolism was favored in the 5xFAD mice as an alternative energy source (**Figure 4.3F**) which was unexpected considering the pre-existing lipid metabolism defects reported in this transgenic line (Bai et al., 2020).

In various neurological disorders, cognitive decline has been associated with hippocampal hyperactivity and the failure to deactivate brain regions consisting the default mode network (e.g. posterior cingulate cortex, precuneus, retrosplenial cortex) (Koh et al., 2010; Oser et al., 2014; Palop and Mucke, 2016; Putcha et al., 2011; Seidman et al., 2014; Sperling et al., 2009). Reducing neuronal hyperactivity pharmacologically has been also found to improve cognitive performance in humans with mild cognitive decline (Bakker et al., 2012; Miller et al., 2008) suggesting that neuronal hyperactivity is a cause and not a compensatory mechanism of cognitive decline. But neuronal hyperactivity may have broader implications in disease onset. Apart from contributing to cognitive deficits, neuronal hyperactivity could drive several other pathological aspects related to AD, such as Aβ release (Yamamoto et al., 2015), synaptic loss (Hefendehl et al., 2016; Lacor et al., 2007) and neuronal degeneration (Putcha et al., 2011).

It has been shown before that electrical, pharmacological and optogenetic neuronal stimulation can augment the secretion of Aβ from the presynaptic terminals in various APP transgenic mouse lines (Bero et al., 2011; Cirrito et al., 2005; Kamenetz et al., 2003; Yamamoto et al., 2015). In turn, elevated Aβ levels have been shown to induce neural overexcitability and hyperactivity disrupting neural circuits both in wild-type and APP transgenic mouse lines (Busche et al., 2008, 2012; Zott et al., 2019). Moreover, in humans, within the brain regions where Aβ aggregation is most profound, the basal metabolic rates and neuronal activity are elevated (Bassett et al., 2006; Bero et al., 2011; Buckner et al., 2005). These findings support the hypothesis of a significant unclamped cycle facilitating an Aβ-dependent neuronal hyperactivity in AD (Zott et al., 2019) and are in line with our results showing an increase in soluble Aβ42 secretion and a multifactorial perturbation of synaptic transmission in wild-type animals following neuronal hyperactivity.

Finally, the absence of an overt effect of the chronic optogenetic stimulation in the 5xFAD, at least at the synaptic protein level, suggests an occlusion of the detrimental effects of evoked neuronal hyperactivity in AD, or a potential pre-existing loss of synaptic reserve. This is in line with the observations indicating that neuronal hyperactivity manifests early in AD resulting in synapse and circuit disruption (Palop and Mucke, 2016). And yet, while these deficits in circuits arising from neuronal degeneration in AD might appear beyond repair, suppressing excessive neuronal activity early in the progression of the disease may represent a possible therapeutic modality to delay or modify the disease progression and cease the vicious cycle of relentless hyperactivity.

4.6 Experimental Procedures

Animals

Rodent experiments were carried out on male 5xFAD mice, and their wild-type littermates bred and housed in the CERVO Brain Research Centre animal facility. The male 5xFAD and female B6SJLF1/J breeders were purchased from the Jackson Laboratory (#34840-JAX and #100012, respectively). Mice were housed on a 12 h day/night cycle with ad libitum access to food and water. Only male mice were used in this study and were randomly assigned to experimental groups. All experiments were approved by the committee for animal protection of Université Laval (CPAUL) and followed the guidelines from the Canadian Council for Animal Care.

Surgical Procedures and viral transduction

The optic fibers (200 µm core, 0.39 NA on 2.5 mm ceramic ferrules) flat-cleaved tip was coated with 100 nL of a 1:1 mix of silk fibroin solution (Sigma cat# 5154-20ML) and the viral vector AAV2/5-CaMKIIa-hChR2(C128S/D156A)-mCherry (called AAV2/5-CaMKIIa-SSFO-mCherry here after; titer: 7.7 x 1012 GC/mL, Canadian Neurophotonics Platform Viral Vector Core) or AAV2/8.CaMKIIa.tdTomato (titer: 1.3 x 1013 GC/mL, Canadian Neurophotonics Platform Viral Vector Core, RRID: SCR_016477). The optic fibers were left to dry for 15 hrs at 4 ^{o}C prior the surgery as described in (Jackman et al., 2018). Stereotaxic surgery was performed on mice (4-weeks old) maintained on isoflurane anaesthesia. Briely, a circular craniotomy was drilled above the hippocampus with coordinates: -2.30 mm rostro-caudal and - 2.00 mm latero-medial. The optic fiber cannula was lowered 1.60 mm into the brain (dorso-ventral - 1.60 mm) and fixed on the cranium with C&B Metabond® (Parkell Inc.). Following the surgery, mice were single-housed and the chronic optogenetic stimulation experiments started 4-5 weeks later.

For the optrode recordings, the same viral vectors were unilaterally infused into each side of the hippocampal CA1 (rostro-caudal: -2.30 mm, latero-medial: 2.00 mm, dorso-ventral: 1.60 mm). The infusion was performed with pulled borosilicate glass capillaries and a NANOLITER2020 injector (World Precision Instruments LLC). The *in vivo* optrode experiments started a minimum of 4 weeks later.

Optogenetic stimulation

After 4-5 weeks from the optic fiber implantation mice were optically stimulated for 2 s every 24 hrs (starting at 2-months of age) for 4 weeks by blue light (470 nm, 1 mW). The

light was generated by an LED diode (ThorLabs cat# M470F3) and delivered through fiber optics (200 µm core, 0.39 NA) to the implanted fiber optic cannulae.

In vivo extracellular optrode recordings

Simultaneous optical stimulation and electrical extracellular recording in the hippocampal CA1 was performed in B6SJLF1 male mice previously transduced with SSFO or tdTomato using a micro-optrode (LeChasseur et al., 2011). Briefly, mice were anesthetized with a mix of 100 mg ketamine, 15 mg xylazine and 2.5 acepromazine per kg and placed in a stereotaxic frame on a temperature control pad. A craniotomy was drilled above the hippocampus with coordinates: -2.30 mm rostro-caudal and - 2.00 mm latero-medial. A micro-optrode (6-8 µm tip diameter; 550 µm optical core; 0.22 NA; 100 µm hollow core) was filled with 0.5 M potassium acetate solution, connected to a 470 nm laser diode (Doric lenses) through a multimode optical fiber (600 µm optical core; 0.22 NA; ThorLabs) and lowered vertically to the brain. Electrophysiological recordings were initiated at -1,3 mm ventral. A 2s long light pulse was delivered to activate the SSFO. The extracellular electrophysiological signal was amplified (Neurodata IR183, Cygnus technology), filtered (band pass, 300–3,000 Hz, model 440, Brownlee Precision), and digitized. The filtered traces were analyzed with Spike2 (Cambridge Electronic Design). Events were isolated, clustered and quantified to plot the peristimulus time histogram.

Samples Preparation

For the proteomics analysis, brains were excised from anesthetized mice (30% urethane in saline) within 30 min after optogenetic stimulation. The hippocampi were dissected, collected in sample tubes, frozen immediately in liquid nitrogen and stored at -80 ºC until use. 25 mg of frozen tissue was lysed in 150 µL of freshly made lysis buffer (4% SDS, 0.1 M DTT, 100 mM Tris/HCl; pH 7.6) and homogenized with an electric FisherBrandTM Pellet PestleTM homogenizer (Thermo Fisher Scientific, cat# 12141361). Homogenates were incubated at 95 ºC for 3 min and centrifuged at 16,000 g for 5 min. The supernatants were transferred into sample tubes and stored at -80 ºC.

For ELISA, tissue was harvested as before within 30 min after optogenetic stimulation. 25 mg of frozen hippocampus tissue was homogenized in 150 µL of RIPA buffer (50 mM Tris-HCl, 150 mM NaCl, 1% Triton X-100, 0.5% Na deoxycholate, 0.1% SDS; pH 8.0). Homogenates were incubated under constant agitation for 4 hrs at 4 ºC for lysis.

Lysates were centrifuged at 17,200 g and 4 ºC for 10 min. Supernatants were collected and stored at -30 ºC.

Protein mass spectrometry

Protein mass spectrometry analysis was performed in the Proteomics Facility of Biomedical Sciences Research Centre Alexander Fleming. Four to five biological replicas for each condition (wild-type + AAV2/8-CaMKIIa-tdTomato; wild-type + AAV2/8-CaMKIIa-SSFO-mCherry; 5xFAD + AAV2/5-CaMKIIa-tdTomato; 5xFAD + AAV2/5-CaMKIIa-SSFO-mCherry) were analyzed. Briefly, proteins of the lysed samples were processed according to the sensitive Sp3 protocol (Hughes et al., 2018). The reduced cysteine residues were alkylated in 200 mM iodoacetamide (Acros Organics). 20 μg of beads (1:1 mixture of hydrophilic and hydrophobic SeraMag carboxylate-modified beads; GE Life Sciences) were added to each sample in 50% ethanol. Protein clean-up was performed on a magnetic rack. The beads were washed twice with 80% ethanol followed by one wash with 100% acetonitrile (Fisher Chemical). The beads-captured proteins were digested overnight at 37 ºC with trypsin (0.5 μg trypsin/LysC mix in 25 mM ammonium bicarbonate) under vigorous shaking (1200 rpm, Eppendorf Thermomixer). The supernatants were collected, and the peptides were purified by a modified Sp3 clean-up protocol and finally solubilized in the mobile phase A (0.1% formic acid in water), and sonicated. Peptides concentration was determined through absorbance measurement at 280 nm using a nanodrop instrument.
Peptides were analyzed by a liquid chromatography tandem mass spectrometry (LS-MS/MS) on a setup consisting of a Dionex Ultimate 3000 nanoRSLC online with a Thermo Q Exactive HF-X Orbitrap mass spectrometer. Peptidic samples were directly injected and separated on a 25 cm-long analytical C18 column (PepSep, 1.9 μm3 beads, 75 μm ID) using a 90 min long run. The full MS was acquired in profile mode using a Q Exactive HF-X Hybrid Quadropole-Orbitrap mass spectrometer operating in the scan range of 375-1400 m/z using 120 K resolving power with an AGC of 3x 106 and a max IT of 60 ms followed by data independent analysis using 8 Th windows (39 loops counts) with 15 K resolving power with an AGC of 3x 105, a max IT of 22 ms and normalized collision energy (NCE) of 26.

Label-free quantification and data analysis

Orbitrap raw data were analyzed in DIA-NN 1.8 (Data-Independent Acquisition by Neural Networks) against the complete Uniprot Mus musculus proteome (Downloaded April 16, 2021) supplemented with APP, presenilin, mCherry and ChR2. Search parameters were

set to allow up to two possible trypsin/P enzyme missed cleavages. A spectra library was generated from the DIA runs and used to reanalyze them. Cysteine carbamidomethylation was set as a fixed modification while N-terminal acetylation and methionine oxidations were set as variable modifications. The match between runs (MBR) feature was used for all the analyses and the output (precursor) was filtered at 0.01 false discovery rate (FDR). The protein inference was performed on the gene level using only proteotypic peptides. The double pass mode of the neural network classifier was also activated. Perseus (version 1.6.15.0) (Tyanova et al., 2016) was used for data processing and statistical analysis. A total of 6,426 label free quantified proteins were subjected to statistical analysis with ANOVA test (p-value 0.05 cutoff) for the comparison of groups. The statistically significant proteins were then Z-scored and visualized by Euclidean hierarchical clustering as heat maps.

Cellular component analysis was performed with DAVID Gene-ontology analysis of the biological processes associated with upregulated and downregulated proteins and interaction network analysis of functional or physical protein to protein associations were performed with STRING (version 11.5). Circos plots were drawn using RStudio by uploading the list of proteins enriched in our samples for each biological process selected by the gene-ontology analysis. Volcano plots were generated with GraphPad Prism 9 (GraphPad software).

ELISA

Levels of Aβ40 and Aβ42 in hippocampal samples were quantitated by Human/Rat β Amyloid (40) ELISA kit (Wako catalog# 294-62501, LOT# WTL5240) and Human/Rat β Amyloid (42) ELISA kit (Wako catalog# 290-62601, LOT# WTM4353) respectively. Both ELISAs were performed according to the manufacturer recommendations, and the plates were read at 450 nm using an Eon microplate reader (BioTek).

Immunofluorescence

A Leica Vibratome VT1220S (Leica Microsystems) was used to cut 100 µm coronal sections of paraformaldehyde fixed brain tissue. Sections were rinsed 3 times in 0.1M PBS with 0.2% Triton X-100 (PBST) for 10 min, blocked for 1 hr with 10% Normal Goat Serum (NGS) in PBST and then incubated for 15 hrs at 4 ºC in primary anti-c-Fos (rabbit monoclonal, 1:2000, Cell Signaling catalog# 2250S) diluted in PBST containing 4% NGS. Sections were washed in PBST and subsequently incubated for 2 hrs at room temperature in AlexaFluor™ 488-conjugated goat anti-rabbit (1:500, Invitrogen catalog# A11008) diluted

in PBST containing 4% NGS. Tissue was mounted on SuperFrost™ slides (Thermo Fisher Scientific catalog# 12-550-15) using a fluorescence mounting medium with DAPI (Abcam catalog# ab104139) and cover-slipped.

All confocal images were acquired with a Zeiss LSM710 confocal laser scanning microscope. Acquisitions were 12-bit images, 2048x2048 pixels with a pixel dwell time of 3.15 µs. A 40x Plan-Apochromat oil objective (1.4 NA) was used for magnification. Tile scans were acquired at 12-bits, 512x512 pixels (each tile) with a pixel dwell time of 0.64 µs and an x5 EC-Plan-Neofluar objective (0.16 NA). Laser power, photomultiplier tube (PMT) settings, filters, dichroic mirrors, scanning speed were kept constant for all acquisitions.

Y-maze spatial memory test

The Y-maze apparatus consisted of 3 identical arms (each 36.2 x 8.25 cm) in a Y configuration (placed at 120° to each other) connected by a center polygonal area. The walls of the arms were transparent so the animals could identify two distinct visual cues placed outside the apparatus to facilitate spatial navigation. During the training phase, the mice were placed individually in the maze and left freely to explore two arms, for 10 minutes, while the third arm was blocked by a removable door. An hour later, the mice were returned to the maze and allowed to explore all arms. The latency to enter the new (third) arm was measured for each mouse and used to score the spatial memory performance of the mice. Between mice, the maze was cleaned with 70% isopropyl solution to minimize scent cues. Entry into the arm was defined as a mouse placing all four paws on the arm. For the mice receiving the daily optogenetic stimulation, the spatial memory test was performed after the end of the 4 weeks-long stimulation protocol. The day of the test, the mice receive a 2s light pulse before the beginning of the training phase.

Statistical Analysis

For the proteomic experiments, the statistical analysis of the label-free quantification intensities was performed with Perseus (version 1.6.15) using a two sample t-test with a *p* value of 0.05 or an ANOVA for multiple sample tests with Benjamini-Hochberg correction and an FDR of 0.05. For estimation statistics based on effect size and confidence intervals (Ho et al., 2019), the raw data were uploaded in the https://www.estimationstats.com/ and results were downloaded. The estimation plots show the mean difference between the groups and the 95% confidence interval by the ends of the vertical error bar.

Data and code availability

The code used to generate the circos plot is available upon request. Any additional information required to reanalyze the data reported in this paper is available from the corresponding author upon request.

4.7 Acknowledgements

The authors thank Camille Sugère and Lyane Méthot for assistance with the daily optogenetic stimulation protocol and Efthimios Skoulakis (Biomedical Sciences Research Centre Alexander Fleming) and Nicolò Ilacqua (Université Laval) for the invaluable comments on proteomics data. The authors also thank Dominique Isabel for assistance with RStudio and data visualization.

4.8 Author contributions

IK, KP and YDK designed the experiments. IK performed all the surgeries. IK and RS performed the optogenetic stimulation and immunohistochemistry experiments. IK and JA conducted and analyzed the optrode experiments. MS performed the mass spectrometry analysis. IK performed the behavioral tests. IK and KP analyzed the proteomics data. IK, KP and YDK interpreted the data and wrote the manuscript. YDK obtained funding and supervised all aspects of the present study. All the authors read and approved the final version of the manuscript.

4.9 Figures

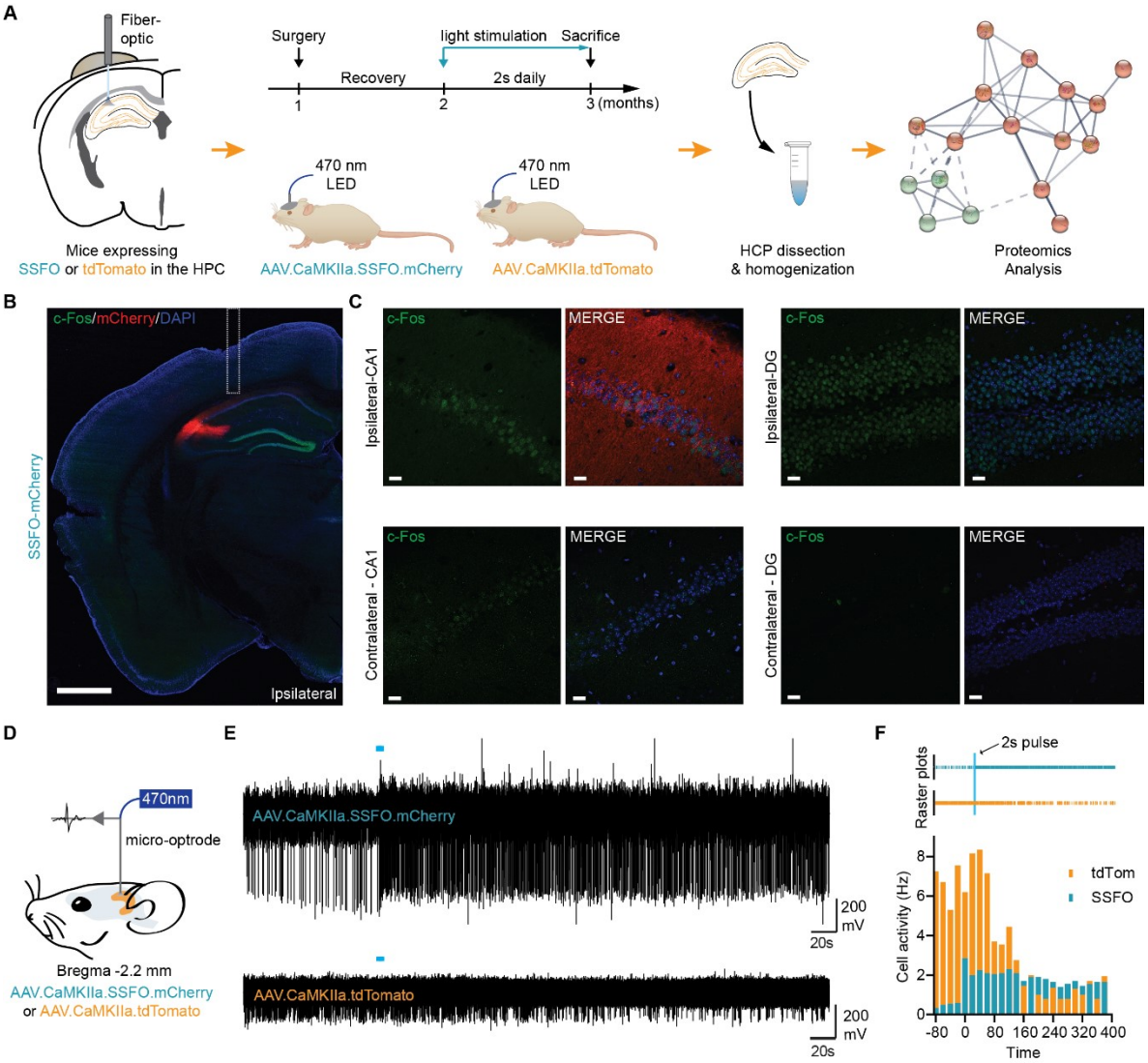

Figure 4.1 Optogenetic stimulation activates hippocampal neurons and evokes neuronal hyperactivity.

(**A**) Diagram showing an overview of the proteome experiment following chronic optogenetic stimulation of the hippocampus. (**B - C**) Confocal images showing immunofluorescence labeling of c-Fos (green) and mCherry (virus expression reporter protein, red) in coronal sections of mice infected with AAV-SSFO (Scale bars: 1 mm in **B** and 20 μm in **C**; DAPI in blue). Expression of SSFO was observed in the ipsilateral side of infection, but not the contralateral side. Unilateral light stimulation increased the levels of c-Fos at ipsilateral CA1 and DG but not the contralateral side. (**D**) Micro-optrode recording configuration. A 470 nm laser was coupled to an optrode probe for electrical recordings and advanced into the brain. (**E**) Example traces recorded in AAV-SSFO (top) or AAV-tdTomato (bottom) infected mice. 470 nm activation pulse is indicated with a blue bar. (**F**) Raster plot and peristimulus time histogram of the events detected prior and following the 470 nm activation pulse

for the example traces shown in **E** (AAV-SSFO in cyan and AAV-tdTomato in orange). Blue line indicates the activation pulse in the raster plot.

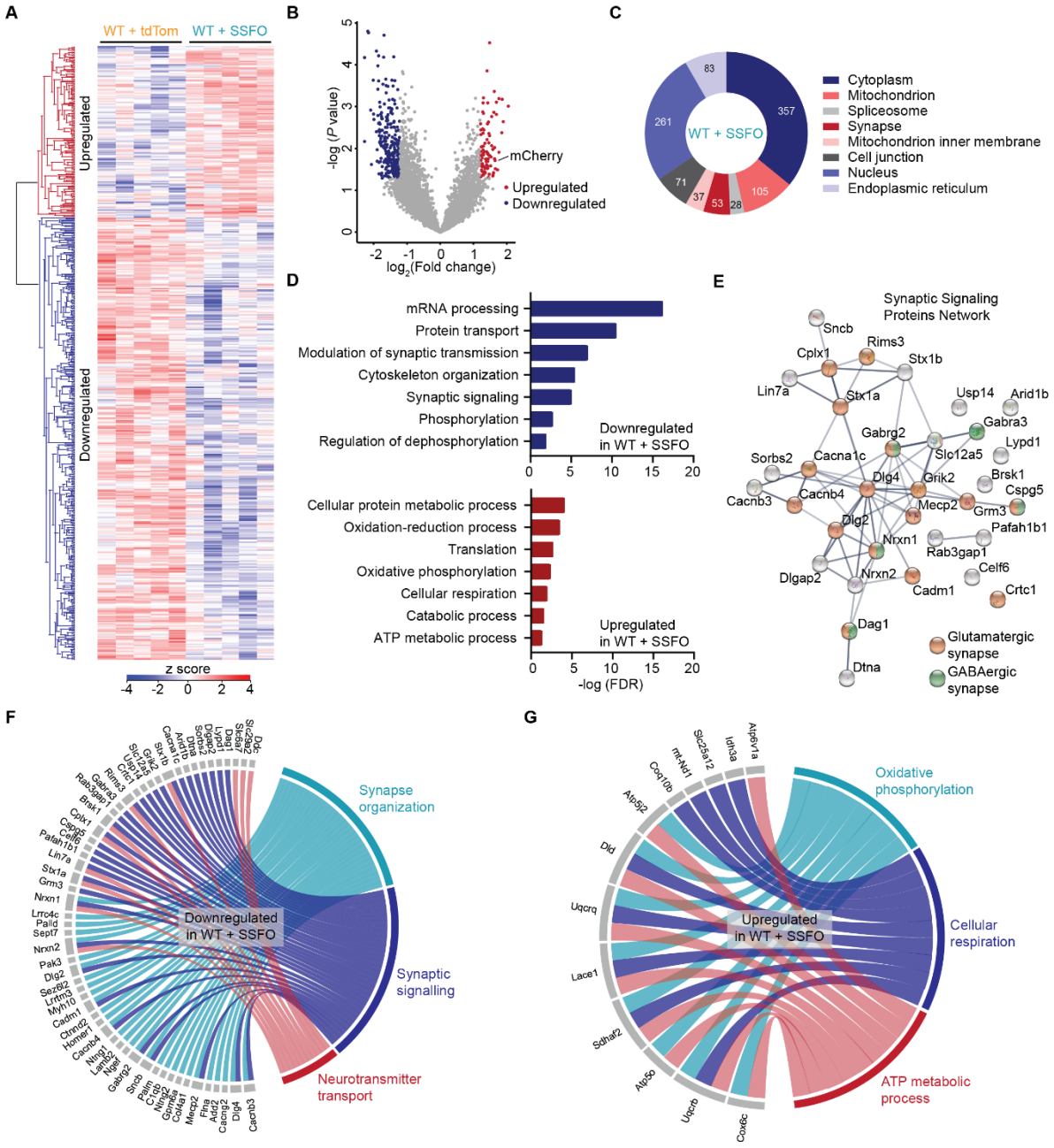

Figure 4.2 Chronic optogenetic stimulation elicits synaptic signalling protein downregulation in wild-type mice.

(**A**) Heat map revealing the scaled protein levels in the hippocampus of wild-type mice expressing AAV-SSFO or AAV-tdTomato after 4 weeks of daily optogenetic stimulation. (**B**) Volcano plot depicting upregulated (red) and downregulated (blue) proteins in the hippocampus of WT+SSFO mice compared to WT+tdTom mice. Proteins significant at P values ≤ 0.05 and fold change ≥ 1.2 are shown in red or blue. (**C**) Cellular component enrichment analysis of the proteins significantly altered following stimulation in WT+SSFO mice. (**D**) GO analysis of upregulated (red) and downregulated

(blue) biological processes in the hippocampus of WT+SSFO mice. (**E**) Interactome of functional or physical protein to protein associations of the synaptic signaling proteins downregulated in WT+SSFO mice. The proteins in orange are associated with glutamatergic synapses while the proteins in green with GABAergic. (**F** - **G**) Circos plots showing the proteins and selected biological processes downregulated (**F**) or upregulated (**G**) in WT+SSFO mice.

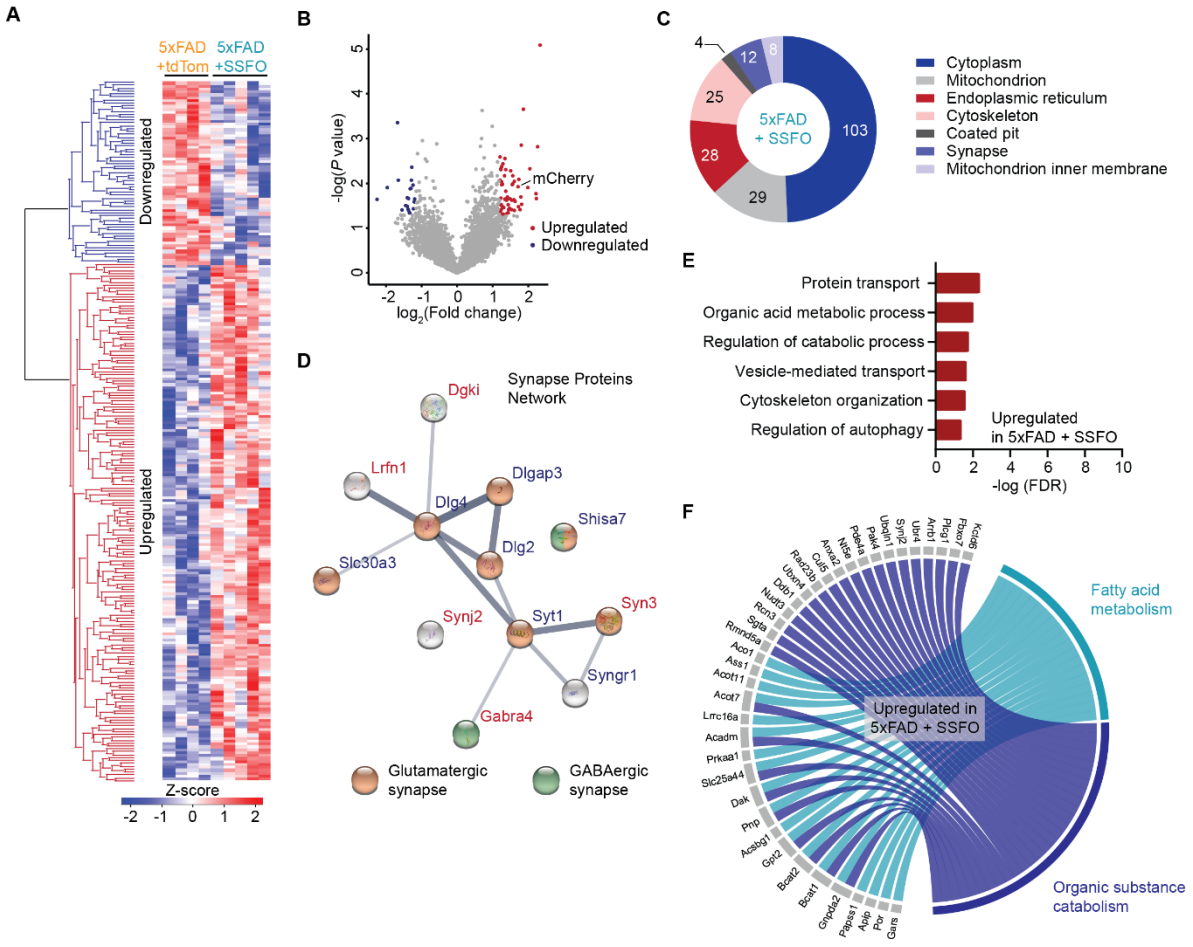

Figure 4.3 Chronic optogenetic stimulation upregulates lipid metabolism in 5xFAD mice.

(**A**) Heat map revealing the scaled protein levels in the hippocampus of 5xFAD mice expressing AAV-SSFO or AAV-tdTomato after 4 weeks of daily optogenetic stimulation. (**B**) Volcano plot depicting upregulated (red) and downregulated (blue) proteins in the hippocampus of 5xFAD+SSFO mice compared to 5xFAD+tdTom mice. Proteins significant at P values ≤ 0.05 and fold change ≥ 1.2 are shown in red or blue. (**C**) Cellular component enrichment analysis of the proteins significantly altered following stimulation in 5xFAD+SSFO mice. (**D**) GO analysis of upregulated biological processes in the hippocampus of 5xFAD+SSFO mice. (**E**) Interactome of functional or physical protein to protein associations of the synaptic proteins altered in 5xFAD+SSFO mice after optogenetic stimulation. The orange circles represent glutamatergic synapse proteins while the green GABAergic. The proteins written in red are upregulated while the proteins in blue are downregulated (**F**) Circos plots showing the proteins and selected biological processes upregulated in 5xFAD+SSFO mice.

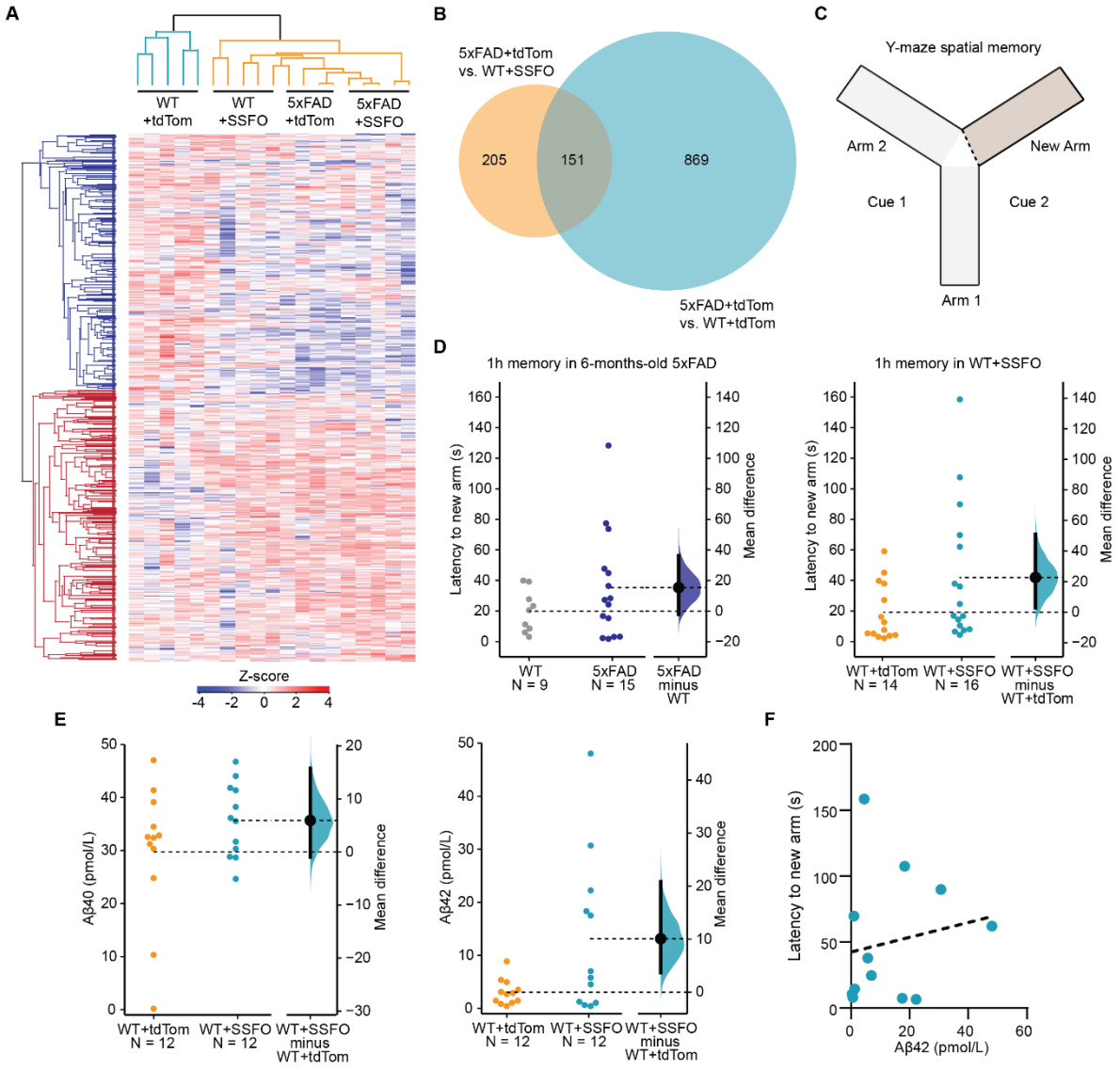

Figure 4.4 Chronic hippocampal optogenetic activation induces spatial memory deficits and elevates secretion of Aβ42 in wild-type mice.

(**A**) Heat map revealing the hierarchical clustering of 5xFAD and wild-type (WT) mice expressing AAV-SSFO or AAV-tdTomato based on their scaled protein levels in the hippocampus after 4 weeks of daily optogenetic stimulation. (**B**) Venn diagram showing the number of common proteins when comparing the differentially expressed proteins in 5xFAD mice as compared to wild-type (5xFAD+tdTom vs. WT+tdTom) and the proteins differentially expressed between the 5xFAD+tdTom and the WT+SSFO. (**C**) Schematic representation of the experimental setup of the Y-maze spatial memory test. (**D**) The latency to the new arm during the one hour Y-maze spatial memory test. The data are analyzed with estimation statistics. Each point represents an individual mouse. The mean difference is dissipated as a dot and the 95% confidence interval by the ends of the vertical error bars. (**E**) The concentration of soluble Aβ40 and Aβ42 in the hippocampus of WT+SSFO (cyan) as

compared to WT+tdTom (orange). Each point represents an individual mouse. The mean difference is dissipated as a dot and the 95% confidence interval by the ends of the vertical error bars. (**F**) The correlation of Aβ42 levels to the spatial memory performance measured as the latency to the new arm during the Y-maze test.

4.10 Supplementary materials

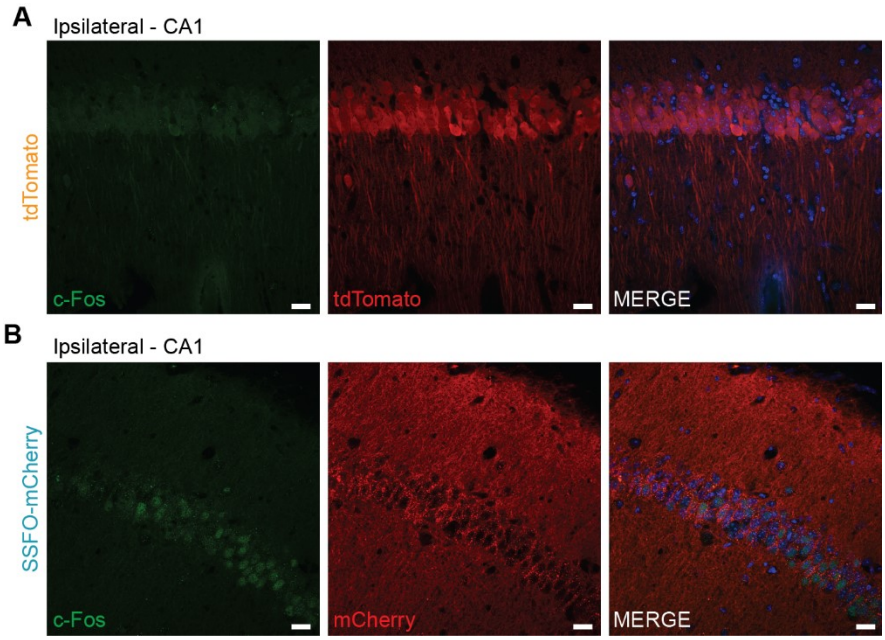

Suppl. Figure 4.5. c-Fos expression in the hippocampus of AAV-CaMKIIa-tdTomato or AAV-CaMKIIa-SSFO-mCherry infected mice.

(**A**) Confocal images showing labeling for c-Fos (green) and tdTomato (reporter protein, red) in coronal sections of mice infected with AAV-CaMKIIa-tdTomato. (**B**) Confocal images showing labeling for c-Fos (green) and Cherry (SSFO expression reporter protein, red) in coronal sections of mice infected with AAV-CaMKIIa-SFFO. Scale bars 20 µm, DAPI in blue.

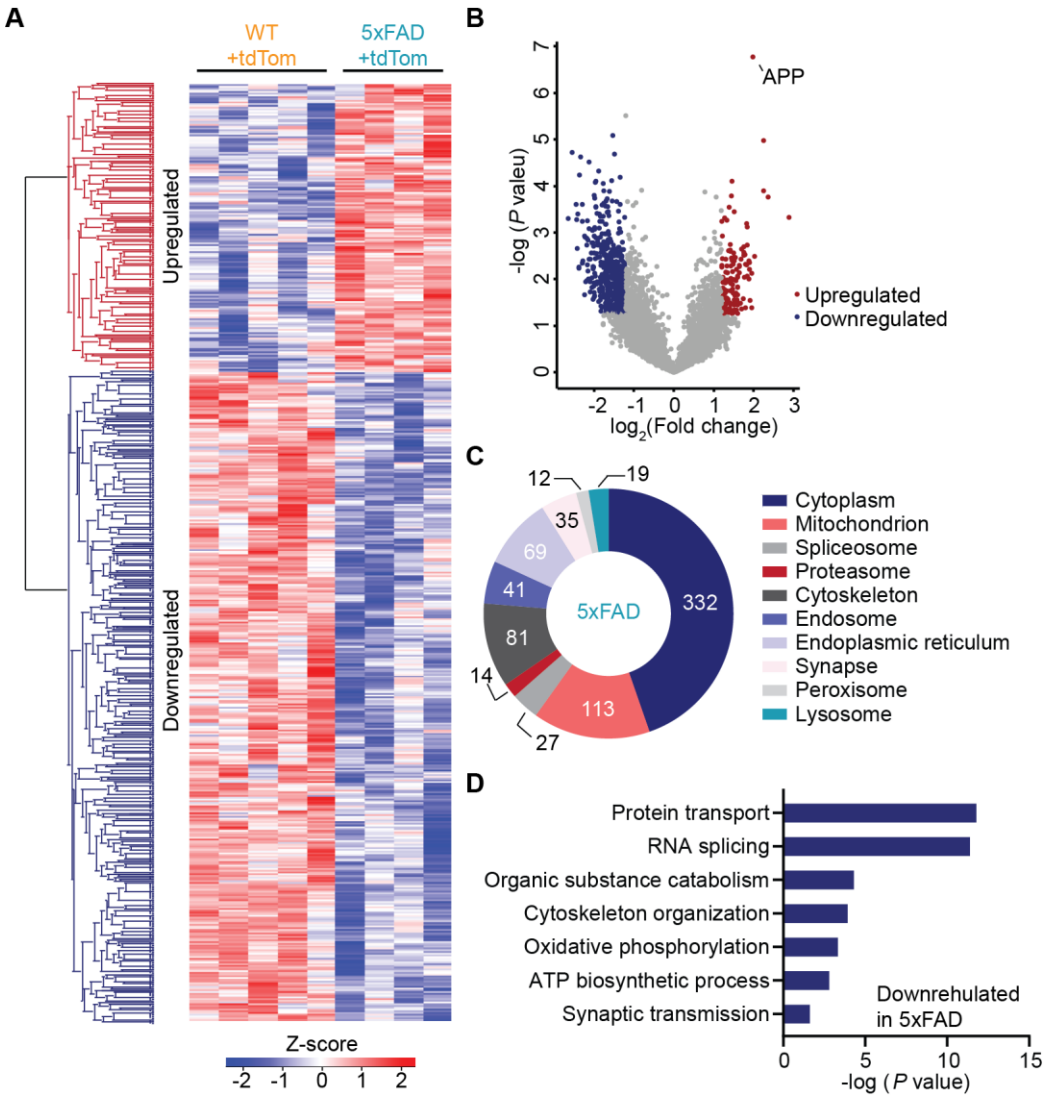

Suppl. Figure 4.6. The 5xFAD mice display defects on OXPHOS, ATP synthesis and lipid metabolism in the hippocampus.

(**A**) Heat map representing protein expression changes in 5xFAD mice as compared to WT mice. (**B**) Volcano plot depicting the proteins with the highest statistically significant (P values ≤ 0.05 and fold change ≥ 1.2) upregulation (red) and downregulation (blue) in the hippocampus of 5xFAD mice. (**C** - **D**) Results of the GO enrichment analysis of the top 10 most abundant cellular components (**C**) and selected biological processes downregulated in 5xFAD (**D**).

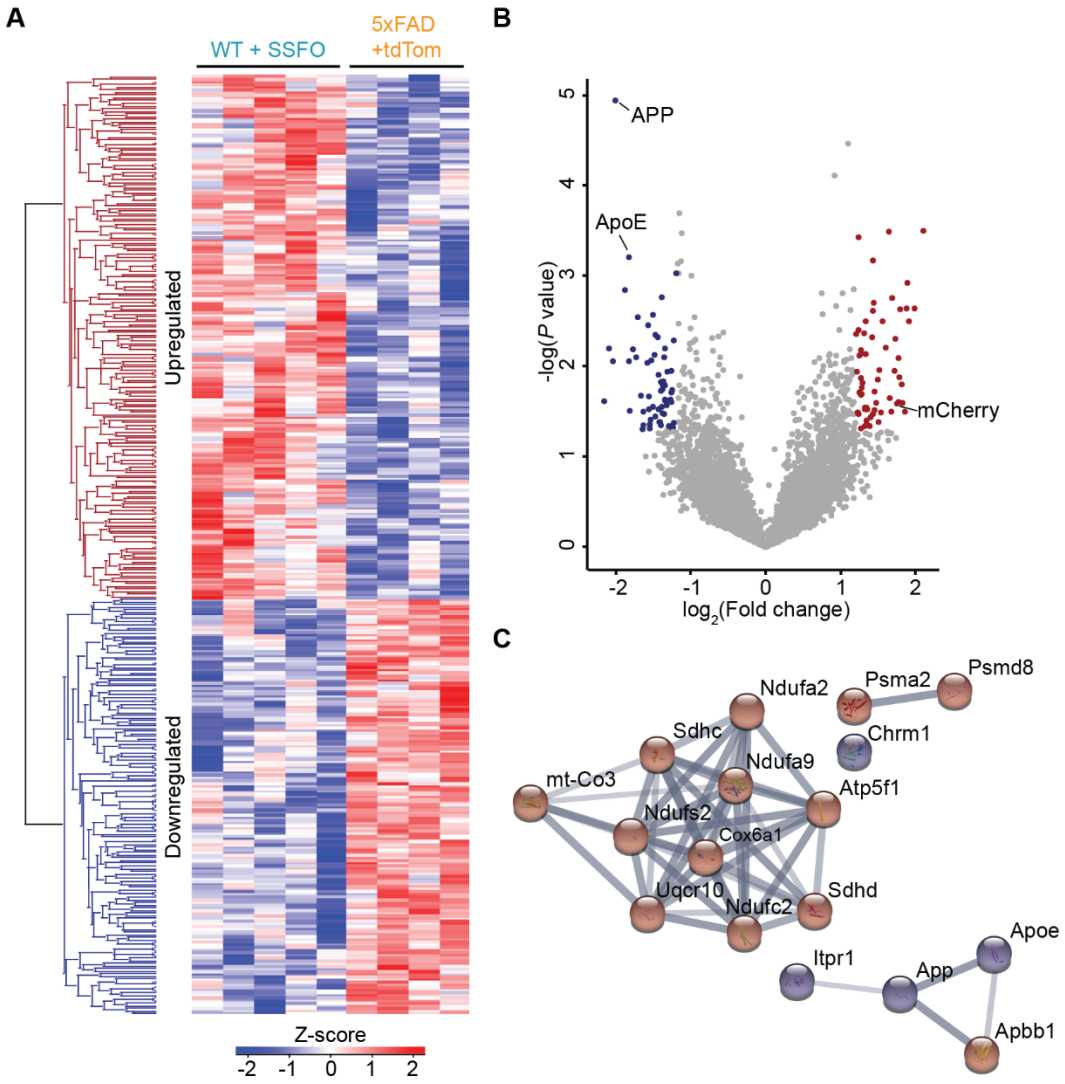

Suppl. Figure 4.7. Proteins altered by evoked neuronal hyperactivity in WT mice as compared to those altered due to mutations in 5xFAD mice.

(**A**) Heat map representing scaled expression levels of the statistically significant altered proteins in WT+SSFO compared to 5xFAD+tdTom. (**B**) Volcano plot exhibiting the proteins showing the greatest fold change in WT+SSFO vs. 5xFAD+tdTom. Upregulated proteins in red and downregulated proteins in blue. (**C**) Functional interaction network of proteins involved in Alzheimer's disease pathways showing expression change in WT+SSFO mice identified with GO pathway enrichment analysis. Proteins in red are upregulated and proteins in blue are downregulated.

Protein ID	Gene Name	-LOG(P-value)	Difference WT+SSFO – WT+tdTom
Akap5	A kinase (PRKA) anchor protein 5	1.478559835	0.502140045
Arl8b	ADP-ribosylation factor-like 8B	2.004810578	0.240664291
Atp6v1e1	ATPase, H+ transporting, lysosomal V1 subunit E1	1.417462418	-0.170627594
Brsk1	BR serine/threonine kinase 1	2.916066873	0.228399658
Cops5	COP9 signalosome subunit 5	2.443347154	-0.153899002
Dlgap2	DLG associated protein 2	1.475970462	0.344342041
Grk2	G protein-coupled receptor kinase 2	1.907290481	0.235454178
Gripap1	GRIP1 associated protein 1	2.175491422	0.187366104
Iqsec1	IQ motif and Sec7 domain 1	1.947854154	0.144786072
Pdlim5	PDZ and LIM domain 5	1.561244522	0.280237198
Rab11b	RAB11B, member RAS oncogene family	2.13743559	-0.503410339
Rasgrp2	RAS, guanyl releasing protein 2	1.407895903	0.502393341
Sh3gl2	SH3-domain GRB2-like 2	1.301907589	-0.147069168
Baalc	brain and acute leukemia, cytoplasmic	2.335699601	0.570791245
Cacna1c	calcium channel, voltage-dependent, L type, alpha 1C subunit	1.429482299	0.587653732
Cacng2	calcium channel, voltage-dependent, gamma subunit 2	1.402720659	0.510936737
Cadm1	cell adhesion molecule 1	2.114760942	0.479909515
Cspg5	chondroitin sulfate proteoglycan 5	2.585752912	0.596991348
Cplx1	complexin 1	1.692414471	0.260537338
Cdk16	cyclin-dependent kinase 16	1.306921675	-0.262182236
Dlg2	discs large MAGUK scaffold protein 2	1.506059748	0.268368912
Dlg4	discs large MAGUK scaffold protein 4	1.435203453	0.201265717
Dtna	dystrobrevin alpha	2.439720869	0.157659149
Dag1	dystroglycan 1	1.907415426	0.230922699
Dmd	dystrophin, muscular dystrophy	2.132238682	0.235076904
Eps8	epidermal growth factor receptor pathway substrate 8	1.646121952	0.341037369
Fam107a	family with sequence similarity 107, member A	1.548813676	-0.979149246
Gabra3	gamma-aminobutyric acid (GABA) A receptor, subunit alpha 3	1.516946376	1.384323502
Gabrg1	gamma-aminobutyric acid (GABA) A receptor, subunit gamma 1	1.517024267	-1.348511314
Gabrg2	gamma-aminobutyric acid (GABA) A receptor, subunit gamma 2	1.716423653	0.273066711
Grik2	glutamate receptor, ionotropic, kainate 2 (beta 2)	1.907290481	0.235454178
Gpm6a	glycoprotein m6a	2.971972376	0.501918411
Gap43	growth associated protein 43	1.351147259	0.301823044
Homer1	homer scaffolding protein 1	1.756048526	0.216147995

Kif3b	kinesin family member 3B	2.642100797	0.276025009
Lrrc4c	leucine rich repeat containing 4C	1.48520899	0.416059494
Lrrtm3	leucine rich repeat transmembrane neuronal 3	1.363043884	1.444319725
Lin7a	lin-7 homolog A, crumbs cell polarity complex component	2.387155448	0.320999908
Mff	mitochondrial fission factor	1.937312815	0.191346741
Nectin1	nectin cell adhesion molecule 1	1.538838542	0.363574219
Nrxn1	neurexin I	1.475274347	0.196094131
Palm	paralemmin	2.70169	0.213194
Phactr1	phosphatase and actin regulator 1	1.87081939	0.251573944
Kctd16	potassium channel tetramerisation domain containing 16	1.745617186	0.305397415
Kcna1	potassium voltage-gated channel, shaker-related subfamily, member 1	1.916655315	-0.194697189
Ppp1r9b	protein phosphatase 1, regulatory subunit 9B	1.376266728	0.221435165
Rims3	regulating synaptic membrane exocytosis 3	1.33269186	0.584886169
Rgs17	regulator of G-protein signaling 17	1.306421494	-0.389675903
Sorcs2	sortilin-related VPS10 domain containing receptor 2	2.311952474	0.481020355
Stx1a	syntaxin 1A (brain)	1.53514505	0.341389084
Tln2	talin 2	1.565125206	0.23805275
Tor1a	torsin family 1, member A (torsin A)	2.373399451	0.54083519
Tmem240	transmembrane protein 240	2.500850725	1.838264847

Suppl. Table 4.1. The 53 synaptic proteins altered in WT + SSFO mice upon chronic optogenetic stimulation.

Protein ID	Gene Name	-LOG(P-value)	Difference WT+SSFO – 5xFAD+tdTom
Sdhd	succinate dehydrogenase complex, subunit C, integral membrane protein	1.955492	1.517831
Ndufs2	NADH:ubiquinone oxidoreductase core subunit S2	1.684709	0.872116
Ndufa2	NADH:ubiquinone oxidoreductase subunit A2	1.339693	1.339693
Itpr1	inositol 1,4,5-trisphosphate receptor 1	1.583373	-0.93539
Ndufc2	NADH:ubiquinone oxidoreductase subunit C2	1.480365	0.951946
Chrm1	cholinergic receptor, muscarinic 1, CNS	1.851256	-0.83787
Cox6a1	cytochrome c oxidase subunit 6A1	1.605674	1.173535
Psmd8	proteasome (prosome, macropain) 26S subunit, non-ATPase, 8	1.522368	1.360535
Uqcr10	ubiquinol-cytochrome c reductase, complex III subunit X	2.093132	0.710384
mt-Co3	cytochrome c oxidase III, mitochondrial	1.436133	0.818438
Ndufa9	NADH:ubiquinone oxidoreductase subunit A9	1.385648	0.927287
Sdhc	succinate dehydrogenase complex, subunit C, integral membrane protein	1.566704	0.936176
Atp5f1	ATP synthase, H+ transporting mitochondrial F1 complex, beta subunit	2.368052	1.312024
Psma2	proteasome subunit alpha 2	1.485332	1.232026
Apoe	apolipoprotein E	3.210177	-1.82654
Apbb1	amyloid beta (A4) precursor protein-binding, family B, member 1	1.514134	1.054535
App	amyloid beta (A4) precursor protein	4.943931	-2.00642

Suppl. Table 4.2. The 17 proteins involved in Alzheimer's disease pathways altered specifically in WT+SSFO mice upon stimulation.

Chapter 5 – Discussion

5.1 Summary

The main focus of this thesis is to explore the various mechanisms by which abnormal brain activity in Alzheimer's disease and normal aging can induce memory deficits and cognitive decline. First, I described that restoring KCC2 function and chloride transport in AD-like transgenic mice we can prevent cortical hyperactivity and reverse spatial memory deficits and social dysfunction. Second, I showed that a subset of old mice develops an overt cognitive decline which is correlated with an increase in the levels of inhibitory synaptic proteins within the mPFC. Driving inhibition in the mPFC of young mice, then, was sufficient to replicate similar cognitive deficits to the ones presented in old cognitively impaired mice. Third, inducing chronic neuronal hyperactivity within the hippocampus of young mice was sufficient to elicit synapse disruption and give rise to spatial memory deficits. This chronically evoked hyperactivity also resulted in downregulation of KCC2 but also in boosting the amyloidogenic processing of APP and a subsequent elevation in soluble Aβ42 secretion. Altogether, these results provide evidence that disruption of inhibitory control, disinhibition, or excessive excitatory signaling can disturb normal brain functioning and evoke cognitive decline.

5.2 Chloride transport disruption in AD

In Chapter 2, I presented evidence supporting a chloride transport dysregulation manifesting in the PFC and the hippocampus of mice carrying several AD-linked mutations. This is in line with previous observations reporting a disinhibition in mice overexpressing AD-linked mutations (Busche and Konnerth, 2016; Busche et al., 2008, 2012; Palop and Mucke, 2016; Verret et al., 2012). Indeed soluble Aβ and plaques have been found to induce neuronal overexcitability leading to cortical and hippocampal hyperactivity (Zott et al., 2018). Hyperexcitability, in turn, has been associated with cognitive decline (Dickerson et al., 2005; Palop and Mucke, 2009) suggesting a causal link between aberrant brain activity and cognitive frailty in AD. More importantly, since this neuronal activity disruption appears to arise from impaired $GABA_A$-mediated inhibition, the idea of chloride homeostasis as a potential mechanism of memory deficits in AD is further supported.

Recent studies have tried to link chloride homeostasis deficits with disinhibition in AD (Bie et al., 2022; Chen et al., 2017; Doshina et al., 2017; Shen et al., 2022), however no

direct link has been established with KCC2. In the study conducted by Chen and colleagues, APP is suggested to interact with KCC2, and the disruption of this interaction seems to affect GABAergic signaling resulting in an depolarizing reversal for GABA (Chen et al., 2017). However, the interaction of the two proteins have been only demonstrated by exogenous *in vitro* overexpression of the two proteins in HEK293 cells. This interaction was not identified in a thorough KCC2 interactome study conducted in mouse brain samples (Mahadevan et al., 2017), nor has it been reproduced with co-immunoprecipitation in the brain of wild-type with specific antibodies targeting the Aβ unique sequence of App (**Figure 5.1**). Thus, one could argue that the reported interaction (Chen et al., 2017) could be an artifact of protein overexpression. However, the depolarizing E_{GABA} described in the brain of *APP*$^{-/-}$ animals in the same study (Chen et al., 2017) can still be mediated through a KCC2 downregulation and chloride transport disruption via another mechanism.

On the other hand, overexpression of hAPP in cultured neurons, or mice (in the absence of elevated Aβ) significantly alters GABAergic transmission (Doshina et al., 2017; Kreis et al., 2021) potentially through a loss of KCC2 function. Furthermore, Aβ fibrils injection directly to the CA1 of mice have been shown to reduce KCC2 levels and shift E_{Cl-} (Bie et al., 2022). Finally, a recent computational study has identified bumetanide, a NKCC1 inhibitor, as a good repurposed candidate drug to prevent AD in humans (Taubes et al., 2021), further supporting the hypothesis that chloride transport and inhibitory signaling are disrupted in AD. Altogether, these findings suggest that overexpression of APP, or Aβ can disrupt chloride homeostasis in AD and induce some of the brain network abnormalities and cognitive deficits characterizing the early stages of the disease.

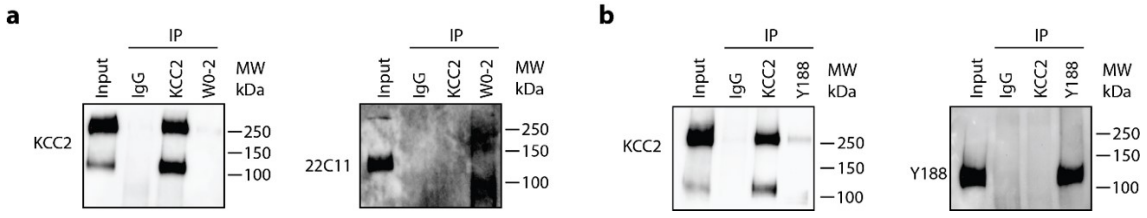

Figure 5.1. Co-immunoprecipitation experiment for KCC2 and APP in the mouse brain.

(**a**) KCC2 does not interact with APP in mouse brain by co-IP with either KCC2 antibodies or APP antibodies targeting specifically the amyloid-β sequence. Rabbit IgG (IP:IgG) was used as a negative control. (**b**) KCC2 does not interact weakly with APP in the mouse brain by co-IP with APP antibodies targeting APP between the 1-100 aa (similar to the one used by (Chen et al., 2017)).

It is important to highlight that, so far, overexpression of APP appears to result in KCC2 downregulation (Doshina et al., 2017) and yet most of the first generation amyloidogenic transgenic lines are based on overexpression of the human *app* gene. Thus, one could argue that the reduced KCC2 membrane levels reported here in the brain of 5xFAD mice might be driven by the APP overexpression. However, the levels of KCC2 seem to be unaltered in brain regions less affected by the AD pathology, such as the nucleus accumbens (**Suppl. Figure 2.8**) or remain unaltered in young 5xFAD mice (**Figure 2.1**) excluding the possibility of an effect of the genetic background and APP overexpression. Moreover, comparable KCC2 downregulation was observed in the APP^{NL-F-G} brains where APP is not overexpressed, but Aβ accumulation and precipitation is still observed (**Figure 2.1**).

Understanding the mechanism by which chloride transport is impaired in AD is crucial for restoring GABAergic signalling. The robustness of $GABA_AR$ neurotransmission relies on low intracellular chloride concentrations, so that chloride flows into the cell when $GABA_ARs$ open. In the mature brain, KCC2 is the key regulator of chloride levels and, therefore, of inhibitory signaling (Doyon et al., 2016). Thus, the findings presented here regarding the diminished KCC2 levels in brain regions greatly affected by Aβ can explain the neuronal hyperexcitability associated with AD through disinhibition (Doyon et al., 2016). While enhancing $GABA_A$-mediated inhibitory transmission has been proposed as a treatment for AD before, the use of benzodiazepines has yielded inconclusive results in patients. This is consistent with a deficit in KCC2 and chloride transport since it can lead to paradoxical and detrimental effects of targeting $GABA_A$ function directly. Targeting KCC2 alone (Gagnon et al., 2013) or combined with targeting $GABA_A$ (Lorenzo et al., 2020) appears as a more promising strategy to restore inhibition.

KCC2 hypofunction can also lead to loss of synaptic specificity (Ferando et al., 2016), enhanced NMDA receptor function (Hildebrand et al., 2016), and to disruption of TASK-3 channels and AMPA receptors trafficking (Chevy et al., 2015; Goutierre et al., 2019) suggesting that KCC2 is important for both GABAergic and glutamatergic transmission. In such a way, enhancing KCC2 and chloride transport present a particularly promising strategy to restore normal neuronal excitability, synaptic precision and cognitive impairments associated with AD.

5.3 KCC2 dysfunction as a cause of network alterations

The work presented in this thesis shows KCC2 dysfunction in the PFC and the hippocampus of mice overexpressing AD-linked mutations specifically, although dysregulation of chloride homeostasis through a KCC2 hypofunction has been described throughout the CNS and in various pathological conditions. For instance, chloride transport goes awry in the superficial dorsal horn in chronic pain (Coull et al., 2003; Ferrini et al., 2020; Lorenzo et al., 2020), during stress in the hypothalamus (Hewitt et al., 2009), in epilepsy in the hippocampus (Sivakumaran et al., 2015) and in alcohol or diazepam addiction in the VTA (Ostroumov et al., 2016, 2020). In all these situations, chloride transport dysregulation results in neuronal disinhibition or disruption of neuronal plasticity.

When E_{Cl^-} is depolarized (due to overt KCC2 downregulation) and the opening of $GABA_AR$ (or the glycine receptor in the spinal cord) results in outward movement of chloride, synaptic inhibition is lost, neuronal processing is altered, and network disruption follows. However, even a mild KCC2 downregulation can be detrimental to neuronal coding, in the absence of a shift in E_{GABA} polarity. Neurons with reduced chloride extrusion capacity are incapable of handling transient chloride loads due to neuronal activity resulting in chloride accumulation and gradient collapse (Ferrini et al., 2020). As such, neurons lose their ability to process the various synaptic inputs (especially high frequency inputs) causing information transfer loss (Doyon et al., 2015).

KCC2 dysfunction, in addition, reduces the synapse specificity of LTP, promoting a runaway spread of potentiation to functionally unrelated synapses (Ferando et al., 2016). This can lead to further interference of the input-output function of neurons and the loss of signal specificity critical for networks dynamics and neural coding (Doyon et al., 2011). Once again, this spread of plasticity to unrelated functional clusters appears to emerge by altered E_{GABA} and chloride dynamics.

However, diminished KCC2 can affect neuronal function independently of GABA signaling and its chloride transport function. KCC2 is regulating the activity-driven trafficking of AMPA receptors in glutamatergic synapses (Chevy et al., 2015), thereby controlling LTP induction. Moreover, silencing of KCC2 increases neuronal excitability and impairs network activity specifically in the range of slow and fast gamma oscillations (Simonnet et al., 2022). These recent experimental data are consistent with the computational studies predicting that KCC2 hypofunction could result in filtering of inhibitory synaptic events (Doyon et al., 2011). Interestingly, the neuronal overexcitability induced by KCC2 downregulation, can be

occluded by activation of the leak potassium channels Task-3 (Simonnet et al., 2022) which as mentioned earlier have been found to interact with KCC2 (Goutierre et al., 2019).

All these findings demonstrating the involvement of KCC2 in controlling synaptic specificity, neuronal excitability, and brain rhythms closely resemble the synaptic and neuronal network dysfunction reported in AD. Previous studies have shown a loss of gamma power in AD models (for review (Palop and Mucke, 2016)). When the power of gamma oscillations is restored either by increasing inhibitory activity (Martinez-Losa et al., 2018; Verret et al., 2012) or by multi-sensory gamma power entrainment (Iaccarino et al., 2016), cognitive deficits were mitigated and epileptiform activity was greatly reduced. We have shown that an age-dependent cortical hyperactivity and hypersynchrony in the gamma frequency range is observed in the brains of 5xFAD mice (**Figure 2.4**). And yet, the loss of gamma power in AD described by others is restricted in a task-related manner (Martinez-Losa et al., 2018; Verret et al., 2012). These task-related changes in gamma oscillations power differ mechanistically from aberrant increases in gamma power during rest (consistent with our observations, Chapter 2) reported in APP23 and APPswe/PS1dE9 mice (Gurevicius et al., 2013; Ittner et al., 2014) in the cortex and hippocampus. Interestingly, long-term CLP290 treatment in aged 5xFAD mice prevented cortical hyperactivity (**Figure 2.4**; consistent with the computational predictions from (Doyon et al., 2011, 2015)) and improved learning performance during a spatial memory task (**Figure 2.3**). In agreement, KCC2 downregulation has been shown to impair network rhythmogenesis and deteriorate spatial and contextual memory in mice (Simonnet et al., 2022). Finally, a similar scenario with an increase in overall spontaneous gamma activity and a reduction in task/sensory-evoked activity manifests in various autism spectrum disorders (Kayarian et al., 2020) highlighting the importance of normal brain network activity for successful cognitive processing.

5.4 Potential mechanism of KCC2 downregulation in AD

The expression, trafficking, and function of KCC2 are modulated by an array of distinct intracellular and intercellular mechanisms (Doyon et al., 2016). The first includes transcriptional regulation by two neuron-specific silencing elements (NRSEs) and the transcription factor of the early grow response family (EGR) (Ludwig et al., 2011) and posttranscriptional processes such as phosphorylation and dephosphorylation of KCC2 in key intracellular residues by protein kinase C (PKC) and protein phosphatase 1 (PP1) respectively (Kahle et al., 2013). Ca^{2+} levels also participate in the intracellular regulation of

KCC2 expression and its cleavage by calpain (Puskarjov et al., 2012). Among the intercellular mechanisms regulating KCC2 expression/function are BDNF signaling through TrkB receptors, serotonin and the 5HT2A receptors, potentiation of NMDA receptors, Zn^{2+} and the mZnR/GPR39 receptors and finally adenosine and the A3AR receptors (Bos et al., 2013; Coull et al., 2003; Ferrini et al., 2013; Ford et al., 2015; Gilad et al., 2015; Hewitt et al., 2009; Lee et al., 2011). And yet it appears that Aβ can also participate in the regulation KCC2 expression potentially through an activity-dependent disinhibitory or BDNF/Trk-B signaling (Bie et al., 2022).

The findings presented here strongly suggest that KCC2 downregulation and chloride dyshomeostasis in AD are downstream from Aβ secretion and accumulation. It has been shown that direct injection of Aβ in the rat CA1 results in a reduction of KCC2 monomers (and results in significant increase in E_{Cl-}) which can be prevented by concurrent injection of BDNF and a pro-BDNF inhibitor (Bie et al., 2022). Thus, Aβ appears to regulate KCC2 expression though disruption of BDNF maturation and a loss of the BDNF/Trk-B signaling and Shc pathway activation which has been shown to upregulate KCC2 (Rivera et al., 2004). However, concurrent phosphorylation of Trk-B receptors by PLCγ and Shc can result in activation of CREB and a subsequent downregulation of KCC2, highlighting the complexity of this regulatory mechanism. This latter signaling cascade might also act as an alternative mechanism of KCC2 downregulation in AD. Enlarged microglia have been found to infiltrate and engulf amyloid plaques in various AD-like transgenic mouse lines, including the 5xFAD mice (Oakley et al., 2006; Simard et al., 2006; Wegiel et al., 2001). In parallel, microglia have been found to secrete BDNF in chronic pain models, which in turn activates Trk-B resulting in KCC2 downregulation (Coull et al., 2005). Thus, activated microglia surrounding plaques in AD could respond similar to what have been shown in the chronic pain paradigms and reduce the protein levels of KCC2. However, considering that plaques deposit in advanced AD, and that Aβ fibrils can induce neuronal overexcitability and hyperactivity prior to plaques formation, this BDNF/Trk-B-mediated KCC2 downregulation might be less involved in AD and an activity-dependent regulation of KCC2 expression may precede.

Here, I have shown that incubation of hippocampal neurons in culture with Aβ42 resulted in a profound reduction in membrane KCC2 which can be restored partly with acute CLP257, short-term (4 hours) treatment (**Suppl. Figure 2.11**). This *in vitro* experimental paradigm could be utilized to further investigate the mechanism by which Aβ downregulates KCC2 and explore the signaling cascades that mediate, in turn, the restoration of KCC2 by

the CLP enhancing molecules following Aβ. Although, as just discussed before, the mechanisms by which Aβ acts to downregulate KCC2 potentially involve signaling cascades activated by neuronal activity.

I have already discussed how Aβ can induce neuronal overexcitability which in turn evokes cortical and hippocampal hyperactivity (Palop and Mucke, 2016), either via suppression of glutamate reuptake (Zott et al., 2019) or through a disruption of pre-synaptic inhibition (Martinez-Losa et al., 2018; Verret et al., 2012). Consecutively, neuronal hyperactivity can directly reduce the levels and function of KCC2 (Ferando et al., 2016; Rivera et al., 2004) disrupting $GABA_A$-mediated neurotransmission. This latter finding of an activity-dependent control of KCC2 expression is consistent with the proteomics data presented in Chapter 4 showing an approximate 1.5-fold reduction of KCC2 protein levels in wild-type mice following evoked chronic neuronal hyperactivity (**Figure 4.2**). Additionally, evoked neuronal hyperactivity in the hippocampus of wild-type mice resulted in a profound increase in the levels of soluble Aβ42 (**Figure 4.4**), further supporting the previous observations linking neuronal activity with Aβ secretion and deposition (Bero et al., 2011; Cirrito et al., 2005).

Taking into consideration all the points discussed above on how neuronal activity, amyloid, and KCC2 are connected one could probably suggest not only a sequential pathway of Aβ-dependent neuronal hyperactivity and KCC2 downregulation, but potentially a positive feedback cycle which can maintain neuronal hyperactivity, augment Aβ secretion and disrupt chloride transport and GABAergic transmission through KCC2 (**Figure 5.2**). This cycle has the potential of trapping neurons in an unclamped spiral of escalating hyperexcitability and Aβ secretion which can eventually result in excitotoxicity and neuronal degeneration.

It still remains unknown whether disruption of KCC2 can directly result in the abnormal processing of APP and Aβ secretion. The data presented here, support that KCC2 dysfunction is downstream to Aβ accumulation. However, I have shown in this thesis that the spontaneous multi-unit activity of the fast gamma (60-120 Hz) and ripple (120-200 Hz) bands in the retrosplenial cortex and hippocampus increase with age in transgenic mice carrying AD-linked mutations (**Figure 2.4**). Long-term treatment of 5xFAD mice with CLP290 (a KCC2 enhancer) protected from a KCC2 reduction (**Suppl. Figure 2.14**) and prevented the age-dependent increase in high-frequency oscillations (**Figure 2.4**) suggesting that restoring chloride transport in AD can can restore normal neural excitability which in turn can slow down the Aβ-dependent pathology in AD and allow neuronal networks to escape

from the vicious cycle of escalating hyperactivity. Therefore, enhancing KCC2 may represent a particular promising therapeutic avenue for restoring normal neuronal activity in AD and restoring cognitive functions in patients.

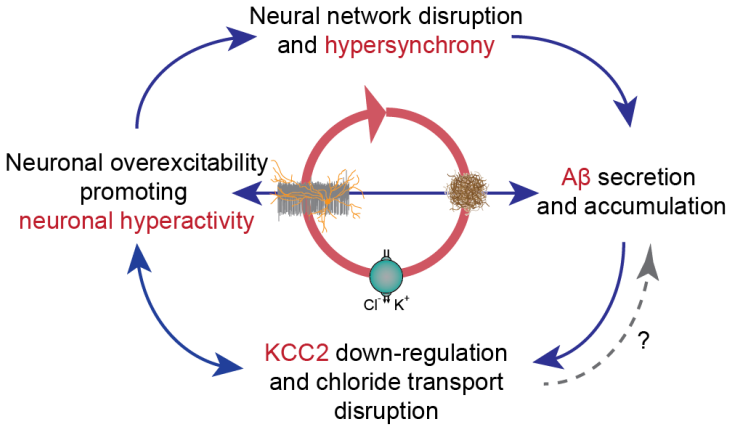

Figure 5.2. Vicious cycle of Aβ-dependent neuronal hyperactivity, network disruption and KCC2 dysfunction.

Amyloid-β secretion can downregulate KCC2 expression resulting in a neuronal chloride transport disruption which in turn alters neuronal excitability. Neuronal overexcitability translates in neuronal hyperactivity and under certain conditions to network hypersynchrony. This neuronal network disruption has been found to affect augment the Aβ load in the brain.

5.5 When does excessive inhibition become detrimental?

In Chapter 3 of this thesis, I presented results indicating elevated inhibitory input in the layer II/III of the mPFC of old cognitively impaired mice based on the levels of inhibitory pre- and post-synaptic proteins. Furthermore, activating GABAergic inhibitory neurons in young mice, in turn, was sufficient to induce cognitive deficits. On that account, one should wonder how or why uncontrolled, excessive inhibitory signalling can have such a detrimental effect in cognitive performance.

Inhibition in the cortex is generated by interneurons (neurons releasing GABA) which account for approximately 20% of the cortical neurons (Meinecke and Peters, 1987). And still, even if interneurons are simply differentiated by excitatory neurons based on their morphology and their ability to release GABA, they represent a highly heterogeneous

population of neurons. This heterogeneity of GABAergic interneurons within the cortex reflects the vast complexity of the GABAergic inhibitory neurotransmission in the CNS (Kepecs and Fishell, 2014).

However, the functional complexity of GABAergic inhibition may not be solely based upon the diversity of its interneurons. The synaptic connections these neurons form with excitatory pyramidal neurons, but also with other neighboring interneurons further diversifies the effect of GABAergic inhibition (Pfeffer et al., 2013; Tremblay et al., 2016). Feedback inhibition is generated when excitatory pyramidal neurons form synapses with interneurons that in turn form synapses with surrounding excitatory neurons. Contrary, feedforward inhibition arises when long-range excitatory neurons contact both local interneurons and other surrounding excitatory neurons. Finally, disinhibition is achieved when an interneuron forms synapses with another interneuron preventing it from inhibiting an excitatory neuron. Nevertheless, the inhibitory input generated by interneurons appears to gate signal flow to and from the cortex, and generate oscillatory rhythms (Buzsáki and Draguhn, 2004; Buzśaki and Wang, 2012; Tremblay et al., 2016) which are essential for cognitive performance and successful memory encoding (Abadchi et al., 2020; Palop and Mucke, 2016; Remondes and Wilson, 2015; Yamamoto et al., 2014).

It is important to also highlight, that the contribution of interneurons in shaping and controlling the E/I balance and network activity in the neocortex might be even more profound in humans based on the recent observations indicating a 2.5 fold increase in the number of interneurons in the human cortex as compared to the mouse brain and the almost ten times higher number of interneuron to interneuron connections (Loomba et al., 2022).

Having clarified the complexity of the inhibitory signalling let us try to answer our initial question. Uncontrolled inhibitory input can: (1) shutdown completely a local neuronal network by inhibiting excitatory neurons; (2) alter the frequency of oscillatory firing within the network; (3) result in disinhibition and subsequently to a rampant excitatory activity. All these three scenarios can be detrimental for normal brain functioning and disrupt information processing further supporting the significance of inhibition to cognitive performance.

Another really interesting observation of a detrimental effect of enhanced GABAergic input has been made in some types of epilepsy. In general, enhanced inhibition has been reported in the hippocampus or the neocortex of numerous rodent models of epilepsy (Klaassen et al., 2006; Scimemi et al., 2005; Zhan and Nadler, 2009) which acts as a compensatory mechanism against neuronal hyperactivity and seizures. However, in absence epilepsy, the excessive GABAergic inhibitory has been found to paradoxically

promote the seizures (Cope et al., 2009; Klaassen et al., 2006). In this type of epilepsy enhanced extra-synaptic tonic inhibition persistently hyperpolarizes thalamocortical relay neurons resulting in the generation of epileptiform discharges in the neocortex and behavioral arrest and unresponsiveness. Notably, this work highlights again how enhanced GABAergic inhibitory input can have adverse, opposing effects than the commonly expected and how it can be detrimental in some cases for network activity.

Since enhanced inhibition can have such a dramatic effect on network activity and cognitive performance, neurons undergo homeostatic changes regulating synaptic strength in order to maintain their characteristic firring patterns (Turrigiano and Nelson, 2004). In addition, compensatory mechanisms can evoke concomitant changes in excitatory signalling to counter the increase in the inhibitory input and maintain the E/I balance (Van Vreeswijk and Sompolinsky, 1996). This means that in pathological conditions the majority of these protective mechanisms fail to counter and control alterations in either the excitatory or inhibitory transmission resulting in neuronal network disruption and the onset of disease.

5.6 Future avenues

The study of AD-like mouse transgenic lines presented in Chapter 2 provides significant evidence of a KCC2 hypofunction and a subsequent chloride transport disruption in two distinct brain regions (the mPFC and the CA1; **Figure 2.1**) involved in memory formation and the development of AD-pathology. This is consistent with previous reports linking Aβ and deficits in inhibitory neurotransmission ensuing cortical and hippocampal hyperactivity resulting in memory deficits (Palop and Mucke, 2016; Zott et al., 2018). Preventing KCC2 decrease in the 5xFAD was sufficient to protect against the age-dependent emergence of cortical hyperactivity suggesting that GABAergic neurotransmission is indeed disrupted. However, no direct link between the loss of membrane KCC2 and a shift in E_{GABA} has been drawn in the 5xFAD mice. Therefore, it will be useful to measure the GABA reversal in brain slices derived from 5xFAD and non-transgenic mice.

It is also critical to verify whether the reduction in membrane KCC2 is specific for excitatory neurons, and it does not extend to inhibitory neurons. The chloride transport experiments presented here have been conducted exclusively in CaMKIIa positive neurons, therefore in excitatory neurons, in both the mPFC and the CA1, suggesting that chloride transport is impaired primarily in excitatory neurons. However, it is necessary to assess if

KCC2 levels (and chloride transport) are altered in inhibitory neurons too. This is the case, for instance, in spinal cord injury models, where KCC2 is downregulated in local inhibitory neurons surrounding the injury sites (Chen et al., 2018). When KCC2 was selectively restored in inhibitory interneurons, the E/I ratio was rebalanced allowing for normal network activity and a recovery in the stepping ability of injured mice (Chen et al., 2018). Regulating the intracellular chloride levels in excitatory neurons is crucial for controlling the excitability of these neurons and their response to inhibitory input, however ensuring that the inhibitory input *per se* is intact is also necessary for maintaining specific firing patterns within a neuronal network (Möhler et al., 2004). We have developed a viral construct allowing for the transduction of SuperClomeleon in inhibitory neurons (**Figure 5.3**) which can be used to measure the rate of chloride transport specifically in this subtype of neurons. In turn, the levels of membrane KCC2 can be quantified as before in CaMKIIa and GAD67 positive neurons respectively in 5xFAD mice and provide all the necessary data to assess the extend of chloride dyshomeostasis in AD-like transgenic mouse lines.

Understanding the contribution of Aβ pathology in the downregulation of KCC2 is pivotal. It has been discussed earlier that the membrane KCC2 loss appears to be downstream to Aβ secretion, however we should not exclude the possibility of KCC2 downregulation being sufficient to augment Aβ secretion in AD-like transgenic lines. Thus, treating transgenic mice with a KCC2 enhancer prior to Aβ accumulation, or upregulating KCC2 in CNS neurons via a systemic viral infection with an AAV-PHP.B-syn-HA-KCC2 (Chen et al., 2018) at an early timepoint will allow us to understand the directionality of the KCC2 and Aβ interaction.

Considering the reported loss of KCC2 in the hippocampus of 5xFAD and APP^{NL-G-F} mice, and the resultant chloride transport impairment, it will be important to study the LTP specificity within the hippocampus in AD-like transgenic mice. It has been shown that hypofunction of KCC2 in the hippocampus of aged mice resulted in a runaway LTP relaying in unstimulated synapses (Ferando et al., 2016). This unspecific spread of LTP to unrelated synapses can disrupt memory formation and give rise to cognitive decline. Therein, testing whether such process occurs in AD-like transgenic mice resulting from a KCC2-mediated shift in E_{GABA} should provide additional mechanistic evidence of a hippocampus-related memory loss in AD. In addition to measuring LTP induction in two independently stimulated pathways following the protocol described by (Ferando et al., 2016), it will be important to record the induction and the strength of LTP in 5xFAD prior to the reported KCC2 downregulation as the function of the co-transporter might be affected before any significant

change in its protein levels. Moreover, recording LTP induction in the presence of a KCC2 blocker (such as VU0240551) or $GABA_AR$ antagonist in 5xFAD will provide further evidence on the extent of disruption of chloride transport and in these mice.

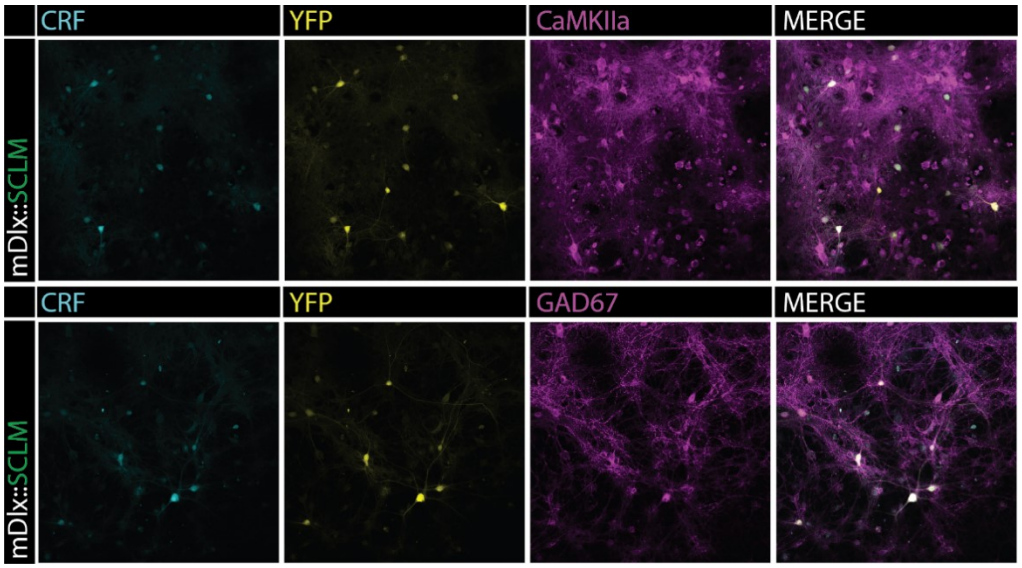

Figure 5.3. The AAV-mDlx-SCLM allowing for transduction of the chloride sensor (SCLM) in inhibitory neurons.

Confocal images of AAV2/9-mDlx-SCLM infected hippocampal neurons in culture. The neurons are stained against CaMKIIa (top) and GAD67 (bottom). The SCLM construct is a FRET pair of mCerrulean (CRP) and the yellow fluorescent protein (YFP).

The progression of AD pathology and symptoms are influenced by sex. Women show reliably higher levels of Aβ and pTAU than men, but also the cognitive decline rates differ between sexes (Buckley et al., 2020). Consistently, sex differences have been described in various AD-like transgenic lines (Bories et al., 2012; King et al., 1999; Sil et al., 2022), with females showing more profound phenotypes in some lines and males in others. In the study presented in chapter 2, both sexes have been included in all the experimental setups, however sex differences have not been studied. It will be therefore intriguing to extend the scope of this study and investigate whether chloride transport dysregulation manifests earlier in one of the two sexes and whether the mechanisms of KCC2 downregulation are

similar between sexes. Recent work in human spinal cords have demonstrated a sex-specific mechanism of KCC2 downregulation (Dedek et al., 2022), which could probably be true under pathological conditions, such as AD.

The study on normal aging nicely demonstrates the contribution of uncontrolled inhibitory input in the development of cognitive decline. However, the study could have been designed accordingly to further validate if the cognitive decline observed in a subpopulation of old mice can be rescued by restoring the E/I balance in the mPFC. For instance, a group of old mice could have been cognitively characterized first and then infected with a virus overexpressing ChR2 in either CaMKIIa or mDlx neurons within the mPFC, implanted with an optic fiber and tested again behaviorally upon light stimulation. If the ARCD is associated with a shift towards inhibition, then activating inhibitory neurons in cognitively impaired mice should have no effect while activating excitatory neurons should compete the pre-existing excessive inhibitory input and potentially rescue some of the cognitive deficits. In contrast, activating inhibitory neurons in cognitively intact old mice should replicate the phenotype seen in young mice when GABAergic neurons were optogenetically activated (**Figure 3.4**). Optogenetic activation of GABAergic neurons in young mice was sufficient to replicate cognitive deficits observed in a subpopulation of old, cognitively impaired mice. And yet, it is crucial to measure the net activity of the mPFC during this high frequency optogenetic stimulation to ensure that the general activity of the mPFC was reduced. Similar LFP recordings to the ones performed in the 5xFAD mice could shed light on the effect of such optogenetic manipulation and help us understand if driving inhibition in the brain of young mice generates the expected outcome. Similar LFP recordings (or *in vivo* multi-unit recordings to detect spiking activity) needs to be performed to verify whether the neuronal activity of the mPFC is altered in cognitively impaired old mice consistently with the synaptic protein findings described here (**Figure 3.2**) or the slice recordings indicating an excessive inhibitory input in pyramidal neurons shown before by others (Bories et al., 2013; Wong et al., 2006).

It will be of great interest to measure the KCC2 protein levels in the old cognitively-impaired mice, especially since previous work have shown an activity-dependent downregulation of KCC2 in the hippocampus of aged mice (Ferando et al., 2016). It might be possible, that chloride transport is disrupted in old mice and thus the excessive inhibitory tone in the mPFC could finally translate in uncontrolled excitatory neuronal activity during memory encoding tasks.

In Chapter 4, I presented the effects of chronic evoked hyperactivity in the hippocampus of wild-type and 5xFAD. This work was meant to explore the contribution of neuronal hyperactivity to the disruption of synaptic transmission and the induction of several signalling cascades promoting neurodegeneration in non-pathological conditions and in disease. The results of the proteomics analysis in wild-type mice strongly supported the notion that unrestrained neuronal hyperactivity alters several cellular mechanisms regulating synthesis and degradation of synaptic proteins and impairs memory formation. In contrast, the effect of rampart neuronal hyperactivity was occluded in the 5xFAD mice. This occlusion could result from a pre-existing synaptic dysfunction in the 5xFAD and a loss of synaptic reserve that could support the sustained evoked neuronal activity. Thus, it will be interesting to assess whether the multi-unit firing rates increase upon light stimulation of the SSFO in 5xFAD, similar to what happens in the wild-type mice (**Figure 4.1D** and **4.1E**). This experiment could also help to understand the extent of synaptic loss in pre-symptomatic 5xFAD mice. In this thesis I have shown that hippocampal hyperactivity emerges with age in the 5xFAD mice consistent with what has been reported in other AD-like mouse transgenic lines (Gurevicius et al., 2013; Ittner et al., 2014). Still, one could speculate that by challenging the system (by bringing hippocampal neurons in a depolarizing state with the SSFO activation) a runaway neuronal hyperactivity might occur as early as 2 months of age in the 5xFAD, which should be further explored. In addition, behavioral testing 3-month-old 5xFAD mice after a month of daily optogenetic activation of the hippocampus (stimulation beginning at 2 months of age) might reveal memory deficits similar or even more profound than the ones observed in the wild-type animals (**Figure 4.4D**) which will further support the hypothesis that neuronal hyperactivity can accelerate the progression of disease in AD patients.

Of particular interest will also be to study if and how fast the wild-type mice receiving the chronic optogenetic stimulation for a month can recover from the detrimental effects of neuronal hyperactivity. Hence, analyzing the proteome and the memory performance of mice at different time points after a month of optogenetic stimulation will allow us to understand if the brain is still able to recover from chronic neuronal hyperactivity. In addition, it will be interesting to study the effect of evoked neuronal hyperactivity in older wild-type mice and compare their proteome alterations to the ones already described here in young mice. It might be possible that sustain hippocampal hyperactivity has minimal effect in the homeostatic mechanisms regulating the expression and degradation of synaptic proteins in old animals, like what happened in the 5xFAD mice. Cognitive decline in aged rodents has

been linked with hippocampal hyperactivity (Koh et al., 2010; Wilson et al., 2005), thus the effect of optogenetic activation seen in young mice might be occluded in old mice.

Moreover, it will be informative to replicate the same series of experiments described in Chapter 4 in wild-type mice receiving an acute optogenetic activation of the SSFO (single trial activation as opposed to a month of daily activation). This will allow us to understand whether a single event of evoked hyperactivity can be equally detrimental to chronic neuronal overexcitability and hyperactivity. Controlled and well-restrained elevated synaptic activity within a neuronal network evokes LTP. Along this line, acute optogenetic elevation of neuronal activity, under non-pathological conditions, should result in activation of regulatory mechanism facilitating LTP, opposed to what is described here followed chronic neuronal hyperactivity.

The results of an increase in the soluble Aβ42 in the wild-type mice upon chronic optogenetic stimulation are consistent with previous observations showing that pharmacological and optogenetic neuronal stimulation can augment the secretion of Aβ (Bero et al., 2011; Cirrito et al., 2005; Kamenetz et al., 2003; Yamamoto et al., 2015). Interestingly, the proteomics analysis conducted in the hippocampal samples of these mice revealed that from among all the proteins implemented on the cleavage of APP and the production of Aβ, only the anterior pharynx-defective 1 protein (APH-1) is upregulated upon stimulation. However, during the mass spectrometry analysis, the spectrum of presenilin-1 was not identified for instance. Thus, it will be critical to further investigate if BACE1 or the principal components of γ-secretase are upregulated followed chronic neuronal hyperactivity.

Finally, another really interesting finding from the proteomic analysis is that Rheb, the only direct activator of mTOR (Crino, 2016), is upregulated following the chronic optogenetic stimulation in wild-type mice. Hyperactivation of the mTOR pathway has been linked to the pathogenesis of various neurological and neurodegenerative disorders (Crino, 2016). mTOR signalling can evoke structural changes in neurons, such as somatic and dendritic hypertrophy or axon tract enlargement which in turn can alter neuronal excitability (Lasarge and Danzer, 2014). Moreover, mTOR has been found to phosphorylate 4E-BP1, a translation repressor, resulting in activation of cap-dependent translation and the development of cortical seizures and epilepsy (Nguyen et al., 2022). Therein, verifying with immunoblots if Rhed is upregulated followed chronic neuronal hyperactivity and whether 4E-BP1 is phosphorylated will provide further evidence of mTOR hyperactivity and of a potential molecular mechanism supporting pathology and neurodegeneration.

Conclusion

The work presented in this thesis indicates that disruption of inhibitory control or excessive excitatory signaling can obstruct normal brain functioning and induce cognitive decline. Cognitive frailty by itself represents a widely diverse phenotype which has been described for a variety of neurological and neurodegenerative disorders. In parallel, it appears that several distinct mechanisms can induce cognitive decline depending on the nature and the pathophysiology of each disease leading to cognitive impairment. Is it loss of inhibition and sustained neuronal hyperactivity in Alzheimer's disease? Exaggerated inhibitory control in normal aging? The end point of either is a significant deterioration in cognitive performance. Therefore, one could speculate that regardless of the driving mechanisms or associated disease leading to cognitive disruption, restoring a fine-tuned neuronal activity, and preserving the coordination of assorted brain states should be key to slowdown or rescue cognitive decline. To that end, we need to better understand the regulatory mechanisms maintaining the E/I balance within neuronal networks in non-pathological conditions but also investigate the changes in E/I balance occurring within each aberrant neuronal network in disease to finally identify effective strategies to treat cognitive decline.

Bibliography

Abadchi, J.K., Nazari-Ahangarkolaee, M., Gattas, S., Bermudez-Contreras, E., Luczak, A., McNaughton, B.L., and Mohajerani, M.H. (2020). Spatiotemporal patterns of neocortical activity around hippocampal sharp-wave ripples. Elife *9*.

Abbott, L.F., and Regehr, W.G. (2004). Synaptic computation. Nat. 2004 4317010 *431*, 796–803.

Abdulla, F.A., Abu-Bakra, M.A.J., Calaminici, M.R., Stephenson, J.D., and Sinden, J.D. (1995). Importance of forebrain cholinergic and GABAergic systems to the age-related deficits in water maze performance of rats. Neurobiol. Aging *16*, 41–52.

Adolfsson, R., Gottfries, C.G., Roos, B.E., and Winblad, B. (1979). Changes in the brain catecholamines in patients with dementia of Alzheimer type. Br. J. Psychiatry *135*, 216–223.

Agarwal, S., Tannenberg, R.K., and Dodd, P.R. (2008). Reduced Expression of the Inhibitory Synapse Scaffolding Protein Gephyrin in Alzheimer's Disease. J. Alzheimer's Dis. *14*, 313–321.

Agez, M., Schultz, P., Medina, I., Baker, D.J., Burnham, M.P., Cardarelli, R.A., Conway, L.C., Garnier, K., Geschwindner, S., Gunnarsson, A., et al. (2017). Molecular architecture of potassium chloride co-transporter KCC2. Sci. Reports 2017 71 *7*, 1–14.

Ahmed, T., Van der Jeugd, A., Blum, D., Galas, M.C., D'Hooge, R., Buee, L., and Balschun, D. (2014). Cognition and hippocampal synaptic plasticity in mice with a homozygous tau deletion. Neurobiol. Aging *35*, 2474–2478.

Alessi, D.R., Zhang, J., Khanna, A., Hochdörfer, T., Shang, Y., and Kahle, K.T. (2014). The WNK-SPAK/OSR1 pathway: master regulator of cation-chloride cotransporters. Sci. Signal. *7*.

Amatniek, J.C., Hauser, W.A., DelCastillo-Castaneda, C., Jacobs, D.M., Marder, K., Bell, K., Albert, M., Brandt, J., and Stern, Y. (2006). Incidence and Predictors of Seizures in Patients with Alzheimer's Disease. Epilepsia *47*, 867–872.

Andreadis, A., Brown, W.M., and Kosik, K.S. (1992). Structure and novel exons of the human tau gene. Biochemistry *31*, 10626–10633.

Andrews-Hanna, J.R., Snyder, A.Z., Vincent, J.L., Lustig, C., Head, D., Raichle, M.E.E., and Buckner, R.L. (2007). Disruption of Large-Scale Brain Systems in Advanced Aging. Neuron *56*, 924–935.

Andrews-Zwilling, Y., Gillespie, A.K., Kravitz, A. V., Nelson, A.B., Devidze, N., Lo, I., Yoon, S.Y., Bien-Ly, N., Ring, K., Zwilling, D., et al. (2012). Hilar GABAergic Interneuron Activity Controls Spatial Learning and Memory Retrieval. PLoS One *7*, e40555.

Anggono, V., and Huganir, R.L. (2012). Regulation of AMPA receptor trafficking and synaptic plasticity. Curr. Opin. Neurobiol. *22*, 461–469.

Angulo, S.L., Orman, R., Neymotin, S.A., Liu, L., Buitrago, L., Cepeda-Prado, E., Stefanov, D., Lytton, W.W., Stewart, M., Small, S.A., et al. (2017). Tau and amyloid-related pathologies in the entorhinal cortex have divergent effects in the hippocampal circuit. Neurobiol. Dis. *108*, 261–276.

Anticevic, A., Cole, M.W., Murray, J.D., Corlett, P.R., Wang, X.-J., and Krystal, J.H. (2012). The role of default network deactivation in cognition and disease. Trends Cogn. Sci. *16*, 584–592.

Armenta-Resendiz, M., Assali, A., Tsvetkov, E., Cowan, C.W., and Lavin, A. (2022). Repeated methamphetamine administration produces cognitive deficits through augmentation of GABAergic synaptic transmission in the prefrontal cortex. Neuropsychopharmacol. 2022 4710 *47*, 1816–1825.

Arrasate, M., Pérez, M., and Avila, J. (2000). Tau dephosphorylation at tau-1 site correlates with its association to cell membrane. Neurochem. Res. *25*, 43–50.

Attwell, D., and Gibb, A. (2005). Neuroenergetics and the kinetic design of excitatory synapses. Nat. Rev. Neurosci. 2005 611 *6*, 841–849.

Aubert, G., and Lansdorp, P.M. (2008). Telomeres and aging. Physiol. Rev. *88*, 557–579.

Auger, M.L., and Floresco, S.B. (2015). Prefrontal Cortical GABA Modulation of Spatial Reference and Working Memory. Int. J. Neuropsychopharmacol. *18*, 1–11.

Bai, B., Wang, X., Li, Y., Chen, P.C., Yu, K., Dey, K.K., Yarbro, J.M., Han, X., Lutz, B.M., Rao, S., et al. (2020). Deep Multilayer Brain Proteomics Identifies Molecular Networks in

Alzheimer's Disease Progression. Neuron *105*, 975-991.e7.

Bai, L., Hof, P.R., Standaert, D.G., Xing, Y., Nelson, S.E., Young, A.B., and Magnusson, K.R. (2004). Changes in the expression of the NR2B subunit during aging in macaque monkeys. Neurobiol. Aging *25*, 201–208.

Bakker, A., Krauss, G.L., Albert, M.S., Speck, C.L., Jones, L.R., Stark, C.E., Yassa, M.A., Bassett, S.S., Shelton, A.L., and Gallagher, M. (2012). Reduction of Hippocampal Hyperactivity Improves Cognition in Amnestic Mild Cognitive Impairment. Neuron *74*, 467–474.

Bakker, A., Albert, M.S., Krauss, G., Speck, C.L., and Gallagher, M. (2015). Response of the medial temporal lobe network in amnestic mild cognitive impairment to therapeutic intervention assessed by fMRI and memory task performance. NeuroImage Clin. *7*, 688–698.

Bakkour, A., Morris, J.C., Wolk, D.A., and Dickerson, B.C. (2013). The effects of aging and Alzheimer's disease on cerebral cortical anatomy: Specificity and differential relationships with cognition. Neuroimage *76*, 332–344.

Báldi, R., Varga, C., and Tamás, G. (2010). Differential distribution of KCC2 along the axo-somato-dendritic axis of hippocampal principal cells. Eur. J. Neurosci. *32*, 1319–1325.

Bañuelos, C., Sofia Beas, B., McQuail, J.A., Gilbert, R.J., Frazier, C.J., Setlow, B., and Bizon, J.L. (2014). Prefrontal Cortical GABAergic Dysfunction Contributes to Age-Related Working Memory Impairment. J. Neurosci. *34*, 3457–3466.

Barense, M.D., Fox, M.T., and Baxter, M.G. (2002). Aged Rats Are Impaired on an Attentional Set-Shifting Task Sensitive to Medial Frontal Cortex Damage in Young Rats. Learn. Mem. *9*, 191.

Baroncelli, L., Braschi, C., Spolidoro, M., Begenisic, T., Maffei, L., and Sale, A. (2011). Brain Plasticity and Disease: A Matter of Inhibition. Neural Plast. *2011*, 1–11.

Bartzokis, G., Cummings, J.L., Sultzer, D., Henderson, V.W., Nuechterlein, K.H., and Mintz, J. (2003). White Matter Structural Integrity in Healthy Aging Adults and Patients With Alzheimer Disease: A Magnetic Resonance Imaging Study. Arch. Neurol. *60*, 393–398.

Bassett, S.S., Yousem, D.M., Cristinzio, C., Kusevic, I., Yassa, M.A., Caffo, B.S., and Zeger, S.L. (2006). Familial risk for Alzheimer's disease alters fMRI activation patterns. Brain *129*, 1229–1239.

Bateman, R.J., Siemers, E.R., Mawuenyega, K.G., Wen, G., Browning, K.R., Sigurdson, W.C., Yarasheski, K.E., Friedrich, S.W., DeMattos, R.B., May, P.C., et al. (2009). A γ-secretase inhibitor decreases amyloid-β production in the central nervous system. Ann. Neurol. *66*, 48–54.

Bateman, R.J., Xiong, C., Benzinger, T.L.S., Fagan, A.M., Goate, A., Fox, N.C., Marcus, D.S., Cairns, N.J., Xie, X., Blazey, T.M., et al. (2012). Clinical and Biomarker Changes in Dominantly Inherited Alzheimer's Disease. N. Engl. J. Med. *367*, 795–804.

Beas, B.S., Setlow, B., and Bizon, J.L. (2013). Distinct manifestations of executive dysfunction in aged rats. Neurobiol. Aging *34*, 2164–2174.

Béïque, J.C., and Huganir, R.L. (2009). AMPA Receptor Subunits Get Their Share of the Pie. Neuron *62*, 165–168.

Bekris, L.M., Yu, C.E., Bird, T.D., and Tsuang, D.W. (2010). Review article: Genetics of Alzheimer disease. J. Geriatr. Psychiatry Neurol. *23*, 213–227.

Ben-Ari, Y. (2002). Excitatory actions of gaba during development: the nature of the nurture. Nat. Rev. Neurosci. 2002 39 *3*, 728–739.

Ben-Ari, Y., Gaiarsa, J.L., Tyzio, R., and Khazipov, R. (2007). GABA: A pioneer transmitter that excites immature neurons and generates primitive oscillations. Physiol. Rev. *87*, 1215–1284.

Bergeron, M.J., Castonguay, A., and De Koninck, Y. (2014). KCC2 : nouvelle cible thérapeutique pour le traitement de pathologies neurologiques. Médecine/Sciences *30*, 514–517.

Bero, A.W., Yan, P., Roh, J.H., Cirrito, J.R., Stewart, F.R., Raichle, M.E., Lee, J.-M., and Holtzman, D.M. (2011). Neuronal activity regulates the regional vulnerability to amyloid-β deposition. Nat. Neurosci. *14*, 750–756.

Berry, K.P., and Nedivi, E. (2017). Spine Dynamics: Are They All the Same? Neuron *96*,

43–55.

Betz, H. (1998). Gephyrin, a major player in GABAergic postsynaptic membrane assembly? Nat. Neurosci. 1998 17 *1*, 541–543.

Bie, B., Wu, J., Lin, F., Naguib, M., and Xu, J. (2022). Suppression of hippocampal GABAergic transmission impairs memory in rodent models of Alzheimer's disease. Eur. J. Pharmacol. *917*, 174771.

Bishop, N.A., Lu, T., and Yankner, B.A. (2010). Neural mechanisms of ageing and cognitive decline. Nat. 2010 4647288 *464*, 529–535.

Bizon, J.L., LaSarge, C.L., Montgomery, K.S., McDermott, A.N., Setlow, B., and Griffith, W.H. (2009). Spatial reference and working memory across the lifespan of male Fischer 344 rats. Neurobiol. Aging *30*, 646–655.

Blaesse, P., Guillemin, I., Schindler, J., Schweizer, M., Delpire, E., Khiroug, L., Friauf, E., and Nothwang, H.G. (2006). Oligomerization of KCC2 Correlates with Development of Inhibitory Neurotransmission. J. Neurosci. *26*, 10407–10419.

Blazer, D.G. (2000). Psychiatry and the oldest old. Am. J. Psychiatry *157*, 1915–1924.

Bloss, E.B., Janssen, W.G., McEwen, B.S., and Morrison, J.H. (2010). Interactive effects of stress and aging on structural plasticity in the prefrontal cortex. J. Neurosci. *30*, 6726–6731.

Bloss, E.B., Janssen, W.G., Ohm, D.T., Yuk, F.J., Wadsworth, S., Saardi, K.M., McEwen, B.S., and Morrison, J.H. (2011). Evidence for Reduced Experience-Dependent Dendritic Spine Plasticity in the Aging Prefrontal Cortex. J. Neurosci. *31*, 7831–7839.

Bonnert, T.P., Mckernan, R.M., Farrar, S., Le Bourdellès, B., Heavens, R.P., Smith, D.W., Hewson, L., Rigby, M.R., Sirinathsinghji, D.J.S., Brown, N., et al. (1999). θ, a novel γ-aminobutyric acid type A receptor subunit. Proc. Natl. Acad. Sci. U. S. A. *96*, 9891–9896.

Bookheimer, S.Y., Strojwas, M.H., Cohen, M.S., Saunders, A.M., Pericak-Vance, M.A., Mazziotta, J.C., and Small, G.W. (2000). Patterns of Brain Activation in People at Risk for Alzheimer's Disease. N. Engl. J. Med. *343*, 450–456.

Bories, C., Guitton, M.J., Julien, C., Tremblay, C., Vandal, M., Msaid, M., De Koninck, Y.,

and Calon, F. (2012). Sex-Dependent Alterations in Social Behaviour and Cortical Synaptic Activity Coincide at Different Ages in a Model of Alzheimer's Disease. PLoS One *7*, e46111.

Bories, C., Husson, Z., Guitton, M.J., and De Koninck, Y. (2013). Differential balance of prefrontal synaptic activity in successful versus unsuccessful cognitive aging. J. Neurosci. *33*, 1344–1356.

Born, H.A., Kim, J.Y., Savjani, R.R., Das, P., Dabaghian, Y.A., Guo, Q., Yoo, J.W., Schuler, D.R., Cirrito, J.R., Zheng, H., et al. (2014). Genetic Suppression of Transgenic APP Rescues Hypersynchronous Network Activity in a Mouse Model of Alzeimer's Disease. J. Neurosci. *34*, 3826–3840.

Bos, R., Sadlaoud, K., Boulenguez, P., Buttigieg, D., Liabeuf, S., Brocard, C., Haase, G., Bras, H., and Vinay, L. (2013). Activation of 5-HT2A receptors upregulates the function of the neuronal K-Cl cotransporter KCC2. Proc. Natl. Acad. Sci. U. S. A. *110*, 348–353.

Boulenguez, P., Liabeuf, S., Bos, R., Bras, H., Jean-Xavier, C., Brocard, C., Stil, A., Darbon, P., Cattaert, D., Delpire, E., et al. (2010). Down-regulation of the potassium-chloride cotransporter KCC2 contributes to spasticity after spinal cord injury. Nat. Med. 2010 163 *16*, 302–307.

Bourgeois, J.P., Goldman-Rakic, P.S., and Rakic, P. (1994). Synaptogenesis in the Prefrontal Cortex of Rhesus Monkeys. Cereb. Cortex *4*, 78–96.

Bourne, J., and Harris, K.M. (2007). Do thin spines learn to be mushroom spines that remember? Curr. Opin. Neurobiol. *17*, 381–386.

Brabander, de, Kramers, and Uylings (1998). Layer-specific dendritic regression of pyramidal cells with ageing in the human prefrontal cortex. Eur. J. Neurosci. *10*, 1261–1269.

Brown, V.J., and Bowman, E.M. (2002). Rodent models of prefrontal cortical function. Trends Neurosci. *25*, 340–343.

Bu, X.-L., Xiang, Y., Jin, W.-S., Wang, J., Shen, L.-L., Huang, Z.-L., Zhang, K., Liu, Y.-H., Zeng, F., Liu, J.-H., et al. (2018). Blood-derived amyloid-β protein induces Alzheimer's disease pathologies. Mol. Psychiatry *23*, 1–9.

Buckley, R.F., Scott, M.R., Jacobs, H.I.L., Schultz, A.P., Properzi, M.J., Amariglio, R.E.,

Hohman, T.J., Mayblyum, D. V., Rubinstein, Z.B., Manning, L., et al. (2020). Sex Mediates Relationships Between Regional Tau Pathology and Cognitive Decline. Ann. Neurol. *88*, 921–932.

Buckner, R.L., Snyder, A.Z., Shannon, B.J., LaRossa, G., Sachs, R., Fotenos, A.F., Sheline, Y.I., Klunk, W.E., Mathis, C.A., Morris, J.C., et al. (2005). Molecular, Structural, and Functional Characterization of Alzheimer's Disease: Evidence for a Relationship between Default Activity, Amyloid, and Memory. J. Neurosci. *25*, 7709–7717.

Buell, S.J., and Coleman, P.D. (1981). Quantitative evidence for selective dendritic growth in normal human aging but not in senile dementia. Brain Res. *214*, 23–41.

Burianova, J., Ouda, L., Profant, O., and Syka, J. (2009). Age-related changes in GAD levels in the central auditory system of the rat. Exp. Gerontol. *44*, 161–169.

Burke, S.N., and Barnes, C.A. (2006). Neural plasticity in the ageing brain. Nat. Rev. Neurosci. 2006 71 *7*, 30–40.

Burke, S.N., and Barnes, C.A. (2010). Senescent synapses and hippocampal circuit dynamics. Trends Neurosci. *33*, 153–161.

Busche, M.A., and Konnerth, A. (2016). Impairments of neural circuit function in Alzheimer's disease. Philos. Trans. R. Soc. B Biol. Sci. *371*, 20150429.

Busche, M.A., Eichhoff, G., Adelsberger, H., Abramowski, D., Wiederhold, K.-H., Haass, C., Staufenbiel, M., Konnerth, A., and Garaschuk, O. (2008). Clusters of hyperactive neurons near amyloid plaques in a mouse model of Alzheimer's disease. Science *321*, 1686–1689.

Busche, M.A., Chen, X., Henning, H.A., Reichwald, J., Staufenbiel, M., Sakmann, B., and Konnerth, A. (2012). Critical role of soluble amyloid-β for early hippocampal hyperactivity in a mouse model of Alzheimer's disease. Proc. Natl. Acad. Sci. U. S. A. *109*, 8740–8745.

Busche, M.A., Kekuš, M., Adelsberger, H., Noda, T., Förstl, H., Nelken, I., and Konnerth, A. (2015). Rescue of long-range circuit dysfunction in Alzheimer's disease models. Nat. Neurosci. *18*, 1623–1630.

Busche, M.A., Wegmann, S., Dujardin, S., Commins, C., Schiantarelli, J., Klickstein, N., Kamath, T. V., Carlson, G.A., Nelken, I., and Hyman, B.T. (2019). Tau impairs neural

circuits, dominating amyloid-β effects, in Alzheimer models in vivo. Nat. Neurosci. *22*, 57–64.

Buzsáki, G., and Chrobak, J.J. (1995). Temporal structure in spatially organized neuronal ensembles: a role for interneuronal networks. Curr. Opin. Neurobiol. *5*, 504–510.

Buzsáki, G., and Draguhn, A. (2004). Neuronal Oscillations in Cortical Networks. Science (80-.). *304*, 1926–1929.

Buzśaki, G., and Wang, X.J. (2012). Mechanisms of gamma oscillations. Annu. Rev. Neurosci. *35*, 203–225.

Cabeza, R. (2002). Hemispheric asymmetry reduction in older adults: the HAROLD model. Psychol. Aging *17*, 85–100.

Cabeza, R., Grady, C.L., Nyberg, L., McIntosh, A.R., Tulving, E., Kapur, S., Jennings, J.M., Houle, S., and Craik, F.I.M. (1997). Age-Related Differences in Neural Activity during Memory Encoding and Retrieval: A Positron Emission Tomography Study. J. Neurosci. *17*, 391–400.

Cabeza, R., Anderson, N.D., Locantore, J.K., and McIntosh, A.R. (2002). Aging Gracefully: Compensatory Brain Activity in High-Performing Older Adults. Neuroimage *17*, 1394–1402.

Canter, R.G., Penney, J., and Tsai, L.-H. (2016). The road to restoring neural circuits for the treatment of Alzheimer's disease. Nature *539*, 187–196.

Carpenter, H.E., Kelly, K.B., Bizon, J.L., and Frazier, C.J. (2016). Age-related changes in tonic activation of presynaptic versus extrasynaptic γ-amniobutyric acid type B receptors in rat medial prefrontal cortex. Neurobiol. Aging *45*, 88–97.

Carr, D.B., Goate, A., Phil, D., and Morris, J.C. (1997). Current concepts in the pathogenesis of Alzheimer's disease. Am. J. Med. *103*, 3S-10S.

Caspary, D.M., Hughes, L.F., and Ling, L.L. (2013). Age-related GABAA receptor changes in rat auditory cortex. Neurobiol. Aging *34*, 1486–1496.

Cavelier, P., Hamann, M., Rossi, D., Mobbs, P., and Attwell, D. (2005). Tonic excitation and inhibition of neurons: ambient transmitter sources and computational consequences. Prog.

Biophys. Mol. Biol. *87*, 3–16.

Celone, K.A., Calhoun, V.D., Dickerson, B.C., Atri, A., Chua, E.F., Miller, S.L., DePeau, K., Rentz, D.M., Selkoe, D.J., Blacker, D., et al. (2006). Alterations in Memory Networks in Mild Cognitive Impairment and Alzheimer's Disease: An Independent Component Analysis. J. Neurosci. *26*, 10222–10231.

Chamma, I., Chevy, Q., Poncer, J.C., and Lévi, S. (2012). Role of the neuronal K-Cl co-transporter KCC2 in inhibitory and excitatory neurotransmission. Front. Cell. Neurosci. *6*.

Chamma, I., Heubl, M., Chevy, Q., Renner, M., Moutkine, I., Eugène, E., Poncer, J.C., and Lévi, S. (2013). Activity-Dependent Regulation of the K/Cl Transporter KCC2 Membrane Diffusion, Clustering, and Function in Hippocampal Neurons. J. Neurosci. *33*, 15488–15503.

Chandrasekaran, K., Giordano, T., Brady, D.R., Stoll, J., Martin, L.J., and Rapoport, S.I. (1994). Impairment in mitochondrial cytochrome oxidase gene expression in Alzheimer disease. Mol. Brain Res. *24*, 336–340.

Chang, Y.M., Rosene, D.L., Killiany, R.J., Mangiamele, L.A., and Luebke, J.I. (2005). Increased Action Potential Firing Rates of Layer 2/3 Pyramidal Cells in the Prefrontal Cortex are Significantly Related to Cognitive Performance in Aged Monkeys. Cereb. Cortex *15*, 409–418.

Chartier-Harlin, M.C., Crawford, F., Houlden, H., Warren, A., Hughes, D., Fidani, L., Goate, A., Rossor, M., Roques, P., Hardy, J., et al. (1991). Early-onset Alzheimer's disease caused by mutations at codon 717 of the β-amyloid precursor protein gene. Nat. 1991 3536347 *353*, 844–846.

Chaudhry, F.A., Reimer, R.J., Bellocchio, E.E., Danbolt, N.C., Osen, K.K., Edwards, R.H., and Storm-Mathisen, J. (1998). The Vesicular GABA Transporter, VGAT, Localizes to Synaptic Vesicles in Sets of Glycinergic as Well as GABAergic Neurons. J. Neurosci. *18*, 9733–9750.

Chen, B., Li, Y., Yu, B., Zhang, Z., Brommer, B., Williams, P.R., Liu, Y., Hegarty, S.V., Zhou, S., Zhu, J., et al. (2018). Reactivation of Dormant Relay Pathways in Injured Spinal Cord by KCC2 Manipulations. Cell *174*, 521-535.e13.

Chen, M., Wang, J., Jiang, J., Zheng, X., Justice, N.J., Wang, K., Ran, X., Li, Y., Huo, Q., Zhang, J., et al. (2017). APP modulates KCC2 expression and function in hippocampal GABAergic inhibition. Elife *6*.

Chevy, Q., Heubl, M., Goutierre, M., Backer, S., Moutkine, I., Eugène, E., Bloch-Gallego, E., Lévi, S., and Poncer, J.C. (2015). KCC2 Gates Activity-Driven AMPA Receptor Traffic through Cofilin Phosphorylation. J. Neurosci. *35*, 15772–15786.

Choi, D.W. (1994). Chapter 6 Glutamate receptors and the induction of excitotoxic neuronal death. Prog. Brain Res. *100*, 47–51.

Choii, G., and Ko, J. (2015). Gephyrin: a central GABAergic synapse organizer. Exp. Mol. Med. 2015 474 *47*, e158–e158.

Choquet, D., and Triller, A. (2013). The Dynamic Synapse. Neuron *80*, 691–703.

Chu, D.C.M., Penney, J.B., and Young, A.B. (1987). Quantitative autoradiography of hippocampal GABAB and GABAA receptor changes in Alzheimer's disease. Neurosci. Lett. *82*, 246–252.

Cirrito, J.R., Yamada, K.A., Finn, M.B., Sloviter, R.S., Bales, K.R., May, P.C., Schoepp, D.D., Paul, S.M., Mennerick, S., and Holtzman, D.M. (2005). Synaptic activity regulates interstitial fluid amyloid-beta levels in vivo. Neuron *48*, 913–922.

Cleary, J.P., Walsh, D.M., Hofmeister, J.J., Shankar, G.M., Kuskowski, M.A., Selkoe, D.J., and Ashe, K.H. (2004). Natural oligomers of the amyloid-β protein specifically disrupt cognitive function. Nat. Neurosci. 2004 81 *8*, 79–84.

Cobb, S.R., Buhl, E.H., Halasy, K., Paulsen, O., and Somogyi, P. (1995). Synchronization of neuronal activity in hippocampus by individual GABAergic interneurons. Nat. 1995 3786552 *378*, 75–78.

Collinson, N., Kuenzi, F.M., Jarolimek, W., Maubach, K.A., Cothliff, R., Sur, C., Smith, A., Otu, F.M., Howell, O., Atack, J.R., et al. (2002). Enhanced Learning and Memory and Altered GABAergic Synaptic Transmission in Mice Lacking the α5 Subunit of the GABAAReceptor. J. Neurosci. *22*, 5572–5580.

Côme, E., Heubl, M., Schwartz, E.J., Poncer, J.C., and Lévi, S. (2019). Reciprocal regulation

of KCC2 trafficking and synaptic activity. Front. Cell. Neurosci. *13*, 48.

Cope, D.W., Di Giovanni, G., Fyson, S.J., Orbán, G., Errington, A.C., Lrincz, M.L., Gould, T.M., Carter, D.A., and Crunelli, V. (2009). Enhanced tonic GABAA inhibition in typical absence epilepsy. Nat. Med. 2009 1512 *15*, 1392–1398.

Cordero-Erausquin, M., Coull, J.A.M., Boudreau, D., Rolland, M., and De Koninck, Y. (2005). Differential Maturation of GABA Action and Anion Reversal Potential in Spinal Lamina I Neurons: Impact of Chloride Extrusion Capacity. J. Neurosci. *25*, 9613–9623.

Cordshagen, A., Busch, W., Winklhofer, M., Nothwang, H.G., and Hartmann, A.M. (2018). Phosphoregulation of the intracellular termini of K-Cl cotransporter 2 (KCC2) enables flexible control of its activity. J. Biol. Chem. *293*, 16984–16993.

Correia, S.S., Bassani, S., Brown, T.C., Lisé, M.F., Backos, D.S., El-Husseini, A., Passafaro, M., and Esteban, J.A. (2008). Motor protein–dependent transport of AMPA receptors into spines during long-term potentiation. Nat. Neurosci. 2008 114 *11*, 457–466.

Coull, J.A.M., Boudreau, D., Bachand, K., Prescott, S.A., Nault, F., Sík, A., De Koninck, P., and De Koninck, Y. (2003). Trans-synaptic shift in anion gradient in spinal lamina I neurons as a mechanism of neuropathic pain. Nat. 2003 4246951 *424*, 938–942.

Coull, J.A.M., Beggs, S., Boudreau, D., Boivin, D., Tsuda, M., Inoue, K., Gravel, C., Salter, M.W., and De Koninck, Y. (2005). BDNF from microglia causes the shift in neuronal anion gradient underlying neuropathic pain. Nat. 2005 4387070 *438*, 1017–1021.

Cramer, P.E., Cirrito, J.R., Wesson, D.W., Lee, C.Y.D., Karlo, J.C., Zinn, A.E., Casali, B.T., Restivo, J.L., Goebel, W.D., James, M.J., et al. (2012). ApoE-directed therapeutics rapidly clear β-amyloid and reverse deficits in AD mouse models. Science (80-.). *335*, 1503–1506.

Crary, J.F., Trojanowski, J.Q., Schneider, J.A., Abisambra, J.F., Abner, E.L., Alafuzoff, I., Arnold, S.E., Attems, J., Beach, T.G., Bigio, E.H., et al. (2014). Primary age-related tauopathy (PART): a common pathology associated with human aging. Acta Neuropathol. *128*, 755–766.

Cretin, B., Sellal, F., Philippi, N., Bousiges, O., Di Bitonto, L., Martin-Hunyadi, C., and Blanc, F. (2016). Epileptic Prodromal Alzheimer's Disease, a Retrospective Study of 13 New

Cases: Expanding the Spectrum of Alzheimer's Disease to an Epileptic Variant? J. Alzheimer's Dis. *52*, 1125–1133.

Crino, P.B. (2016). The mTOR signalling cascade: paving new roads to cure neurological disease. Nat. Rev. Neurol. 2016 127 *12*, 379–392.

Crystal, H., Dickson, D., Fuld, P., Masur, D., Scott, R., Mehler, M., Masdeu, J., Kawas, C., Aronson, M., and Wolfson, L. (1988). Clinico-pathologic studies in dementia: Nondemented subjects with pathologically confirmed alzheimer's disease. Neurology *38*, 1682–1687.

Damoiseaux, J.S., Prater, K.E., Miller, B.L., and Greicius, M.D. (2012). Functional connectivity tracks clinical deterioration in Alzheimer's disease. Neurobiol. Aging *33*, 828.e19-828.e30.

Danbolt, N.C. (2001). Glutamate uptake. Prog. Neurobiol. *65*, 1–105.

Dawson, R., Wallace, D.R., and Meldrum, M.J. (1989). Endogenous glutamate release from frontal cortex of adult and aged rats. Neurobiol. Aging *10*, 665–668.

Dedek, A., Xu, J., Kandegedara, C.M., Lorenzo, L.É., Godin, A.G., De Koninck, Y., Lombroso, P.J., Tsai, E.C., and Hildebrand, M.E. (2019). Loss of STEP61 couples disinhibition to N-methyl-d-aspartate receptor potentiation in rodent and human spinal pain processing. Brain *142*, 1535–1546.

Dedek, A., Xu, J., Lorenzo, L.É., Godin, A.G., Kandegedara, C.M., Glavina, G., Landrigan, J.A., Lombroso, P.J., De Koninck, Y., Tsai, E.C., et al. (2022). Sexual dimorphism in a neuronal mechanism of spinal hyperexcitability across rodent and human models of pathological pain. Brain *145*, 1124–1138.

Dehury, B., Somavarapu, A.K., and Kepp, K.P. (2020). A computer-simulated mechanism of familial Alzheimer's disease: Mutations enhance thermal dynamics and favor looser substrate-binding to γ-secretase. J. Struct. Biol. *212*.

Deidda, G., Parrini, M., Naskar, S., Bozarth, I.F., Contestabile, A., and Cancedda, L. (2015). Reversing excitatory GABAAR signaling restores synaptic plasticity and memory in a mouse model of Down syndrome. Nat. Med. *21*, 318–326.

Delpire, E., and Lauf, P.K. (1991). Kinetics of Cl-dependent K fluxes in hyposmotically

swollen low K sheep erythrocytes. J. Gen. Physiol. *97*, 173–193.

Delpire, E., Days, E., Lewis, L.M., Mi, D., Kim, K., Lindsley, C.W., and Weaver, C.D. (2009). Small-molecule screen identifies inhibitors of the neuronal K-Cl cotransporter KCC2. Proc. Natl. Acad. Sci. U. S. A. *106*, 5383–5388.

Delpire, E., Baranczak, A., Waterson, A.G., Kim, K., Kett, N., Morrison, R.D., Scott Daniels, J., David Weaver, C., and Lindsley, C.W. (2012). Further optimization of the K-Cl cotransporter KCC2 antagonist ML077: Development of a highly selective and more potent in vitro probe. Bioorg. Med. Chem. Lett. *22*, 4532–4535.

Destexhe, A., Contreras, D., and Steriade, M. (1999). Spatiotemporal Analysis of Local Field Potentials and Unit Discharges in Cat Cerebral Cortex during Natural Wake and Sleep States. J. Neurosci. *19*, 4595–4608.

Van Deursen, J.A., Vuurman, E.F.P.M., Verhey, F.R.J., Van Kranen-Mastenbroek, V.H.J.M., and Riedel, W.J. (2008). Increased EEG gamma band activity in Alzheimer's disease and mild cognitive impairment. J. Neural Transm. *115*, 1301–1311.

Dickerson, B.C., Salat, D.H., Bates, J.F., Atiya, M., Killiany, R.J., Greve, D.N., Dale, A.M., Stern, C.E., Blacker, D., Albert, M.S., et al. (2004). Medial temporal lobe function and structure in mild cognitive impairment. Ann. Neurol. *56*, 27–35.

Dickerson, B.C., Salat, D.H., Greve, D.N., Chua, E.F., Rand-Giovannetti, E., Rentz, D.M., Bertram, L., Mullin, K., Tanzi, R.E., Blacker, D., et al. (2005). Increased hippocampal activation in mild cognitive impairment compared to normal aging and AD. Neurology *65*, 404–411.

Dickstein, D.L., Kabaso, D., Rocher, A.B., Luebke, J.I., Wearne, S.L., and Hof, P.R. (2007). Changes in the structural complexity of the aged brain. Aging Cell *6*, 275–284.

Dinamarca, M.C., Raveh, A., Schneider, A., Fritzius, T., Früh, S., Rem, P.D., Stawarski, M., Lalanne, T., Turecek, R., Choo, M., et al. (2019). Complex formation of APP with GABA B receptors links axonal trafficking to amyloidogenic processing. Nat. Commun. *10*.

Disterhoft, J.F., and Oh, M.M. (2007). Alterations in intrinsic neuronal excitability during normal aging. Aging Cell *6*, 327–336.

Dolev, I., Fogel, H., Milshtein, H., Berdichevsky, Y., Lipstein, N., Brose, N., Gazit, N., and Slutsky, I. (2013). Spike bursts increase amyloid-β 40/42 ratio by inducing a presenilin-1 conformational change. Nat. Neurosci. 2013 165 *16*, 587–595.

Dominguez, L.G., Wennberg, R.A., Gaetz, W., Cheyne, D., Snead, O.C., and Perez Velazquez, J.L. (2005). Enhanced Synchrony in Epileptiform Activity? Local versus Distant Phase Synchronization in Generalized Seizures. J. Neurosci. *25*, 8077–8084.

Doody, R.S., Raman, R., Farlow, M., Iwatsubo, T., Vellas, B., Joffe, S., Kieburtz, K., He, F., Sun, X., Thomas, R.G., et al. (2013). A Phase 3 Trial of Semagacestat for Treatment of Alzheimer's Disease. N. Engl. J. Med. *369*, 341–350.

Doshina, A., Gourgue, F., Onizuka, M., Opsomer, R., Wang, P., Ando, K., Tasiaux, B., Dewachter, I., Kienlen-Campard, P., Brion, J.-P., et al. (2017). Cortical cells reveal APP as a new player in the regulation of GABAergic neurotransmission. Sci. Rep. *7*, 370.

Doyon, N., Prescott, S.A., Castonguay, A., Godin, A.G., Kröger, H., and De Koninck, Y. (2011). Efficacy of synaptic inhibition depends on multiple, dynamically interacting mechanisms implicated in chloride homeostasis. PLoS Comput. Biol. *7*, e1002149.

Doyon, N., Prescott, S.A., and De Koninck, Y. (2015). Mild KCC2 Hypofunction Causes Inconspicuous Chloride Dysregulation that Degrades Neural Coding. Front. Cell. Neurosci. *9*, 516.

Doyon, N., Vinay, L., Prescott, S.A., and De Koninck, Y. (2016). Chloride Regulation: A Dynamic Equilibrium Crucial for Synaptic Inhibition. Neuron *89*, 1157–1172.

Drubin, D.G., and Kirschner, M.W. (1986). Tau protein function in living cells. J. Cell Biol. *103*, 2739–2746.

Drubin, D.G., Caput, D., and Kirschner, M.W. (1984). Studies on the expression of the microtubule-associated protein, tau, during mouse brain development, with newly isolated complementary DNA probes. J. Cell Biol. *98*, 1090–1097.

Duan, H., Wearne, S.L., Rocher, A.B., Macedo, A., Morrison, J.H., and Hof, P.R. (2003). Age-related Dendritic and Spine Changes in Corticocortically Projecting Neurons in Macaque Monkeys. Cereb. Cortex *13*, 950–961.

Van Duijn, C.M., Hendriks, L., Cruts, M., Hardy, J.A., Hofman, A., and Van Broeckhoven, C. (1991). Amyloid precursor protein gene mutation in early-onset Alzheimer's disease. Lancet (London, England) *337*, 978.

Dumitriu, D., Hao, J., Hara, Y., Kaufmann, J., Janssen, W.G.M., Lou, W., Rapp, P.R., and Morrison, J.H. (2010). Selective Changes in Thin Spine Density and Morphology in Monkey Prefrontal Cortex Correlate with Aging-Related Cognitive Impairment. J. Neurosci. *30*, 7507–7515.

van Dyck, C.H., Swanson, C.J., Aisen, P., Bateman, R.J., Chen, C., Gee, M., Kanekiyo, M., Li, D., Reyderman, L., Cohen, S., et al. (2022). Lecanemab in Early Alzheimer's Disease. N. Engl. J. Med.

Egan, M.F., Kost, J., Tariot, P.N., Aisen, P.S., Cummings, J.L., Vellas, B., Sur, C., Mukai, Y., Voss, T., Furtek, C., et al. (2018). Randomized Trial of Verubecestat for Mild-to-Moderate Alzheimer's Disease. N. Engl. J. Med. *378*, 1691–1703.

Elston, G.N., Benavides-Piccione, R., Elston, A., Manger, P.R., and Defelipe, J. (2011). Pyramidal cells in prefrontal cortex of primates: Marked differences in neuronal structure among species. Front. Neuroanat. *5*, 1–17.

Enomoto, T., Tse, M.T., and Floresco, S.B. (2011). Reducing prefrontal gamma-aminobutyric acid activity induces cognitive, behavioral, and dopaminergic abnormalities that resemble schizophrenia. Biol. Psychiatry *69*, 432–441.

Erten-Lyons, D., Woltjer, R.L., Dodge, H., Nixon, R., Vorobik, R., Calvert, J.F., Leahy, M., Montine, T., and Kaye, J. (2009). Factors associated with resistance to dementia despite high Alzheimer disease pathology. Neurology *72*, 354–360.

Essrich, C., Lorez, M., Benson, J.A., Fritschy, J.M., and Lüscher, B. (1998). Postsynaptic clustering of major GABAA receptor subtypes requires the γ2 subunit and gephyrin. Nat. Neurosci. 1998 17 *1*, 563–571.

Farrant, M., and Kaila, K. (2007). The cellular, molecular and ionic basis of GABA(A) receptor signalling. Prog. Brain Res. *160*, 59–87.

Farrant, M., and Nusser, Z. (2005). Variations on an inhibitory theme: phasic and tonic

activation of GABAA receptors. Nat. Rev. Neurosci. 2005 63 *6*, 215–229.

Ferando, I., Faas, G.C., and Mody, I. (2016). Diminished KCC2 confounds synapse specificity of LTP during senescence. Nat. Neurosci. *19*, 1197–1200.

Fernandez, F., Morishita, W., Zuniga, E., Nguyen, J., Blank, M., Malenka, R.C., and Garner, C.C. (2007). Pharmacotherapy for cognitive impairment in a mouse model of Down syndrome. Nat. Neurosci. 2007 104 *10*, 411–413.

Ferrini, F., Trang, T., Mattioli, T.-A.M., Laffray, S., Del'Guidice, T., Lorenzo, L.-E., Castonguay, A., Doyon, N., Zhang, W., Godin, A.G., et al. (2013). Morphine hyperalgesia gated through microglia-mediated disruption of neuronal Cl^- homeostasis. Nat. Neurosci. *16*, 183–192.

Ferrini, F., Lorenzo, L.E., Godin, A.G., Quang, M. Le, and De Koninck, Y. (2017). Enhancing KCC2 function counteracts morphine-induced hyperalgesia. Sci. Rep. *7*, 1–8.

Ferrini, F., Perez-Sanchez, J., Ferland, S., Lorenzo, L.E., Godin, A.G., Plasencia-Fernandez, I., Cottet, M., Castonguay, A., Wang, F., Salio, C., et al. (2020). Differential chloride homeostasis in the spinal dorsal horn locally shapes synaptic metaplasticity and modality-specific sensitization. Nat. Commun. *11*, 1–18.

Filippini, N., MacIntosh, B.J., Hough, M.G., Goodwin, G.M., Frisoni, G.B., Smith, S.M., Matthews, P.M., Beckmann, C.F., and Mackay, C.E. (2009). Distinct patterns of brain activity in young carriers of the APOE-ε4 allele. Proc. Natl. Acad. Sci. U. S. A. *106*, 7209–7214.

Fogel, H., Frere, S., Segev, O., Bharill, S., Shapira, I., Gazit, N., O'Malley, T., Slomowitz, E., Berdichevsky, Y., Walsh, D.M., et al. (2014). APP homodimers transduce an amyloid-β-mediated increase in release probability at excitatory synapses. Cell Rep. *7*, 1560–1576.

Ford, A., Castonguay, A., Cottet, M., Little, J.W., Chen, Z., Symons-Liguori, A.M., Doyle, T., Egan, T.M., Vanderah, T.W., De Konnick, Y., et al. (2015). Engagement of the GABA to KCC2 signaling pathway contributes to the analgesic effects of A3AR agonists in neuropathic pain. J. Neurosci. *35*, 6057–6067.

Forlenza, O. V., Diniz, B.S., Radanovic, M., Santos, F.S., Talib, L.L., and Gattaz, W.F. (2011). Disease-modifying properties of long-term lithium treatment for amnestic mild

cognitive impairment: randomised controlled trial. Br. J. Psychiatry *198*, 351–356.

Foster, T.C. (2007). Calcium homeostasis and modulation of synaptic plasticity in the aged brain. Aging Cell *6*, 319–325.

Frandemiche, M.L., De Seranno, S., Rush, T., Borel, E., Elie, A., Arnal, I., Lanté, F., and Buisson, A. (2014). Activity-Dependent Tau Protein Translocation to Excitatory Synapse Is Disrupted by Exposure to Amyloid-Beta Oligomers. J. Neurosci. *34*, 6084–6097.

Freir, D.B., Holscher, C., and Herron, C.E. (2001). Blockade of long-term potentiation by β-amyloid peptides in the CA1 region of the rat hippocampus in vivo. J. Neurophysiol. *85*, 708–713.

Frick, K.M., Baxter, M.G., Markowska, A.L., Olton, D.S., and Price, D.L. (1995). Age-related spatial reference and working memory deficits assessed in the water maze. Neurobiol. Aging *16*, 149–160.

Friedel, P., Kahle, K.T., Zhang, J., Hertz, N., Pisella, L.I., Buhler, E., Schaller, F., Duan, J., Khanna, A.R., Bishop, P.N., et al. (2015). WNK1-regulated inhibitory phosphorylation of the KCC2 cotransporter maintains the depolarizing action of GABA in immature neurons. Sci. Signal. *8*.

Fuster, J.M. (2001). The Prefrontal Cortex—An Update: Time Is of the Essence. Neuron *30*, 319–333.

Futamachi, K.J., Mutani, R., and Prince, D.A. (1974). Potassium activity in rabbit cortex. Brain Res. *75*, 5–25.

Gagnon, M., Bergeron, M.J., Lavertu, G., Castonguay, A., Tripathy, S., Bonin, R.P., Perez-Sanchez, J., Boudreau, D., Wang, B., Dumas, L., et al. (2013). Chloride extrusion enhancers as novel therapeutics for neurological diseases. Nat. Med. *19*, 1524–1528.

Gallagher, M., and Burwell, R.D. (1989). Relationship of age-related decline across several behavioral domains. Neurobiol. Aging *10*, 691–708.

Gallagher, M., and Rapp, P.R. (2003). THE USE OF ANIMAL MODELS TO STUDY THE EFFECTS OF AGING ON COGNITION. Http://Dx.Doi.Org/10.1146/Annurev.Psych.48.1.339 *48*, 339–370.

Gamba, G., Saltzberg, S.N., Lombardi, M., Miyanoshita, A., Lytton, J., Hediger, M.A., Brenner, B.M., and Hebert, S.C. (1993). Primary structure and functional expression of a cDNA encoding the thiazide-sensitive, electroneutral sodium-chloride cotransporter. Proc. Natl. Acad. Sci. U. S. A. *90*, 2749–2753.

Games, D., Adams, D., Alessandrini, R., Barbour, R., Berthelette, P., Blackwell, C., Carr, T., Clemens, J., Donaldson, T., and Gillespie, F. (1995). Alzheimer-type neuropathology in transgenic mice overexpressing V717F beta-amyloid precursor protein. Nature *373*, 523–527.

Garcia-Marin, V., Blazquez-Llorca, L., Rodriguez, J.R., Boluda, S., Muntane, G., Ferrer, I., and DeFelipe, J. (2009). Diminished perisomatic GABAergic terminals on cortical neurons adjacent to amyloid plaques. Front. Neuroanat. *3*, 28.

Gassmann, M., and Bettler, B. (2012). Regulation of neuronal GABAB receptor functions by subunit composition. Nat. Rev. Neurosci. 2012 136 *13*, 380–394.

Geinisman, Y., De Toledo-Morrell, L., and Morrell, F. (1986). Loss of perforated synapses in the dentate gyrus: morphological substrate of memory deficit in aged rats. Proc. Natl. Acad. Sci. *83*, 3027–3031.

Geschwind, D.H. (2003). Tau phosphorylation, tangles, and neurodegeneration: The chicken or the egg? Neuron *40*, 457–460.

Gilad, D., Shorer, S., Ketzef, M., Friedman, A., Sekler, I., Aizenman, E., and Hershfinkel, M. (2015). Homeostatic regulation of KCC2 activity by the zinc receptor mZnR/GPR39 during seizures. Neurobiol. Dis. *81*, 4–13.

Gilbert, S.F. (2000). Aging: The Biology of Senescence.

Glykys, J., and Mody, I. (2007). Activation of GABAA Receptors: Views from Outside the Synaptic Cleft. Neuron *56*, 763–770.

Goate, A., Chartier-Harlin, M.C., Mullan, M., Brown, J., Crawford, F., Fidani, L., Giuffra, L., Haynes, A., Irving, N., and James, L. (1991). Segregation of a missense mutation in the amyloid precursor protein gene with familial Alzheimer's disease. Nature *349*, 704–706.

Goedert, M., Wischik, C.M., Crowther, R.A., Walker, J.E., and Klug, A. (1988). Cloning and

sequencing of the cDNA encoding a core protein of the paired helical filament of Alzheimer disease: identification as the microtubule-associated protein tau. Proc. Natl. Acad. Sci. U. S. A. *85*, 4051–4055.

Goedert, M., Spillantini, M.G., Jakes, R., Rutherford, D., and Crowther, R.A. (1989). Multiple isoforms of human microtubule-associated protein tau: sequences and localization in neurofibrillary tangles of Alzheimer's disease. Neuron *3*, 519–526.

Goldman-Rakic, P.S., and Brown, R.M. (1981). Regional changes of monoamines in cerebral cortex and subcortical structures of aging rhesus monkeys. Neuroscience *6*, 177–187.

Götz, J., and Ittner, L.M. (2008). Animal models of Alzheimer's disease and frontotemporal dementia. Nat. Rev. Neurosci. 2008 97 *9*, 532–544.

Götz, J., Bodea, L.G., and Goedert, M. (2018). Rodent models for Alzheimer disease. Nat. Rev. Neurosci. *19*, 583–598.

Götz, J., Halliday, G., and Nisbet, R.M. (2019). Molecular Pathogenesis of the Tauopathies. Https://Doi-Org.Acces.Bibl.Ulaval.ca/10.1146/Annurev-Pathmechdis-012418-012936 *14*, 239–261.

Goutierre, M., Al Awabdh, S., Donneger, F., François, E., Gomez-Dominguez, D., Irinopoulou, T., Menendez de la Prida, L., and Poncer, J.C. (2019). KCC2 Regulates Neuronal Excitability and Hippocampal Activity via Interaction with Task-3 Channels. Cell Rep. *28*, 91-103.e7.

Grady, C.L. (2008). Cognitive neuroscience of aging. Ann. N. Y. Acad. Sci. *1124*, 127–144.

Grady, C.L., McIntosh, A.R., Horwitz, B., Maisog, J.M., Ungerleider, L.G., Mentis, M.J., Pietrini, P., Schapiro, M.B., and Haxby, J. V. (1995). Age-Related Reductions in Human Recognition Memory Due to Impaired Encoding. Science (80-.). *269*, 218–221.

Gralle, M., and Ferreira, S.T. (2007). Structure and functions of the human amyloid precursor protein: The whole is more than the sum of its parts. Prog. Neurobiol. *82*, 11–32.

Grégoire, J., and Van der Linden, M. (2007). Effect of age on forward and backward digit spans. Http://Dx.Doi.Org/10.1080/13825589708256642 *4*, 140–149.

Greicius, M.D., Srivastava, G., Reiss, A.L., and Menon, V. (2004). Default-mode network activity distinguishes Alzheimer's disease from healthy aging: Evidence from functional MRI. Proc. Natl. Acad. Sci. U. S. A. *101*, 4637–4642.

Grill, J.D., and Riddle, D.R. (2002). Age-related and laminar-specific dendritic changes in the medial frontal cortex of the rat. Brain Res. *937*, 8–21.

Grimley, J.S., Li, L., Wang, W., Wen, L., Beese, L.S., Hellinga, H.W., and Augustine, G.J. (2013). Visualization of Synaptic Inhibition with an Optogenetic Sensor Developed by Cell-Free Protein Engineering Automation. J. Neurosci. *33*, 16297.

Groth, R., and Aanonsen, L. (2002). Spinal brain-derived neurotrophic factor (BDNF) produces hyperalgesia in normal mice while antisense directed against either BDNF or trkB, prevent inflammation-induced hyperalgesia. Pain *100*, 171–181.

Guillon, J., Attal, Y., Colliot, O., La Corte, V., Dubois, B., Schwartz, D., Chavez, M., and De Vico Fallani, F. (2017). Loss of brain inter-frequency hubs in Alzheimer's disease. Sci. Reports 2017 71 *7*, 1–13.

Gulyás, A.I., Sík, A., Payne, J.A., Kaila, K., and Freund, T.F. (2001). The KCl cotransporter, KCC2, is highly expressed in the vicinity of excitatory synapses in the rat hippocampus. Eur. J. Neurosci. *13*, 2205–2217.

Gunning-Dixon, F.M., and Raz, N. (2000). The cognitive correlates of white matter abnormalities in normal aging: A quantitative review. Neuropsychology *14*, 224–232.

Gurevicius, K., Lipponen, A., and Tanila, H. (2013). Increased cortical and thalamic excitability in freely moving APPswe/PS1dE9 mice modeling epileptic activity associated with Alzheimer's disease. Cereb. Cortex *23*, 1148–1158.

Gutiérrez, A., Khan, Z.U., Ruano, D., Miralles, C.P., Vitorica, J., and De Blas, A.L. (1996). Aging-related subunit expression changes of the GABAA receptor in the rat hippocampus. Neuroscience *74*, 341–348.

Guttmann, C.R.G., Jolesz, F.A., Kikinis, R., Killiany, R.J., Moss, M.B., Sandor, T., and Albert, M.S. (1998). White matter changes with normal aging. Neurology *50*, 972–978.

Haass, C. (2010). Initiation and propagation of neurodegeneration. Nat. Med. 2010 1611 *16*,

1201–1204.

El Haj, M., Antoine, P., Amouyel, P., Lambert, J.C., Pasquier, F., and Kapogiannis, D. (2016). Autobiographical memory decline in Alzheimer's Disease. Ageing Res. Rev. *27*, 15.

Hall, C.N., Klein-Flügge, M.C., Howarth, C., and Attwell, D. (2012). Oxidative phosphorylation, not glycolysis, powers presynaptic and postsynaptic mechanisms underlying brain information processing. J. Neurosci. *32*, 8940–8951.

Hammond, C. (2015). Cellular and Molecular Neurophysiology: Fourth Edition. Cell. Mol. Neurophysiol. Fourth Ed. 1–433.

Hanger, D.P., Anderton, B.H., and Noble, W. (2009). Tau phosphorylation: the therapeutic challenge for neurodegenerative disease. Trends Mol. Med. *15*, 112–119.

Hansen, K.B., Yi, F., Perszyk, R.E., Furukawa, H., Wollmuth, L.P., Gibb, A.J., and Traynelis, S.F. (2018). Structure, function, and allosteric modulation of NMDA receptors. J. Gen. Physiol. *150*, 1081–1105.

Hara, Y., Rapp, P.R., and Morrison, J.H. (2012). Neuronal and morphological bases of cognitive decline in aged rhesus monkeys. Age (Omaha). *34*, 1051.

Hardy, J., and Selkoe, D.J. (2002). The amyloid hypothesis of Alzheimer's disease: progress and problems on the road to therapeutics. Science *297*, 353–356.

Hardy, J.A., and Higgins, G.A. (1992). Alzheimer's disease: The amyloid cascade hypothesis. Science (80-.). *256*, 184–185.

Hardy, J., Cowburn, R., Barton, A., Reynolds, G., Lofdahl, E., O'Carroll, A.M., Wester, P., and Winblad, B. (1987). Region-specific loss of glutamate innervation in Alzheimer's disease. Neurosci. Lett. *73*, 77–80.

Hardy, J., Duff, K., Hardy, K.G., Perez-Tur, J., and Hutton, M. (1998). Genetic dissection of Alzheimer's disease and related dementias: amyloid and its relationship to tau. Nat. Neurosci. 1998 15 *1*, 355–358.

Harris, K.M. (1999). Structure, development, and plasticity of dendritic spines. Curr. Opin. Neurobiol. *9*, 343–348.

Harris, K.M., and Kater, S.B. (2003). Dendritic Spines: Cellular Specializations Imparting Both Stability and Flexibility to Synaptic Function. Http://Dx.Doi.Org.Acces.Bibl.Ulaval.ca/10.1146/Annurev.Ne.17.030194.002013 *17*, 341–371.

Hartley, D.M., Walsh, D.M., Ye, C.P., Diehl, T., Vasquez, S., Vassilev, P.M., Teplow, D.B., and Selkoe, D.J. (1999). Protofibrillar intermediates of amyloid beta-protein induce acute electrophysiological changes and progressive neurotoxicity in cortical neurons. J. Neurosci. *19*, 8876–8884.

Hartmann, A.M., and Nothwang, H.G. (2015). Molecular and evolutionary insights into the structural organization of cation chloride cotransporters. Front. Cell. Neurosci. *8*, 1–14.

He, Z., Guo, J.L., McBride, J.D., Narasimhan, S., Kim, H., Changolkar, L., Zhang, B., Gathagan, R.J., Yue, C., Dengler, C., et al. (2018). Amyloid-β plaques enhance Alzheimer's brain tau-seeded pathologies by facilitating neuritic plaque tau aggregation. Nat. Med. *24*, 29–38.

Head, D., Buckner, R.L., Shimony, J.S., Williams, L.E., Akbudak, E., Conturo, T.E., McAvoy, M., Morris, J.C., and Snyder, A.Z. (2004). Differential Vulnerability of Anterior White Matter in Nondemented Aging with Minimal Acceleration in Dementia of the Alzheimer Type: Evidence from Diffusion Tensor Imaging. Cereb. Cortex *14*, 410–423.

Hebert, L.E., Scherr, P.A., Bienias, J.L., Bennett, D.A., and Evans, D.A. (2003a). Alzheimer Disease in the US Population: Prevalence Estimates Using the 2000 Census. Arch. Neurol. *60*, 1119–1122.

Hebert, S.C., Mount, D.B., and Gamba, G. (2003b). Molecular physiology of cation-coupled Cl− cotransport: the SLC12 family. Pflügers Arch. 2004 4475 *447*, 580–593.

Hedden, T., and Gabrieli, J.D.E. (2004). Insights into the ageing mind: a view from cognitive neuroscience. Nat. Rev. Neurosci. 2004 52 *5*, 87–96.

Hedden, T., Lautenschlager, G., and Park, D.C. (2005). Contributions of processing ability and knowledge to verbal memory tasks across the adult life-span. Q. J. Exp. Psychol. A. *58*, 169–190.

Hedden, T., Van Dijk, K.R.A., Becker, J.A., Mehta, A., Sperling, R.A., Johnson, K.A., and Buckner, R.L. (2009). Disruption of Functional Connectivity in Clinically Normal Older Adults Harboring Amyloid Burden. J. Neurosci. *29*, 12686–12694.

Hefendehl, J.K., LeDue, J., Ko, R.W.Y., Mahler, J., Murphy, T.H., and MacVicar, B.A. (2016). Mapping synaptic glutamate transporter dysfunction in vivo to regions surrounding Aβ plaques by iGluSnFR two-photon imaging. Nat. Commun. 2016 71 *7*, 1–13.

Herl, L., Thomas, A. V., Lill, C.M., Banks, M., Deng, A., Jones, P.B., Spoelgen, R., Hyman, B.T., and Berezovska, O. (2009). Mutations in amyloid precursor protein affect its interactions with presenilin/γ-secretase. Mol. Cell. Neurosci. *41*, 166–174.

Herndon, J.G., Moss, M.B., Rosene, D.L., and Killiany, R.J. (1997). Patterns of cognitive decline in aged rhesus monkeys. Behav. Brain Res. *87*, 25–34.

Herrmann, C., and Demiralp, T. (2005). Human EEG gamma oscillations in neuropsychiatric disorders. Clin. Neurophysiol. *116*, 2719–2733.

Hertz, L., and Zielke, H.R. (2004). Astrocytic control of glutamatergic activity: astrocytes as stars of the show. Trends Neurosci. *27*, 735–743.

Heuser, J.E., and Reese, T.S. (1977). Structure of the Synapse. Compr. Physiol. 261–294.

Hewitt, S.A., Wamsteeker, J.I., Kurz, E.U., and Bains, J.S. (2009). Altered chloride homeostasis removes synaptic inhibitory constraint of the stress axis. Nat. Neurosci. 2009 124 *12*, 438–443.

Hildebrand, M.E., Xu, J., Dedek, A., Li, Y., Sengar, A.S., Beggs, S., Lombroso, P.J., and Salter, M.W. (2016). Potentiation of Synaptic GluN2B NMDAR Currents by Fyn Kinase Is Gated through BDNF-Mediated Disinhibition in Spinal Pain Processing. Cell Rep. *17*, 2753–2765.

Hines, R.M., Wu, L., Hines, D.J., Steenland, H., Mansour, S., Dahlhaus, R., Singaraja, R.R., Cao, X., Sammler, E., Hormuzdi, S.G., et al. (2008). Synaptic Imbalance, Stereotypies, and Impaired Social Interactions in Mice with Altered Neuroligin 2 Expression. J. Neurosci. *28*, 6055–6067.

Hoe, H.S., Kea, J.L., Carney, R.S.E., Lee, J., Markova, A., Lee, J.Y., Howell, B.W., Hyman,

B.T., Pak, D.T.S., Bu, G., et al. (2009). Interaction of Reelin with Amyloid Precursor Protein Promotes Neurite Outgrowth. J. Neurosci. *29*, 7459–7473.

Hof, P.R., and Morrison, J.H. (2004). The aging brain: morphomolecular senescence of cortical circuits. Trends Neurosci. *27*, 607–613.

Hof, P.R., Duan, H., Page, T.L., Einstein, M., Wicinski, B., He, Y., Erwin, J.M., and Morrison, J.H. (2002). Age-related changes in GluR2 and NMDAR1 glutamate receptor subunit protein immunoreactivity in corticocortically projecting neurons in macaque and patas monkeys. Brain Res. *928*, 175–186.

Honig, L.S., Vellas, B., Woodward, M., Boada, M., Bullock, R., Borrie, M., Hager, K., Andreasen, N., Scarpini, E., Liu-Seifert, H., et al. (2018). Trial of Solanezumab for Mild Dementia Due to Alzheimer's Disease. N. Engl. J. Med. *378*, 321–330.

Hormuzdi, S.G., Filippov, M.A., Mitropoulou, G., Monyer, H., and Bruzzone, R. (2004). Electrical synapses: a dynamic signaling system that shapes the activity of neuronal networks. Biochim. Biophys. Acta - Biomembr. *1662*, 113–137.

Hornykiewicz, O. (2002). Dopamine miracle: From brain homogenate to dopamine replacement. Mov. Disord. *17*, 501–508.

Horváth, A., Szcs, A., Barcs, G., Noebels, J.L., and Kamondi, A. (2016). Epileptic Seizures in Alzheimer Disease. Alzheimer Dis. Assoc. Disord. *30*, 186–192.

Hou, Y., Dan, X., Babbar, M., Wei, Y., Hasselbalch, S.G., Croteau, D.L., and Bohr, V.A. (2019). Ageing as a risk factor for neurodegenerative disease. Nat. Rev. Neurol. 2019 1510 *15*, 565–581.

Hsia, A.Y., Masliah, E., Mcconlogue, L., Yu, G.Q., Tatsuno, G., Hu, K., Kholodenko, D., Malenka, R.C., Nicoll, R.A., and Mucke, L. (1999). Plaque-independent disruption of neural circuits in Alzheimer's disease mouse models. Proc. Natl. Acad. Sci. U. S. A. *96*, 3228–3233.

Hsieh, H., Boehm, J., Sato, C., Iwatsubo, T., Tomita, T., Sisodia, S., and Malinow, R. (2006). AMPAR Removal Underlies Aβ-Induced Synaptic Depression and Dendritic Spine Loss. Neuron *52*, 831–843.

Huberfeld, G., Wittner, L., Clemenceau, S., Baulac, M., Kaila, K., Miles, R., and Rivera, C. (2007). Perturbed Chloride Homeostasis and GABAergic Signaling in Human Temporal Lobe Epilepsy. J. Neurosci. *27*, 9866–9873.

Hübner, C.A., Stein, V., Hermans-Borgmeyer, I., Meyer, T., Ballanyi, K., and Jentsch, T.J. (2001). Disruption of KCC2 reveals an essential role of K-Cl cotransport already in early synaptic inhibition. Neuron *30*, 515–524.

Hughes, C.S., Moggridge, S., Müller, T., Sorensen, P.H., Morin, G.B., and Krijgsveld, J. (2018). Single-pot, solid-phase-enhanced sample preparation for proteomics experiments. Nat. Protoc. 2018 141 *14*, 68–85.

Huijbers, X.W., Schultz, A.P., Papp, K. V., Lapoint, M.R., Hanseeuw, X., Chhatwal, X.J.P., Hedden, T., Johnson, X.A., and Sperling, X.R.A. (2019). Tau Accumulation in Clinically Normal Older Adults Is Associated with Hippocampal Hyperactivity. J. Neurosci. *39*, 548–556.

Van Hummel, A., Bi, M., Ippati, S., Van Der Hoven, J., Volkerling, A., Lee, W.S., Tan, D.C.S., Bongers, A., Ittner, A., Ke, Y.D., et al. (2016). No Overt Deficits in Aged Tau-Deficient C57Bl/6.Mapttm1(EGFP)Kit GFP Knockin Mice. PLoS One *11*, e0163236.

Hutton, M., Lendon, C.L., Rizzu, P., Baker, M., Froelich, S., Houlden, H.H., Pickering-Brown, S., Chakraverty, S., Isaacs, A., Grover, A., et al. (1998). Association of missense and 5′-splice-site mutations in tau with the inherited dementia FTDP-17. Nat. 1998 3936686 *393*, 702–705.

Hyde, T.M., Lipska, B.K., Ali, T., Mathew, S. V., Law, A.J., Metitiri, O.E., Straub, R.E., Ye, T., Colantuoni, C., Herman, M.M., et al. (2011). Expression of GABA Signaling Molecules KCC2, NKCC1, and GAD1 in Cortical Development and Schizophrenia. J. Neurosci. *31*, 11088–11095.

Hyman, B.T., Phelps, C.H., Beach, T.G., Bigio, E.H., Cairns, N.J., Carrillo, M.C., Dickson, D.W., Duyckaerts, C., Frosch, M.P., Masliah, E., et al. (2012). National Institute on Aging-Alzheimer's Association guidelines for the neuropathologic assessment of Alzheimer's disease. Alzheimers. Dement. *8*, 1–13.

Iaccarino, H.F., Singer, A.C., Martorell, A.J., Rudenko, A., Gao, F., Gillingham, T.Z., Mathys,

H., Seo, J., Kritskiy, O., Abdurrob, F., et al. (2016). Gamma frequency entrainment attenuates amyloid load and modifies microglia. Nature *540*, 230–235.

Ikeda, K., Onimaru, H., Yamada, J., Inoue, K., Ueno, S., Onaka, T., Toyoda, H., Arata, A., Ishikawa, T.O., Taketo, M.M., et al. (2004). Malfunction of Respiratory-Related Neuronal Activity in Na+, K+-ATPase α2 Subunit-Deficient Mice Is Attributable to Abnormal Cl- Homeostasis in Brainstem Neurons. J. Neurosci. *24*, 10693–10701.

Irizarry, M.C., Jin, S., He, F., Emond, J.A., Raman, R., Thomas, R.G., Sano, M., Quinn, J.F., Tariot, P.N., Galasko, D.R., et al. (2012). Incidence of New-Onset Seizures in Mild to Moderate Alzheimer Disease. Arch. Neurol. *69*, 368–372.

Ising, C., Gallardo, G., Leyns, C.E.G., Wong, C.H., Jiang, H., Stewart, F., Koscal, L.J., Roh, J., Robinson, G.O., Serrano, J.R., et al. (2017). AAV-mediated expression of anti-tau scFvs decreases tau accumulation in a mouse model of tauopathy. J. Exp. Med. *214*, 1227–1238.

Ittner, A.A., Gladbach, A., Bertz, J., Suh, L.S., and Ittner, L.M. (2014). p38 MAP kinase-mediated NMDA receptor-dependent suppression of hippocampal hypersynchronicity in a mouse model of Alzheimer's disease. Acta Neuropathol. Commun. *2*, 1–17.

Ittner, L.M., Ke, Y.D., and Götz, J. (2009). Phosphorylated Tau interacts with c-Jun N-terminal kinase-interacting protein 1 (JIP1) in Alzheimer disease. J. Biol. Chem. *284*, 20909–20916.

Ittner, L.M., Ke, Y.D., Delerue, F., Bi, M., Gladbach, A., van Eersel, J., Wölfing, H., Chieng, B.C., Christie, M.J., Napier, I.A., et al. (2010a). Dendritic function of tau mediates amyloid-beta toxicity in Alzheimer's disease mouse models. Cell *142*, 387–397.

Ittner, L.M., Ke, Y.D., Delerue, F., Bi, M., Gladbach, A., van Eersel, J., Wölfing, H., Chieng, B.C., Christie, M.J., Napier, I.A., et al. (2010b). Dendritic function of tau mediates amyloid-β toxicity in alzheimer's disease mouse models. Cell *142*, 387–397.

Ivakine, E.A., Acton, B.A., Mahadevan, V., Ormond, J., Tang, M., Pressey, J.C., Huang, M.Y., Ng, D., Delpire, E., Salter, M.W., et al. (2013). Neto2 is a KCC2 interacting protein required for neuronal Cl- regulation in hippocampal neurons. Proc. Natl. Acad. Sci. U. S. A. *110*, 3561–3566.

Jacob, T.C., Moss, S.J., and Jurd, R. (2008). GABAA receptor trafficking and its role in the dynamic modulation of neuronal inhibition. Nat. Rev. Neurosci. 2008 95 *9*, 331–343.

Jagust, W. (2018). Imaging the evolution and pathophysiology of Alzheimer disease. Nat. Rev. Neurosci. 2018 1911 *19*, 687–700.

Jankowsky, J.L., Slunt, H.H., Ratovitski, T., Jenkins, N.A., Copeland, N.G., and Borchelt, D.R. (2001). Co-expression of multiple transgenes in mouse CNS: a comparison of strategies. Biomol. Eng. *17*, 157–165.

Janus, C., Pearson, J., McLaurin, J.A., Mathews, P.M., Jiang, Y., Schmidt, S.D., Chishti, M.A., Horne, P., Heslin, D., French, J., et al. (2000). Aβ peptide immunization reduces behavioural impairment and plaques in a model of Alzheimer's disease. Nat. 2000 4086815 *408*, 979–982.

Jarrett, J.T., Berger, E.P., and Lansbury, P.T. (1993). The C-Terminus of the β Protein is Critical in Amyloidogenesisa. Ann. N. Y. Acad. Sci. *695*, 144–148.

Jawhar, S., Trawicka, A., Jenneckens, C., Bayer, T.A., and Wirths, O. (2012). Motor deficits, neuron loss, and reduced anxiety coinciding with axonal degeneration and intraneuronal Aβ aggregation in the 5XFAD mouse model of Alzheimer's disease. Neurobiol. Aging *33*, 196.e29-40.

De Jeu, M., and Pennartz, C. (2002). Circadian modulation of GABA function in the rat suprachiasmatic nucleus: Excitatory effects during the night phase. J. Neurophysiol. *87*, 834–844.

Jiang, J., and Jiang, H. (2015). Efficacy and adverse effects of memantine treatment for Alzheimer's disease from randomized controlled trials. Neurol. Sci. 2015 369 *36*, 1633–1641.

Jing, Y., Liu, P., and Leitch, B. (2016). Region-specific changes in presynaptic agmatine and glutamate levels in the aged rat brain. Neuroscience *312*, 10–18.

Johnson, E.C.B., Ho, K., Yu, G.Q., Das, M., Sanchez, P.E., Djukic, B., Lopez, I., Yu, X., Gill, M., Zhang, W., et al. (2020). Behavioral and neural network abnormalities in human APP transgenic mice resemble those of App knock-in mice and are modulated by familial

Alzheimer's disease mutations but not by inhibition of BACE1. Mol. Neurodegener. *15*, 1–26.

Jonsson, T., Atwal, J.K., Steinberg, S., Snaedal, J., Jonsson, P. V., Bjornsson, S., Stefansson, H., Sulem, P., Gudbjartsson, D., Maloney, J., et al. (2012). A mutation in APP protects against Alzheimer's disease and age-related cognitive decline. Nature *488*, 96–99.

Jucker, M., and Walker, L.C. (2013). Self-propagation of pathogenic protein aggregates in neurodegenerative diseases. Nature *501*, 45–51.

Jucker, M., and Walker, L.C. (2018). Propagation and spread of pathogenic protein assemblies in neurodegenerative diseases. Nat. Neurosci. 2018 2110 *21*, 1341–1349.

Kabaso, D., Coskren, P.J., Henry, B.I., Hof, P.R., and Wearne, S.L. (2009). The electrotonic structure of pyramidal neurons contributing to prefrontal cortical circuits in macaque monkeys is significantly altered in aging. Cereb. Cortex *19*, 2248–2268.

Kahle, K.T., Staley, K.J., Nahed, B. V., Gamba, G., Hebert, S.C., Lifton, R.P., and Mount, D.B. (2008). Roles of the cation-chloride cotransporters in neurological disease. Nat. Clin. Pract. Neurol. *4*, 490–503.

Kahle, K.T., Rinehart, J., and Lifton, R.P. (2010). Phosphoregulation of the Na–K–2Cl and K–Cl cotransporters by the WNK kinases. Biochim. Biophys. Acta - Mol. Basis Dis. *1802*, 1150–1158.

Kahle, K.T., Deeb, T.Z., Puskarjov, M., Silayeva, L., Liang, B., Kaila, K., and Moss, S.J. (2013). Modulation of neuronal activity by phosphorylation of the K–Cl cotransporter KCC2. Trends Neurosci. *36*, 726–737.

Kaila, K. (1994). Ionic basis of GABAA receptor channel function in the nervous system. Prog. Neurobiol. *42*, 489–537.

Kaila, K., Price, T.J., Payne, J.A., Puskarjov, M., and Voipio, J. (2014). Cation-chloride cotransporters in neuronal development, plasticity and disease. Nat. Rev. Neurosci. *15*, 637–654.

Kamal, A., Almenar-Queralt, A., LeBlanc, J.F., Roberts, E.A., and Goldstein, L.S.B. (2001). Kinesin-mediated axonal transport of a membrane compartment containing β-secretase and

presenilin-1 requires APP. Nat. 2001 4146864 *414*, 643–648.

Kamenetz, F., Tomita, T., Hsieh, H., Seabrook, G., Borchelt, D., Iwatsubo, T., Sisodia, S., and Malinow, R. (2003). APP Processing and Synaptic Function. Neuron *37*, 925–937.

Kandel, E.R., and Spencer, W.A. (1961). ELECTROPHYSIOLOGY OF HIPPOCAMPAL NEURONS: II. AFTER-POTENTIALS AND REPETITIVE FIRING. Https://Doi.Org/10.1152/Jn.1961.24.3.243 *24*, 243–259.

Kandel, M.B., Yamamoto, S., Midorikawa, R., Morise, J., Wakazono, Y., Oka, S., and Takamiya, K. (2018). N-glycosylation of the AMPA-type glutamate receptor regulates cell surface expression and tetramer formation affecting channel function. J. Neurochem. *147*, 730–747.

Kang, J., Lemaire, H.G., Unterbeck, A., Salbaum, J.M., Masters, C.L., Grzeschik, K.H., Multhaup, G., Beyreuther, K., and Müller-Hill, B. (1987). The precursor of Alzheimer's disease amyloid A4 protein resembles a cell-surface receptor. Nat. 1987 3256106 *325*, 733–736.

Kang, J.E., Lim, M.M., Bateman, R.J., Lee, J.J., Smyth, L.P., Cirrito, J.R., Fujiki, N., Nishino, S., and Holtzman, D.M. (2009). Amyloid-beta dynamics are regulated by orexin and the sleep-wake cycle. Science *326*, 1005–1007.

Kasai, H., Matsuzaki, M., Noguchi, J., Yasumatsu, N., and Nakahara, H. (2003). Structure–stability–function relationships of dendritic spines. Trends Neurosci. *26*, 360–368.

Kayarian, F.B., Jannati, A., Rotenberg, A., and Santarnecchi, E. (2020). Targeting Gamma-Related Pathophysiology in Autism Spectrum Disorder Using Transcranial Electrical Stimulation: Opportunities and Challenges. Autism Res. *13*, 1051–1071.

Kehrer, C. (2008). Altered excitatory-inhibitory balance in the NMDA-hypofunction model of schizophrenia. Front. Mol. Neurosci. *1*, 6.

Kepecs, A., and Fishell, G. (2014). Interneuron cell types are fit to function. Nature *505*, 318–326.

Keramidis, I., Vourkou, E., Papanikolopoulou, K., and Skoulakis, E.M.C. (2020). Functional Interactions of Tau Phosphorylation Sites That Mediate Toxicity and Deficient Learning in

Drosophila melanogaster. Front. Mol. Neurosci. *13*.

Kesner, R.P., and Churchwell, J.C. (2011). An analysis of rat prefrontal cortex in mediating executive function. Neurobiol. Learn. Mem. *96*, 417–431.

Kessels, H.W., Nabavi, S., and Malinow, R. (2013). Metabotropic NMDA receptor function is required for β-amyloid-induced synaptic depression. Proc. Natl. Acad. Sci. U. S. A. *110*, 4033–4038.

Khedr, E.M., Ahmed, M.A., Hamdy, A., and Shawky, O.A. (2011). Cortical excitability of amyotrophic lateral sclerosis: Transcranial magnetic stimulation study. Neurophysiol. Clin. Neurophysiol. *41*, 73–79.

Kim, C.K., Adhikari, A., and Deisseroth, K. (2017). Integration of optogenetics with complementary methodologies in systems neuroscience. Nat. Rev. Neurosci. 2017 184 *18*, 222–235.

Kim, J.H., Anwyl, R., Suh, Y.H., Djamgoz, M.B.A., and Rowan, M.J. (2001). Use-Dependent Effects of Amyloidogenic Fragments of β-Amyloid Precursor Protein on Synaptic Plasticity in Rat Hippocampus In Vivo. J. Neurosci. *21*, 1327–1333.

Kimura, R., and Ohno, M. (2009). Impairments in remote memory stabilization precede hippocampal synaptic and cognitive failures in 5XFAD Alzheimer mouse model. Neurobiol. Dis. *33*, 229–235.

Kimura, T., Whitcomb, D.J., Jo, J., Regan, P., Piers, T., Heo, S., Brown, C., Hashikawa, T., Murayama, M., Seok, H., et al. (2014). Microtubule-associated protein tau is essential for long-term depression in the hippocampus. Philos. Trans. R. Soc. B Biol. Sci. *369*.

King, D.L., Arendash, G.W., Crawford, F., Sterk, T., Menendez, J., and Mullan, M.J. (1999). Progressive and gender-dependent cognitive impairment in the APPSW transgenic mouse model for Alzheimer's disease. Behav. Brain Res. *103*, 145–162.

Klaassen, A., Glykys, J., Maguire, J., Labarca, C., Mody, I., and Boulter, J. (2006). Seizures and enhanced cortical GABAergic inhibition in two mouse models of human autosomal dominant nocturnal frontal lobe epilepsy. Proc. Natl. Acad. Sci. U. S. A. *103*, 19152–19157.

Klausberger, T., and Somogyi, P. (2008). Neuronal diversity and temporal dynamics: The

unity of hippocampal circuit operations. Science (80-.). *321*, 53–57.

Klunk, W.E., Engler, H., Nordberg, A., Wang, Y., Blomqvist, G., Holt, D.P., Bergström, M., Savitcheva, I., Huang, G.F., Estrada, S., et al. (2004). Imaging brain amyloid in Alzheimer's disease with Pittsburgh Compound-B. Ann. Neurol. *55*, 306–319.

Kneussel, M., Brandstätter, J.H., Laube, B., Stahl, S., Müller, U., and Betz, H. (1999). Loss of Postsynaptic GABAA Receptor Clustering in Gephyrin-Deficient Mice. J. Neurosci. *19*, 9289–9297.

Kneussel, M., Helmut Brandstätter, J., Gasnier, B., Feng, G., Sanes, J.R., and Betz, H. (2001). Gephyrin-Independent Clustering of Postsynaptic GABAA Receptor Subtypes. Mol. Cell. Neurosci. *17*, 973–982.

Koh, M.T., Haberman, R.P., Foti, S., McCown, T.J., and Gallagher, M. (2010). Treatment strategies targeting excess hippocampal activity benefit aged rats with cognitive impairment. Neuropsychopharmacology *35*, 1016–1025.

Kohli, B.M., Pflieger, D., Mueller, L.N., Carbonetti, G., Aebersold, R., Nitsch, R.M., and Konietzko, U. (2012). Interactome of the amyloid precursor protein APP in brain reveals a protein network involved in synaptic vesicle turnover and a close association with synaptotagmin-1. J. Proteome Res. *11*, 4075–4090.

Kowal, P. (2016). An Aging World: 2015.

Kreis, A., Desloovere, J., Suelves, N., Pierrot, N., Yerna, X., Issa, F., Schakman, O., Gualdani, R., de Clippele, M., Tajeddine, N., et al. (2021). Overexpression of wild-type human amyloid precursor protein alters GABAergic transmission. Sci. Reports 2021 111 *11*, 1–18.

Kuhn, P.H., Wang, H., Dislich, B., Colombo, A., Zeitschel, U., Ellwart, J.W., Kremmer, E., Roßner, S., and Lichtenthaler, S.F. (2010). ADAM10 is the physiologically relevant, constitutive α-secretase of the amyloid precursor protein in primary neurons. EMBO J. *29*, 3020–3032.

Kunz, L., Schröder, T.N., Lee, H., Montag, C., Lachmann, B., Sariyska, R., Reuter, M., Stirnberg, R., Stöcker, T., Messing-Floeter, P.C., et al. (2015). Reduced grid-cell-like

representations in adults at genetic risk for Alzheimer's disease. Science (80-.). *350*, 430–433.

Kursan, S., McMillen, T.S., Beesetty, P., Dias-Junior, E., Almutairi, M.M., Sajib, A.A., Kozak, J.A., Aguilar-Bryan, L., and Di Fulvio, M. (2017). The neuronal K+Cl− co-transporter 2 (Slc12a5) modulates insulin secretion. Sci. Reports 2017 71 *7*, 1–14.

Kurudenkandy, F.R., Zilberter, M., Biverstål, H., Presto, J., Honcharenko, D., Strömberg, R., Johansson, J., Winblad, B., and Fisahn, A. (2014). Amyloid-β-induced action potential desynchronization and degradation of hippocampal gamma oscillations is prevented by interference with peptide conformation change and aggregation. J. Neurosci. *34*, 11416–11425.

Lacor, P.N., Buniel, M.C., Furlow, P.W., Clemente, A.S., Velasco, P.T., Wood, M., Viola, K.L., and Klein, W.L. (2007). Aβ Oligomer-Induced Aberrations in Synapse Composition, Shape, and Density Provide a Molecular Basis for Loss of Connectivity in Alzheimer's Disease. J. Neurosci. *27*, 796–807.

Lacoursiere, S.G., Safar, J., Westaway, D., Mohajerani, M.H., and Sutherland, R.J. (2022). The effect of Aβ seeding is dependent on the presence of knock-in genes in the AppNL−G−F mice. Front. Dement. *0*, 2.

Lai, F., and Williams, R.S. (1989). A Prospective Study of Alzheimer Disease in Down Syndrome. Arch. Neurol. *46*, 849–853.

Lalonde, R., Dumont, M., Staufenbiel, M., and Strazielle, C. (2005). Neurobehavioral characterization of APP23 transgenic mice with the SHIRPA primary screen. Behav. Brain Res. *157*, 91–98.

Lam, A.D., Deck, G., Goldman, A., Eskandar, E.N., Noebels, J., and Cole, A.J. (2017). Silent hippocampal seizures and spikes identified by foramen ovale electrodes in Alzheimer's disease. Nat. Med. *23*, 678–680.

Lanctôt, K.L., Herrmaan, N., Mazzotta, P., Khan, L.R., and Ingber, N. (2004). GABAergic function in Alzheimer's disease: Evidence for dysfunction and potential as a therapeutic target for the treatment of behavioral and psychological symptoms of dementia. Can. J. Psychiatry *49*, 439–453.

Lapray, D., Lasztoczi, B., Lagler, M., Viney, T.J., Katona, L., Valenti, O., Hartwich, K., Borhegyi, Z., Somogyi, P., and Klausberger, T. (2012). Behavior-dependent specialization of identified hippocampal interneurons. Nat. Neurosci. 2012 159 *15*, 1265–1271.

Lasarge, C.L., and Danzer, S.C. (2014). Mechanisms regulating neuronal excitability and seizure development following mTOR pathway hyperactivation. Front. Mol. Neurosci. *7*, 18.

LaSarge, C.L., Montgomery, K.S., Tucker, C., Slaton, G.S., Griffith, W.H., Setlow, B., and Bizon, J.L. (2007). Deficits across multiple cognitive domains in a subset of aged Fischer 344 rats. Neurobiol. Aging *28*, 928–936.

Laxton, A.W., Tang-Wai, D.F., McAndrews, M.P., Zumsteg, D., Wennberg, R., Keren, R., Wherrett, J., Naglie, G., Hamani, C., Smith, G.S., et al. (2010). A phase I trial of deep brain stimulation of memory circuits in Alzheimer's disease. Ann. Neurol. *68*, 521–534.

Leal, S.L., and Yassa, M.A. (2015). Neurocognitive Aging and the Hippocampus across Species. Trends Neurosci. *38*, 800–812.

LeChasseur, Y., Dufour, S., Lavertu, G., Bories, C., Deschênes, M., Vallée, R., and De Koninck, Y. (2011). A microprobe for parallel optical and electrical recordings from single neurons in vivo. Nat. Methods *8*, 319–325.

Lee, H.H.C., Walker, J.A., Williams, J.R., Goodier, R.J., Payne, J.A., and Moss, S.J. (2007). Direct Protein Kinase C-dependent Phosphorylation Regulates the Cell Surface Stability and Activity of the Potassium Chloride Cotransporter KCC2 *. J. Biol. Chem. *282*, 29777–29784.

Lee, H.H.C., Jurd, R., and Moss, S.J. (2010). Tyrosine phosphorylation regulates the membrane trafficking of the potassium chloride co-transporter KCC2. Mol. Cell. Neurosci. *45*, 173–179.

Lee, H.H.C., Deeb, T.Z., Walker, J.A., Davies, P.A., and Moss, S.J. (2011). NMDA receptor activity downregulates KCC2 resulting in depolarizing GABAA receptor–mediated currents. Nat. Neurosci. 2011 146 *14*, 736–743.

Legon, W., Punzell, S., Dowlati, E., Adams, S.E., Stiles, A.B., and Moran, R.J. (2016). Altered Prefrontal Excitation/Inhibition Balance and Prefrontal Output: Markers of Aging in Human Memory Networks. Cereb. Cortex *26*, 4315–4326.

Lerma, J., and Marques, J.M. (2013). Kainate Receptors in Health and Disease. Neuron *80*, 292–311.

Lerma, J., Herranz, A.S., Herreras, O., Abraira, V., and del Rio, R.M. (1986). In vivo determination of extracellular concentration of amino acids in the rat hippocampus. A method based on brain dialysis and computerized analysis. Brain Res. *384*, 145–155.

Lesné, S.E., Sherman, M.A., Grant, M., Kuskowski, M., Schneider, J.A., Bennett, D.A., and Ashe, K.H. (2013). Brain amyloid-β oligomers in ageing and Alzheimer's disease. Brain *136*, 1383–1398.

Lévi, S., Logan, S.M., Tovar, K.R., and Craig, A.M. (2004). Gephyrin Is Critical for Glycine Receptor Clustering But Not for the Formation of Functional GABAergic Synapses in Hippocampal Neurons. J. Neurosci. *24*, 207–217.

Lewis, D.A., Hashimoto, T., and Volk, D.W. (2005). Cortical inhibitory neurons and schizophrenia. Nat. Rev. Neurosci. 2005 64 *6*, 312–324.

Lewis, J., Dickson, D.W., Lin, W.L., Chisholm, L., Corral, A., Jones, G., Yen, S.H., Sahara, N., Skipper, L., Yager, D., et al. (2001). Enhanced neurofibrillary degeneration in transgenic mice expressing mutant tau and APP. Science (80-.). *293*, 1487–1491.

Li, C., and Götz, J. (2017). Somatodendritic accumulation of Tau in Alzheimer's disease is promoted by Fyn-mediated local protein translation. EMBO J. *36*, 3120–3138.

Li, H., Khirug, S., Cai, C., Ludwig, A., Blaesse, P., Kolikova, J., Afzalov, R., Coleman, S.K., Lauri, S., Airaksinen, M.S., et al. (2007). KCC2 Interacts with the Dendritic Cytoskeleton to Promote Spine Development. Neuron *56*, 1019–1033.

Li, S., Hong, S., Shepardson, N.E., Walsh, D.M., Shankar, G.M., and Selkoe, D. (2009). Soluble oligomers of amyloid Beta protein facilitate hippocampal long-term depression by disrupting neuronal glutamate uptake. Neuron *62*, 788–801.

Liabeuf, S., Stuhl-Gourmand, L., Gackière, F., Mancuso, R., Sanchez Brualla, I., Marino, P., Brocard, F., and Vinay, L. (2017). Prochlorperazine Increases KCC2 Function and Reduces Spasticity after Spinal Cord Injury. Https://Home.Liebertpub.Com/Neu *34*, 3397–3406.

Liguz-Lecznar, M., Lehner, M., Kaliszewska, A., Zakrzewska, R., Sobolewska, A., and

Kossut, M. (2014). Altered glutamate/GABA equilibrium in aged mice cortex influences cortical plasticity. Brain Struct. Funct. 2014 2203 *220*, 1681–1693.

Limon, A., Reyes-Ruiz, J.M., and Miledi, R. (2012). Loss of functional GABA A receptors in the Alzheimer diseased brain. Proc. Natl. Acad. Sci. U. S. A. *109*, 10071–10076.

Ling, L.L., Hughes, L.F., and Caspary, D.M. (2005). Age-related loss of the GABA synthetic enzyme glutamic acid decarboxylase in rat primary auditory cortex. Neuroscience *132*, 1103–1113.

Liu, L., Wong, T.P., Pozza, M.F., Lingenhoehl, K., Wang, Y., Sheng, M., Auberson, Y.P., and Wang, Y.T. (2004). Role of NMDA Receptor Subtypes in Governing the Direction of Hippocampal Synaptic Plasticity. Science (80-.). *304*, 1021–1024.

Liu, X., Erikson, C., and Brun, A. (1996). Cortical Synaptic Changes and Gliosis in Normal Aging, Alzheimer's Disease and Frontal Lobe Degeneration. Dement. Geriatr. Cogn. Disord. *7*, 128–134.

Lleó, A., Greenberg, S.M., and Growdon, J.H. (2006). Current Pharmacotherapy for Alzheimer's Disease. Https://Doi.Org/10.1146/Annurev.Med.57.121304.131442 *57*, 513–533.

Logan, J.M., Sanders, A.L., Snyder, A.Z., Morris, J.C., and Buckner, R.L. (2002). Under-Recruitment and Nonselective Recruitment: Dissociable Neural Mechanisms Associated with Aging. Neuron *33*, 827–840.

Loomba, S., Straehle, J., Gangadharan, V., Heike, N., Khalifa, A., Motta, A., Ju, N., Sievers, M., Gempt, J., Meyer, H.S., et al. (2022). Connectomic comparison of mouse and human cortex. Science (80-.).

Lorenzo, L.E., Godin, A.G., Ferrini, F., Bachand, K., Plasencia-Fernandez, I., Labrecque, S., Girard, A.A., Boudreau, D., Kianicka, I., Gagnon, M., et al. (2020). Enhancing neuronal chloride extrusion rescues α2/α3 GABAA-mediated analgesia in neuropathic pain. Nat. Commun. *11*, 1–23.

Lu, T., Pan, Y., Kao, S.Y., Li, C., Kohane, I., Chan, J., and Yankner, B.A. (2004). Gene regulation and DNA damage in the ageing human brain. Nature *429*, 883–891.

Lu, W., Shi, Y., Jackson, A.C., Bjorgan, K., During, M.J., Sprengel, R., Seeburg, P.H., and Nicoll, R.A. (2009). Subunit Composition of Synaptic AMPA Receptors Revealed by a Single-Cell Genetic Approach. Neuron *62*, 254–268.

Luchetti, S., Huitinga, I., and Swaab, D.F. (2011). Neurosteroid and GABA-A receptor alterations in Alzheimer's disease, Parkinson's disease and multiple sclerosis. Neuroscience *191*, 6–21.

Ludwig, A., Uvarov, P., Soni, S., Thomas-Crusells, J., Airaksinen, M.S., and Rivera, C. (2011). Early Growth Response 4 Mediates BDNF Induction of Potassium Chloride Cotransporter 2 Transcription. J. Neurosci. *31*, 644–649.

Luebke, J.I., and Rosene, D.L. (2003). Aging alters dendritic morphology, input resistance, and inhibitory signaling in dentate granule cells of the rhesus monkey. J. Comp. Neurol. *460*, 573–584.

Luebke, J., Barbas, H., and Peters, A. (2010). Effects of normal aging on prefrontal area 46 in the rhesus monkey. Brain Res. Rev. *62*, 212–232.

Luebke, J.I., Chang, Y.M., Moore, T.L., and Rosene, D.L. (2004). Normal aging results in decreased synaptic excitation and increased synaptic inhibition of layer 2/3 pyramidal cells in the monkey prefrontal cortex. Neuroscience *125*, 277–288.

Lukasiewicz, P.D. (1996). GABAC receptors in the vertebrate retina. Mol. Neurobiol. *12*, 181–194.

Luscher, B., Fuchs, T., and Kilpatrick, C.L. (2011). GABAA Receptor Trafficking-Mediated Plasticity of Inhibitory Synapses. Neuron *70*, 385–409.

Mackenzie, I.R.A., and Miller, L.A. (1994). Senile plaques in temporal lobe epilepsy. Acta Neuropathol. 1994 875 *87*, 504–510.

Maconochie, D.J., Zempel, J.M., and Steinbach, J.H. (1994). How quickly can GABAA receptors open? Neuron *12*, 61–71.

Madisen, L., Mao, T., Koch, H., Zhuo, J.M., Berenyi, A., Fujisawa, S., Hsu, Y.W.A., Garcia, A.J., Gu, X., Zanella, S., et al. (2012). A toolbox of Cre-dependent optogenetic transgenic mice for light-induced activation and silencing. Nat. Neurosci. 2012 155 *15*, 793–802.

Maeda, S., Djukic, B., Taneja, P., Yu, G.-Q., Lo, I., Davis, A., Craft, R., Guo, W., Wang, X., Kim, D., et al. (2016). Expression of A152T human tau causes age-dependent neuronal dysfunction and loss in transgenic mice. EMBO Rep. *17*, 530–551.

Magi, S., Piccirillo, S., Amoroso, S., and Lariccia, V. (2019). Excitatory Amino Acid Transporters (EAATs): Glutamate Transport and Beyond. Int. J. Mol. Sci. *20*.

Magnusson, K.R., and Cotman, C.W. (1993a). Effects of aging on NMDA and MK801 binding sites in mice. Brain Res. *604*, 334–337.

Magnusson, K.R., and Cotman, C.W. (1993b). Age-related changes in excitatory amino acid receptors in two mouse strains. Neurobiol. Aging *14*, 197–206.

Mahadevan, V., Pressey, J.C., Acton, B.A., Uvarov, P., Huang, M.Y., Chevrier, J., Puchalski, A., Li, C.M., Ivakine, E.A., Airaksinen, M.S., et al. (2014). Kainate Receptors Coexist in a Functional Complex with KCC2 and Regulate Chloride Homeostasis in Hippocampal Neurons. Cell Rep. *7*, 1762–1770.

Mahadevan, V., Khademullah, C.S., Dargaei, Z., Chevrier, J., Uvarov, P., Kwan, J., Bagshaw, R.D., Pawson, T., Emili, A., De Koninck, Y., et al. (2017). Native KCC2 interactome reveals PACSIN1 as a critical regulator of synaptic inhibition. Elife *6*.

Mandell, J.W., and Banker, G.A. (1996). A spatial gradient of tau protein phosphorylation in nascent axons. J. Neurosci. *16*, 5727–5740.

Marder, E., and Prinz, A.A. (2002). Modeling stability in neuron and network function: the role of activity in homeostasis. BioEssays *24*, 1145–1154.

Markkanen, M., Karhunen, T., Llano, O., Ludwig, A., Rivera, C., Uvarov, P., and Airaksinen, M.S. (2014). Distribution of neuronal KCC2a and KCC2b isoforms in mouse CNS. J. Comp. Neurol. *522*, 1897–1914.

Markram, H., Toledo-Rodriguez, M., Wang, Y., Gupta, A., Silberberg, G., and Wu, C. (2004). Interneurons of the neocortical inhibitory system. Nat. Rev. Neurosci. 2004 510 *5*, 793–807.

Martin, D.L., and Barke, K.E. (1998). Are GAD65 and GAD67 associated with specific pools of GABA in brain? Perspect. Dev. Neurobiol. *5*, 119–129.

Martina, M., Royer, S., and Paré, D. (2001). Cell-type-specific GABA responses and chloride homeostasis in the cortex and amygdala. J. Neurophysiol. *86*, 2887–2895.

Martinez-Losa, M., Tracy, T.E., Ma, K., Verret, L., Clemente-Perez, A., Khan, A.S., Cobos, I., Ho, K., Gan, L., Mucke, L., et al. (2018). Nav1.1-Overexpressing Interneuron Transplants Restore Brain Rhythms and Cognition in a Mouse Model of Alzheimer's Disease. Neuron *98*, 75-89.e5.

Masliah, E., Crews, L., and Hansen, L. (2006). Synaptic remodeling during aging and in Alzheimer's disease. J. Alzheimer's Dis. *9*, 91–99.

Masuda, A., Kobayashi, Y., Kogo, N., Saito, T., Saido, T.C., and Itohara, S. (2016). Cognitive deficits in single App knock-in mouse models. Neurobiol. Learn. Mem. *135*, 73–82.

Matsumoto, J.Y., Stead, M., Kucewicz, M.T., Matsumoto, A.J., Peters, P.A., Brinkmann, B.H., Danstrom, J.C., Goerss, S.J., Marsh, W.R., Meyer, F.B., et al. (2013). Network oscillations modulate interictal epileptiform spike rate during human memory. Brain *136*, 2444–2456.

Matsuzaki, M., Ellis-Davies, G.C.R., Nemoto, T., Miyashita, Y., Iino, M., and Kasai, H. (2001). Dendritic spine geometry is critical for AMPA receptor expression in hippocampal CA1 pyramidal neurons. Nat. Neurosci. *4*, 1086–1092.

McKhann, G.M., Knopman, D.S., Chertkow, H., Hyman, B.T., Jack, C.R., Kawas, C.H., Klunk, W.E., Koroshetz, W.J., Manly, J.J., Mayeux, R., et al. (2011). The diagnosis of dementia due to Alzheimer's disease: recommendations from the National Institute on Aging-Alzheimer's Association workgroups on diagnostic guidelines for Alzheimer's disease. Alzheimers. Dement. *7*, 263–269.

McNaughton, D., Knight, W., Guerreiro, R., Ryan, N., Lowe, J., Poulter, M., Nicholl, D.J., Hardy, J., Revesz, T., Lowe, J., et al. (2012). Duplication of amyloid precursor protein (APP), but not prion protein (PRNP) gene is a significant cause of early onset dementia in a large UK series. Neurobiol. Aging *33*, 426.e13-426.e21.

Meinecke, D.L., and Peters, A. (1987). GABA immunoreactive neurons in rat visual cortex. J. Comp. Neurol. *261*, 388–404.

Menéndez, M. (2005). Down syndrome, Alzheimer's disease and seizures. Brain Dev. *27*, 246–252.

Meneses, S., Galicia, O., and Brailowsky, S. (1993). Chronic infusions of GABA into the medial prefrontal cortex induce spatial alternation deficits in aged rats. Behav. Brain Res. *57*, 1–7.

Mercado, A., Broumand, V., Zandi-Nejad, K., Enck, A.H., and Mount, D.B. (2006). A C-terminal Domain in KCC2 Confers Constitutive K+-Cl- Cotransport *. J. Biol. Chem. *281*, 1016–1026.

Meyer-Luehmann, M., Coomaraswamy, J., Bolmont, T., Kaeser, S., Schaefer, C., Kilger, E., Neuenschwander, A., Abramowski, D., Frey, P., Jaton, A.L., et al. (2006). Exogenous induction of cerebral β-amyloidogenesis is governed bf agent and host. Science (80-.). *313*, 1781–1784.

Miller, E.K., and Cohen, J.D. (2003). An Integrative Theory of Prefrontal Cortex Function. Http://Dx.Doi.Org/10.1146/Annurev.Neuro.24.1.167 *24*, 167–202.

Miller, S.L., Celone, K., DePeau, K., Diamond, E., Dickerson, B.C., Rentz, D., Pihlajamäki, M., and Sperling, R.A. (2008). Age-related memory impairment associated with loss of parietal deactivation but preserved hippocampal activation. Proc. Natl. Acad. Sci. U. S. A. *105*, 2181–2186.

Mizukami, K., Grayson, D.R., Ikonomovic, M.D., Sheffield, R., and Armstrong, D.M. (1998). GABAA receptor β2 and β3 subunits mRNA in the hippocampal formation of aged human brain with Alzheimer-related neuropathology. Mol. Brain Res. *56*, 268–272.

Mody, I., De Koninck, Y., Otis, T.S., and Soltesz, I. (1994). Bridging the cleft at GABA synapses in the brain. Trends Neurosci. *17*, 517–525.

Moehlmann, T., Winkler, E., Xia, X., Edbauer, D., Murrell, J., Capell, A., Kaether, C., Zheng, H., Ghetti, B., Haass, C., et al. (2002). Presenilin-1 mutations of leucine 166 equally affect the generation of the Notch and APP intracellular domains independent of their effect on Aβ42 production. Proc. Natl. Acad. Sci. U. S. A. *99*, 8025–8030.

Möhler, H., Fritschy, J.M., Crestani, F., Hensch, T., and Rudolph, U. (2004). Specific GABAA

circuits in brain development and therapy. Biochem. Pharmacol. *68*, 1685–1690.

Mondragón-Rodríguez, S., Trillaud-Doppia, E., Dudilot, A., Bourgeois, C., Lauzon, M., Leclerc, N., and Boehm, J. (2012). Interaction of endogenous tau protein with synaptic proteins is regulated by N-methyl-D-aspartate receptor-dependent tau phosphorylation. J. Biol. Chem. *287*, 32040–32053.

Morales, R., Duran-Aniotz, C., Castilla, J., Estrada, L.D., and Soto, C. (2011). De novo induction of amyloid-β deposition in vivo. Mol. Psychiatry 2012 1712 *17*, 1347–1353.

Morgan, D., Diamond, D.M., Gottschall, P.E., Ugen, K.E., Dickey, C., Hardy, J., Duff, K., Jantzen, P., DiCarlo, G., Wilcock, D., et al. (2000). Aβ peptide vaccination prevents memory loss in an animal model of Alzheimer's disease. Nat. 2000 4086815 *408*, 982–985.

Morris, J.C., and Price, J.L. (2001). Pathologic correlates of nondemented aging, mild cognitive impairment, and early-stage Alzheimer's disease. J. Mol. Neurosci. *17*, 101–118.

Morris, M., Maeda, S., Vossel, K., and Mucke, L. (2011). The Many Faces of Tau. Neuron *70*, 410–426.

Morris, M., Knudsen, G.M., Maeda, S., Trinidad, J.C., Ioanoviciu, A., Burlingame, A.L., and Mucke, L. (2015). Tau post-translational modifications in wild-type and human amyloid precursor protein transgenic mice. Nat. Neurosci. 2015 188 *18*, 1183–1189.

Morrison, J.H., and Baxter, M.G. (2012). The ageing cortical synapse: hallmarks and implications for cognitive decline. Nat. Rev. Neurosci. *13*, 240–250.

Morrison, J.H., and Hof, P.R. (1997). Life and death of neurons in the aging brain. Science (80-.). *278*, 412–419.

Morrison, J.H., and Hof, P.R. (2007). Life and Death of Neurons in The Aging Cerebral Cortex. Int. Rev. Neurobiol. *81*, 41–57.

Mortensen, M., Patel, B., and Smart, T.G. (2012). GABA potency at GABA A receptors found in synaptic and extrasynaptic zones. Front. Cell. Neurosci. *0*, 1.

Mower, G.D., and Guo, Y. (2001). Comparison of the expression of two forms of glutamic acid decarboxylase (GAD67 and GAD65) in the visual cortex of normal and dark-reared

cats. Dev. Brain Res. *126*, 65–74.

Murray, J.D., Anticevic, A., Gancsos, M., Ichinose, M., Corlett, P.R., Krystal, J.H., and Wang, X.J. (2014). Linking Microcircuit Dysfunction to Cognitive Impairment: Effects of Disinhibition Associated with Schizophrenia in a Cortical Working Memory Model. Cereb. Cortex *24*, 859–872.

Nguyen, L.H., Xu, Y., Mahadeo, T., Zhang, L., Lin, T. V., Born, H.A., Anderson, A.E., and Bordey, A. (2022). Expression of 4E-BP1 in juvenile mice alleviates mTOR-induced neuronal dysfunction and epilepsy. Brain *145*, 1310–1325.

Nicholson, D.A., Yoshida, R., Berry, R.W., Gallagher, M., and Geinisman, Y. (2004). Reduction in Size of Perforated Postsynaptic Densities in Hippocampal Axospinous Synapses and Age-Related Spatial Learning Impairments. J. Neurosci. *24*, 7648–7653.

Nicolll, J.A.R., Wilkinson, D., Holmes, C., Steart, P., Markham, H., and Weller, R.O. (2003). Neuropathology of human Alzheimer disease after immunization with amyloid-β peptide: a case report. Nat. Med. 2003 94 *9*, 448–452.

Nikolaev, A., McLaughlin, T., O'Leary, D.D.M., and Tessier-Lavigne, M. (2009). APP binds DR6 to trigger axon pruning and neuron death via distinct caspases. Nat. 2009 4577232 *457*, 981–989.

Nisbet, R.M., Van Der Jeugd, A., Leinenga, G., Evans, H.T., Janowicz, P.W., and Götz, J. (2017). Combined effects of scanning ultrasound and a tau-specific single chain antibody in a tau transgenic mouse model. Brain *140*, 1220–1230.

Nishimura, I., Yang, Y., and Lu, B. (2004). PAR-1 kinase plays an initiator role in a temporally ordered phosphorylation process that confers tau toxicity in Drosophila. Cell *116*, 671–682.

Nowak, L., Bregestovski, P., Ascher, P., Herbet, A., and Prochiantz, A. (1984). Magnesium gates glutamate-activated channels in mouse central neurones. Nat. 1984 3075950 *307*, 462–465.

O'Leary, T.P., Robertson, A., Chipman, P.H., Rafuse, V.F., and Brown, R.E. (2018). Motor function deficits in the 12 month-old female 5xFAD mouse model of Alzheimer's disease. Behav. Brain Res. *337*, 256–263.

Oakley, H., Cole, S.L., Logan, S., Maus, E., Shao, P., Craft, J., Guillozet-Bongaarts, A., Ohno, M., Disterhoft, J., Van Eldik, L., et al. (2006). Intraneuronal beta-amyloid aggregates, neurodegeneration, and neuron loss in transgenic mice with five familial Alzheimer's disease mutations: potential factors in amyloid plaque formation. J. Neurosci. *26*, 10129–10140.

Oblak, A.L., Lin, P.B., Kotredes, K.P., Pandey, R.S., Garceau, D., Williams, H.M., Uyar, A., O'Rourke, R., O'Rourke, S., Ingraham, C., et al. (2021). Comprehensive Evaluation of the 5XFAD Mouse Model for Preclinical Testing Applications: A MODEL-AD Study. Front. Aging Neurosci. *13*, 431.

Olsen, R.W., and Sieghart, W. (2009). GABAA receptors: Subtypes provide diversity of function and pharmacology. Neuropharmacology *56*, 141–148.

Oser, N., Hubacher, M., Specht, K., Datta, A.N., Weber, P., and Penner, I.K. (2014). Default mode network alterations during language task performance in children with benign epilepsy with centrotemporal spikes (BECTS). Epilepsy Behav. *33*, 12–17.

Ostroumov, A., Thomas, A.M., Kimmey, B.A., Karsch, J.S., Doyon, W.M., and Dani, J.A. (2016). Stress Increases Ethanol Self-Administration via a Shift toward Excitatory GABA Signaling in the Ventral Tegmental Area. Neuron *92*, 493–504.

Ostroumov, A., Wittenberg, R.E., Kimmey, B.A., Taormina, M.B., Holden, W.M., McHugh, A.T., and Dani, J.A. (2020). Acute Nicotine Exposure Alters Ventral Tegmental Area Inhibitory Transmission and Promotes Diazepam Consumption. ENeuro *7*.

Palmqvist, S., Schöll, M., Strandberg, O., Mattsson, N., Stomrud, E., Zetterberg, H., Blennow, K., Landau, S., Jagust, W., and Hansson, O. (2017). Earliest accumulation of β-amyloid occurs within the default-mode network and concurrently affects brain connectivity. Nat. Commun. 2017 81 *8*, 1–13.

Palop, J.J., and Mucke, L. (2009). Epilepsy and Cognitive Impairments in Alzheimer Disease. Arch. Neurol. *66*, 435–440.

Palop, J.J., and Mucke, L. (2010a). Amyloid-beta-induced neuronal dysfunction in Alzheimer's disease: from synapses toward neural networks. Nat. Neurosci. *13*, 812–818.

Palop, J.J., and Mucke, L. (2010b). Synaptic depression and aberrant excitatory network

activity in Alzheimer's disease: two faces of the same coin? Neuromolecular Med. *12*, 48–55.

Palop, J.J., and Mucke, L. (2016). Network abnormalities and interneuron dysfunction in Alzheimer disease. Nat. Rev. Neurosci. *17*, 777–792.

Palop, J.J., Chin, J., Roberson, E.D., Wang, J., Thwin, M.T., Bien-Ly, N., Yoo, J., Ho, K.O., Yu, G.-Q., Kreitzer, A., et al. (2007). Aberrant excitatory neuronal activity and compensatory remodeling of inhibitory hippocampal circuits in mouse models of Alzheimer's disease. Neuron *55*, 697–711.

Palva, J.M., Palva, S., and Kaila, K. (2005). Phase Synchrony among Neuronal Oscillations in the Human Cortex. J. Neurosci. *25*, 3962–3972.

Pang, K., Jiang, R., Zhang, W., Yang, Z., Li, L.L., Shimozawa, M., Tambaro, S., Mayer, J., Zhang, B., Li, M., et al. (2021). An App knock-in rat model for Alzheimer's disease exhibiting Aβ and tau pathologies, neuronal death and cognitive impairments. Cell Res. 2021 322 *32*, 157–175.

Paoletti, P., Bellone, C., and Zhou, Q. (2013). NMDA receptor subunit diversity: impact on receptor properties, synaptic plasticity and disease. Nat. Rev. Neurosci. 2013 146 *14*, 383–400.

Papanikolopoulou, K., and Skoulakis, E.M.C. (2014). Temporally distinct phosphorylations differentiate Tau-dependent learning deficits and premature mortality in Drosophila. Hum. Mol. Genet. 1–13.

Park, D.C., Lautenschlager, G., Smith, A.D., Earles, J.L., Frieske, D., Zwahr, M., and Gaines, C.L. (1996). Mediators of long-term memory performance across the life span. Psychol. Aging *11*, 621–637.

Payne, J.A. (1997). Functional characterization of the neuronal-specific K-Cl cotransporter: Implications for [K+](o) regulation. Am. J. Physiol. - Cell Physiol. *273*.

Payne, J.A., Stevenson, T.J., and Donaldson, L.F. (1996). Molecular characterization of a putative K-Cl cotransporter in rat brain. A neuronal-specific isoform. J. Biol. Chem. *271*, 16245–16252.

Payne, J.A., Rivera, C., Voipio, J., and Kaila, K. (2003). Cation–chloride co-transporters in neuronal communication, development and trauma. Trends Neurosci. *26*, 199–206.

Peacock, M.L., Warren, J.T., Roses, A.D., and Fink, J.K. (1993). Novel polymorphism in the A4 region of the amyloid precursor protein gene in a patient without Alzheimer's disease. Neurology *43*, 1254–1254.

Pedersen, J.T., and Sigurdsson, E.M. (2015). Tau immunotherapy for Alzheimer's disease. Trends Mol. Med. *21*, 394–402.

Perrin, R.J., Fagan, A.M., and Holtzman, D.M. (2009). Multimodal techniques for diagnosis and prognosis of Alzheimer's disease. Nature *461*, 916–922.

Persson, J., Lind, J., Larsson, A., Ingvar, M., Sleegers, K., Van Broeckhoven, C., Adolfsson, R., Nilsson, L.G., and Nyberg, L. (2008). Altered deactivation in individuals with genetic risk for Alzheimer's disease. Neuropsychologia *46*, 1679–1687.

Pfeffer, C.K., Xue, M., He, M., Huang, Z.J., and Scanziani, M. (2013). Inhibition of inhibition in visual cortex: the logic of connections between molecularly distinct interneurons. Nat. Neurosci. 2013 168 *16*, 1068–1076.

Piala, A.T., Moon, T.M., Akella, R., He, H., Cobb, M.H., and Goldsmith, E.J. (2014). Chloride sensing by WNK1 involves inhibition of autophosphorylation. Sci. Signal. *7*.

Pin, J.P., and Bettler, B. (2016). Organization and functions of mGlu and GABAB receptor complexes. Nat. 2016 5407631 *540*, 60–68.

Pinard, A., Seddik, R., and Bettler, B. (2010). GABAB Receptors: Physiological Functions and Mechanisms of Diversity. Adv. Pharmacol. *58*, 231–255.

Poulopoulos, A., Aramuni, G., Meyer, G., Soykan, T., Hoon, M., Papadopoulos, T., Zhang, M., Paarmann, I., Fuchs, C., Harvey, K., et al. (2009). Neuroligin 2 Drives Postsynaptic Assembly at Perisomatic Inhibitory Synapses through Gephyrin and Collybistin. Neuron *63*, 628–642.

Price, G.D., and Trussell, L.O. (2006). Estimate of the chloride concentration in a central glutamatergic terminal: a gramicidin perforated-patch study on the calyx of Held. J. Neurosci. *26*, 11432–11436.

Priller, C., Bauer, T., Mitteregger, G., Krebs, B., Kretzschmar, H.A., and Herms, J. (2006). Synapse formation and function is modulated by the amyloid precursor protein. J. Neurosci. *26*, 7212–7221.

Puskarjov, M., Ahmad, F., Kaila, K., and Blaesse, P. (2012). Activity-dependent cleavage of the K-Cl cotransporter KCC2 mediated by calcium-activated protease calpain. J. Neurosci. *32*, 11356–11364.

Putcha, D., Brickhouse, M., O'Keefe, K., Sullivan, C., Rentz, D., Marshall, G., Dickerson, B., and Sperling, R. (2011). Hippocampal Hyperactivation Associated with Cortical Thinning in Alzheimer's Disease Signature Regions in Non-Demented Elderly Adults. J. Neurosci. *31*, 17680–17688.

Puzzo, D., Privitera, L., Leznik, E., Fà, M., Staniszewski, A., Palmeri, A., and Arancio, O. (2008). Picomolar Amyloid-β Positively Modulates Synaptic Plasticity and Memory in Hippocampus. J. Neurosci. *28*, 14537–14545.

Pyapali, G.K., and Turner, D.A. (1996). Increased dendritic extent in hippocampal CA1 neurons from aged F344 rats. Neurobiol. Aging *17*, 601–611.

Quiroz, Y.T., Budson, A.E., Celone, K., Ruiz, A., Newmark, R., Castrillón, G., Lopera, F., and Stern, C.E. (2010). Hippocampal hyperactivation in presymptomatic familial Alzheimer's disease. Ann. Neurol. *68*, 865–875.

Raichle, M.E., MacLeod, A.M., Snyder, A.Z., Powers, W.J., Gusnard, D.A., and Shulman, G.L. (2001). A default mode of brain function. Proc. Natl. Acad. Sci. U. S. A. *98*, 676–682.

Rajah, M.N., and D'Esposito, M. (2005). Region-specific changes in prefrontal function with age: a review of PET and fMRI studies on working and episodic memory. Brain *128*, 1964–1983.

Rajan, K.B., Weuve, J., Barnes, L.L., McAninch, E.A., Wilson, R.S., and Evans, D.A. (2021). Population estimate of people with clinical Alzheimer's disease and mild cognitive impairment in the United States (2020–2060). Alzheimer's Dement. *17*, 1966–1975.

Rapp, P.R., and Amaral, D.G. (1989). Evidence for task-dependent memory dysfunction in the aged monkey. J. Neurosci. *9*, 3568–3576.

Raz, N., Rodrigue, K.M., Kennedy, K.M., Head, D., Gunning-Dixon, F., and Acker, J.D. (2003). Differential Aging of the Human Striatum: Longitudinal Evidence. Am. J. Neuroradiol. *24*.

Raz, N., Gunning-Dixon, F., Head, D., Rodrigue, K.M., Williamson, A., and Acker, J.D. (2004). Aging, sexual dimorphism, and hemispheric asymmetry of the cerebral cortex: replicability of regional differences in volume. Neurobiol. Aging *25*, 377–396.

Reed, L.A., Wszolek, Z.K., and Hutton, M. (2001). Phenotypic correlations in FTDP-17. Neurobiol. Aging *22*, 89–107.

Reish, N.J., Jamshidi, P., Stamm, B., Flanagan, M.E., Sugg, E., Tang, M., Donohue, K.L., McCord, M., Krumpelman, C., Mesulam, M.-M., et al. (2023). Multiple Cerebral Hemorrhages in a Patient Receiving Lecanemab and Treated with t-PA for Stroke. Https://Doi.Org/10.1056/NEJMc2215148.

Remondes, M., and Wilson, M.A. (2015). Slow-γ Rhythms Coordinate Cingulate Cortical Responses to Hippocampal Sharp-Wave Ripples during Wakefulness. Cell Rep. *13*, 1327–1335.

Resnick, S.M., Pham, D.L., Kraut, M.A., Zonderman, A.B., and Davatzikos, C. (2003). Longitudinal Magnetic Resonance Imaging Studies of Older Adults: A Shrinking Brain. J. Neurosci. *23*, 3295–3301.

Reuter-Lorenz, P.A., Jonides, J., Smith, E.E., Hartley, A., Miller, A., Marshuetz, C., and Koeppe, R.A. (2000). Age Differences in the Frontal Lateralization of Verbal and Spatial Working Memory Revealed by PET. J. Cogn. Neurosci. *12*, 174–187.

Rhein, V., Song, X., Wiesner, A., Ittner, L.M., Baysang, G., Meier, F., Ozmen, L., Bluethmann, H., Dröse, S., Brandt, U., et al. (2009). Amyloid-beta and tau synergistically impair the oxidative phosphorylation system in triple transgenic Alzheimer's disease mice. Proc. Natl. Acad. Sci. U. S. A. *106*, 20057–20062.

Rice, H.C., De Malmazet, D., Schreurs, A., Frere, S., Van Molle, I., Volkov, A.N., Creemers, E., Vertkin, I., Nys, J., Ranaivoson, F.M., et al. (2019). Secreted amyloid-b precursor protein functions as a GABA B R1a ligand to modulate synaptic transmission. Science (80-.). *363*.

Richard, B.C., Kurdakova, A., Baches, S., Bayer, T.A., Weggen, S., and Wirths, O. (2015). Gene Dosage Dependent Aggravation of the Neurological Phenotype in the 5XFAD Mouse Model of Alzheimer's Disease. J. Alzheimers. Dis. *45*, 1223–1236.

Richardson, B.D., Ling, L.L., Uteshev, V. V., and Caspary, D.M. (2013). Reduced GABAA Receptor-Mediated Tonic Inhibition in Aged Rat Auditory Thalamus. J. Neurosci. *33*, 1218–1227.

Rissman, R.A., and Mobley, W.C. (2011). Implications for treatment: GABAA receptors in aging, Down syndrome and Alzheimer's disease. J. Neurochem. *117*, 613–622.

Rissman, R.A., Mishizen-Eberz, A.J., Carter, T.L., Wolfe, B.B., De Blas, A.L., Miralles, C.P., Ikonomovic, M.D., and Armstrong, D.M. (2003). Biochemical analysis of GABAA receptor subunits α1, α5, β1, β2 in the hippocampus of patients with Alzheimer's disease neuropathology. Neuroscience *120*, 695–704.

Rissman, R.A., De Blas, A.L., and Armstrong, D.M. (2007). GABAA receptors in aging and Alzheimer's disease. J. Neurochem. *103*, 1285–1292.

Rivera, C., Voipio, J., Payne, J.A., Ruusuvuori, E., Lahtinen, H., Lamsa, K., Pirvola, U., Saarma, M., and Kaila, K. (1999). The K+/Cl- co-transporter KCC2 renders GABA hyperpolarizing during neuronal maturation. Nature *397*, 251–255.

Rivera, C., Li, H., Thomas-Crusells, J., Lahtinen, H., Viitanen, T., Nanobashvili, A., Kokaia, Z., Airaksinen, M.S., Voipio, J., Kaila, K., et al. (2002). BDNF-induced TrkB activation down-regulates the K+–Cl− cotransporter KCC2 and impairs neuronal Cl− extrusion. J. Cell Biol. *159*, 747–752.

Rivera, C., Voipio, J., Thomas-Crusells, J., Li, H., Emri, Z., Sipilä, S., Payne, J.A., Minichiello, L., Saarma, M., and Kaila, K. (2004). Mechanism of Activity-Dependent Downregulation of the Neuron-Specific K-Cl Cotransporter KCC2. J. Neurosci. *24*, 4683–4691.

Roberson, E.D., Scearce-Levie, K., Palop, J.J., Yan, F., Cheng, I.H., Wu, T., Gerstein, H., Yu, G.Q., and Mucke, L. (2007). Reducing endogenous tau ameliorates amyloid β-induced deficits in an Alzheimer's disease mouse model. Science (80-.). *316*, 750–754.

Roberson, E.D., Halabisky, B., Yoo, J.W., Yao, J., Chin, J., Yan, F., Wu, T., Hamto, P., Devidze, N., Yu, G.-Q., et al. (2011). Amyloid-β/Fyn-induced synaptic, network, and cognitive impairments depend on tau levels in multiple mouse models of Alzheimer's disease. J. Neurosci. *31*, 700–711.

Romanelli, M.F., Ashkin, K., Morris, J.C., and Coben, L.A. (1990). Advanced Alzheimer's Disease Is a Risk Factor for Late-Onset Seizures. Arch. Neurol. *47*, 847–850.

Rose, M.R. (2009). Adaptation, aging, and genomic information. Aging (Albany. NY). *1*, 444–450.

Roselli, F., Tirard, M., Lu, J., Hutzler, P., Lamberti, P., Livrea, P., Morabito, M., and Almeida, O.F.X. (2005). Soluble β-Amyloid1-40 Induces NMDA-Dependent Degradation of Postsynaptic Density-95 at Glutamatergic Synapses. J. Neurosci. *25*, 11061–11070.

Rosen, A.C., Prull, M.W., O'Hara, R., Race, E.A., Desmond, J.E., Glover, G.H., Yesavage, J.A., and Gabrieli, J.D.E. (2002). Variable effects of aging on frontal lobe contributions to memory. Neuroreport *13*, 2425–2428.

Rosenzweig, E.S., and Barnes, C.A. (2003). Impact of aging on hippocampal function: plasticity, network dynamics, and cognition. Prog. Neurobiol. *69*, 143–179.

Rowley, N.M., Madsen, K.K., Schousboe, A., and Steve White, H. (2012). Glutamate and GABA synthesis, release, transport and metabolism as targets for seizure control. Neurochem. Int. *61*, 546–558.

Rozycka, A., and Liguz-Lecznar, M. (2017). The space where aging acts: focus on the GABAergic synapse. Aging Cell *16*, 634–643.

Rubenstein, J.L.R., and Merzenich, M.M. (2003). Model of autism: increased ratio of excitation/inhibition in key neural systems. Genes. Brain. Behav. *2*, 255–267.

Ruthazer, E.S., Béïque, J.C., and De Koninck, Y. (2022). Editorial: Shedding Light on the Nervous System: Progress in Neurophotonics Research. Front. Neural Circuits *16*, 49.

Saito, T., Matsuba, Y., Mihira, N., Takano, J., Nilsson, P., Itohara, S., Iwata, N., and Saido, T.C. (2014). Single App knock-in mouse models of Alzheimer's disease. Nat. Neurosci. *17*, 661–663.

Saito, T., Matsuba, Y., Yamazaki, N., Hashimoto, S., and Saido, T.C. (2016). Calpain Activation in Alzheimer's Model Mice Is an Artifact of APP and Presenilin Overexpression. J. Neurosci. *36*, 9933–9936.

Saito, T., Mihira, N., Matsuba, Y., Sasaguri, H., Hashimoto, S., Narasimhan, S., Zhang, B., Murayama, S., Higuchi, M., Lee, V.M.Y., et al. (2019). Humanization of the entire murine Mapt gene provides a murine model of pathological human tau propagation. J. Biol. Chem. *294*, 12754–12765.

Sallinen, R., Tornberg, J., Putkiranta, M., Horelli-Kuitunen, N., Airaksinen, M.S., and Wessman, M. (2001). Chromosomal localization of SLC12A5/Slc12a5, the human and mouse genes for the neuron-specific K+-Cl– cotransporter (KCC2) defines a new region of conserved homology. Cytogenet. Genome Res. *94*, 67–70.

Salloway, S., Sperling, R., Fox, N.C., Blennow, K., Klunk, W., Raskind, M., Sabbagh, M., Honig, L.S., Porsteinsson, A.P., Ferris, S., et al. (2014). Two Phase 3 Trials of Bapineuzumab in Mild-to-Moderate Alzheimer's Disease. N. Engl. J. Med. *370*, 322–333.

Salter, M.W., and Kalia, L. V. (2004). Src kinases: a hub for NMDA receptor regulation. Nat. Rev. Neurosci. 2004 54 *5*, 317–328.

Sattler, R., and Tymianski, M. (2001). Molecular mechanisms of glutamate receptor-mediated excitotoxic neuronal cell death. Mol. Neurobiol. 2001 241 *24*, 107–129.

Schacter, D.L., Kaszniak, A.W., Kihlstrom, J.F., and Valdiserri, M. (1991). The relation between source memory and aging. Psychol. Aging *6*, 559–568.

Schaie, K.W. (1996). Intellectual Development in Adulthood: The Seattle Longitudinal Study - K. Warner Schaie, Professor of Psychology K Warner Schaie, PhD PhD - Google Books.

Scheff, S.W., Price, D.A., Schmitt, F.A., Dekosky, S.T., and Mufson, E.J. (2007). Synaptic alterations in CA1 in mild Alzheimer disease and mild cognitive impairment. Neurology *68*, 1501–1508.

Scheibel, M.E., Lindsay, R.D., Tomiyasu, U., and Scheibel, A.B. (1975). Progressive dendritic changes in aging human cortex. Exp. Neurol. *47*, 392–403.

Scheibel, M.E., Lindsay, R.D., Tomiyasu, U., and Scheibel, A.B. (1976). Progressive

dendritic changes in the aging human limbic system. Exp. Neurol. *53*, 420–430.

Schenk, D., Barbour, R., Dunn, W., Gordon, G., Grajeda, H., Guldo, T., Hu, K., Huang, J., Johnson-Wood, K., Khan, K., et al. (1999). Immunization with amyloid-β attenuates Alzheimer-disease-like pathology in the PDAPP mouse. Nat. 1999 4006740 *400*, 173–177.

Schwenk, J., Pérez-Garci, E., Schneider, A., Kollewe, A., Gauthier-Kemper, A., Fritzius, T., Raveh, A., Dinamarca, M.C., Hanuschkin, A., Bildl, W., et al. (2015). Modular composition and dynamics of native GABAB receptors identified by high-resolution proteomics. Nat. Neurosci. 2015 192 *19*, 233–242.

Scimemi, A., Semyanov, A., Sperk, G., Kullmann, D.M., and Walker, M.C. (2005). Multiple and plastic receptors mediate tonic GABAA receptor currents in the hippocampus. J. Neurosci. *25*, 10016–10024.

Segovia, G., Porras, A., Del Arco, A., and Mora, F. (2001a). Glutamatergic neurotransmission in aging: a critical perspective. Mech. Ageing Dev. *122*, 1–29.

Segovia, G., Del Arco, A., Prieto, L., and Mora, F. (2001b). Glutamate-glutamine cycle and aging in striatum of the awake rat: effects of a glutamate transporter blocker. Neurochem. Res. *26*, 37–41.

Seidman, L.J., Rosso, I.M., Thermenos, H.W., Makris, N., Juelich, R., Gabrieli, J.D.E., Faraone, S. V., Tsuang, M.T., and Whitfield-Gabrieli, S. (2014). Medial temporal lobe default mode functioning and hippocampal structure as vulnerability indicators for schizophrenia: A MRI study of non-psychotic adolescent first-degree relatives. Schizophr. Res. *159*, 426–434.

Selimbeyoglu, A., Kim, C.K., Inoue, M., Lee, S.Y., Hong, A.S.O., Kauvar, I., Ramakrishnan, C., Fenno, L.E., Davidson, T.J., Wright, M., et al. (2017). Modulation of prefrontal cortex excitation/inhibition balance rescues social behavior in CNTNAP2-deficient mice. Sci. Transl. Med. *9*, eaah6733.

Selkoe, D.J. (2001). Alzheimer's disease: genes, proteins, and therapy. Physiol. Rev. *81*, 741–766.

Selkoe, D.J. (2008). Soluble oligomers of the amyloid β-protein impair synaptic plasticity and behavior. Behav. Brain Res. *192*, 106–113.

Serrano-Pozo, A., Frosch, M.P., Masliah, E., and Hyman, B.T. (2011). Neuropathological alterations in Alzheimer disease. Cold Spring Harb. Perspect. Med. *1*.

Sevigny, J., Chiao, P., Bussière, T., Weinreb, P.H., Williams, L., Maier, M., Dunstan, R., Salloway, S., Chen, T., Ling, Y., et al. (2016). The antibody aducanumab reduces Aβ plaques in Alzheimer's disease. Nature *537*, 50–56.

Shankar, G.M., Li, S., Mehta, T.H., Garcia-Munoz, A., Shepardson, N.E., Smith, I., Brett, F.M., Farrell, M.A., Rowan, M.J., Lemere, C.A., et al. (2008). Amyloid-beta protein dimers isolated directly from Alzheimer's brains impair synaptic plasticity and memory. Nat. Med. *14*, 837–842.

Shao, E., Chang, C.-W., Li, Z., Yu, X., Ho, K., Zhang, M., Wang, X., Simms, J., Lo, I., Speckart, J., et al. (2022). TAU ablation in excitatory neurons and postnatal TAU knockdown reduce epilepsy, SUDEP, and autism behaviors in a Dravet syndrome model. Sci. Transl. Med. *14*.

Shen, Q., Wu, X., Zhang, Z., Zhang, D., Yang, S., and Xing, D. (2022). Gamma frequency light flicker regulates amyloid precursor protein trafficking for reducing β-amyloid load in Alzheimer's disease model. Aging Cell *21*, e13573.

Sherzai, D., Losey, T., Vega, S., and Sherzai, A. (2014). Seizures and dementia in the elderly: Nationwide Inpatient Sample 1999–2008. Epilepsy Behav. *36*, 53–56.

Shi, L., Argenta, A.E., Winseck, A.K., and Brunso-Bechtold, J.K. (2004). Stereological quantification of GAD-67–immunoreactive neurons and boutons in the hippocampus of middle-aged and old Fischer 344 × Brown Norway rats. J. Comp. Neurol. *478*, 282–291.

Sigurdsson, E.M., and Sigurdsson, M. (2016). Tau Immunotherapy. Neurodegener. Dis. *16*, 34–38.

Sil, A., Erfani, A., Lamb, N., Copland, R., Riedel, G., and Platt, B. (2022). Sex Differences in Behavior and Molecular Pathology in the 5XFAD Model. J. Alzheimer's Dis. *85*, 755–778.

Silayeva, L., Deeb, T.Z., Hines, R.M., Kelley, M.R., Munoz, M.B., Lee, H.H.C., Brandon, N.J., Dunlop, J., Maguire, J., Davies, P.A., et al. (2015). KCC2 activity is critical in limiting the onset and severity of status epilepticus. Proc. Natl. Acad. Sci. U. S. A. *112*, 3523–3528.

Simard, A.R., Soulet, D., Gowing, G., Julien, J.P., and Rivest, S. (2006). Bone Marrow-Derived Microglia Play a Critical Role in Restricting Senile Plaque Formation in Alzheimer's Disease. Neuron *49*, 489–502.

Simon, N.W., LaSarge, C.L., Montgomery, K.S., Williams, M.T., Mendez, I.A., Setlow, B., and Bizon, J.L. (2010). Good things come to those who wait: Attenuated discounting of delayed rewards in aged Fischer 344 rats. Neurobiol. Aging *31*, 853–862.

Simonnet, C., Sinha, M., Goutierre, M., Moutkine, I., Daumas, S., and Poncer, J.C. (2022). Silencing KCC2 in mouse dorsal hippocampus compromises spatial and contextual memory. BioRxiv 2022.02.18.481031.

Sivakumaran, S., Cardarelli, R.A., Maguire, J., Kelley, M.R., Silayeva, L., Morrow, D.H., Mukherjee, J., Moore, Y.E., Mather, R.J., Duggan, M.E., et al. (2015). Selective Inhibition of KCC2 Leads to Hyperexcitability and Epileptiform Discharges in Hippocampal Slices and In Vivo. J. Neurosci. *35*, 8291–8296.

Siwek, M.E., Müller, R., Henseler, C., Trog, A., Lundt, A., Wormuth, C., Broich, K., Ehninger, D., Weiergräber, M., and Papazoglou, A. (2015). Altered theta oscillations and aberrant cortical excitatory activity in the 5XFAD model of Alzheimer's disease. Neural Plast. *2015*.

Small, S.A., Schobel, S.A., Buxton, R.B., Witter, M.P., and Barnes, C.A. (2011). A pathophysiological framework of hippocampal dysfunction in ageing and disease. Nat. Rev. Neurosci. 2011 1210 *12*, 585–601.

Smith, K.R., and Kittler, J.T. (2010). The cell biology of synaptic inhibition in health and disease. Curr. Opin. Neurobiol. *20*, 550–556.

Snyder, E.M., Nong, Y., Almeida, C.G., Paul, S., Moran, T., Choi, E.Y., Nairn, A.C., Salter, M.W., Lombroso, P.J., Gouras, G.K., et al. (2005). Regulation of NMDA receptor trafficking by amyloid-β. Nat. Neurosci. 2005 88 *8*, 1051–1058.

Soba, P., Eggert, S., Wagner, K., Zentgraf, H., Siehl, K., Kreger, S., Löwer, A., Langer, A., Merdes, G., Paro, R., et al. (2005). Homo- and heterodimerization of APP family members promotes intercellular adhesion. EMBO J. *24*, 3624–3634.

Sohal, V.S., Zhang, F., Yizhar, O., and Deisseroth, K. (2009). Parvalbumin neurons and

gamma rhythms enhance cortical circuit performance. Nat. 2009 4597247 *459*, 698–702.

Somogyi, P., and Klausberger, T. (2005). Defined types of cortical interneurone structure space and spike timing in the hippocampus. J. Physiol. *562*, 9–26.

Sorrentino, V., Romani, M., Mouchiroud, L., Beck, J.S., Zhang, H., D'Amico, D., Moullan, N., Potenza, F., Schmid, A.W., Rietsch, S., et al. (2017). Enhancing mitochondrial proteostasis reduces amyloid-β proteotoxicity. Nat. 2017 5527684 *552*, 187–193.

Specchio, N., Di Micco, V., Trivisano, M., Ferretti, A., and Curatolo, P. (2022). The epilepsy-autism spectrum disorder phenotype in the era of molecular genetics and precision therapy. Epilepsia *63*, 6–21.

Sperling, R., Mormino, E., and Johnson, K. (2014). The Evolution of Preclinical Alzheimer's Disease: Implications for Prevention Trials. Neuron *84*, 608–622.

Sperling, R.A., Laviolette, P.S., O'Keefe, K., O'Brien, J., Rentz, D.M., Pihlajamaki, M., Marshall, G., Hyman, B.T., Selkoe, D.J., Hedden, T., et al. (2009). Amyloid deposition is associated with impaired default network function in older persons without dementia. Neuron *63*, 178–188.

Sperling, R.A., Dickerson, B.C., Pihlajamaki, M., Vannini, P., LaViolette, P.S., Vitolo, O. V., Hedden, T., Becker, J.A., Rentz, D.M., Selkoe, D.J., et al. (2010). Functional Alterations in Memory Networks in Early Alzheimer's Disease. NeuroMolecular Med. *12*, 27–43.

Spillantini, M.G., Murrell, J.R., Goedert, M., Farlow, M.R., Klug, A., and Ghetti, B. (1998). Mutation in the tau gene in familial multiple system tauopathy with presenile dementia. Proc. Natl. Acad. Sci. U. S. A. *95*, 7737–7741.

Spruston, N. (2008). Pyramidal neurons: dendritic structure and synaptic integration. Nat. Rev. Neurosci. 2008 93 *9*, 206–221.

Staley, K. (1994). The role of an inwardly rectifying chloride conductance in postsynaptic inhibition. Https://Doi.Org/10.1152/Jn.1994.72.1.273 *72*, 273–284.

Stambolic, V., Ruel, L., and Woodgett, J.R. (1996). Lithium inhibits glycogen synthase kinase-3 activity and mimics Wingless signalling in intact cells. Curr. Biol. *6*, 1664–1669.

Steinbach, J.P., Müller, U., Leist, M., Li, Z.W., Nicotera, P., and Aguzzi, A. (1998). Hypersensitivity to seizures in β-amyloid precursor protein deficient mice. Cell Death Differ. 1998 510 *5*, 858–866.

Stéphan, A., Laroche, S., and Davis, S. (2001). Generation of Aggregated β-Amyloid in the Rat Hippocampus Impairs Synaptic Transmission and Plasticity and Causes Memory Deficits. J. Neurosci. *21*, 5703–5714.

Strittmatter, W.J., Saunders, A.M., Schmechel, D., Pericak-Vance, M., Enghild, J., Salvesen, G.S., and Roses, A.D. (1993). Apolipoprotein E: high-avidity binding to beta-amyloid and increased frequency of type 4 allele in late-onset familial Alzheimer disease. Proc. Natl. Acad. Sci. U. S. A. *90*, 1977–1981.

De Strooper, B., and Karran, E. (2016). The Cellular Phase of Alzheimer's Disease. Cell *164*, 603–615.

De Strooper, B., Iwatsubo, T., and Wolfe, M.S. (2012). Presenilins and γ-Secretase: Structure, Function, and Role in Alzheimer Disease. Cold Spring Harb. Perspect. Med. *2*, a006304.

Sturchler-Pierrat, C., Abramowski, D., Duke, M., Wiederhold, K.H., Mistl, C., Rothacher, S., Ledermann, B., Bürki, K., Frey, P., Paganetti, P.A., et al. (1997). Two amyloid precursor protein transgenic mouse models with Alzheimer disease-like pathology. Proc. Natl. Acad. Sci. U. S. A. *94*, 13287–13292.

Sullivan, B.J., Kipnis, P.A., Carter, B.M., Shao, L.R., and Kadam, S.D. (2021). Targeting ischemia-induced KCC2 hypofunction rescues refractory neonatal seizures and mitigates epileptogenesis in a mouse model. Sci. Signal. *14*.

Summers, W.K., Majovski, L. V, Marsh, G.M., Tachiki, K., and Kling, A. (1986). Oral tetrahydroaminoacridine in long-term treatment of senile dementia, Alzheimer type. N. Engl. J. Med. *315*, 1241–1245.

Szklarczyk, D., Gable, A.L., Nastou, K.C., Lyon, D., Kirsch, R., Pyysalo, S., Doncheva, N.T., Legeay, M., Fang, T., Bork, P., et al. (2021). The STRING database in 2021: customizable protein-protein networks, and functional characterization of user-uploaded gene/measurement sets. Nucleic Acids Res. *49*, D605–D612.

Tackenberg, C., and Brandt, R. (2009). Divergent Pathways Mediate Spine Alterations and Cell Death Induced by Amyloid-β, Wild-Type Tau, and R406W Tau. J. Neurosci. *29*, 14439–14450.

Talbot, C., Lendon, C., Craddock, N., Shears, S., Morris, J.C., and Goate, A. (1994). Protection against Alzheimer's disease with apoE ∈2. Lancet *343*, 1432–1433.

Tampellini, D., Capetillo-Zarate, E., Dumont, M., Huang, Z., Yu, F., Lin, M.T., and Gouras, G.K. (2010). Effects of Synaptic Modulation on β-Amyloid, Synaptophysin, and Memory Performance in Alzheimer's Disease Transgenic Mice. J. Neurosci. *30*, 14299–14304.

Tan, J., and Evin, G. (2012). β-Site APP-cleaving enzyme 1 trafficking and Alzheimer's disease pathogenesis. J. Neurochem. *120*, 869–880.

Taubes, A., Nova, P., Zalocusky, K.A., Kosti, I., Bicak, M., Zilberter, M.Y., Hao, Y., Yoon, S.Y., Oskotsky, T., Pineda, S., et al. (2021). Experimental and real-world evidence supporting the computational repurposing of bumetanide for APOE4-related Alzheimer's disease. Nat. Aging 2021 110 *1*, 932–947.

Thal, D.R., Rüb, U., Orantes, M., and Braak, H. (2002). Phases of Aβ-deposition in the human brain and its relevance for the development of AD. Neurology *58*, 1791–1800.

Tornberg, J., Voikar, V., Savilahti, H., Rauvala, H., and Airaksinen, M.S. (2005). Behavioural phenotypes of hypomorphic KCC2-deficient mice. Eur. J. Neurosci. *21*, 1327–1337.

Tran, T., Gallagher, M., and Kirkwood, A. (2018). Enhanced postsynaptic inhibitory strength in hippocampal principal cells in high-performing aged rats. Neurobiol. Aging *70*, 92–101.

Tremblay, R., Lee, S., and Rudy, B. (2016). GABAergic Interneurons in the Neocortex: From Cellular Properties to Circuits. Neuron *91*, 260–292.

Turner, D.A., and Deupree, D.L. (1991). Functional elongation of CA1 hippocampal neurons with aging in Fischer 344 rats. Neurobiol. Aging *12*, 201–210.

Turrigiano, G.G., and Nelson, S.B. (2004). Homeostatic plasticity in the developing nervous system. Nat. Rev. Neurosci. 2004 52 *5*, 97–107.

Tyagarajan, S.K., and Fritschy, J.M. (2014). Gephyrin: a master regulator of neuronal

function? Nat. Rev. Neurosci. 2014 153 *15*, 141–156.

Tyanova, S., Temu, T., Sinitcyn, P., Carlson, A., Hein, M.Y., Geiger, T., Mann, M., and Cox, J. (2016). The Perseus computational platform for comprehensive analysis of (prote)omics data. Nat. Methods *13*, 731–740.

Uvarov, P., Ludwig, A., Markkanen, M., Pruunsild, P., Kaila, K., Delpire, E., Timmusk, T., Rivera, C., and Airaksinen, M.S. (2007). A novel N-terminal isoform of the neuron-specific K-Cl cotransporter KCC2. J. Biol. Chem. *282*, 30570–30576.

Uvarov, P., Ludwig, A., Markkanen, M., Soni, S., Hübner, C.A., Rivera, C., and Airaksinen, M.S. (2009). Coexpression and heteromerization of two neuronal K-Cl cotransporter isoforms in neonatal brain. J. Biol. Chem. *284*, 13696–13704.

Uylings, H.B.M., Groenewegen, H.J., and Kolb, B. (2003). Do rats have a prefrontal cortex? Behav. Brain Res. *146*, 3–17.

Vandenberg, R.J., and Ryan, R.M. (2013). Mechanisms of glutamate transport. Physiol. Rev. *93*, 1621–1657.

Varoqueaux, F., Jamain, S., and Brose, N. (2004). Neuroligin 2 is exclusively localized to inhibitory synapses. Eur. J. Cell Biol. *83*, 449–456.

Vattikuti, S., and Chow, C.C. (2010). A Computational Model for Cerebral Cortical Dysfunction in Autism Spectrum Disorders. Biol. Psychiatry *67*, 672–678.

Verret, L., Mann, E.O., Hang, G.B., Barth, A.M.I., Cobos, I., Ho, K., Devidze, N., Masliah, E., Kreitzer, A.C., Mody, I., et al. (2012). Inhibitory interneuron deficit links altered network activity and cognitive dysfunction in alzheimer model. Cell *149*, 708–721.

Villemagne, V.L., Pike, K.E., Chételat, G., Ellis, K.A., Mulligan, R.S., Bourgeat, P., Ackermann, U., Jones, G., Szoeke, C., Salvado, O., et al. (2011). Longitudinal assessment of Aβ and cognition in aging and Alzheimer disease. Ann. Neurol. *69*, 181–192.

Villette, V., Poindessous-Jazat, F., Simon, A., Léna, C., Roullot, E., Bellessort, B., Epelbaum, J., Dutar, P., and Stéphan, A. (2010). Decreased Rhythmic GABAergic Septal Activity and Memory-Associated θ Oscillations after Hippocampal Amyloid-β Pathology in the Rat. J. Neurosci. *30*, 10991–11003.

Volkow, N.D., Wang, G.J., Fowler, J.S., Logan, J., Gatley, S.J., MacGregor, R.R., Schlyer, D.J., Hitzemann, R., and Wolf, A.P. (1996). Measuring age-related changes in dopamine D2 receptors with 11C-raclopride and 18F-N-methylspiroperidol. Psychiatry Res. Neuroimaging *67*, 11–16.

Volkow, N.D., Wang, G.J., Fowler, J.S., Ding, Y.S., Gur, R.C., Gatley, J., Logan, J., Moberg, P.J., Hitzemann, R., Smith, G., et al. (1998). Parallel loss of presynaptic and postsynaptic dopamine markers in normal aging. Ann. Neurol. *44*, 143–147.

Vossel, K.A., Beagle, A.J., Rabinovici, G.D., Shu, H., Lee, S.E., Naasan, G., Hegde, M., Cornes, S.B., Henry, M.L., Nelson, A.B., et al. (2013). Seizures and Epileptiform Activity in the Early Stages of Alzheimer Disease. JAMA Neurol. *70*, 1158–1166.

Vossel, K.A., Ranasinghe, K.G., Beagle, A.J., Mizuiri, D., Honma, S.M., Dowling, A.F., Darwish, S.M., Van Berlo, V., Barnes, D.E., Mantle, M., et al. (2016). Incidence and impact of subclinical epileptiform activity in Alzheimer's disease. Ann. Neurol. *80*, 858–870.

Vossel, K.A., Tartaglia, M.C., Nygaard, H.B., Zeman, A.Z., and Miller, B.L. (2017). Epileptic activity in Alzheimer's disease: causes and clinical relevance. Lancet Neurol. *16*, 311–322.

Van Vreeswijk, C., and Sompolinsky, H. (1996). Chaos in neuronal networks with balanced excitatory and inhibitory activity. Science *274*, 1724–1726.

Wallace, D.R., and Dawson, R. (1990). Effect of age and monosodium-L-glutamate (MSG) treatment on neurotransmitter content in brain regions from male Fischer-344 rats. Neurochem. Res. *15*, 889–898.

Wallace, D.R., and Dawson, R. (1992). Ammonia regulation of phosphate-activated glutaminase displays regional variation and impairment in the brain of aged rats. Neurochem. Res. *17*, 1113–1122.

Walsh, D.M., Klyubin, I., Fadeeva, J. V., Cullen, W.K., Anwyl, R., Wolfe, M.S., Rowan, M.J., and Selkoe, D.J. (2002). Naturally secreted oligomers of amyloid beta protein potently inhibit hippocampal long-term potentiation in vivo. Nature *416*, 535–539.

Wang, J.Z., and Liu, F. (2008). Microtubule-associated protein tau in development, degeneration and protection of neurons. Prog. Neurobiol. *85*, 148–175.

Wang, Y., and Mandelkow, E. (2015). Tau in physiology and pathology. Nat. Rev. Neurosci. 2015 171 *17*, 22–35.

Wang, F., Bélanger, E., Côté, S.L., Desrosiers, P., Prescott, S.A., Côté, D.C., and De Koninck, Y. (2018). Sensory Afferents Use Different Coding Strategies for Heat and Cold. Cell Rep. *23*, 2001–2013.

Wang, M., Gamo, N.J., Yang, Y., Jin, L.E., Wang, X.J., Laubach, M., Mazer, J.A., Lee, D., and Arnsten, A.F.T. (2011). Neuronal basis of age-related working memory decline. Nat. 2011 4767359 *476*, 210–213.

Wang, Q., Walsh, D.M., Rowan, M.J., Selkoe, D.J., and Anwyl, R. (2004). Block of long-term potentiation by naturally secreted and synthetic amyloid beta-peptide in hippocampal slices is mediated via activation of the kinases c-Jun N-terminal kinase, cyclin-dependent kinase 5, and p38 mitogen-activated protein kinase as well as metabotropic glutamate receptor type 5. J. Neurosci. *24*, 3370–3378.

Wang, Z., Jackson, R.J., Hong, W., Taylor, W.M., Corbett, G.T., Moreno, A., Liu, W., Li, S., Frosch, M.P., Slutsky, I., et al. (2017). Human Brain-Derived Aβ Oligomers Bind to Synapses and Disrupt Synaptic Activity in a Manner That Requires APP. J. Neurosci. *37*, 11947–11966.

Watanabe, M., Wake, H., Moorhouse, A.J., and Nabekura, J. (2009). Clustering of neuronal K+-Cl- cotransporters in lipid rafts by tyrosine phosphorylation. J. Biol. Chem. *284*, 27980–27988.

Weber, M., Hartmann, A.M., Beyer, T., Ripperger, A., and Nothwang, H.G. (2014). A novel regulatory locus of phosphorylation in the C terminus of the potassium chloride cotransporter KCC2 that interferes with n-ethylmaleimide or staurosporine-mediated activation. J. Biol. Chem. *289*, 18668–18679.

Wefelmeyer, W., Puhl, C.J., and Burrone, J. (2016). Homeostatic Plasticity of Subcellular Neuronal Structures: From Inputs to Outputs. Trends Neurosci. *39*, 656–667.

Wegiel, J., Wang, K.C., Imaki, H., Rubenstein, R., Wronska, A., Osuchowski, M., Lipinski, W.J., Walker, L.C., and LeVine, H. (2001). The role of microglial cells and astrocytes in fibrillar plaque evolution in transgenic APPSW mice. Neurobiol. Aging *22*, 49–61.

Wei, W., Nguyen, L.N., Kessels, H.W., Hagiwara, H., Sisodia, S., and Malinow, R. (2010). Amyloid beta from axons and dendrites reduces local spine number and plasticity. Nat. Neurosci. *13*, 190–196.

West, R.L. (1996). An application of prefrontal cortex function theory to cognitive aging. Psychol. Bull. *120*, 272–292.

Williams, J.R., Sharp, J.W., Kumari, V.G., Wilson, M., and Payne, J.A. (1999). The Neuron-specific K-Cl Cotransporter, KCC2: ANTIBODY DEVELOPMENT AND INITIAL CHARACTERIZATION OF THE PROTEIN *. J. Biol. Chem. *274*, 12656–12664.

Wilson, I.A., Ikonen, S., Gallagher, M., Eichenbaum, H., and Tanila, H. (2005). Age-Associated Alterations of Hippocampal Place Cells Are Subregion Specific. J. Neurosci. *25*, 6877–6886.

Wilson, R.S., Beckett, L.A., Bienias, J.L., Evans, D.A., and Bennett, D.A. (2003). Terminal decline in cognitive function. Neurology *60*, 1782–1787.

Winblad, B., and Blum, K.I. (2003). Hints of a Therapeutic Vaccine for Alzheimer's? Neuron *38*, 517–518.

Wolfe, M.S., Xia, W., Ostaszewski, B.L., Diehl, T.S., Kimberly, W.T., and Selkoe, D.J. (1999). Two transmembrane aspartates in presenilin-1 required for presenilin endoproteolysis and γ-secretase activity. Nat. 1999 3986727 *398*, 513–517.

Wong, M. (2010). Too much inhibition leads to excitation in absence epilepsy. Epilepsy Curr. *10*, 131–132.

Wong, D.F., Rosenberg, P.B., Zhou, Y., Kumar, A., Raymont, V., Ravert, H.T., Dannals, R.F., Nandi, A., Brašić, J.R., Ye, W., et al. (2010). In Vivo Imaging of Amyloid Deposition in Alzheimer Disease Using the Radioligand 18F-AV-45 (Flobetapir F 18). J. Nucl. Med. *51*, 913–920.

Wong, T.P., Marchese, G., Casu, M.A., Ribeiro-Da-Silva, A., Cuello, A.C., and De Koninck, Y. (2006). Imbalance towards inhibition as a substrate of aging-associated cognitive impairment. Neurosci. Lett. *397*, 64–68.

Xiao, N.A., Zhang, J., Zhou, M., Wei, Z., Wu, X.L., Dai, X.M., Zhu, Y.G., and Chen, X.C.

(2015). Reduction of glucose metabolism in olfactory bulb is an earlier Alzheimer's disease-related biomarker in 5XFAD mice. Chin. Med. J. (Engl). *128*, 2220–2227.

Xie, Y., Chang, S., Zhao, C., Wang, F., Liu, S., Wang, J., Delpire, E., Ye, S., and Guo, J. (2020). Structures and an activation mechanism of human potassium-chloride cotransporters. Sci. Adv. *6*.

Yamamoto, J., Suh, J., Takeuchi, D., and Tonegawa, S. (2014). Successful execution of working memory linked to synchronized high-frequency gamma oscillations. Cell *157*, 845–857.

Yamamoto, K., Tanei, Z.-I. ichi, Hashimoto, T., Wakabayashi, T., Okuno, H., Naka, Y., Yizhar, O., Fenno, L.E., Fukayama, M., Bito, H., et al. (2015). Chronic Optogenetic Activation Augments Aβ Pathology in a Mouse Model of Alzheimer Disease. Cell Rep. *11*, 859–865.

Yankner, B.A., Dawes, L.R., Fisher, S., Villa-Komaroff, L., Oster-Granite, M. Lou, and Neve, R.L. (1989). Neurotoxicity of a fragment of the amyloid precursor associated with Alzheimer's disease. Science *245*, 417–420.

Yeo, M., Berglund, K., Augustine, G., and Liedtke, W. (2009). Novel Repression of Kcc2 Transcription by REST–RE-1 Controls Developmental Switch in Neuronal Chloride. J. Neurosci. *29*, 14652–14662.

Yizhar, O., Fenno, L.E., Prigge, M., Schneider, F., Davidson, T.J., O'Shea, D.J., Sohal, V.S., Goshen, I., Finkelstein, J., Paz, J.T., et al. (2011a). Neocortical excitation/inhibition balance in information processing and social dysfunction. Nature *477*, 171–178.

Yizhar, O., Fenno, L.E., Davidson, T.J., Mogri, M., and Deisseroth, K. (2011b). Optogenetics in neural systems. Neuron *71*, 9–34.

Yoshikai, S. ichi, Sasaki, H., Doh-ura, K., Furuya, H., and Sakaki, Y. (1990). Genomic organization of the human amyloid beta-protein precursor gene. Gene *87*, 257–263.

Yu, Z.Y., Wang, W., Fritschy, J.M., Witte, O.W., and Redecker, C. (2006). Changes in neocortical and hippocampal GABAA receptor subunit distribution during brain maturation and aging. Brain Res. *1099*, 73–81.

Zempel, H., and Mandelkow, E. (2014). Lost after translation: missorting of Tau protein and

consequences for Alzheimer disease. Trends Neurosci. *37*, 721–732.

Zempel, H., Thies, E., Mandelkow, E., and Mandelkow, E.M. (2010). Aβ Oligomers Cause Localized Ca2+ Elevation, Missorting of Endogenous Tau into Dendrites, Tau Phosphorylation, and Destruction of Microtubules and Spines. J. Neurosci. *30*, 11938–11950.

Zhan, R.Z., and Nadler, J.V. (2009). Enhanced tonic GABA current in normotopic and hilar ectopic dentate granule cells after pilocarpine-induced status epilepticus. J. Neurophysiol. *102*, 670–681.

Zhang, L., Spigelman, I., and Carlen, P.L. (1991). Development of GABA-mediated, chloride-dependent inhibition in CA1 pyramidal neurones of immature rat hippocampal slices. J. Physiol. *444*, 25–49.

Zhang, S., Zhou, J., Zhang, Y., Liu, T., Friedel, P., Zhuo, W., Somasekharan, S., Roy, K., Zhang, L., Liu, Y., et al. (2021). The structural basis of function and regulation of neuronal cotransporters NKCC1 and KCC2. Commun. Biol. 2021 41 *4*, 1–15.

Zheng, H., and Koo, E.H. (2006). The amyloid precursor protein: Beyond amyloid. Mol. Neurodegener. *1*, 1–12.

Zhou, H.Y., Chen, S.R., Byun, H.S., Chen, H., Li, L., Han, H.D., Lopez-Berestein, G., Sood, A.K., and Pan, H.L. (2012). N-methyl-D-aspartate receptor- and calpain-mediated proteolytic cleavage of K+-Cl- cotransporter-2 impairs spinal chloride homeostasis in neuropathic pain. J. Biol. Chem. *287*, 33853–33864.

Zhou, Y., Cheng, Y., Li, Y., Ma, J., Wu, Z., Chen, Y., Mei, J., and Chen, M. (2021). Soluble β-amyloid impaired the GABA inhibition by mediating KCC2 in early APP/PS1 mice. Biosci. Trends *15*, 330–340.

Zott, B., Busche, M.A., Sperling, R.A., and Konnerth, A. (2018). What Happens with the Circuit in Alzheimer's Disease in Mice and Humans? Annu. Rev. Neurosci. *41*, 277–297.

Zott, B., Simon, M.M., Hong, W., Unger, F., Chen-Engerer, H.J., Frosch, M.P., Sakmann, B., Walsh, D.M., and Konnerth, A. (2019). A vicious cycle of β amyloid−dependent neuronal hyperactivation. Science (80-.). *365*, 559–565.